BEHAVIOR OF STRAIGHT SKEWED I-GIRDER BRIDGES WITH SKEW INDEX APPROACHING 0.3

A Dissertation
Presented to
The Academic Faculty

by

Ajit Manohar Kamath

In Partial Fulfillment
of the Requirements for the Degree
Master of Science in Civil Engineering in the
School of Civil and Environmental Engineering

Georgia Institute of Technology
December 2019

BEHAVIOR OF STRAIGHT SKEWED I-GIRDER BRIDGES WITH SKEW INDEX APPROACHING 0.3

Approved by:

Dr. Donald W. White, Advisor
School of Civil and Environmental Engineering
Georgia Institute of Technology

Dr. Yang Wang
School of Civil and Environmental Engineering
Georgia Institute of Technology

Dr. Ryan Sherman
School of Civil and Environmental Engineering
Georgia Institute of Technology

Date Approved: December 6, 2019

To my family, for their unconditional love and support

ACKNOWLEDGEMENTS

I would like to express my sincere gratitude and appreciation for the opportunity provided by my advisor, Dr. Donald W. White, without which this work would not have been possible. His expertise in the field of structural engineering and his love for research is remarkable. Additionally, I would like to thank John Heath, Brian Adams and Amrithraj Anand from Heath and Lineback Engineers Inc. for their invaluable insights.

I also wish to thank the rest of my committee members, Dr. Yang Wang and Dr. Ryan Sherman for their valuable comments and suggestions.

I would like to thank my friends for their valuable help and support, especially Ryan Slein, Oghuzhan Togay and Ajinkya Lokhande for the constant support and motivation.

TABLE OF CONTENTS

LIST OF TABLES

LIST OF FIGURES

SUMMARY

The skew index is often used to quantify the extent of skew of girder bridges. The skew index of a bridge span can be defined as $w_g \tan \theta / L_s$, where w_g is the framing width between the fascia girders, θ is the maximum angle of skew, and L_s is the span length under consideration. Many straight skewed I-girder bridges have skew indices less than or equal to 0.3, or only slightly larger. Prior research has shown that transverse load path effects can start to become relatively significant for $I_s > 0.3$. It is anticipated that bridge owners and consultants are increasingly using refined methods of analysis – 2D grid, plate and eccentric beam or 3D Finite Element Analysis (3D FEA) for certain I-girder bridge geometries. However, traditionally, many straight skewed I-girder bridges have been designed using 1D line girder analysis (LGA). 3D FEA requires expensive software, time to develop a working finite element model and staff that have adequate knowledge of finite element modeling and its nuances.

The FDOT Structures Design Guidelines currently require a refined method of analysis for straight steel I-girder bridges with a skew index greater than 0.2 and less than or equal to 0.6. They require a 3D FEA if the skew index is greater than 0.6. Based on current FDOT design policy, over one-third of their existing bridges with a skew index less than 0.3 would therefore require a refined analysis for design, when line girder models may have sufficed. Application of LGA in lieu of 3D FEA for such bridges has the potential to simplify the workflow and allow concentration of resources on other important matters, if it can be understood that LGA provides acceptable designs for a wider range of straight skewed I-girder bridges.

This research seeks to improve the understanding of the behavior of straight steel I-girder skewed bridges having skew indices up to and slightly larger than 0.3 and evaluate the applicability of simplified methods of analysis. To achieve this goal, comparative parametric 3D FEA and LGA studies are conducted on a suite of 26 bridges with skew indices up to and slightly exceeding 0.3. These bridges are configured from a suite of 57 bridges sampled from the Florida DOT bridge inventory. Key response quantities studied include total dead load displacements and girder layovers, girder moments and shears, bearing reactions, girder flange lateral bending stresses, and cross-frame forces. The suite of 26 bridges represents a gamut of skewed bridges including parallel and non-parallel skew, cross-frames parallel to the skew or perpendicular to the girders, contiguous and staggered cross-frame layouts, and girder splay. The parametric study evaluates the extent to which LGA can adequately calculate the response quantities for straight steel I-girder bridges with small to moderate skew.

It is found that the accuracy of LGA procedures with respect to 3D FEA methods depends on a complex combination of numerous structural attributes. These include:

- The skew index,
- The actual skew angle at the bearing lines, and
- The framing arrangement of the cross-frames.

Regarding the framing arrangement of the cross-frames, some of the factors involved are:

a) Contiguous cross-frame arrangements tend to result in larger cross-frame forces and smaller girder flange lateral bending. However, if a contiguous cross-frame line is discontinued with a relatively short stagger between this line and a bearing line

or another intermediate cross-frame line, substantial girder flange lateral bending can be introduced at the location where the line is discontinued.

b) Generous use of staggers and offsets tends to reduce the cross-frame forces at the expense of some additional girder flange lateral bending.

c) Intermediate cross-frames lines framed across interior bearings tend to exhibit significant transverse cantilever action, resulting in large cross-frame forces. Any discontinuities at the ends of these types of cross-frames tends to attract large girder flange lateral bending.

d) Cross-frames framed directly into or relatively close to bearing locations often attract excessive forces, unless local lean-on details are used (i.e., leaving the cross-frame diagonals out). Large girder flange lateral bending stress can occur at locations where these types of cross-frames are discontinued.

The comparative studies conducted in this research show that LGA estimates of girder maximum Strength I bending moments and shear forces are less than 10% unconservative for all the bridges studied. However, the accuracy of total dead load vertical displacements used in camber calculations is not adequate for bridges having larger skew, and/or cross-frame arrangements exhibiting significant transverse load path effects. In addition, transverse load path effects have a significant impact on the accuracy of LGA estimates of vertical reactions, fatigue live load forces and cross-frame forces. Recommendations are developed for the application of LGA based on these findings. The synthesized results from this research provide detailed insight into various structural attributes influencing the behavior of straight skewed I-girder bridges.

CHAPTER 1. INTRODUCTION

1.1 Background

Line girder analysis (LGA) is the simplest and most basic method used in the analysis and design of girder bridges. With LGA, bridge girders are analyzed individually, and the interaction between the girders via the cross-frames, diaphragms and bridge deck is ignored or accounted for only in a coarse approximate fashion. In contrast, refined methods of analysis involve the direct modeling of the interactions between the girders, cross-frames and bridge deck to various degrees of rigor. 3D Finite Element Analysis (3D FEA) is the most rigorous refined method and commonly involves a detailed three-dimensional representation of the bridge deck, girders, cross-frames, diaphragms, and bearings, and potentially other substructure elements, capturing their collaboration and interaction in resisting the loads. In 3D FEA methods, the girders, cross-frames, diaphragms, bridge deck, bearings and other structural components typically are modeled at their specific locations in three-dimensional space. Other refined methods of analysis include 2D grid and plate-eccentric beam analysis models. In 2D grid analysis methods, the girders, cross-frames, and potentially various longitudinal and transverse widths of the deck are modeled as line elements in a single horizontal plane. In the final composite constructed condition, the bridge deck is typically modeled by using the composite properties of the girders in these procedures. Refined methods of analysis are typically specified to be used for bridges that are expected to exhibit interaction between the girders, bridge deck and the cross-frames that cannot be captured by LGA.

The Florida DOT Structures Design Guidelines (FDOT, 2019a) currently limit the use of line girder analysis methods for straight steel I-girder bridges based on the value of the skew index,

$$I_s = \frac{w_g \tan\theta}{L_s} \tag{1}$$

where

w_g = width of the bridge measured between fascia girders

θ = skew angle at a support defined as the difference between the alignment of the support and a line perpendicular to the longitudinal axis of the bridge

L_s = Length of the span under consideration.

The skew index for a bridge is generally taken as the maximum value from Eq. 1, calculated considering each of the bearing lines and each of the spans. FDOT requires a refined method of analysis for straight steel I-girder bridges when the skew index is greater than 0.2 and less than or equal to 0.6. They require a 3D FEA when the skew index is greater than 0.6. Approximately 250 steel I-girder bridges were constructed in Florida from the years 2000 to 2014, with over 90% having a skew index of less than 0.3. NCHRP Report 725 (White et al., 2012) indicates that LGA is capable of predicting girder noncomposite major-axis bending stresses and vertical displacements with a worst-case mean normalized error less than or equal to 12 % when the skew index is less than or equal to 0.3. Based on current FDOT design policy, over one-third of the above bridges with a skew index less than 0.3 would require a 2D grid or 3D FEA for design, when line girder models may have

sufficed. Most of the prior research on skewed steel I-girder bridges has focused predominantly on more heavily skewed geometries rather than geometries that reflect the majority of the Department's steel I-girder bridge inventory. Moreover, a detailed study focused on the application of LGA for moderately skewed bridges is lacking in the literature.

1.2 Objectives of this Research

The objective of this research is to understand more fully the behavior of steel I-girder bridges with skew indices up to and slightly above 0.3, and to determine when, for these types of bridges, Line Girder Analysis (LGA) will yield results that are very similar to those obtained from 3D FEA. This includes the direct estimation of major-axis bending stresses and vertical displacements from the LGA, nearly direct estimation of girder layover at the bearings, and indirect estimation of girder flange lateral bending stresses and cross-frame forces. Guidance on sufficient application of LGA to bridges with skew indices up to and potentially beyond 0.3 would allow for potential revisions to the current FDOT (2019a) requirements for use of refined analysis in design.

1.3 Organization of the Thesis

This thesis is organized in five main chapters. Chapter 2 provides a broad review of prior research and guidelines. The objectives of the research are achieved by a comparative parametric 3D FEA and LGA studies on a suite of 26 bridges that have skew indices up to and slightly exceeding 0.3. The 26 bridges are selected from a set of 57 bridges sampled from the FDOT inventory. Chapter 3 presents a data analysis of these bridges and outlines the development of the suite of 26 bridges for the parametric studies. Chapter 4 discusses

key LGA and 3D FEA modeling idealizations and identifies key bridge responses that effectively describe the behavior of skewed I-girder bridges. Furthermore, considerations related to load and response calculations for the parametric studies are explained. Chapter 5 focuses on detailed comparisons of the LGA and 3D FEA results, considering each of the key bridge responses. Chapter 6 summarizes the specific findings and recommendations from this research.

CHAPTER 2. LITERATURE REVIEW

This chapter reviews the present knowledge within the literature regarding the behavior of skewed I-girder bridges subjected to dead live gravity loads, the influence of cross-frame arrangements and cross-frame detailing on bridge responses, as well as bridge behavior during deck placement. The chapter concludes with a summary of current guidance regarding the limits of applicability of line girder analysis for the design of straight skewed I-girder bridges.

2.1. Behavior of Skewed Bridges

Geometrically, a skewed bridge is one in which one or more lines of support are not oriented perpendicular to the longitudinal axis of the bridge. The effects of skew on structural behavior depend largely on the magnitude of the skew, quantified by the skew angle θ and the skew index I_s (see Eq. 1), and the layout of cross-frames in the structure. The behavior of straight skewed I-girder bridges becomes increasingly three-dimensional with increasing skew. Sanchez (2011) shows that the skew index, I_s, is a coarse indicator of the sensitivity of steel I-girder bridges to skew.

The structural behavior of a skewed bridge is influenced both by the end bearing-line and intermediate cross-frames. End bearing-line cross-frames oriented along the skew twist the girders to maintain continuity between the skewed bearing-line cross-frames and the girders (NSBA 2016). Figure 1 illustrates the behavior for two girders connected along a skewed bearing line. The bearings are assumed to be fixed (laterally and longitudinally restrained) for simplicity of the discussion. The major-axis bending rotation of the girders induces a longitudinal displacement Δ_z of the top flange relative to the bottom flange. However, since the girders are attached to the skewed bearing-line cross-frames, which have relatively high in-plane stiffness, the cross-frames can only achieve this longitudinal

displacement by rotating about the axis tangent to the bearing line. This induces a relative lateral displacement between the top and bottom flange, Δ_x, and a twist rotation of the girders at the bearing line. Correspondingly, girder torsional moments are developed. These moments increase the vertical reactions at the obtuse corner and reduce the vertical reactions at the acute corner.

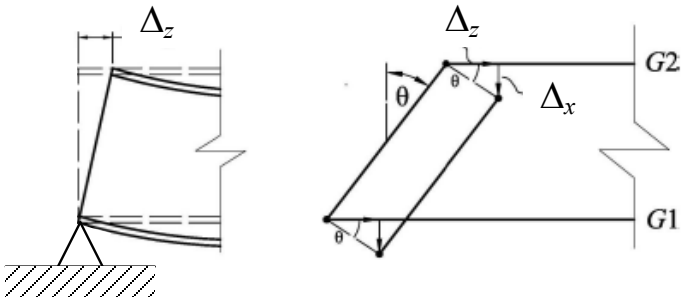

Figure 1. Relative flange displacement in a skewed bridge, adapted from Sanchez (2011).

Figure 2, from White et al. (2012), illustrates the above girder end rotations at the specific bearing on Girder G2. The girder web and the bearing-line cross-frame are assumed to be plumb in the current configuration shown in this figure. The double arrow perpendicular to the girder web represents the major-axis bending rotation of the girder, ϕ_x, about the fixed point. This rotation induces the longitudinal displacement Δ_z at the top flange of the girder. However, since the girder is attached to the skewed bearing line cross-frame, the top flange can only displace significantly in the direction normal to the plane of the cross-frame. This is indicated by the vector labeled Δ. The cross-frame deflects essentially only by rotating about its longitudinal axis through the fixed point. This is shown by the double-arrow vector ϕ. To maintain compatibility between the girder and the cross-frame, the top flange of the girder must deflect by the vector component labeled Δ_x in the figure, in addition to the deflection Δ_z. Therefore, the girder web lays over by the deflection Δ_x relative to the fixed point. This deflection, divided by the height h, gives the girder twist rotation ϕ_z.

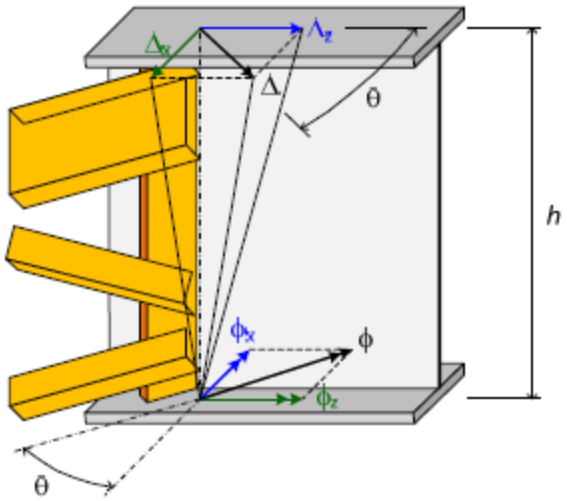

Figure 2. Illustration of the girder major-axis bending and twist rotations required for compatibility at a skewed bearing cross-frame, from NCHRP 725 report (White et al. 2012).

Based on Figures 1 and 2, the girder layover at the bearing locations can be calculated as follows:

$$\Delta = \phi_x h \tan\theta \tag{2}$$

where,

θ = skew angle at the bearing line and

ϕ_x = the girder major-axis bending rotation relative to the ideally plumb position associated with the dead load condition targeted for the cross-frame detailing.

h = girder depth.

When the intermediate cross-frames are perpendicular to the girders, twisting occurs because of the differential vertical deflections between the girders at each of the intermediate cross-frames (NSBA 2016). The differential vertical deflections are due to the fact that the cross-frames connect to different positions within the span of each of the

girders (NSBA 2016). Due to the large in-plane rigidities of typical cross-frames, intermediate cross-frames that are perpendicular to the girders force them to have approximately the same twist and layover at the bracing points (Sanchez 2011). The AASHTO LRFD Bridge Specifications (AASHTO 2017) allow intermediate cross-frames to be oriented parallel to the skew if the skew angle is less than 20°, and it mandates the orientation of cross-frames to be perpendicular to the girders if the skew angle is greater than 20°. If the intermediate cross-frames are oriented parallel to the skew, the differential vertical deflections at the ends of cross-frames are essentially zero in straight bridges with parallel skew. However, the cross-frames still induce a twisting of the girders at these points when there is any major-axis bending rotation of the girders there, due to compatibility of deformations.

Florida DOT and various other states follow the AASHTO (2017) requirements for bridges having a skew angle up to 20°. Kansas DOT extends this limit up to 40° to reduce potential differential deflection and distortion induced fatigue (Zhou et al. 2017)). It should be noted that this may create a more critical detail for evaluation of load-induced fatigue at connection plates turned parallel to the cross-frames and welded to the girder flanges. Wisconsin DOT limits the use of cross-frames parallel to the skewed bearing lines to bridges with a skew angle of less than 15° (WisDOT 2019). Ohio DOT mandates all intermediate cross-frames to be perpendicular to the girder regardless of the skew angle (ODOT 2007).

Figures 3 and 4 show representative skewed bridge deflected shapes for the case where the cross-frames are oriented perpendicular to the girders, by focusing on two girders unconnected and then interconnected by cross-frames.

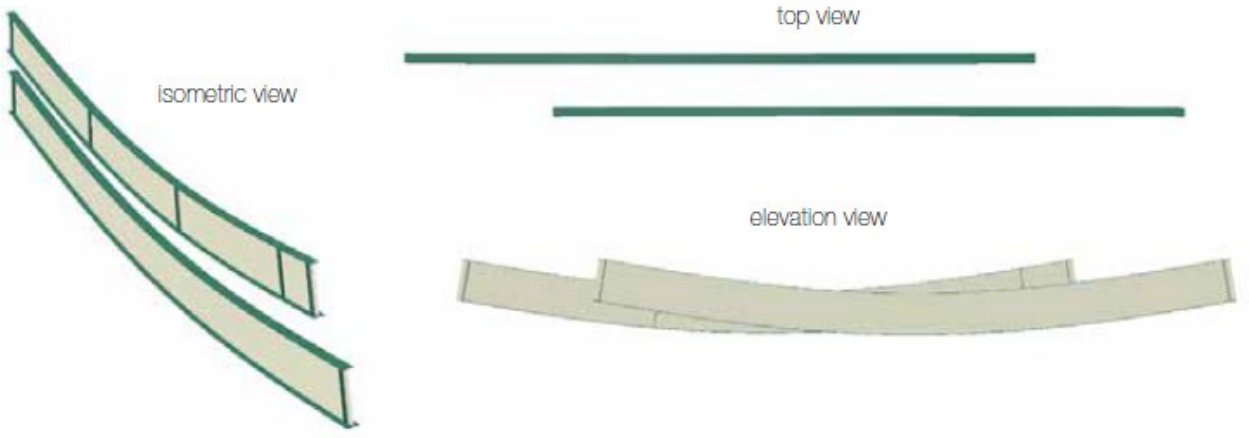

Figure 3. Girder deflections for two simple-span I-girders on parallel skewed supports, subjected steel dead load prior to connecting the cross-frames, from NSBA (2016).

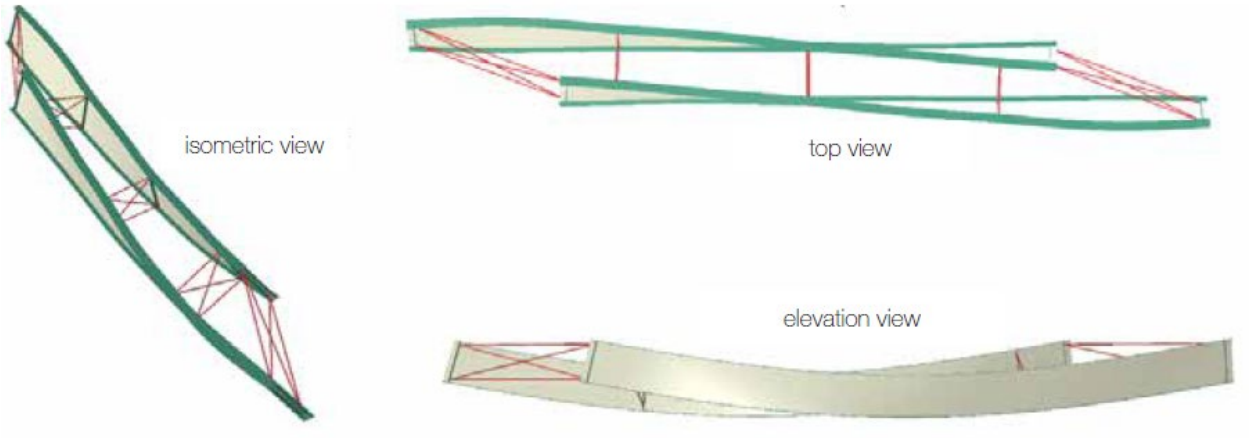

Figure 4. Girder deflections and twist for two simple-span i-girders on parallel skewed supports, subjected to steel dead load, after connecting the cross-frames, from NSBA (2016).

Figure 5 shows a sketch from Sanchez (2011) that illustrates the enforcement of compatibility of layover between adjacent girders by an intermediate cross-frame. Figure 5a shows the twist and vertical deflections of the two girders when only the end-bearing cross-frames are connected to the girders. Figure 5b shows the twist and vertical deflections of the two girders when all the cross-frames – end bearing and intermediate, are connected to the girders.

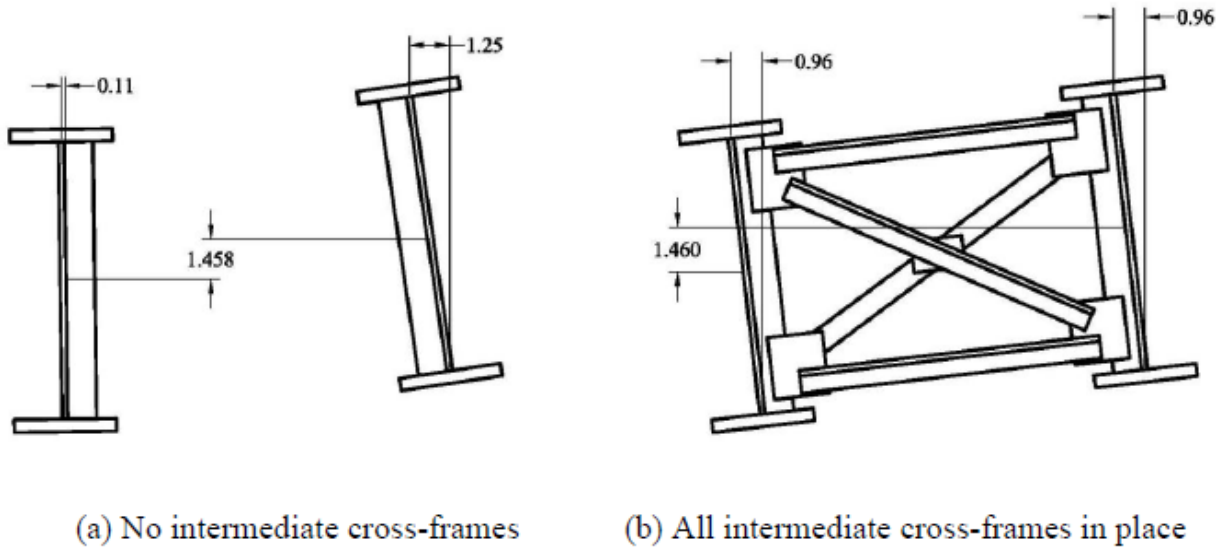

Figure 5. Layover compatibility between adjacent girders enforced by an intermediate cross-frame, from Sanchez (2011).

2.2. Forces in Cross-Frames of a Skewed Bridge

It is shown in Section 2.1 that intermediate cross-frames impart twist and lateral displacement such that the girders have approximately equal layovers at all the bracing points. Compatibility of displacements and rotations develops forces at the connection points of the cross-frames to the girders as shown in Figure 6 (Sanchez 2011). This also induces lateral bending of girder flanges. Furthermore, intermediate cross-frames provide a load path for transfer of vertical forces to the bridge supports. These forces depend on the overall transverse stiffness of the system formed by the grid of girders and cross-frames within the spans.

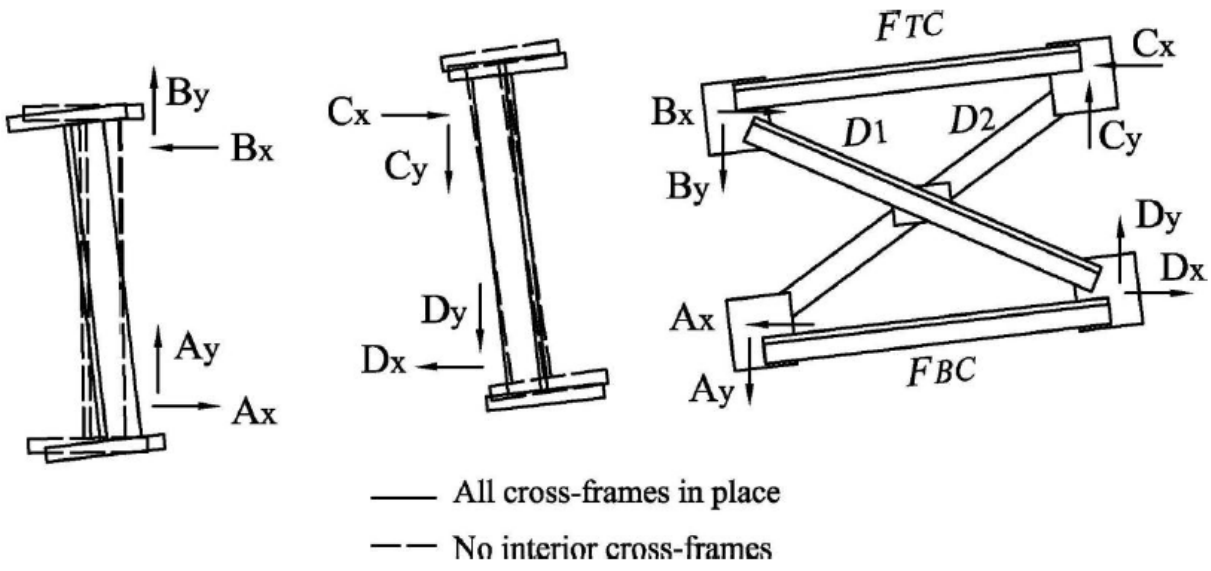

Figure 6. Internal forces in girders and cross-frames due to skew effects, from Sanchez (2011).

Due to larger stiffness of the system of girders and cross-frames along the shorter diagonal direction connecting the obtuse corners of a parallel skew bridge, a significant transverse load path can develop between the supports with large forces being observed near the obtuse corners of the bridge span (White et al. 2015). Kupricka and Poellot (1993) describe this behavior as nuisance stiffness. At contiguous cross-frame lines, the horizontal forces developed in the girder flanges are approximately balanced by the cross-frames connected to the girder from both sides of the girder. Therefore, the girder flange lateral bending stresses tend to be smaller in these situations, although significant flange lateral bending can occur where a contiguous cross-frame line is discontinued.

Conversely, when staggers and offsets in the cross-frame layout are used to mitigate the stiff transverse path, discussed subsequently in Section 2.3, the cross-frame forces tend to be reduced at the expense of the girder flange lateral bending stresses tending to be increased. This needs to be accounted in the proportioning of the girder flanges. The AASHTO LRFD Specifications (AASHTO 2017) advise that, in such cases, flange lateral bending stresses are best determined by direct structural analysis. However, in many

situations, these lateral bending stresses have a relatively minor influence on the girder design. Furthermore, offsets and staggers can provide a desirable reduction in the cross-frame/diaphragm forces (NHI 2011, NSBA 2016, and AASHTO 2017). The AASHTO LRFD Specifications (AASHTO, 2017) indicate that, in some cases, the flange lateral bending stresses are reduced due to this decrease in the cross-frame forces.

The next section discusses a few strategies for mitigating the stiff transverse load path effects.

2.3. Strategies for Mitigating Transverse Load Path Effects

It is explained in Section 2.1 that intermediate cross-frames impart twist and lateral displacement such that the girders have approximately equal layovers at the bracing points. Compatibility of displacements and rotations develops forces at the connection points of the cross-frames to the girders as shown in Figure 6. This induces lateral bending of the girder flanges when there are offsets, staggers or general discontinuities in the cross-frame lines. Furthermore, intermediate cross-frames provide a load path for transfer of vertical forces to the bridge supports. These forces depend on the overall transverse stiffness of the system formed by the grid of girders and cross-frames within the spans.

If the first intermediate cross-frame within a span is connected too close to a bearing, high internal forces should be expected (Sanchez 2011). Therefore, a strategy for mitigating the nuisance stiffness is to offset the intermediate cross-frames from the bearings in the vicinity of the skewed supports.

White et al. (2015) and NSBA (2016) recommend that, where support lines are skewed more than 20° from normal and cross-frames or diaphragms are provided along the skewed support line, the first intermediate cross-frames or diaphragms placed normal to the girders adjacent to the skewed support ideally should be offset, where practicable, by a minimum of the larger of $4b_f$ or $0.4L_b$ from the support, where b_f is the largest girder flange width

within the unbraced length on either side of the first cross-frame or diaphragm, and L_b is the unbraced length between the first and the second intermediate cross-frame or diaphragm from the support along the girder under consideration. The AASHTO LRFD Specifications (AASHTO 2017) have adopted these recommendations. Figure 7 shows an illustration of the application of this concept from NCHRP 20-07/Task 355 (White et al. 2015). In this example, staggering of the cross-frames is achieved by omitting alternate cross-frames within the bays between the interior girders.

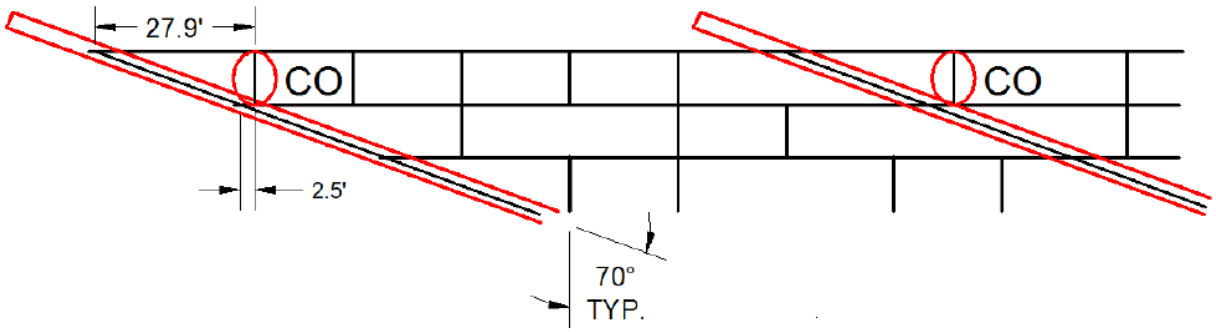

Figure 7. Use of a staggered cross-frame layout plus isolated (local) lean-on bracing, from NCHRP 20-07/Task 355 report (CO indicates cross-frames in which the diagonals are taken out, and only of top and bottom chords are employed).

The above practice helps to alleviate the introduction of a stiff load path that will attract and transfer large transverse forces to the skewed support lines, particularly at the obtuse corners of a parallel skewed span. At the acute corners of severely skewed bridge spans, the above offset requirements may result in an excessive unbraced length on the fascia girder as can be observed in Figure 7. In this case, a cross-frame with only top and bottom chords (no diagonal members) can be framed from the first interior girder to the fascia girder at a small offset from the support, perpendicular to the girders, to avoid inducing a large transverse stiffness while also providing adequate lateral support to the fascia girder (White et al. 2015). The use of unbraced lengths smaller than $4b_f$ or $0.4L_b$ often tends to result in the associated cross-frames working more like a contiguous cross-frame line rather than a discontinuous one.

Figure 8, from White et al. (2015), illustrates the above concept on a bridge with an extreme non-parallel skew. NSBA (2016) explains that a cross-frame must be provided on at least one side of a girder at each bracing location to provide the required lateral bracing. In some situations, additional cross-frames may be required to provide sufficient lateral bracing stiffness. However, the alternate removal of intermediate cross-frames is usually structurally sufficient (White et al. 2015).

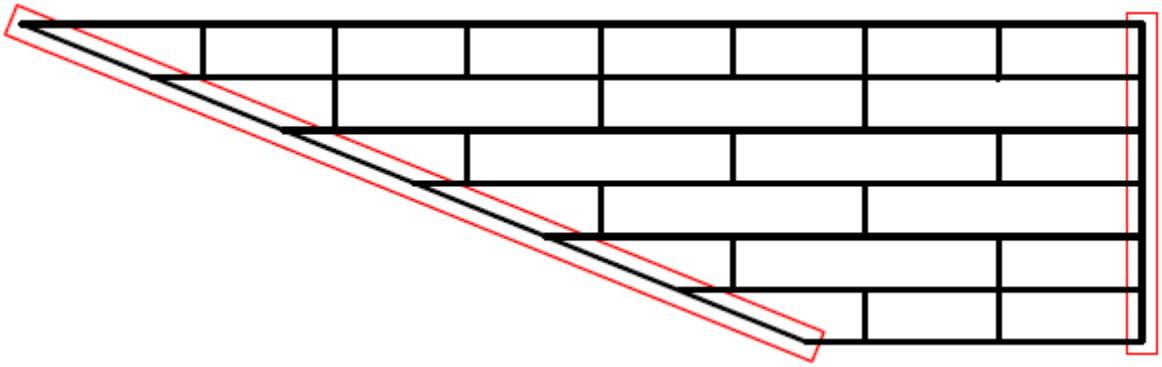

Figure 8. Use of staggered cross-frame layout for a bridge with extreme non-parallel skew, from NCHRP 20-07/Task 355 report and NSBA (2016).

For continuous span bridges, the AASHTO LRFD 7th Edition (AASHTO 2015) Article 6.7.4.2 states that at the discretion of the Owner, cross-frames/diaphragms need not be provided along skewed interior support lines if cross-frames/diaphragms normal to the girders are provided at bearings that resist lateral forces. Figure 9 provides an example of this type of framing arrangement from the bridges sampled from the FDOT inventory for this research. This framing arrangement causes substantial nuisance stiffness effects, since the cross-frames join points of zero vertical displacement on the bearing line and finite non-zero displacement on the other side of the cross-frame. A cantilever-type action occurs for these cross-frames when they are framed across a bearing line. Framing of an intermediate cross-frame perpendicular to the girders and into or near a bearing location along a skewed support is highly discouraged unless the cross-frames diagonals are omitted (NSBA 2016). The AASHTO LRFD 8th Edition (AASHTO 2017) has revised its

recommendations to indicate a preference for offsets of the intermediate cross-frames from the bearing lines, and the provision of cross-frames between the girders along all bearing lines.

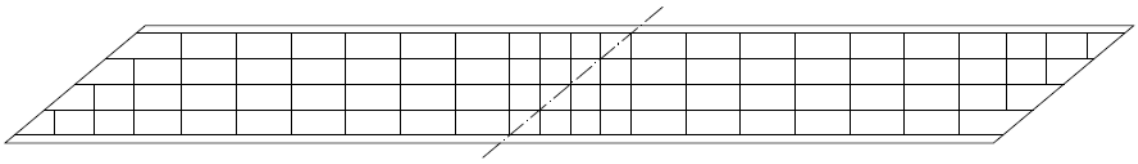

Figure 9. Bridge F31, from FDOT database.

The NHI (2011) and NCHRP 20-07/Task 355 (White et al. 2015) reports find that transverse stiffness effects are alleviated most effectively by placing diaphragms or cross-frames along the bearing lines, and locating perpendicular intermediate diaphragms or cross-frames at greater than or equal to the minimum offset from skewed bearing lines as discussed above (in the context of bridges with skew angle $\theta > 20°$). Figure 10 shows an example of this type of framing arrangement. NSBA (2016) explains that the lines through the work-points at the mid-length of the intermediate cross-frames are all parallel to the bearing lines in this bridge. However, given the skew angle in the bridge, the stagger distances between the intermediate cross-frame locations within the span are both greater than $4b_f$ and $0.4L_{b,adj}$, where b_f is the largest girder flange width within the unbraced length on either side of the intermediate cross-frame, and $L_{b,adj}$ is the unbraced length between intermediate cross-frame under consideration and the adjacent cross-frames.

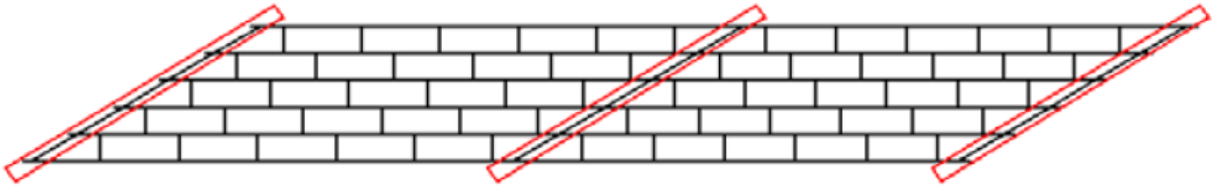

Figure 10. Recommended staggered framing arrangement for straight skewed bridges with parallel skew angles at bearing lines, from NSBA (2016).

The NCHRP 20-07/Task 355 report also suggests an arrangement that places the cross-frames perpendicular to the girders in a staggered arrangement (with skews greater than 20°), but positions a common "work point" on the different cross-frames at locations parallel to the skew. That is, the work points are "fanned" approximately between the skew angles at the ends of the span. Such an arrangement is shown in Figure 11.

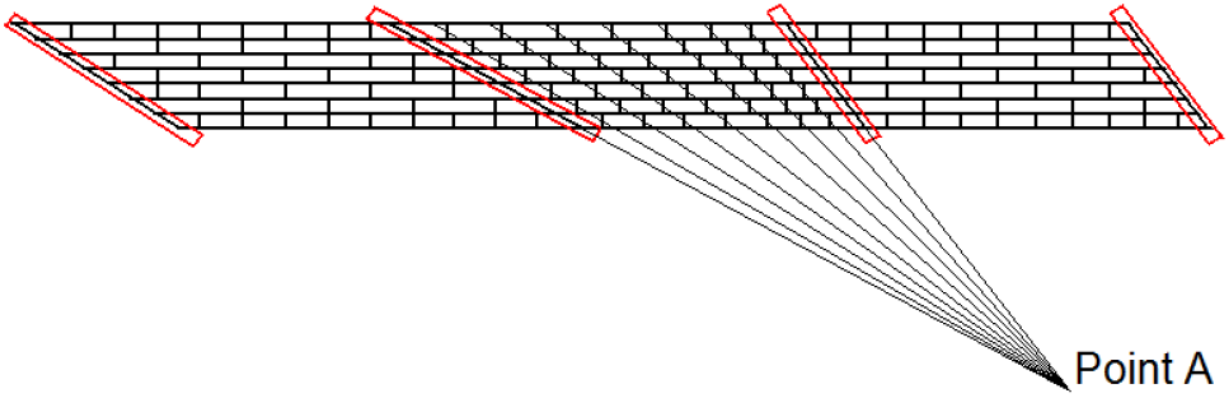

Figure 11. Sketch of an alternative staggered "fanned" cross-frame layout for a non-parallel skewed bridge, from the NCHRP 20-07/Task 355 report (White et al., 2015).

Furthermore, generally diaphragms or cross-frames can be omitted to alleviate uplift considerations at certain bearings, as well as potentially to relieve excessive diaphragm or cross-frame forces due to transverse stiffness effects if the skew is significant. (White et. al. 2015; AASHTO 2017)

Another approach to mitigate significant transverse load path effects is to use a lean-on cross-frame system arrangement in parallel skew bridges, as shown in Figure 12 (Romage 2008; Zhou 2006; Helwig and Yura (2015)). In this structural system, the diagonals are left out of a large number of the cross-frames. Only the top and bottom chords are installed, providing a load path to resist the torsional rotation of all the girders connected along contiguous cross-frame lines by one or only a few cross-frames on each line (Helwig and Yura 2012). This basically provides a "shear release," removing the restraint of the differential displacements between the girders throughout much of the

bridge plan. However, the top and bottom chords connect the girders together such that equal layover is enforced among the girders connected at the lean-on bracing location.

The NCHRP 20-07/Task 355 research (White et al. 2015) studied a bridge with a lean-on cross-frame system, also studied extensively by Romage (2008). The Task 355 research showed that a staggered cross-frame arrangement gives lower average maximum cross-frame forces for all cross-frame detailing methods (NLF, SDLF and TDLF) than the lean-on-bracing arrangement. It should also be noted that the shear release provided by the lean-on framing arrangement can allow excessive differential vertical deflections between the girders, resulting in large deviations in the final elevations. In some cases, this attribute must be considered when designing lean-on systems.

The Task 355 research concludes that the lean-on and the recommended staggered cross-frame framing systems are comparable in terms of achieving the desired results of mitigating nuisance transverse stiffness effects. The use of staggered cross-frames provides more overall continuity between the girders throughout the span, and a staggered arrangement in which every other intermediate cross-frame is removed within the span results in a substantial reduction in the number of cross-frames within the overall bridge system (White et al. 2015).

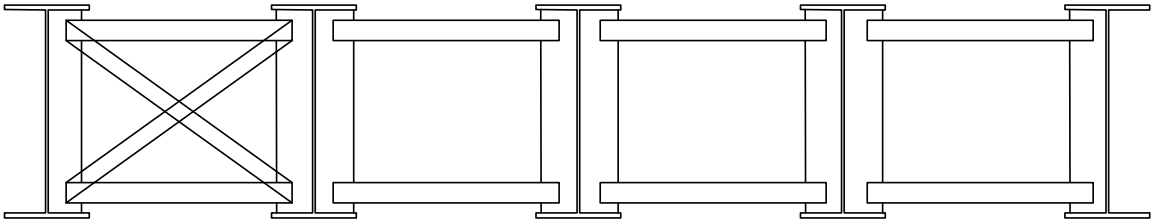

Figure 12. Lean-on bracing system for bridge girders.

It should be noted that the above recommendations were developed focusing on a wide range of skewed bridge geometries, with the bridge skew in many of the cases being relatively large. These concepts should be beneficial for bridges with less severely skewed

geometry as well, but the impact of these changes in the cross-frame framing arrangement will not be as dramatic. The softening of the transverse load path obtained using staggered cross-frame arrangements can potentially increase the range of applicability of line girder analysis for straight skewed bridges.

The AASHTO LRFD Bridge Specifications (AASHTO 2017) allow intermediate cross-frames to be oriented parallel to the skew for bridges if the skew angle is less than 20°, and they mandate the orientation of cross-frames to be perpendicular to the girders if the skew angle is greater than 20°. Kansas DOT extends this limit up to 40° as discussed above in Section 2.1. Although cross-frames oriented parallel to the skewed bearing lines can be effective with skew angles larger than 20°, the influence of bent plate connection flexibilities can become an issue (Wang and Helwig, 2008). Wang and Helwig (2008) further state that when a brace is oriented parallel to the skewed supports, the stiffness and strength of the brace can be significantly reduced. The stiffness reduction is due to the fact that the full stiffness of the brace is not engaged in resisting twist of the girder cross-section due to the angled orientation of the brace. In addition, the orientation of the brace parallel to the skew results in longer lengths in the brace member, which reduces the stiffness of the bracing in restraining girder torsional rotations. However, this reduction in stiffness also can be beneficial potentially, by reducing the tendency of the cross-frames to attract force within the statically indeterminate bridge structural system.

Zhou et. al (2017) studied the behavior of straight skewed I-girder bridges having skew angles of 0°, 20° and 40°, for a staggered cross-frame arrangement and a contiguous cross-frame arrangement where cross-frames are placed parallel to skew. Each of these bridges were investigated for different types of cross-frame connections that included a half-pipe stiffener, bent-plate and transverse stiffeners. Cross-frames oriented parallel to skew often are connected to the girder via a bent plate. The bent plate connection provided excessive flexibility into the system. This can be eliminated by using a half-pipe stiffener connection

(Quadrato, 2010). Girders in bridges that employed half-pipe stiffeners resulted in smaller lateral displacements in the study by Zhou et al. (2017). The bridge models that include the half-pipe stiffeners produced higher compression axial stresses near the connection ends. However, the stress magnitudes at locations away from the connection were similar in all the bridge models. The cross-frame forces in a bridge with a half-pipe connection were generally observed to be lower than with other types of connection.

2.4. "Fit" Considerations for Skewed Bridges

Skewed I-girder bridges undergo torsional displacements of the individual girders, as discussed in the previous sections. As a result, the girder webs can be plumb only under one loading condition. To achieve approximately plumb girder geometries for a given dead load condition (e.g., steel dead load or total dead load), the cross-frames and diaphragms are detailed to "fit" to the conceptually plumb girders once they are vertically deflected (from their initial cambered geometry) under this load condition. Thus, a "fit" condition can be defined as the deflected or undeflected girder geometry under which the cross-frames or diaphragms are detailed to connect to theoretically plumb girders (NSBA 2016). A fit condition is selected to offset, or compensate for (to different extents), the twisting of the I-girders under dead load. According to NSBA (2016), the detailer accomplishes I-girder bridge fit by setting the "drops" between the girders for the fabrication of the cross-frames and connection plates. Drops are calculated as the difference in the vertical elevation between the tops of the girder webs at the cross-frame connections to the girders under the targeted dead load condition (initial cambered elevations minus the estimated vertical deflections of the girders under the targeted dead load condition).

Table 1 (NSBA 2016) summarizes the three most common fit conditions considered in steel I-girder bridge construction. SDLF gives approximately plumb girder webs after the erection of all the steel components, and TDLF gives approximately plumb girder webs after the bridge is subjected to its total dead load (NSBA 2016). In this context, total dead

load typically refers to loads that include the weight of the steel components and the concrete deck. The cross-frames are erected before the deck is cast. The girders are fabricated with a camber calculated on the basis of total dead loads. Therefore, for both SDLF and TDLF detailing, a lack-of-fit force is developed in the cross-frames that can be calculated based on the changes in the ideal plumb girder geometry between the initial no-load cambered positions and the idealized plumb girder positions under the targeted dead load.

Table 1. Common fit conditions, from NSBA (2016).

Loading Condition Fit	Construction Stage Fit	Description	Practice
No-Load Fit (NLF)	Fully-Cambered Fit	The cross-frames are detailed to fit to the girders in their fabricated, plumb, fully-cambered position under zero dead load	The fabricator (detailer) sets the drops using the no-load elevations of the girders (i.e., the fully cambered girder profiles)
Steel Dead Load Fit (SDLF)	Erected Fit	The cross-frames are detailed to fit to the girders in their ideally plumb as-deflected positions under the bridge steel dead load at the completion of the erection.	The fabricator (detailer) sets the drops using the girder vertical elevations at steel dead load, calculated as the fully cambered girder profiles minus the steel dead load deflections.
Total Dead Load Fit (TDLF)	Final Fit	The cross-frames are detailed to fit to the girders in their ideally plumb as-deflected positions under the bridge total dead load.	The fabricator (detailer) sets the drops using the girder vertical elevations at total dead load, which are equal to the fully cambered girder profiles minus the total dead load deflections.

The FDOT Structures Design Guidelines Section 5.1 mandate the use of SDLF. No Load Fit (NLF) and Steel Dead Load Fit (SDLF) may be used where appropriate (NLF can be acceptable when the bearings are at a small skew angle; however, NLF detailing leads to girder layovers at end bearings that are larger than they really should need to be when

the end bearing line is skewed (NSBA 2016).) Total Dead Load Fit (TDLF) is not permitted by FDOT without Structures Design Office (SDO) approval.

NCHRP 20-07/Task 355 (White et al. 2015) report that in straight skewed bridges, SDLF using Line Girder Analysis (LGA) cambers results theoretically in zero cross-frame forces, zero flange lateral bending stresses and perfectly plumb girders in the SDL condition. Similarly, TDLF using LGA cambers results theoretically in zero cross-frame forces, zero flange lateral bending stresses and perfectly plumb girders in the TDL condition. This is based on the idealization that the deck forms and the bridge deck in the early condition during concrete placement do not provide any interconnection between the girders in resisting TDL, i.e., the concrete deck is assumed to not have any setup that would resist the girder displacements under subsequent concrete placement. The above behavior for SDLF and TDLF is the same regardless of whether the bridge has parallel or non-parallel skew of its bearing lines.

White et al. (2015) further report that, for straight skewed bridges, theoretically the most accurate girder cambers, which should be fabricated into the girders to achieve the targeted elevations under the TDL (when the cross-frames are detailed based on the LGA cambers), are:

- For TDLF, the negative of the girder TDL vertical deflections obtained from the LGA.
- For SDLF, the negative of the girder SDL vertical deflections obtained from the LGA plus the negative of the Concrete Dead Load (CDL) vertical deflections obtained from a NLF 3D Refined Analysis (RA). This solution considers the fact that the behavior of the bridge subjected to the steel dead load, where the SDLF detailing effects offset the SDL twist rotations of the girders, is different than the behavior of the bridge for the CDL, where the bridge deflects as a three-

dimensional system in resisting the weight of the concrete. For SDLF using the theoretical girder elevations obtained by subtracting the LGA steel dead load deflections from the above cambers, the girders will be theoretically plumb and the cross-frame forces will be theoretically zero under the steel dead load.

It is important to include the lack-of-fit effects associated with the fit condition in refined analysis to obtain accurate cross-frame forces (White et al. 20115, Azizinamini et al. 2014b). That is, for SDLF or TDLF detailing, the cross-frames do not fit to the girders in their initial cambered no-load geometry, and this lack-of-fit in the initial no-load condition has a significant impact on the bridge internal forces. Azizinamini (2014b) achieves this in ANSYS (ANSYS 2019) by using the "Element Birth and Death" feature of this software. For SDLF, the cross-frames can be modeled as inactive until the erection of steel and this is achieved by using the "Death" command. After girder erection, the unstressed cross-frames can be incorporated into the subsequent 3D refined analysis model, at the current deformed configuration of the structure, using the "Birth" command.

SDLF can be simulated in CSiBridge (Computers and Structures 2018) using its staged construction capabilities and appropriate stiffness modifiers. A very small number such as 1E-20 is used to make the cross-frames conceptually inactive during the stage involving application of the steel dead load. This stage consists of the steel girders and the cross-frames deflecting under their self-weight. At this stage in the analysis, it is essential to ensure lateral stability of the girders. The easiest way to ensure this is to support the girders laterally using fictitious supports. The subsequent stage of the analysis includes activating the cross-frames in the deflected configuration of the girders, by resetting the cross-frame members to their actual stiffness, and applying the wet concrete loads to the noncomposite bridge structure composed of the girders and cross-frames.

NCHRP 20-07/Task 355 (White et al. 2015) uses initial strains to simulate lack-of-fit effects in refined analysis. The initial strains are calculated based on a position vector analysis between the initial locations of the connection workpoints in the initial no-load geometry of the girders and the final position of the connection workpoints in the targeted dead load condition. The corresponding strains associated with the deflections between these configurations can be inserted as temperature loads in the FEA model if the software does not directly allow for insertion of initial strains from this lack-of-fit in the targeted girder geometry. This type of approach is recommended to address the lack-of-fit effects in curved bridges. This is because curved bridge girders are often not stable, or would deflect excessively if the cross-frame systems are theoretically removed. RA cambers (i.e., cambers calculated entirely from refined analysis of the connected three-dimensional bridge structural system) are recommended for the position vector analysis since it becomes difficult to use LGA for such bridges to determine the deflection profiles (White et al. 2015). Additionally, RA better accommodates the consideration of staged concrete deck placement, its influence on the CDL deflections and the resulting appropriate cambers. White et al. (2015) discusses these aspects in detail.

Both of the above approaches can be useful, depending on the context and depending on the capabilities of the software system being employed for the structural analysis.

2.5. Distribution of Girder Dead and Live Loads for Line Girder Analysis

The accuracy of line girder analysis is influenced directly by the assumed distribution of the loads from the physical three-dimensional structural system to the individual girders. The following sections discuss common assumptions for the distribution of the dead loads, and calculations for the distribution of the live loads.

2.5.1 Dead Loads

There are numerous approaches for distributing dead loads to bridge girders for a line girder analysis. The following is a sample of recommendations:

- In steel bridges, the action of the cross-frames tends to distribute the weight of the wet concrete deck so that the girders deflect nearly equally on a straight bridge with right supports. As such, if all the girders are of equal or nearly equal stiffness, the deck weight will be carried nearly equally by all the girders via the restoring forces in the cross-frames. That is, although the loads applied directly to the girders from the formwork will be essentially based on the tributary width of the deck associated with each girder, the cross-frames (if they are essentially rigid compared to the girders) force the girders to deflect equally. Therefore, if the girders have equal stiffness, the restoring forces from the girders will be equal in resisting the loads. Shear forces are developed in the cross-frames that distribute the loads directly applied to the girders such that the internal forces are approximately the same in all the girders. AASHTO LRFD Article 4.6.2.2.1 (AASHTO 2017) recognizes this fact by stating that for multi-girder bridges satisfying certain conditions (constant deck width, parallel girders having approximately the same stiffness, and at least four girders in the bridge cross-section), the permanent loads "of and on the deck" may be distributed equally to each of the girders for approximate line-girder analyses. However, in the case of more significantly skewed steel-girder bridges, the precise distribution of the deck weight is rather complex and strictly can only be ascertained by refined analysis. An important question in the context of the present research is whether the skew effects in bridges with a skew index up to and slightly above 0.3 are sufficiently small such that the assumption of uniform distribution of the loads still works well. In addition, the commentary to Article 4.6.2.2.1 discusses recommended extensions for handling of live loads in bridges with

splayed girders. The implications are that the uniform distribution of dead loads also may be sufficient for these types of bridges, possibly within certain limits.

- As noted above, AASHTO LRFD Article 4.6.2.2.1 also indicates that for bridges satisfying the above stated conditions, permanent loads applied "on" the deck after the deck is made composite may also be distributed equally to each girder. The permanent loads applied to the composite deck can include the weight of parapets, barriers, sidewalks, wearing surface loads, utility loads, etc. It is apparent that the simple statement in AASHTO LRFD Article 4.6.2.2.1 will likely become invalid for some types of loadings, particularly concentrated loadings near the edges of the bridge deck. However, clearly if concentrated loads are small enough, the coarse approximation of distributing them uniformly to all the girders may be sufficient. Additional considerations for the application of composite dead loads to the bridge girders are discussed below.
- Heavier superimposed dead loads such as parapets, barriers, sidewalks or sound walls should not be distributed equally to all the girders for the analysis (NHI 2015). Engineering judgment should be applied in distributing these loads for approximate line-girder analyses. Usually the largest portion of the parapet load on an overhang is assigned to the fascia girder, or to the fascia girder and the first interior girder. In fact, in some cases, the exterior girder may receive more than the weight of a heavy parapet, sound wall, etc. on the extreme deck overhang due to cantilever effects, with resulting uplift of one or more interior girders. These superimposed dead loads are applied to the long-term composite section for the analysis to account in an approximate fashion for long-term creep effects. The Iowa DOT Bridge Design Manual (IOWA DOT 2018) recommends that the weight of deck (part of DC1 loads) shall be distributed to each girder assuming the slab between girders is simply supported and all of the deck weight from an overhang is distributed to the exterior girder.

- For wearing surface loads and deck overlays, the assumption of an equal distribution of the load to each girder for approximate line-girder analyses is reasonable and has been the customary practice.
- Regarding distribution of weight of railing and sidewalks (DC2) and a future wearing surface (DW), the Iowa DOT Bridge Design Manual (IOWA DOT 2018) recommends that for superstructures with roadway widths not greater than 44 feet, DC2 and DW be distributed equally to all girders. Further, it recommends that for superstructures with roadway widths greater than 44 feet, the future wearing surface shall be distributed equally to all girders. However, it indicates that each railing and raised sidewalk cast after the deck along the edge of the superstructure shall be distributed one-half to the exterior girder, one-quarter to the first interior girder, and one-quarter to the second interior girder.
- For the DC2 loads for very wide bridges (total width > 70 ft), the Georgia DOT Bridge Manual (GDOT, 2019) recommends distributing the sidewalk, barrier and parapet loads to the four exterior girders on each side, and the median loads to the girders under the median.

In a slightly more specific context, Sumner et al. (2006) developed an empirical method, using field testing and FEA predictions, to predict the noncomposite deflections in steel I-girder simply supported skewed bridges. The method involves an initial calculation of the girder deflections using tributary loads followed by the application of an empirical correction factor based on the bridge characteristics. X and K-type intermediate cross-frames without top chords were considered in the study. In addition, axial stiffness of the deck forms was considered in the studies. The interaction of these stiffnesses with the other bridge components provides a mechanism for lateral load transfer between girders.

2.5.2 Live Loads

Determining the value of the maximum moments and shears in girders due to live load is a three-dimensional problem. The load transfer from the concrete slab and cross-frames to the steel girders is quite complex, depending generally on numerous aspects. Distribution factors for live loads are used to estimate the live load effects on individual girders. AASHTO Articles 4.6.2.2.2 and 4.6.2.2.3 recommend various distribution factor equations to calculate the amount of live load felt or resisted by each girder in different types of bridge. The distribution factors account for the differences between interior and exterior girders, and simple and continuous spans (NHI, 2011). NCHRP Project 12-26 (Zokaie et al. 1991) explains the development of these equations in detail. These live load distribution factor equations are significantly more accurate, specifically less conservative, than the traditional *S*/5.5 rule on the wheel loads, etc. in the AASHTO Standard Specifications (AASHTO 2002).

It should be noted that the NCHRP 12-26 study (Zokaie et al. 1991) was carried out for bridges without cross-frames/diaphragms. Cross-frames/diaphragms effectively increase the moments in exterior girders and decrease the moments in interior girders, implying that cross-frames/diaphragms further tie the girders together and the girders and cross-frames act as a three-dimensional unit. The width and stiffness of concrete parapets was also often neglected. These parapets, when they act structurally, increase the load in the outer two girders due to the additional stiffness. The effect of bottom lateral bracing in steel I-girder bridges was not considered, and is not addressed by the live load distribution factors (LLDF) equations. To assure conservative results, the constants in the LLDF formulas were adjusted so that the ratio of the value computed using the approximate LLDF to the more accurate distribution factor obtained using 3D FEA methods would in most cases be greater than 1.0 (NHI 2015).

AASHTO LRFD Article 4.6.2.2.2d (AASHTO 2017) mandates that in steel beam-slab bridge cross-sections with cross-frames/diaphragms, the live load distribution factor for the exterior girder/beam/stringer is not to be taken to be less than that which would be obtained by assuming the cross-section deflects and rotates as a rigid cross-section. This additional requirement is needed since the live load distribution factors were developed without taking the effect of cross-frames into consideration. Therefore, the rigid cross section requirement ensures that this deficiency is addressed, albeit with some potential conservatism.

The equations for the live load distribution factor (LLDF) for beam-slab bridges from AASHTO 4.6.2.2, applicable to the AASHTO lane loads, are as follows:

For moment in interior girders for single-lane loading

$$g_{mint} = 0.06 + \left(\frac{S}{14'}\right)^{0.4}\left(\frac{S}{L}\right)^{0.3}\left(\frac{K_g}{Lt_s^{\,3}}\right)^{0.1} \tag{3}$$

For moment in interior girders for multi-lane loading

$$g_{mint} = 0.075 + \left(\frac{S}{9.5'}\right)^{0.6}\left(\frac{S}{L}\right)^{0.2}\left(\frac{K_g}{Lt_s^{\,3}}\right)^{0.1} \tag{4}$$

where K_g, L and t_s are written in consistent units in the last expression,

S = girder spacing $(3.5' \le S \le 16')$

L = span length $(20' \le L \le 200')$

$$K_g = n\left(I + Ae^2\right) \tag{5}$$

K_g = longitudinal stiffness parameter $(1000 \le K_g \le 7x10^6 in^4)$

n = modular ratio of girder material to slab material

I = girder moment of inertia, in^4

e = distance from centroid of girder to midpoint of slab, in

t_s = slab thickness $(4.4" \le t_s \le 12")$

For the moment in exterior girders, the distribution factor is calculated as

$$g_{mext} = g_{mint} e_m \tag{6}$$

$$e_m = 0.77 + \frac{d_e}{9.1'} \tag{7}$$

where,

d_e = distance from the center of the exterior girder to the edge of the exterior of the curb or traffic barrier in feet

A correction factor for moment to account for the effects of skewed supports can be written as:

$$f_m = 1 - c_{1m} \left(\tan \theta \right)^{1.5} \tag{6}$$

where

$$c_{1m} = 0.25\left(\frac{K_g}{Lt_s^3}\right)^{0.25}\left(\frac{S}{L}\right)^{0.5} \quad (7)$$

with K_g, L, and t_s written in consistent units within the first expression, applicable when the difference between skew angles of two adjacent lines of supports does not exceed 10 degrees, and where c_{1m} is taken equal to zero if θ is less than 30°, and θ is taken as 60° when θ > 60°.

The following are salient features pertaining to the application of these equations:

1. Moment LLDF for interior girders
    a) Use of the span length for which the moment is being calculated, for calculation of positive moments
    b) Use of the average of the adjacent span lengths, for calculation of negative moments.
    c) Use of the maximum S at 2/3 of the span length, for simple-span bridges with unequal girder spacing and/or splayed girders.
    d) For fatigue LLDF, dividing the empirical LLDF from Eq. (3) by 1.2 to remove the multiple presence factor values.
    e) The AASHTO LRFD multiple presence factor values are included implicitly within the empirical formulas.
    f) The skew correction factor for moment is often not applied. It is not applied in this research.
2. Moment LLDF for exterior girders
    a) For two or more lanes, use of the interior LLDF equations with adjustment factor *e* from , using the spacing between the exterior and first interior girder at 2/3 of the span length (for splay).

b) Use of lever rule for one-lane, using spacing between the exterior and first interior girder at 2/3 of the span length (for splay). In this work, the one-lane live load distribution factor is used only for the fatigue live load calculations.

c) The LLDF is never to be taken smaller than value obtained from rigid cross-section analysis (RCA). However, the lever rule (multiplied by the multiple presence factor of 1.2) controls relative to RCA for one-lane cases. For multi-lean cases, the RCA LLDF for each number of lanes considered is multiplied by the corresponding multiple presence factor

d) For fatigue LLDF, no multiple presence factor is included in the calculation. In this case, the lever rule, without any multiple presence factor, governs relative to RCA in all situations.

e) The skew correction factor for moment is often not applied. It is not applied in this research.

For shear in interior girders for single lane loading,

$$g_{sint} = 0.36 + \left(\frac{S}{25'}\right) \tag{8}$$

For shear in interior girders for multi-lane loading,

$$g_{sint} = 0.2 + \left(\frac{S}{12'}\right) - \left(\frac{S}{35'}\right)^2 \tag{9}$$

and for shear in exterior girders

$$g_{sext} = g_{sint} e_s \tag{10}$$

$$e_s = 0.6 + \frac{d_e}{10'} \tag{11}$$

The correction factor for shear at obtuse corners of skewed bridges is given as:

$$f_s = 1 + c_{1s}\left(\tan\theta\right) \tag{12}$$

where

$$c_{1s} = 0.2\left(\frac{Lt_s}{K_g}\right)^{0.3} \tag{13}$$

where K_g, t_s and L are written in consistent units.

The following are salient features for the application of these equations:

1. Shear LLDF for interior girders
   a) Use of the span length for which the shear is being calculated, for calculation of shears.
   b) Use of the maximum S at 2/3 of the span length, for simple-span bridges with unequal girder spacing and/or splayed girders
   c) The AASHTO LRFD multiple presence factor values are included implicitly within the empirical formulas.
   d) To obtain the fatigue LLDF, the empirical LLDF is divided by 1.2 to remove the multiple presence factor.
   e) The skew correction factor may be applied conservatively throughout the length of the exterior girder and the interior girder adjacent to the obtuse corner. It is not applied to the other girders. More precisely, the skew correction factor may be

varied from its value at the bearings at and adjacent to the obtuse corner of the span to 1.0 at the mid-span of these girders, and taken as 1.0 for the remainder of the length of these girders.

2. Shear LLDF for exterior girders
    a) For one-lane loaded cases, the lever rule governs relative to RCA; the one-lane calculation is employed only for the fatigue live load calculations for all the bridges considered in this research.
    b) For two-lane loaded cases, the LLDF is calculated by the applying adjustment factor *e* to the interior LLDF, but is not allowed to be smaller than value obtained from rigid cross-section analysis (RCA)
    c) The AASHTO LRFD multiple presence factor values are included implicitly within the empirical formulas.
    d) For fatigue LLDF, there is no division by the multiple presence factor for the lever rule; the multiple presence factor is not included in these calculations.
    e) Application of the maximum calculated value at the girder end adjacent to the obtuse corner as skew correction throughout the length of the exterior girder and the interior girder adjacent to the obtuse corner

2.6. Deck Placement Considerations in Skewed Bridges

The most economical construction of steel bridges is unshored (NHI 2011). In this case, the bare steel structure consisting of I-girders and cross-frames have to resist their own weight and the weight of the wet concrete deck slab, deck forms and construction equipment. The deck becomes composite with the steel I-girders once the deck hardens. Depending on the length of the bridge, casting of the deck in stages may be required. If the deck is cast in stages, some portions of the deck becomes composite with the girder before other portions. As a result, the behavior of the bridge changes during staged deck casting. This aspect generally needs to be considered in analysis and design of a bridge. For

continuous span bridges, the deck in the positive moment regions is cast before the negative moment regions over the support in order to minimize cracking at the top of the slab as illustrated in Figure 13 for a parallel skew two-span continuous bridge (NHI 2011).

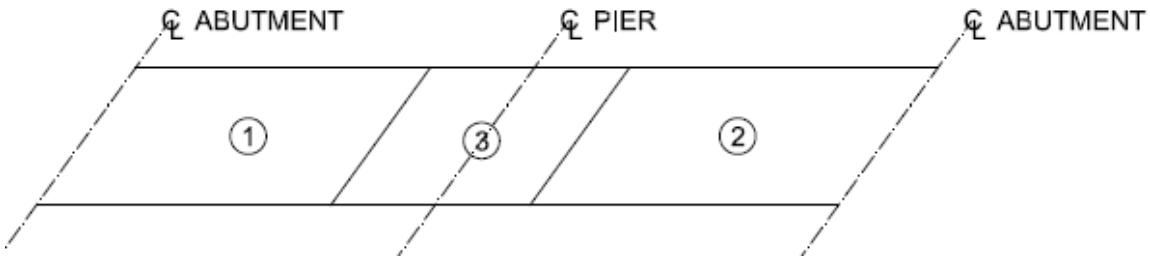

Figure 13. Typical sequence of casting concrete in decks for continuous-span bridges.

For skewed bridges, it becomes important to ensure deck placement is reasonably symmetrical laterally to minimize eccentric or unbalanced loading (NHI 2011). This reduces differential deflections between adjacent girders. It is preferable on skewed bridges where the differential deflection between girders are reasonably small to keep the finishing machine normal to the bridge as it reduces the length required for the machine. In bridges with significant skew, the bridge may twist due to differential deflections during casting due to differential loads on the girders due to the skew. Therefore, in cases with severe skews leading to large differential deflections, it may become necessary to consider skewing the finishing machine to avoid casting significantly more concrete than needed to meet the specified bridge minimum deck thickness or roadway elevations and achieve proper bridge geometry (NHI 2011). This is illustrated in Figure 14.

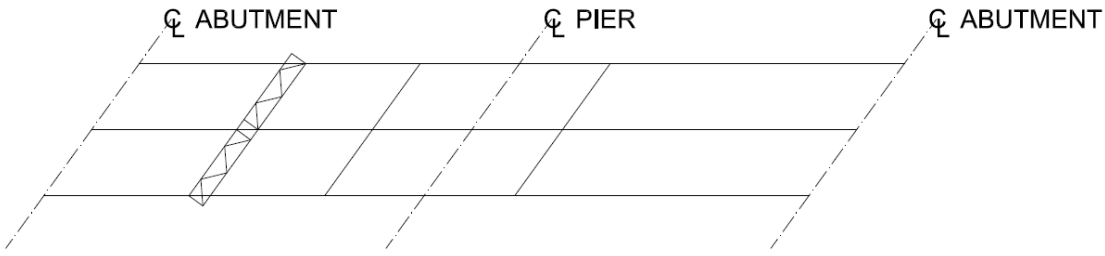

Figure 14. Orientation of screed machine for multi-span continuous bridges having parallel skew.

The twisting of girders due to differential vertical deflections is explained in Section 2.1. One of the sources of differential vertical deflections may be the inaccuracy in camber calculations using LGA vertical displacement estimates. This can potentially result in twist of girders when the cross-frames are erected, if the accuracy of the predictions is different on different girders. The differential vertical deflections may cause the finished deck thicknesses to be incorrect. This is shown in Figure 15, in which δ_{deck} indicates the loss of deck thickness due to the differential vertical deflections and the twist of the girders. Hence, accuracy of the camber calculations is important in ensuring deck placement within tolerances.

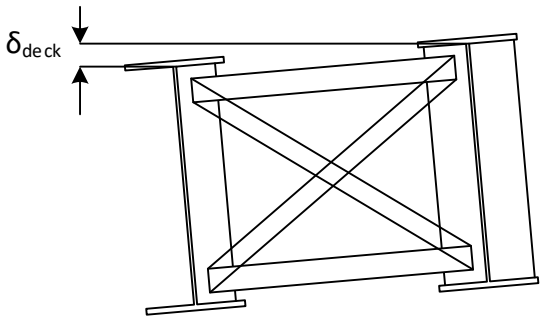

Figure 15. Loss of deck thickness due to twist of girders.

Another aspect to be considered in analysis is that the actual composite stiffness during deck placement depends on whether the concrete has hardened or not before the next pour. NHI (2011) indicates that the stiffness of previously cast portions of the concrete deck when computing deflections considering deck staging should be based on a modular ratio closer to the short-term modular ratio since the concrete does not have enough time to creep between casts.

FDOT Structures Design Guidelines Article 5.2 mandates the design of structures including consideration of the deck casting sequence. Camber diagrams are to be developed accounting for the casting sequence. A grid, 3-D or finite element analysis currently is

required by FDOT to determine girder deflections and required camber for bridges with skews greater than 20°.

2.7. State DOT Restrictions on LGA or Requirements for Refined Analysis

A number of states have specified explicit requirements regarding refined analysis for skewed bridges, or limits on the use of LGA. Sample requirements from a number of states are as follows:

1. Florida DOT (FDOT 2019a):
   a) Use a refined analysis method if the bridge skew index satisfies $0.2 < I_s \leq 0.6$.
   b) Use a 3D FEA is the bridge skew index, $I_s > 0.6$.
2. Pennsylvania DOT (PennDOT 2015):
   a) Simple and continuous-span straight steel girder bridges with skew index $I_s \geq 0.3$ require consideration of uplift potential at acute and obtuse corners by conducting a refined analysis.
   b) Steel structures with skew angles, $\theta \geq 20°$, require a special cross-frame design and the cross-frame members must be considered as main load carrying members.
   c) The design of bearings for bridges with skew angles, $\theta \geq 20°$, require consideration of out-of-plane rotations.
   d) PennDOT does not take advantage of the reduction in load distribution factors for moment due to skew effects.
3. Ohio DOT (ODOT, 2007b): When site conditions require the use of a superstructure type that exceeds the recommended limits set forth by AASHTO LRFD and/or this manual, a special design method may be required using a two-dimensional or three-dimensional model and some type of numerical analysis to solve the model. Examples of special design methods include grillage, finite element, finite strip and classical plate solutions.

CHAPTER 3. DEVELOPMENT OF BRIDGE MATRIX

This chapter documents the development of a matrix of bridges for the parametric study targeted in this research. Section 3.1 summarizes a preliminary data screening of Florida bridges. Section 3.2 identifies key variables that can influence the behavior of skewed bridges, and discusses the characteristics of 57 bridges sampled from the Florida DOT inventory. Section 3.3 identifies 20 bridges selected from this group for parametric study. The bridges selected for the parametric study address the most common geometries in Florida, and provide a broad representation of bridges having skew index up to and slightly larger than 0.3. The bridges with skew indices larger than 0.3 are expected to exhibit more substantial three-dimensional behavior, but are considered important in understanding the behavior of skewed bridges and investigating the potential boundaries of when line girder analysis (LGA) gives acceptable results.

The cross-frame layout heavily influences the structural behavior of skewed bridges via transverse load path effects. Hence, six of the above 20 selected bridges are studied using an alternative cross-frame arrangement that mitigates the transverse load path effects. Section 3.3 summarizes the design of the alternative cross-frame arrangements and also explains the order in which the 26 bridges are studied. Lastly, this section explains the selection of several bridges studied to investigate the impact of staged deck placement.

3.1. Preliminary Screening of Bridges by FDOT

The parametric study plans were initiated by identification of 255 steel I-girder bridges by Florida DOT from their inventory. Of these bridges, 145 qualified as skewed bridges. Out of these 145, 33 bridges were eliminated since they were either curved structures or

bridge plans were not available. Of the remaining bridges, 40% were simple-span bridges, 35% were two-span continuous bridges and the remaining 25% were either three or four-span continuous bridges. As described in Chapter 1, the focus of this research is on bridges that have a skew index up to and slightly exceeding 0.3. However, it is also prudent to study a limited number of bridges with more extreme skew to provide some testing of implications of exceeding the targeted range of skew indices. Therefore, to this end, a total of 51 bridges (23 simple-span, 24 two-span continuous, two three-span continuous bridges and two four-span continuous bridges) were selected with skew indices between 0.05 to 0.4, and an additional six bridges (three simple-span and three two-span continuous) were selected as outliers having a skew index of less than 0.05 (three bridges) or greater than 0.4 (three bridges). Therefore, the total number of bridges for further consideration was 57. These 57 bridges include two bridges (one three-span unit and another two-span unit), which were designed in the early 90s when software tools were not as advanced. These bridges were intended to provide basic sanity checks of the modern design calculations. These 57 bridges are a larger representative set of Florida DOT bridges, from which 20 were selected for the parametric study.

3.2. Data Analysis of 57 Representative Florida DOT Bridges

Based on the literature review in Chapter 2, and also recognizing the fact that design specifications are constantly updated to represent the state-of-the-art, the following variables are identified as the most pertinent for developing a Bridge Inventory Matrix:

1. Date of design
2. Applicable specifications, for the Design of Bridge

3. Bridge articulation (simple-span or continuous)
4. Span lengths (measured along the centerline of the deck)
5. Bridge framing width (between fascia girders)
6. Number of girders
7. Maximum spacing between girders
8. Minimum spacing between girders
9. Support skew angles
10. Support skew indices
11. Cross-frame layout (contiguous or staggered)
12. Cross-frame type (X, K, w/ or w/o top chord, etc.)
13. Specialized cross-frame geometry (e.g., partial or full lean-on cross-frame layout)
14. Maximum cross-frame spacing
15. Minimum cross-frame spacing
16. Averaged cross-frame spacing
17. Cross-frame fit detailing
18. Type of deck forms
19. Deck thickness
20. Deck concrete strength
21. Number of stages of deck placement
22. The ratio of maximum girder spacing to deck thickness
23. Girder span-to-depth ratio
24. Type of bearings

The characteristics of the 57 bridges sampled by FDOT are summarized below. Given the focus of this research, the most important variables are considered to be the bridge articulation (simple or continuous span construction), the skew index, the skew angles of the bearing lines, and the cross-frame type and layout. Table 2 summarizes the bridge articulation for these structures, that is, whether the bridge units are simple span or continuous span, and the number of spans for the continuous-span bridges.

Table 2. Bridge articulation.

Bridge Articulation	Number of Bridges
Simple-Span	26
Two-Span Continuous	27
Three-Span Continuous	2
Four-Span Continuous	2

Tables 3 to 6 list the skew angles, skew indices, span lengths and framing widths between the fascia girders for each of the above four sets of bridges, organized based on the bridge articulation. Tables 7 through 10 show, for each bridge articulation, the position of each of the bridges within a matrix composed of five ranges of the skew index, I_s, for the columns and three ranges of skew angle, θ, for the rows. The footnotes to the cells in these tables summarize noteworthy characteristics of the cross-frame framing arrangements for a number of the bridges. Additional summary tables of various other bridge parameters are presented in Appendix 1.

Table 3. Geometric properties of simple-span bridges.

	Skew Angle at supports		Skew Index at supports		Span	Framing
Identifier	Left	Right	Left	Right	Length (ft)	Width (ft)
F1	-41.5	-41.5	0.276	0.276	202	63.0
F2	-30.0	-30.0	0.062	0.062	195	21.0
F3	-35.9	-35.9	0.185	0.185	202	51.7
F4	-39.7	-39.7	0.202	0.202	212	51.7
F5	-16.5	-16.5	0.108	0.108	202	73.5
F6	21.3	21.3	0.098	0.098	191	48.0
F7	21.3	21.3	0.098	0.098	191	48.0
F8	42.0	42.0	0.183	0.183	165	33.5
F9	11.2	11.2	0.137	0.137	165	114.6
F10	-16.2	-16.2	0.154	0.154	241	128.1
F11	42.1	42.1	0.189	0.189	172	36.0
F12	-8.0	-8.0	0.027	0.027	174	33.8
F13	-29.4	-29.4	0.422	0.422	144	108.3
F14	-15.9	-15.9	0.084	0.084	183	54.0
F15	-20.6	-20.6	0.050	0.050	175	23.2
F16	-18.0	-19.0	0.064	0.068	172	34.0
F17	-43.9	-42.9	0.159	0.154	218	36.0
F18	-36.8	-36.8	0.138	0.138	195	36.0
F19	23.7	23.7	0.124	0.124	198	55.8
F20	23.7	23.7	0.149	0.149	198	66.9
F21	-43.7	-43.7	0.133	0.133	243	33.9
F22	-43.7	-43.7	0.177	0.177	243	45.1
F23	35.5	35.5	0.334	0.334	96	45.1
F24*	52.2	52.2	0.364	0.448	190	55.5, 66.2
F25	-49.4	-49.4	0.462	0.462	208	82.5
F26	7.0	7.0	0.034	0.034	172	48.0

* This is a splayed girder bridge; the widths at each end are reported

Table 4. Geometric properties of two-span continuous bridges.

	Skew Angle at supports*		Skew Index at supports		Span	Framing
Identifier	Left	Right	Left	Right	Length (ft)*	Width (ft)
F27	-36.1	-32.1	0.299	0.258	208.1	85.5
F28	52.9	54.3	0.190	0.200	250.5	36.0
F29	-25.6	-25.6	0.110	0.110	175.9	40.3
F30	-50.3	-50.3	0.281	0.281	250.2	58.3
F31	-50.2	-50.2	0.246	0.246	248.2	51.0
F32	-50.7	-50.7	0.372	0.372	251.8	76.6
F33	-23.4	-23.4	0.274	0.274	147.7	93.3
F34	-17.5	-17.5	0.076	0.076	166.7	40.3
F35	26.0	26.0	0.242	0.242	168.9	83.9
F36	-8.5	-8.5	0.028	0.028	128.8	24.0
F37	-9.0	-9.0	0.059	0.059	128.8	48.0
F38	-9.0	-9.0	0.054	0.054	128.8	44.0
F39	-35.9	-35.9	0.225	0.225	205.2	63.6
F40	-35.9	-35.9	0.187	0.187	205.2	52.9
F41	-17.5	-17.5	0.080	0.080	114.5	29.0
F42	52.7	52.7	0.372	0.372	169.8	48.3
F43	54.5	54.5	0.251	0.251	196.4	35.3
F44	57.2	57.2	0.460	0.460	160.0	47.5
F45	-23.0	-23.0	0.105	0.105	121.7	30.0
F46	-39.8	-39.8	0.184	0.184	216.5	48.0
F47	-38.9	-42.4	0.209	0.237	231.7	60.0
F48	-38.2	-38.2	0.386	0.386	185.2	91.0
F49	13.9	13.9	0.029	0.029	183.7	21.7
F50	15.1	15.1	0.144	0.144	171.8	91.9
F51	13.9	13.9	0.032	0.032	168.5	21.7
F52	-20.7	-20.7	0.345	0.345	115.8	106.0
F53	-10.0	-10.0	0.150	0.150	79.4	67.5

* The skew angles, skew indices at the supports, and the span lengths are reported for the span having the largest skew index

Table 5. Geometric properties of three-span continuous bridges.

	Skew Angle at supports*		Skew Index at supports		Span	Framing
Identifier	Left	Right	Left	Right	Length (ft)*	Width (ft)
F54	58.7	58.7	0.317	0.317	182.0	35.0
F55	-38.1	-38.1	0.258	0.258	184.8	61.0

* The skew angles, skew indices at the supports, and the span lengths are reported for the span having the largest skew index

Table 6. Geometric properties of four-span continuous bridges.

	Skew Angle at supports*		Skew Index at supports		Span	Framing
Identifier	Left	Right	Left	Right	Length (ft)*	Width (ft)
F56	0.0	50.1	0.000	0.233	184.5	36.0
F57	-53.4	-36.2	0.352	0.191	188.2	49.2

* The skew angles, skew indices at the supports, and the span lengths are reported for the span having the largest skew index

Table 7. Classification of simple-span bridges.

		Skew Index, I_s				
		<0.1	0.1-0.2	0.2-0.3	0.3-0.4	>0.4
Maximum Skew Angle, θ (degrees)	<20	F12, F14, F16, F26	F5, F9, *F10*[+]			
	20-30	F6, F7, F15,	F19, F20			*F13*
	30-60	F2	F3, F8, F11, F17, F18, F21, F22	*F1*, *F4**	*F23(S), F24*[&]	*F25*

[+]Cross-frames parallel to skew, *Staggered cross-frame arrangement, [@]Cross-frames framing into the bearing line, [&]Splayed girder bridge

Table 8. Classification of two-span continuous bridges.

		Skew Index, I_s				
		<0.1	0.1-0.2	0.2-0.3	0.3-0.4	>0.4
Maximum Skew Angle, θ (degrees)	<20	F34, F36, F37, F38, F41[+], F49, F51	F50, *F53*[+]			
	20-30		F29, F45[@]	*F33**, F35	*F52*	
	30-60		F28, F29, F39, F46	F30[@], F31[@], F40, *F43*[@], F47	*F27, F32*[@]*, F42, F48*	*F44*[@]

[+]Cross-frames parallel to skew, *Staggered cross-frame arrangement, [@]Cross-frames framing into the bearing line, [&]Splayed girder bridge

Table 9. Classification of three-span continuous bridges.

		Skew Index, I_s				
		<0.1	0.1-0.2	0.2-0.3	0.3-0.4	>0.4
Maximum Skew Angle, θ (degrees)	<20					
	20-30					
	30-60				F54, F55	

Table 10. Classification of four-span continuous bridges.

		Skew Index, I_s				
		<0.1	0.1-0.2	0.2-0.3	0.3-0.4	>0.4
Maximum Skew Angle, θ (degrees)	<20					
	20-30					
	30-60			F56	F57	

A thorough review of the drawings and attributes of the above 57 bridges leads to the following principal observations:

- The bridges have been designed in the early 2000s, and therefore the specifications followed for bridge design are also those of the late 90s and early 2000s.
- The deck width of the bridges varies from a minimum of 30 ft to a maximum of 135 ft.
- Eight bridges out of the 57 have been constructed in phases (deck placed in different phases transversely). These bridges have special design considerations for the cross-frames between girders at the location of the closure pours.
- Bridge F24 is a splayed girder bridge, and has a maximum total width of 64.1 ft.
- The skew angles of the bridge bearing lines vary from a minimum of 8° to a maximum of 58°. Skew angle is important in the consideration of local "skew" effects (e.g., layover at the end bearing lines), and is an important parameter in the development of bridge matrix as is discussed later. The two-span continuous bridge F27, three-span continuous bridge F54, two four-span continuous bridges F56 and F57 have nonparallel

skew at the ends and at intermediate supports. All the other bridges have parallel skew at the ends and at intermediate supports.

- The skew indices of the bridges vary from 0.03 to 0.47. Tables 3 through 6 show the maximum skew index identified at the bearings lines for all the bridges. The skew index is considered to be the principal parameter typically used for estimating potential nuisance stiffness effects associated with the development of a stiff transverse load path, and is considered to be the most important parameter in the development of bridge matrix. However, it is well known that the cross-frame framing arrangement is also a key factor in determining the magnitude of the skew effects.
- The span-to-depth ratios (span along the centerline of the bridge divided by the web depth) of the bridges varies from 19 to 40. (This data for each of the specific bridges is detailed in Appendix 1.) Most of the bridges have span-depth ratios between 25 and 35. Bridge F25 (simple span bridge) has a span-to-depth ratio of 40. Five additional bridges (all two-span continuous bridges) have a span-to-depth ratio greater than 35. Three bridges have a span-to-depth ratio less than 25.
- The cross-frame layout of all the bridges, with the exception of a few, is contiguous with intermediate cross-frames framing perpendicular to the girders. In bridges F10, F41 and F53, where the skew angle is less than 20°, the cross-frames are parallel to the skew. In bridges F3, F4 and F33 the cross-frames are staggered, although the stagger does not meet current recommendations in commentary of the AASHTO LRFD Specifications (AASHTO 2017). In Bridge F33, the cross-frames are staggered although the start-points of the cross-frames are aligned along the skew. As a result, the offsets of the intermediate cross-frames are relatively small and thus the cross-

frame behavior is closer to a contiguous layout than one with the recommended staggered layout.

- In continuous-span bridges F30, F31, F32, F43, F44 and F45, the cross-frames frame into the skewed bearing line at the bearings and at the pier locations, while the cross-frames or diaphragms are omitted along the skewed pier bearing line. This practice has been suggested as one option in NHI course guidance (NHI, 2011), but has been found in the NHI course guidance and in the NCHRP 20-07/355 (White et al., 2015) studies to not work as well as providing cross-frames along the skewed bearing line combined with offsetting of the cross-frames within the span from the bearing locations.
- The cross-frame detailing is NLF for Bridge F43, SDLF for Bridges F14, F21, F22, F24, F27, F43 and F47, and TDLF for all the other bridges. The requirement that "girder flanges and/or webs and/or stiffeners should be vertical after construction of bridge" was interpreted as Total Dead Load Fit.
- Stay-in-place metal deck forms have been used in all the bridges, in all cases where the detailed deck information is available. The specific characteristics of the deck forms was not available for five of the bridges.
- The deck thickness varies from 8 in to 9.5 in for the bridges considered. The deck concrete strength is a standard of 4.5 ksi, except in Bridge F34 where concrete of strength 5.5 ksi is used.
- Six bridges (all two-span continuous) bridges use pot bearings. All other bridges use elastomeric bearings.

3.3. Selection of Bridges for Further Study

For a skewed bridge, as the skew index of a bridge increases, the structural behavior tends to become more three dimensional due to the development of a stiff transverse path in the short diagonal direction. The stiff transverse path can be mitigated by varying the cross-frame layout as discussed in Section 2.3. Also, the local effects of skew (e.g., layover at abutment bearing lines) increase with higher skew angles. Therefore, it is rational to select bridges with a high skew index and skew angle and at the same time cover the gamut of cross-frame arrangements. Thus the bridges are categorized based on skew indices and maximum skew angles of the bridges in Tables 7 to 10.

Tables 7 and 8 show the categorization of the screened simple-span and two-span continuous bridges respectively, on the basis of skew index and skew angle. The bridges in the last two columns of Tables 7 and 8, which are italicized, are recommended for the research study (total of nine), since skew is expected to significantly affect the structural behavior of these bridges. Bridge F1 is representative of the most common skew bridges in Florida. Hence, Bridge F1, italicized in Table 7, is recommended for the study. Apart from these bridges, four additional bridges are selected in which the cross-frame arrangements are not contiguous. These are underlined in the above tables. In addition to the above 16 bridges, all the three- and four-span continuous bridges listed in Tables 9 and 10 are selected for further study. Therefore, a total of 20 bridges were selected for further study.

In addition, the cross-frame arrangement for the bridges was varied according to recommendations in AASHTO LRFD 8th edition (AASHTO 2017) and NCHRP 20-

07/355 (White et al. 2015) as discussed in the Section 2.3 considering the following key considerations:

- Stagger the cross-frames within the spans.
- Avoid framing cross-frames into bearing locations.
- Frame cross-frames/diaphragms along the bearing line at pier supports, and offset intermediate cross-frames relative to the bearing line.
- For continuous-span bridges, provide diaphragms/cross-frames along the bearing lines with no intermediate cross-frames framing into the bearing line.

Revising the cross-frame arrangements in this way should significantly relieve stiff "nuisance" load paths in the transverse direction, and maximize the applicability of line girder analysis. By having two sets of bridges for selected critical bridges, one with a cross-frame layout that tends to cause larger transverse load path effects and one with cross-frame layout that tends to relieve these effects to the maximum extent possible, the project should be able to provide guidance for what is inferred to be current FDOT practices, as well as gains that could be achieved if FDOT were to adopt practices that are more in the direction of the recommendations in the AASHTO LRFD Specifications. Hence, the six bridges F24, F25, F44, F48, F56 and F57 were studied with an alternate cross-frame arrangement. Thus, a total of 26 bridges were selected for the parametric studies. The characteristics of and the overall plan framing arrangement for these 26 bridges are shown in Figures 16 to 41. Plan sketches of the other 31 bridges not selected from the set of the 57 bridges sampled by FDOT are shown in Appendix 2.

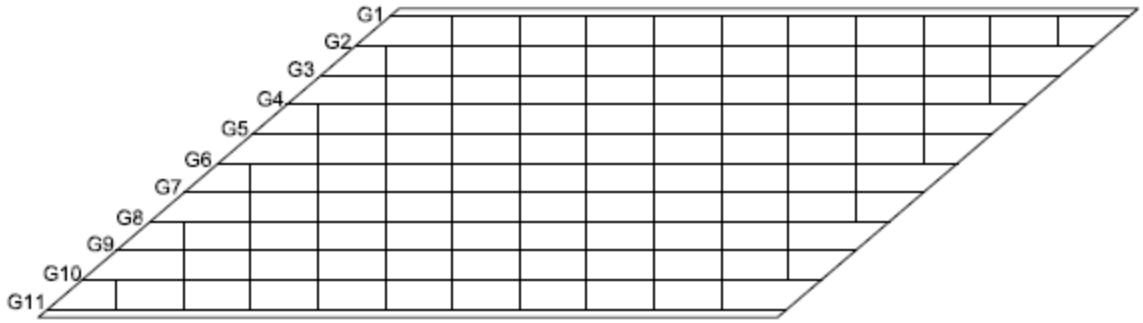

Figure 16. Bridge 1 (F25) (L_s = 208 ft; w_g = 82.5 ft; θ = 49.4°, 49.4°; I_s = 0.46).

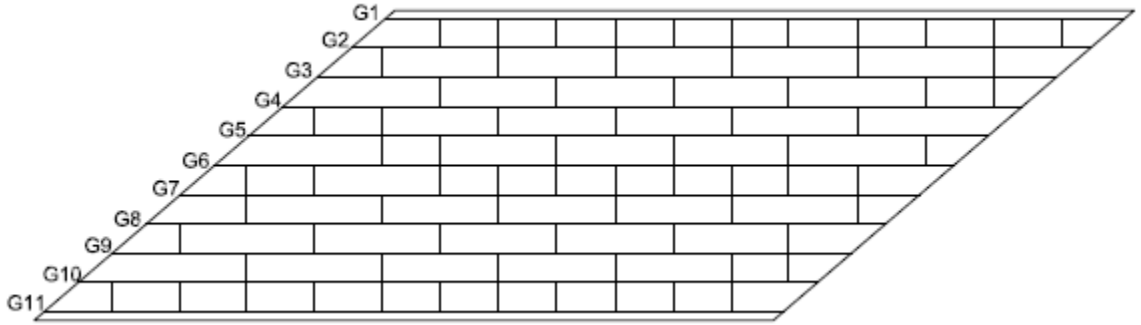

Figure 17. Bridge 2 (F25 Alt) (L_s = 208 ft; w_g = 82.5 ft; θ = 49.4°, 49.4°; I_s = 0.46).

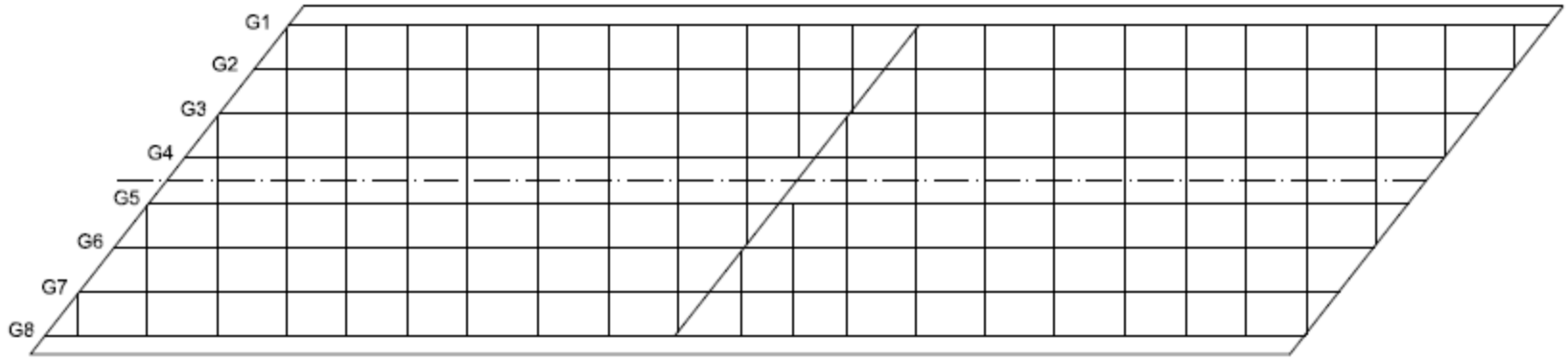

Figure 18. Bridge 3 (F48) (L_s = 185 ft, 185 ft; w_g = 91 ft; θ = 38.2°, 38.2, 38.2°; I_s = 0.39).

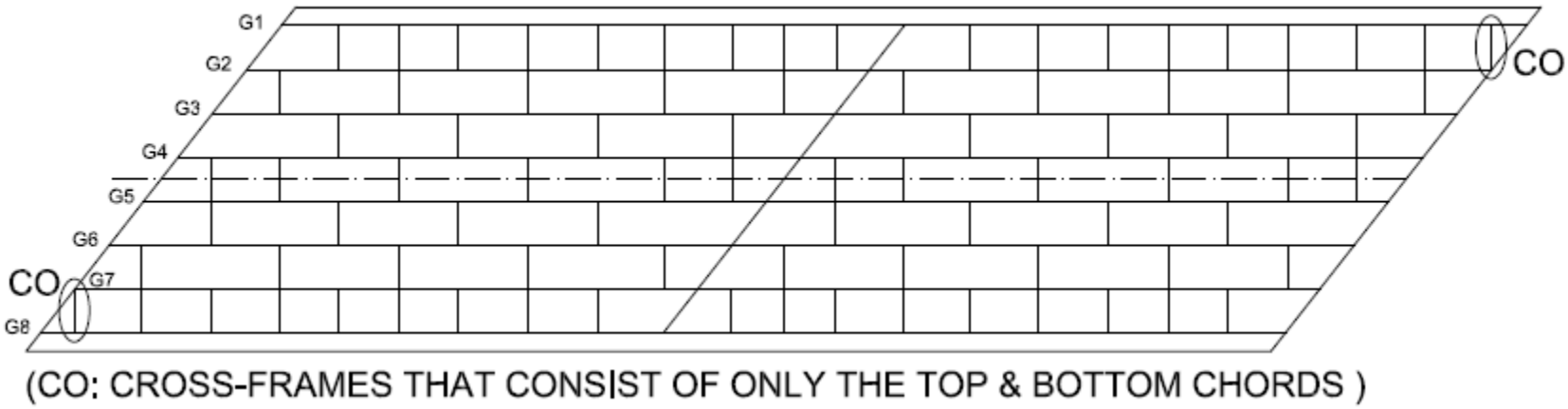

Figure 19. Bridge 4 (F48 Alt) (L_s = 185 ft, 185 ft ; w_g = 91 ft; θ= 38.2°, 38.2, 38.2°; I_s = 0.39).

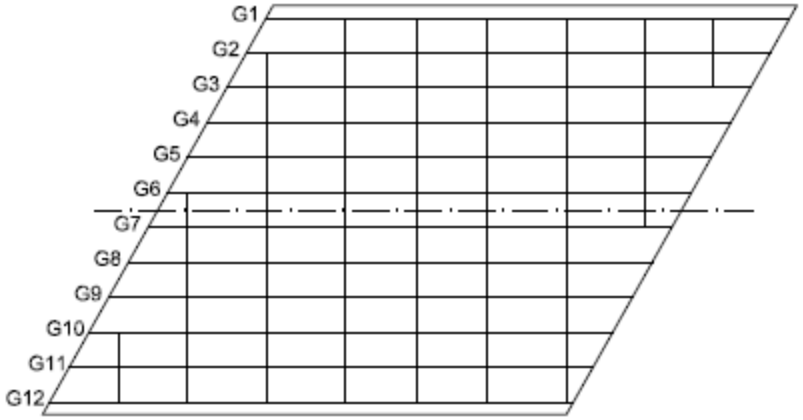

Figure 20. Bridge 5 (F13) (L_s = 144 ft; w_g = 108 ft; θ = 29.4°, 29.4°; I_s = 0.42).

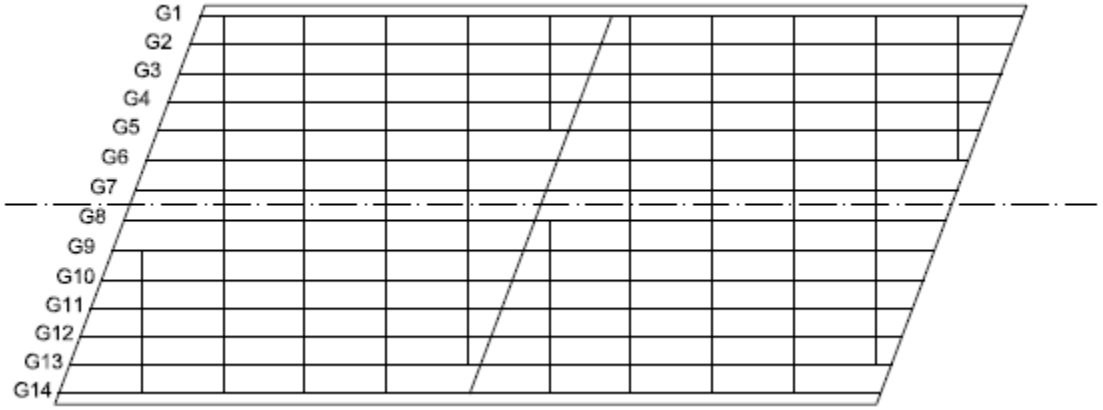

Figure 21. Bridge 6 (F52) (L_s = 116 ft, 116 ft; w_g = 106 ft; θ = 20.7°, 20.7°, 20.7°; I_s = 0.35).

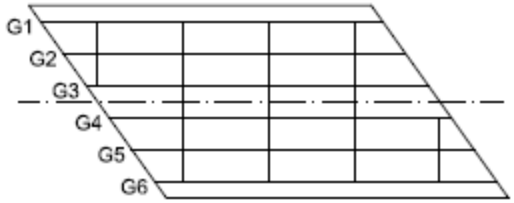

Figure 22. Bridge 7 (F23) (L_s = 96 ft; w_g = 45.1 ft; θ = 35.5°; I_s = 0.33).

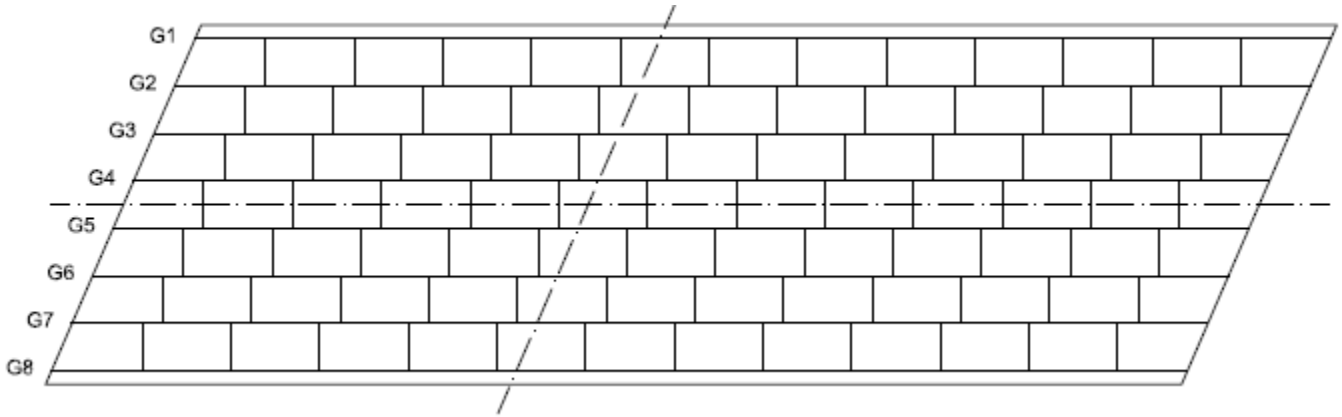

Figure 23. Bridge 8 (F33) (L_s = 148 ft, 173 ft; w_g = 93.3 ft; θ = 23.4°, 23.4°, 23.4°; I_s = 0.27).

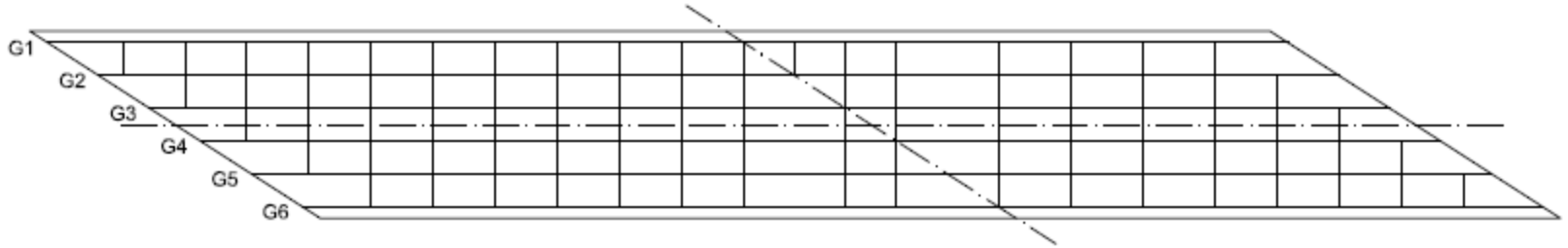

Figure 24. Bridge 9 (F44) (L_s = 202 ft, 158 ft; w_g = 57.5 ft; θ = 57.2°, 57.2°, 57.2°; I_s = 0.47).

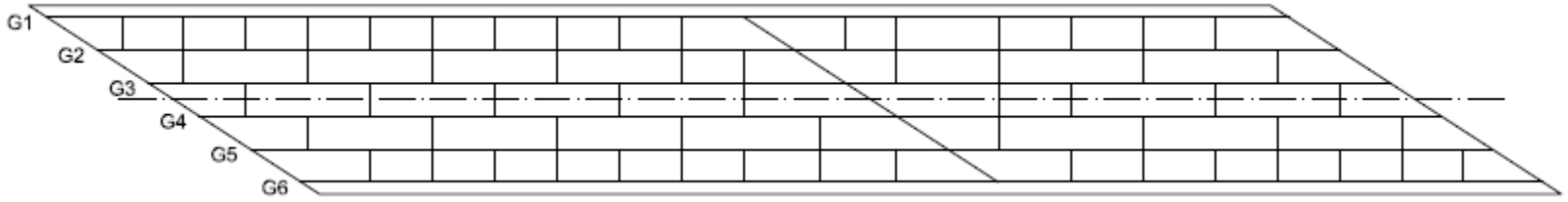

Figure 25. Bridge 10 (F44 Alt) (L_s = 202 ft, 158 ft; w_g = 57.5 ft; θ = 57.2°, 57.2°, 57.2°; I_s = 0.47).

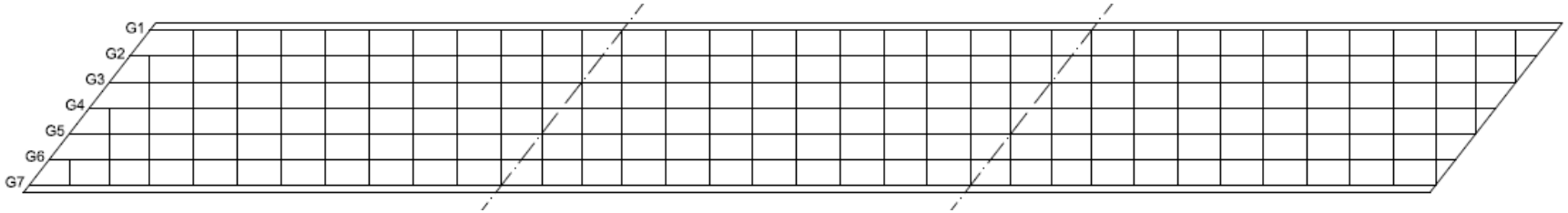

Figure 26. Bridge 11 (F55) (L_s = 188 ft, 186 ft, 185 ft; w_g = 61 ft; θ= 38.1°, 38.1°, 38.1°, 38.1°; I_s=0.26).

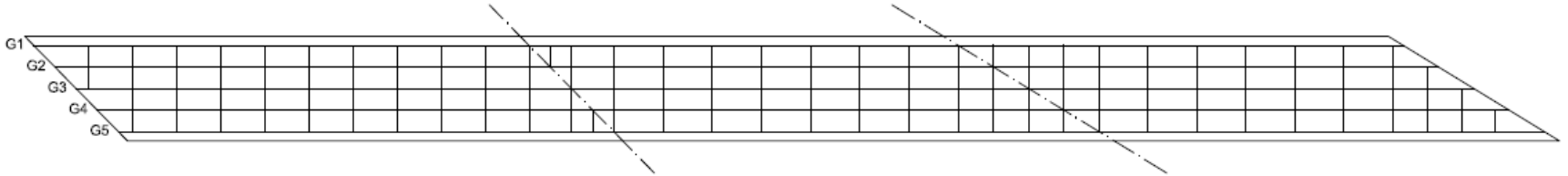

Figure 27. Bridge 12 (F54) (L_s = 202 ft, 187 ft, 182 ft; w_g = 35 ft; θ = 44.7°, 44.7°, 58.7°, 58.7°; I_s = 0.32).

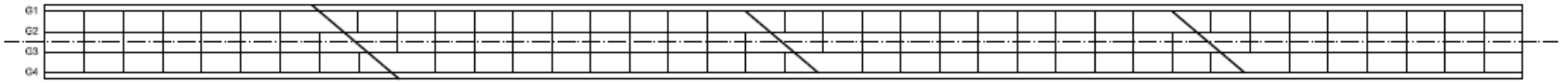

Figure 28. Bridge 13 (F56) (L_s = 185 ft, 253 ft, 253 ft, 186 ft; w_g = 36 ft; θ= 0°, 50.1°, 50.1°, 50.1°, 0°; I_s = 0.23).

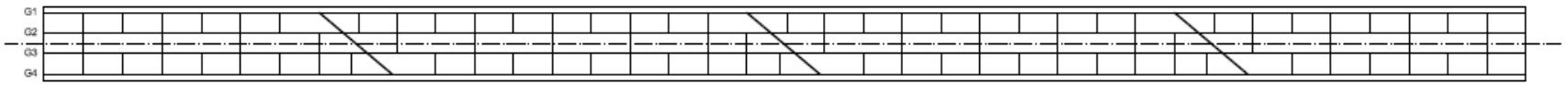

Figure 29. Bridge 14 (F56 Alt) (L_s = 185 ft, 253 ft, 253 ft, 186 ft; w_g = 36 ft; θ = 0°, 50.1°, 50.1°, 50.1°, 0°; I_s = 0.23).

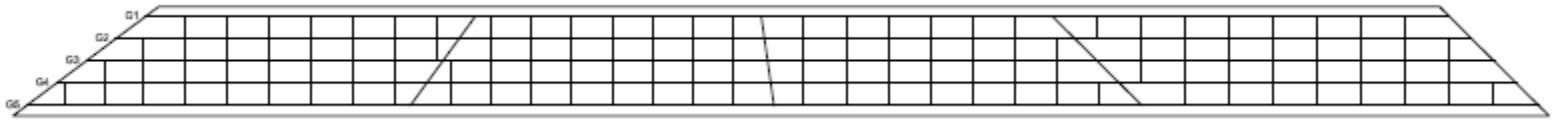

Figure 30. Bridge 15 (F57) (L_s = 188 ft, 156 ft, 159 ft, 226 ft; w_g = 49.2 ft; θ = 53.4°, 36.2°, 8°, 45.3°, 45.3°; I_s = 0.32).

Figure 31. Bridge 16 (F57 Alt) (L_s = 188 ft, 156 ft, 159 ft, 226 ft; w_g = 49.2 ft; θ = 53.4°, 36.2°, 8°, 45.3°, 45.3°; I_s = 0.32).

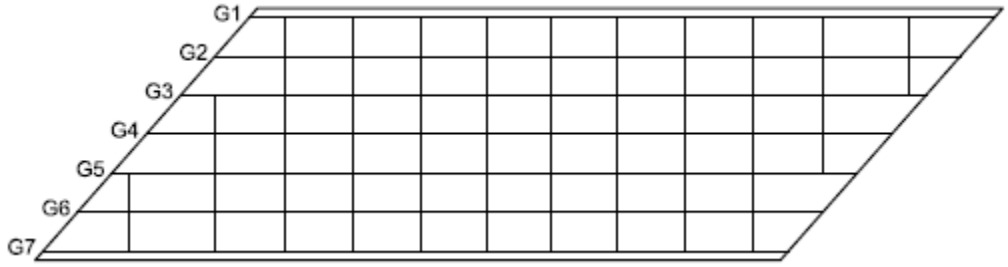

Figure 32. Bridge 17 (F1) (L_s = 202 ft; w_g = 63 ft; θ= 41.5°, 41.5°; I_s = 0.28).

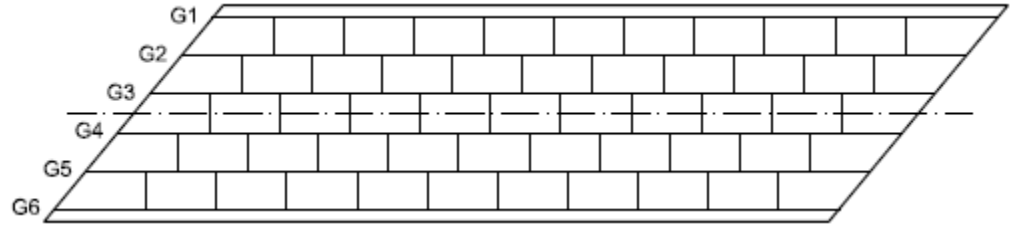

Figure 33. Bridge 18 (F4) (L_s = 212 ft; w_g = 51.7 ft; θ = 39.7°, 39.7°; I_s = 0.2).

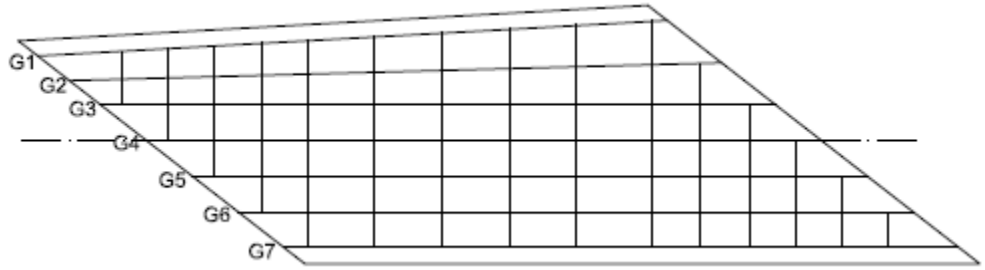

Figure 34. Bridge 19 (F24) (L_s = 196 ft; w_g = 66.2 ft; θ = 52.2°, 52.2°; I_s = 0.45).

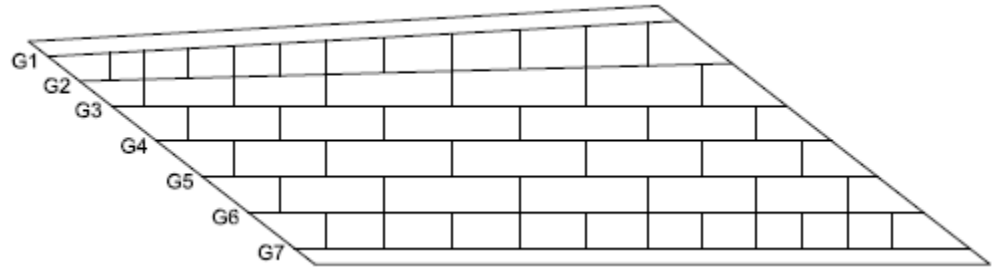

Figure 35. Bridge 20 (F24 Alt) (L_s = 196 ft; w_g = 66.2 ft; θ = 52.2°, 52.2°; I_s = 0.45).

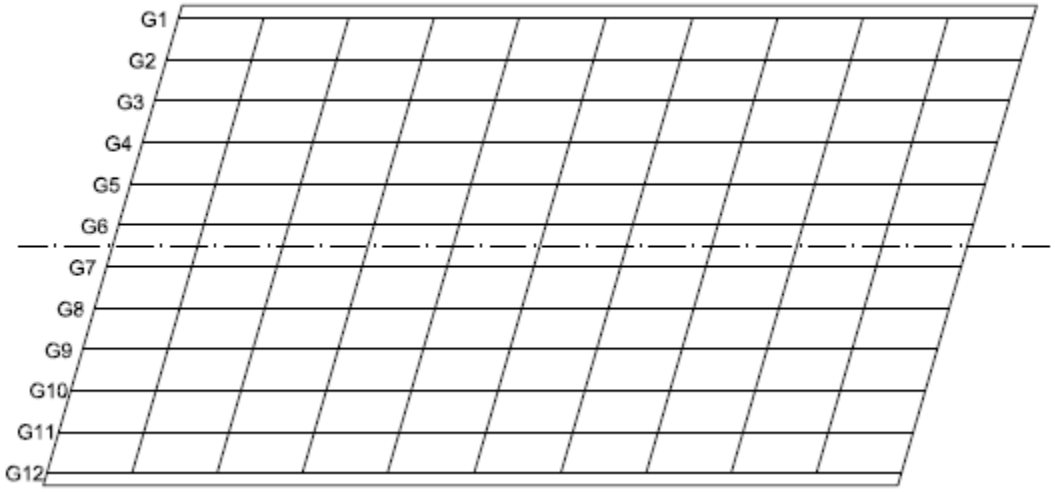

Figure 36. Bridge 21 (F10) (L_s = 241 ft; w_g = 128 ft; θ = 16.2°, 16.2°; I_s = 0.15).

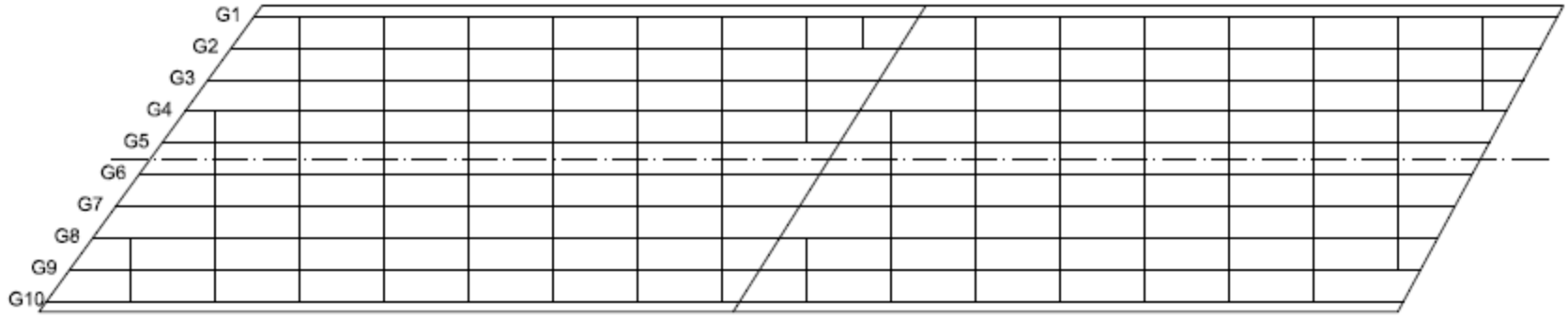

Figure 37. Bridge 22 (F27) (L_s = 204 ft, 195 ft; w_g = 85.5 ft; θ= 36.1°, 32.1°, 28.4°; I_s = 0.31).

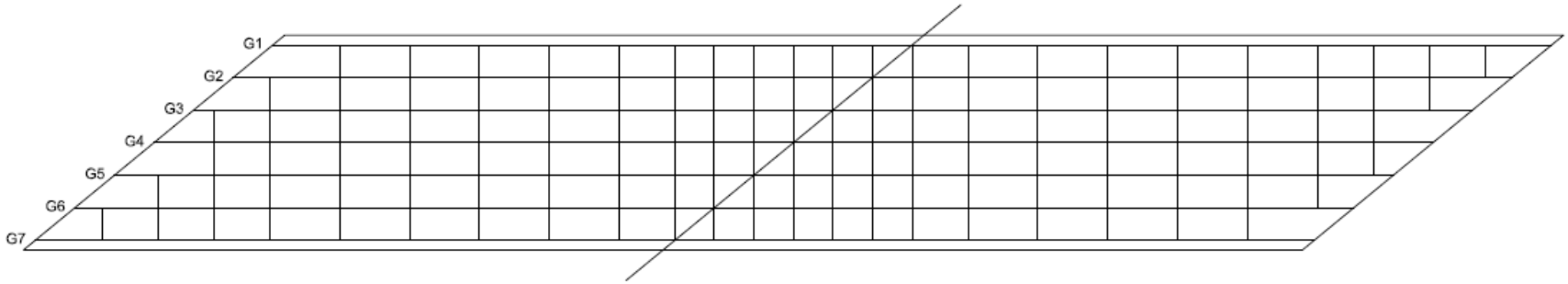

Figure 38. Bridge 23 (F32) (L_s = 202 ft, 158 ft; w_g = 57.5 ft; θ= 57.2°, 57.2°; I_s = 0.47).

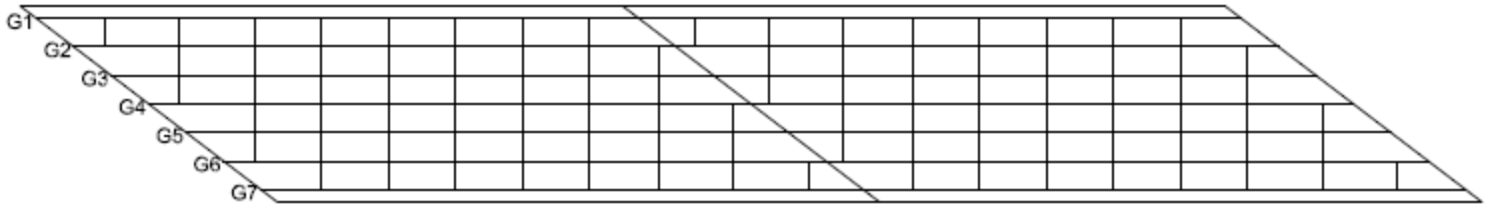

Figure 39. Bridge 24 (F42) (L_s = 170 ft, 170 ft; w_g = 48.3 ft; θ = 52.7°, 52.7°, 52.7°; I_s = 0.37).

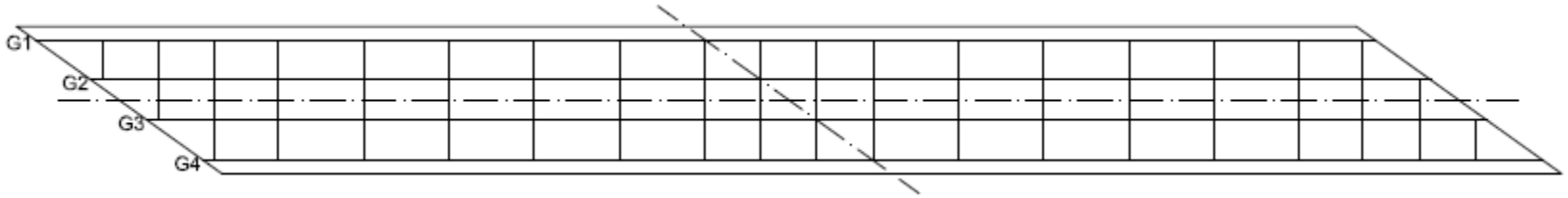

Figure 40. Bridge 25 (F43) (L_s = 196 ft, 196 ft; w_g = 35.3 ft; θ = 54.5°, 54.5°; I_s = 0.25).

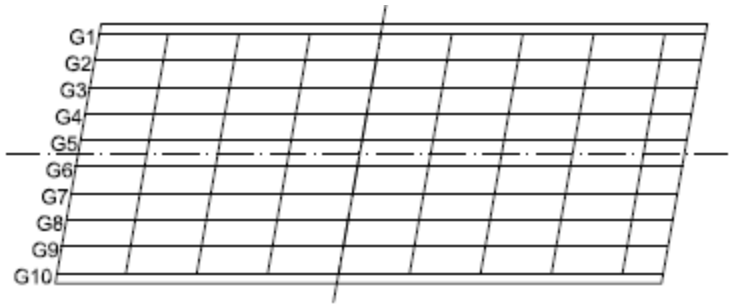

Figure 41. Bridge 26 (F53) (L_s = 79.4 ft, 92 ft; w_g = 67.5 ft; θ = 10°, 10°; I_s = 0.15).

Bridges F24, F25, F44 and F48 are parallel skew bridges. The modifications for these bridges included adding bearing-line cross-frames at the piers (in bridges which do not have bearing-line cross-frames, offsetting the intermediate cross-frames). The alternate cross-frame arrangements are shown in Figures 17, 19, 25 and 35. In addition, the intermediate cross-frames were staggered to soften the stiff transverse path that develops between the two obtuse corners of the spans. Bridges F56 and F57 are non-parallel skew bridges. The modifications for these bridges included staggering of intermediate cross-frames by positioning their work points in a "fanned" pattern between the skew angles at the ends of the span. The alternate cross-frame arrangements are shown in Figures 29 and 31.

In general, the bridges that were apt to cause the most difficulty were analyzed first, e.g., the bridges were studied in the order of decreasing skew indices and skew angles. These results were used to refine our focus in the study of other bridges. Therefore, findings about the behavior of the "difficult" bridges influenced each of the identification/number of additional bridges to be studied with modified cross-frame arrangements.

Furthermore, staged deck placement analysis was carried out for four bridges out of the 26 bridges, the two-span continuous bridges F48 and F48 with and alternative cross-frame arrangement, the three-span continuous bridge F55 and a four-span continuous bridge F57.

The 26 bridges were numbered 1 to 26 in the order they were studied. Figures 16 to 41 show the 26 bridges and provide a summary of its characteristics that include the skew angles at the bearing lines, span lengths, bridge framing width and the skew index. The bridge span lengths are denoted by L_s in the order of the spans, separated by commas. w_g

indicates the bridge framing width between the fascia girders The skew angle magnitudes (θ) are reported at each bearing line, beginning from the left end abutment and moving towards the right end of the bridge. The direction of skew can be identified from the plan sketch. The skew index, I_s, is calculated as the maximum value from Eq. 1 considering each bearing line and the adjacent span lengths.

As an example, consider Bridge 8 (Figure 23). This bridge is two-span continuous. The first and second spans of Bridge 8 have lengths of 148 and 173 ft. The bridge framing width is 93.3 ft. The skew angle magnitudes (23.4°) are reported at each bearing line, beginning from the left end abutment and moving towards the right end of the bridge. The direction of skew can be identified from the plan sketch. Considering a second example, the four-span continuous Bridge 15 (Figure 30) has five bearing lines, the skew angles of which are 53.4°, 36.2°, 8°, 45.3°, and 45.3° respectively. The first two of these bearing lines have a clockwise skew angle whereas the last three have a counterclockwise skew angle. This bridge has four spans with span lengths of 188, 156, 159 and 226 ft.

In summary, the selected bridges numbered according to the order of study and classified according to articulation are:

- Simple span bridges 1(F25), 2(F25 Alt), 5(F13), 7(F23), 17(F1), 18(F4), 19(F24), 20(F24 Alt), 21(F10) Two-span continuous bridges 3(F48), 4(F48 Alt), 6(F52), 8(F33), 9(F44), 10(F44 Alt), 22(F27), 23(F32), 24(F42), 25(F43), 26(F53)
- Three-span continuous bridges 11(F55), 12(F54)
- Four-span continuous bridge 13(F56), 14(F56 Alt), 15(F57), 16(F57 Alt)

CHAPTER 4. MODELING CONSIDERATIONS AND CALCULATION OF RESPONSES

In this research, the commercial software package CSiBridge (V21.0.2) was used for the 3D finite element analysis (3D FEA) and AISC/NSBA LRFD Simon (V10.3.0.0) software was used for the line girder analysis (LGA) of the bridges. The design of a parametric study includes numerous considerations related to definition of loads, creation and execution of the analysis models, and collection of responses. It is imperative that calculation of loads for LGA is consistent with the calculation of loads in 3D FEA. For example, the dead load reactions from the LGA models of the different girders ideally should sum to the total dead load reactions within the 3D FEA model. This chapter summarizes details regarding the modeling idealizations, calculation of loads and calculation of responses in CSiBridge and LRFD Simon. This is followed by an explanation of the procedures and processes developed for efficient execution of the parametric studies comparing LGA and 3D FEA for the suite of 26 bridges identified in Chapter 3.

4.1 Modeling Idealizations for 3D FEA and LGA

4.1.1 3D Finite Element Analysis

The following are key 3D FEA modeling idealizations employed in CSiBridge in the conduct of this research:

1. Frame and shell elements are used by CSiBridge in the modeling of various components of the bridge. “Mixed” frame and shell modeling of the girders is used,

where the web is modeled by shell elements and the flanges are modeled using frame elements. The connection plates are modeled using frame elements. Cross-frames are modeled using frame elements with moment releases at the ends. The deck is modelled using shell elements.

2. To account for the reduced axial stiffness of single angle members in cross-frames due to the eccentricity at end connections, a stiffness reduction factor of 0.65 is used. This is based on the recommendations in AASHTO LRFD Article C4.6.3.3.4.
3. Cross-frames along skewed bearing lines are often connected to the girder connection plates by means of a bent gusset plate. The bent gusset plate provides additional flexibility to the end bearing-line cross-frames that potentially can be beneficial in reducing the skew effects. The bent-plate connection flexibility is not included in the 3D FEA models developed in this research. It is assumed that the connection detail to the girders is such that any additional deformations occurring at the connections are negligible.
4. CSiBridge has the capability to analyze a bridge construction sequence using a staged construction load case. This capability is used to study the effects of staged deck placement in this research. In addition, in this work, a staged construction load case is employed for analyzing noncomposite and composite dead load, as well as for modeling Steel Dead Load Fit (SDLF) detailing effects. These modeling procedures are described in detail in Section 4.5.
5. Live load effects are calculated by CSiBridge using “floating lanes” that is explained in detail in Section 4.2.5.

6. Elastomeric bearings are employed in all the bridges studied in this research. A nominal stiffness of 100 kip/ft is used in the lateral and longitudinal directions. It is assumed that the lateral displacements at the elastomeric bearings are smaller than the tolerances necessary to engage with anchor bolts, guides or other restraining devices, and therefore the lateral displacements are restrained only by the lateral stiffness of the elastomeric bearing pads. As discussed in NHI (2011), rigid modeling of lateral restraint conditions the bearing locations commonly results in unrealistic large lateral forces that then must be equilibrated within the bridge system model.

4.1.2 Line Girder Analysis

Line girder analysis was set up based on the discussion in Section 2.5. Line girder analysis typically was carried out for exterior girder/s (see Section 4.4 for more details), the first interior girder and a "representative" central interior girder. In this project, LRFD Simon was used for line girder analysis of bridges. The following are the specifics of how the line girder analysis was conducted using LRFD Simon:

1. The aspects of calculation of dead loads are explained in Section 2.5.1. For all the bridges considered in these parametric studies, all the dead loads are distributed equally to all the girders.
2. Staged construction can be simulated in LRFD Simon using stage-wise partial uniformly distributed loads.
3. DC1, DC2 and DW loads are calculated for each girder as discussed in Section 4.2. LRFD Simon accepts the input of these loads as uniform loads.

4. Live load calculations are based on distribution factors calculated as per Section 2.5.2. However, the position of the HL-93 truck is based of influence line diagrams for both positive and negative moments. This is handled automatically in LRFD Simon.
5. LRFD Simon provides results for all the design and service load cases including the load case from the concrete deck placement. These can be readily used in the calculation of cambers.

4.2 Load Definitions and their Calculations in CSiBridge and LRFD Simon

This section explains the details pertaining to the definition of loads in CSiBridge and LRFD Simon to maintain consistency in 3D FEA and LGA such that the overall results from each of these two analysis types can be compared within a broader context.

The bridge analyses in the parametric studies have been conducted for the following seven specific load cases:

1a. Steel Dead Load (SDL/SDLF), including the influence of Steel Dead Load Fit (SDLF) effects,

1b. Steel Dead Load (SDL/NLF), not including the influence of Steel Dead Load Fit (SLDF) effects, i.e., based on No-Load Fit,

2a. Concrete Dead Load (CDL), neglecting any influence of prior setup of the concrete during deck placement, or due to staged deck placement or phased construction,

2b. Concrete Dead Load (CDL/SDP), considering the influence of staged deck placement (staged deck placement effects will be studied only for four bridges, as discussed in Section 3.3),

3. Barrier Rail Load (RL),

4. Future Wearing Surface and Utilities Load (DW),

5. Vehicular Live Load (LL),

6a. Live Load with a derived HL-93 vehicle that consists of 25% truck load and 100 % of the lane load (LL Simon),

6b. Live Load with a derived HL-93 vehicle that consists of only the truck load (LL Truck Only),

7. Fatigue Live Load (Fatigue LL).

All of these loadings were unfactored loads. This facilitated the assessment of how the straight skewed bridges considered respond under the different load types. The responses for a given AASHTO LRFD Load Combination was obtained by superimposing the results from the appropriate load cases. All of the analyses were material linear elastic and geometrically linear (i.e., first-order linear elastic) analyses, for which superposition is valid.

The first three load cases provide information about the bridge responses in their noncomposite (DC1) condition. The fourth load case illustrates the influence of staged deck placement. In the fourth case (Case 2b), the concrete deck stiffness for the portions of the

deck placed in previous stages is set to correspond to short-term composite loading (modular ratio of n) while the stiffness of the concrete deck is taken to be negligible for the new loading at a given stage. For the fifth and sixth load cases (RL and DW), the stiffness of the entire concrete deck is set to the long-term composite loading (modular ratio of 3n) value. Lastly, for the vehicular live load cases, the stiffness of the entire concrete deck is set to its short-term composite loading value. The vehicular live load analyses are conducted to determine the maximum and minimum envelope response values in all of the bridge components being assessed.

Load Case 1b is the predominant type of Steel Dead Load analysis performed in current 3D FEA and 2D Grid steel girder bridge design analysis calculations. On the other hand, Load Case 1a recognizes the correct analytical influence of the lack-of-fit of cross-frames relative to the initial no-load cambered geometry of the girders when the cross-frames are detailed for SDLF. For *straight* skewed I-girder bridges with the cross-frames detailed in this way, the girders are theoretically plumb under the steel dead load, and the corresponding steel dead load flange lateral bending stresses and cross-frame forces are zero. This matches with the steel dead load result obtained from LGA. The results from this analysis when contrasted with Load Case 1b, emphasizes that, for SDLF detailing of the cross-frames, refined 3D FEA and 2D Grid analyses generally do not provide the correct analytical steel dead load responses within the structure.

The effect of the SDLF detailing of the cross-frames on the bridge responses can be obtained by subtracting the results of Load Case 1a from the result of Load Case 1b. These results, while not generated in the parametric study, can be readily generated, given the Excel spreadsheets developed. However, it is more informative for bridge engineers to

compare and scrutinize the results for SDL/SDLF and SDL/NLF (Load Cases 1a and 1b), than to study the effects of SDLF in isolation.

The following sections explain further details of the load calculations for each of the above load cases. Although the given loadings constitute the most basic load cases, setting up these basic load cases involves many "approximations" that are described in the next few sections.

4.2.1 Steel Dead Load

Steel dead load is basically the self-weight of the structural steel contained in the superstructure. This includes the steel girders, the cross-frames, and the various miscellaneous steel items including girder splice plates, girder connection plates at the cross-frame locations, girder transverse stiffeners, gusset plates and spacer plates within the cross-frames, bolts and weld material.

Calculation of steel dead load of the bridge superstructure in LRFD Simon LGA models can be summarized as:

- Within each constant-area girder segment (all the bridge girders are prismatic with stepped changes in the cross section at field and/or shop splices in this work), the nominal steel self-weight of the girders is applied as a uniformly distributed load corresponding to the girder cross-section area times the weight density of steel (490 pcf). This load is calculated automatically in LRFD Simon.
- The total additional steel self-weight from a miscellaneous steel allowance of 5 % of the total self-weight of the girders, 130 % of any solid-web diaphragms, and 130

% of the cross-frame member self-weights, is calculated and divided by the total length along all of the steel girders. This uniformly distributed load is applied along all the girder lengths.

- The lengths of the cross-frame members and solid web diaphragms are taken as the lengths between workpoints at the centreline of the girder webs.
- The lengths of the girders are taken as the lengths between the centreline of the bearings. Girder overhangs beyond the bearing lines are neglected.

The applied loads are handled for the 3D FEA in the same manner as described for the LGA, with the following differences:

- The self-weight of the girders, diaphragms and cross-frame members is applied directly as a body load for each of these components based on the areas of the components at any given cross section. The 5 % allowance for the steel self-weight of the girders, and the 30 % allowance corresponding to the steel self-weight of the cross-frames and solid-web diaphragms, is applied directly to the body load for all of the components. Similar to the calculations of the self-weights for the LGA, the length of all the components is determined using the distances between work points at the centreline of the girder webs. In this study, to streamline definition of diaphragms, a rectangular cross-section is specified for each of the cross-frame members composed of angle section or Tee sections. The area of the rectangular section will be the same as the area of the physical member. The height of the rectangular section will be taken as two times the distance from the top of the physical member cross-section to the centroid of the physical member cross-section. This ensures that the cross-frame chords will be modeled at the correct

physical elevations in CSiBridge. The use of rectangular cross-sections for the cross-frame members does not have any impact on the stiffnesses in the bridge model since CSiBridge uses frame elements with end releases to model the chords and diagonals.

- The girder connection plates at diaphragms and cross-frames are explicitly modeled in CSiBridge. Without modeling of the connection plates at these locations, the girder webs, represented by shell finite elements, tends to distort excessively due to the eccentricity of the cross-frame chords relative to the girder flanges. In this study, the weight density of the girder connection plates is set to zero. This simplifies the calculation of consistent self-weights (i.e., same total weight) in CSiBridge and LRFD Simon. The girder connection plate self-weights are assumed to be included within the 30 % miscellaneous steel for the cross-frames.
- Two different 3D FEA calculations are considered for the Steel Dead Load:

  (1a) Steel Dead Load, No Load Fit (SDL-NLF)

  (1b) Steel Dead Load, Steel Dead Load Fit (SDL-SDLF)

  The total steel dead load is the same in both of these analyses. However, for SDL-NLF, the load is applied to the 3D FEA model of the bridge without considering the SDLF effects. That is, the 3D bridge model is constructed and these gravity loads are then simply "turned on." Conversely, SDL-SDLF accounts for the actual detailing of the cross-frames for SDLF. This is accomplished by using the staged construction feature in CSiBridge to analyze the bridge according to the idealization

that the girders are initially stably supported on the vertical supports and the cross-frames are hung from the girders.

Regardless of how the steel self-weight is estimated, it is still largely just a basic *estimate*. The aspect of key importance for this research was that the total of the bearing vertical reactions obtained from the 3D FEA and obtained by summing all the reactions from the LGA idealizations should be the same value (within say 1 percent). This allows for us to state that the 3D FEA and LGA loadings are indeed "equivalent."

4.2.2 Concrete Dead Load

In this study, concrete dead load is taken as the total weight of the concrete bridge deck, including the weight of stay-in-place metal deck forms (and the concrete within the flutes of these forms), the concrete in the overhangs and the concrete within the haunches (i.e., bolsters) over the top of the steel girders.

For the majority of the cases studied, where staged-deck placement is not considered, the total weight of the wet concrete is calculated by considering:

- The weight density of concrete, taken as 150 pcf, times the area of the concrete within the bridge cross-section, obtained as the sum of:
  a) The area of the rectangular structural portion of the deck equal to the structural thickness multiplied by the overall width of the deck.
  b) The area of a sacrificial overlay thickness times the overall width of the deck. (In this work, based on guidance from the FDOT Structural Design Guidelines (FDOT 2019a) and from the FDOT steering group for the research, the sacrificial overlay

thickness is taken as 0.5 inches for decks with a thickness greater than or equal to 8.5 inches. Furthermore, the sacrificial overlay thickness is taken equal to zero for decks with 8.0 inch thickness or less, and it is taken as the specified depth minus 8.0 inches for decks between 8.0 and 8.5 inches in thickness.)

c) The area of the concrete within the girder haunches, taken as the haunch depth minus the thickness of the girder top flange times the flange width for all the girders,

d) A tapered triangular shaped area of the concrete within the two deck overhangs, located below the structural thickness of the deck and varying from zero at the edge of the deck to the haunch depth minus the flange thickness at the tip of the fascia girder top flanges.

- The weight of stay-in-place metal deck forms between the girder flanges, including the weight of the concrete within the flutes of the forms, taken as 20 psf as specified in the FDOT SDG (FDOT 2019a).

These loads are divided by the total number of girders, and then applied as equal line loads in LGA to each of the girders in the bridge cross section.

As a simplification, the temporary bridge form loads on the deck overhangs are neglected. This simplification is applied both in the LGA and in the 3D FEA, so that the LGA and 3D FEA results can be compared on a consistent basis. No specific construction loads, such as screed rail loads, wheel loads from a screed machine, walkway and other related loads supported by the bridge during the deck placement, and loads from the construction operations, are considered in this work, either for the LGA or for the 3D FEA. In conclusion, the wet concrete loads on the overhangs, as modeled, are taken as a representative set of loads for comparison of the LGA and 3D FEA calculations.

Handling of the concrete dead load for staged deck placement is addressed in LRFD Simon by subdividing the girder into lengths corresponding to each stage. The sequence of the placement of these lengths is then specified. LRFD Simon analyzes these successive placements, modeling the concrete in the previously placed stages as composite.

In CSiBridge, the weight of the rectangular structural portion of the bridge deck is considered directly as a body load. All of the other contributions to the concrete dead load are determined in a similar fashion to that described for the LGA, then applied as a uniformly distributed load across the total area of the bridge deck.

It should be noted that this idealization gives a relatively simple approximation of the various torsional effects on the fascia girders from the deck overhangs. In CSiBridge 3D FEA models, the torsion from the overhang is applied entirely to the corresponding fascia girder. In the physical bridge, the above overhang loads, are applied to the corresponding fascia girder during the deck placement. However, when the overhang forms are removed, the direct torsion on the fascia girder from the overhang support brackets is released and the fascia girder exhibits an elastic rebound due to the release of this torsion. In the remaining structure, the concrete dead load on the overhangs is resisted predominantly by the cantilever action of the deck over the top of the fascia girder. Therefore, the torsional moments on the fascia girders, in their final constructed condition, are over-estimated by the "Wet Concrete Loading" procedure in CSiBridge.

The 3D FEA and LGA solutions can be compared consistently based on this approximation. The flange lateral bending stresses in the fascia girders is estimated approximately using AASHTO LRFD Equation C6.10.3.4.1-2 for the purpose of a

consistent comparison with 3D FEA estimates. This is explained in more detail in Section 5.3.11. Further, the total concrete dead load on the bridge, utilized in the 3D FEA and LGA calculations, is the same in both solutions.

4.2.3 Barrier Rail Load

Barriers composed of rails that serve as traffic barriers are placed near the edges of the bridge width and extends throughout the length of the bridge. Barrier rails are erected/installed after the deck hardens and hence the load is applied to the composite bridge section.

In this study, various aspects of calculation of barrier rail loads can be summarized as:

- The weight of the barrier rails is applied as a DC2 load, resisted by the long-term section of the girders. Consideration of barrier rail load in the bridge studies is useful to gage the ability of 1D LGA vs 3D FEA to evaluate the bridge response to a long-term composite superimposed dead load that is applied at concentrated positions across the bridge width. In this study, barrier rail load corresponding to 36 inch single-slope rail was applied in all the bridges. Referring to FDOT (2019a) SDG Table 2.2-1, the 36 inch single-slope rail weighs 430 plf.
- No other barrier loads, sidewalk loads, etc. that would typically be applied as DC2 loads are considered in this research.

In LGA, the total load from the barrier rails, assumed to be two rails, one on each side of the bridge deck, is divided by the total number of girders to obtain an equal line load applied to each of the girders in the bridge cross section.

In the 3D FEA model, the barrier rail loads are applied to the concrete deck at the approximate centroid of the 36 inch single-slope rails. This is taken as nine inches from the edges of the deck.

4.2.4 Future Wearing Surface and Utilities Load

Weight of non-integral wearing surface and utilities supported by the bridge constitute the future wearing surface and utilities load.

In this study, various aspects of calculation of future wearing surface and utilities loads can be summarized as:

- A future wearing surface load of 15 psf = (150 pcf) (1.2 inches) is applied to the overall width of the deck. This is divided by the total number of girders in the bridge cross-section to obtain an equal nominal DW load applied to each of the bridge girders, using the long-term composite properties of the girders.
- No other utility loads are considered in the bridge studies conducted in this research.

In LGA, the total future wearing surface load on the bridge is divided by the total number of girders to obtain an equal line load applied to each of the girders in the bridge cross section.

In 3D FEA, the future wearing surface loads are as specified for the LGA, but are applied directly as a 15 psf load to the full deck area in the CSiBridge models.

4.2.5 Vehicular Live Load

Analysis of live load involves determining the most critical locations of the AASHTO design vehicular live load to estimate the maximum critical responses for the various bridge components. The AASHTO LRFD Specifications require the consideration of *n* live load lanes for a given bridge, where *n* is the number of 12 ft wide lanes that can be placed between the curb lines on the deck. These lanes are to be moved or "floated" across the width of the bridge between the curbs disregarding the presence of medians and sidewalks, to obtain the most critical live load response. In this study, which utilizes a geometric linear and elastic analysis, the maximum responses are obtained using influence surfaces. For a line girder analysis, the maximum responses are obtained using live load distribution factors and influence line diagrams.

In the study, pedestrian live load or special vehicular live loads (e.g., permit loadings, etc.) is not considered. HL-93 vehicular live load defined in the AASHTO LRFD Specifications is used to evaluate the sufficiency of line girder analysis for the bridges to be studied. For the overall system analysis of the bridges studied, the tandem loading in the HL-93 load definitions will never govern. Therefore, the tandem loading is not considered in this project.

<u>Modeling Vehicular Live Load within CSiBridge:</u>

CSiBridge v21 provides very powerful features that greatly facilitate the definition and application of the AASHTO LRFD HL-93 live load model. The standard AASHTO LRFD and HL-93 live load definitions are already included in CSiBridge. The application of this model to a bridge is defined in a succinct way by defining a floating lane set. The overall

width of the bridge that is accessible to vehicular live load, is taken as the width between the exterior barrier rails in this project, is specified as the lane width for the floating lane set. Given the standard lane width of 12 ft, the total width of the floating lane set is divided by 12 ft, then rounded down to the closest integer, *n*. This is the number of live load lanes that the width of the bridge can accommodate. CSiBridge then "floats" the *n* lanes across the width of the bridge, i.e., it positions the lanes at various locations across the bridge width, to generate the maximum live load effects. Within each lane, the HL-93 loading rules apply (again, the tandem load is not included in our analyses). Within the definition of the HL-93 vehicle loading, the dynamic load allowance factor of 1.33 is included in our definition of the "nominal" live load.

Within the floating lane set, CSiBridge considers 1, 2, 3, 4 and up to *n* lanes. For the case of one lane positioned within the width of the floating lane set for maximum effect, a multiple presence factor of 1.2 was employed. For two and three lanes, multiple presence factors of 1.0 and 0.85 are employed. For four or more lanes, a multiple presence factor of 0.65 is used (following the AASHTO LRFD requirements). Floating lanes within a lane set are not allowed to cross or overlap each other. CSiBridge calculates the amount that the floating lanes are allowed to move transversely, based on the total width of the lane set, and the standard 12 ft lane width.

When positioning the floating lanes at a given station, the following possibilities are considered:

- All lanes adjacent in a single group with no intermediate gaps.
- A single gap between two groups of lanes, each group containing no gaps.

For N floating lanes in a lane set, this leads to N possible groupings. This is shown in Figure 42, from the CSiBridge Reference Manual (CSI 2017) for the case where N = 4. For each case, the one or two groups are moved transversely to find the position that leads to the maximum response.

CsiBridge has lane discretization factors for moving the live loads. These will be set to 10 ft in the along lane and across lane directions. In addition, the discretization along the lane will be set that it is never greater than 1/10 of the span length. AASHTO LRFD requires consideration of wheel loads up to 1 ft from the barrier rail (curb) for design of the overhangs. However, the focus in our project was on the overall bridge system design. As such, both edges of all the lanes were considered as "interior edges," meaning that wheel loads do not need to be placed closer than 2 ft from the edge of the lane.

CSiBridge considers traffic moving in either direction within a given lane in obtaining the maximum live load effects. For the bridges considered in this study, the live load was defined by creating a single floating lane set.

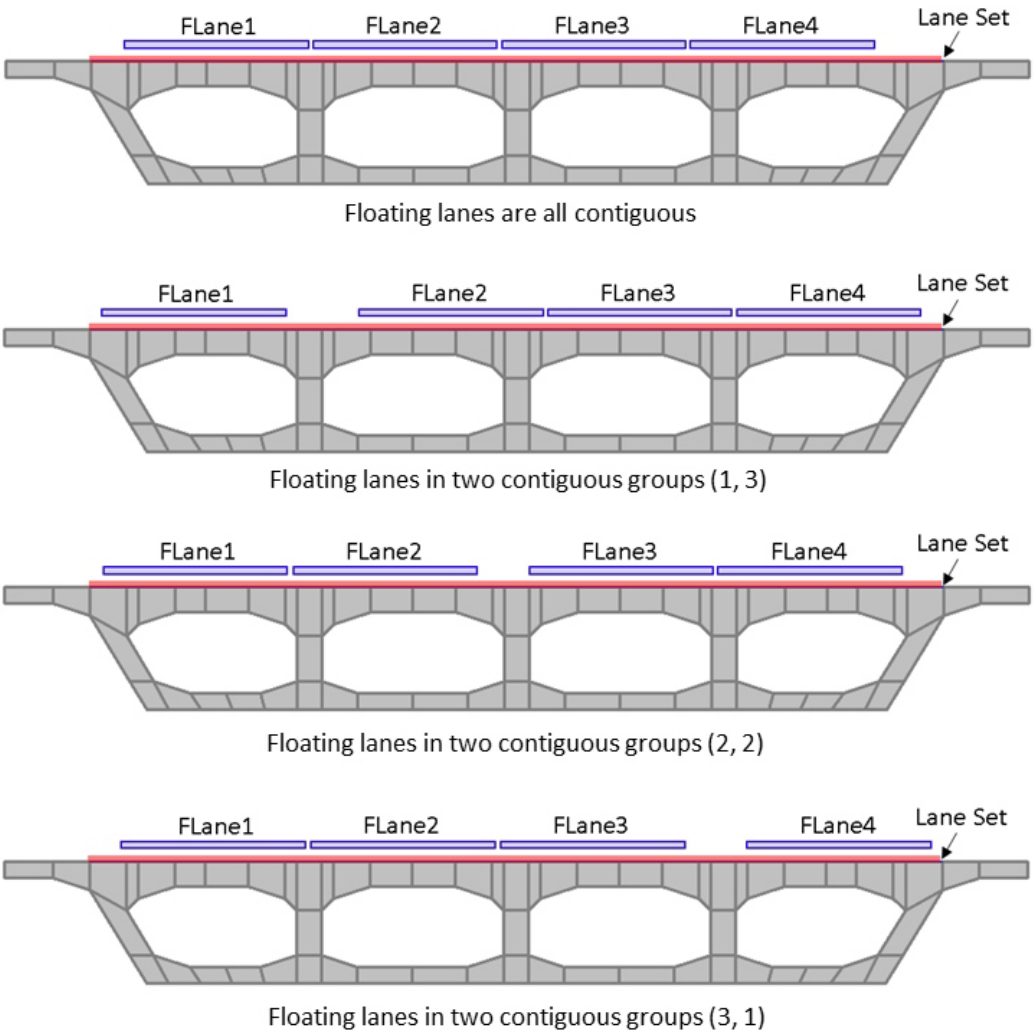

Figure 42. Transverse positioning of four floating lanes showing all possible grouping options from (CSI 2017).

Modeling Vehicular Live Load within LRFD Simon:

In LRFD Simon, live loads are applied to the girders based on AASHTO LRFD load distribution factors, as described in Section 2.5.2. Simon conducts structural analysis to obtain the maximum live load effects, using influence line diagrams to obtain the maximum and minimum envelopes for various response quantities.

4.2.6 Vehicular Live Load for Deflection Calculations

For optional live load deflection evaluation, AASHTO LRFD Specification (AASHTO 2017) Article 3.6.1.3.2 states:

If the owner invokes the optional live load deflection criteria specified in Article 2.5.2.6.2, the deflection should be taken as the larger of:

1. That resulting from the design truck alone, or
2. That resulting from 25% of the design truck taken together with the design lane load

Further, AASHTO LRFD Specification (AASHTO 2017) Article 2.5.2.6.2 states:

1. The vehicular load shall include the dynamic allowance
2. When investigating the maximum absolute deflection for straight girder systems, all design lanes shall be loaded, and all supporting components should be assumed to deflect equally
3. For composite design, the stiffness of the design cross-section used for the determination of deflection should include the entire width of the roadway and the structurally continuous portion of the railings, sidewalks and median barriers (we are assuming none of these are structurally continuous in our calculations).
4. For straight girder systems, the composite bending stiffness may be taken as the stiffness determined as specified above, divided by the number of girders
5. The live load portion of Load Combination Service I of Table 3.4.1-1 should be used including the dynamic load allowance, IM. Basically, a live load multiplier of 1.0 times 1.33 should be used. In addition, the reference to Table 3.4.1-1 indirectly brings in the

consideration of the multiple presence factor, since Article 3.4.1 indicates calls out the use of the multiple presence factor with Table 3.4.1-1.

6. The live load shall be taken from Article 3.6.1.3.2, which brings in the requirement of 25 % of the HL-93 truck with the lane load, or the HL-93 truck alone.

Summarizing, all of the above gives the live load distribution factor of m*(N_L/N_g), applied with 25 % of the HL-93 truck plus the lane load, or the HL-93 truck alone, where, where m is the multiple presence factor, N_L is the maximum number of lanes that can be accommodated on the bridge and N_g is the number of girders in the bridge. The distribution factor obtained is used in calculating an average estimate of live load deflection

However, NHI (2011) note that the assumption of equal deflections is not applicable for bridges that have a skew angle exceeding 20°. This is because the differential deflections that occur between girders is more important than an average estimate of live load deflection obtained from AASHTO optional live load deflection evaluation. Hence, in conclusion, live loading ranging from one to the maximum number of lanes that can be accommodated on the bridge should be employed in the calculation of live load deflection estimates.

Separate load cases 6a, which is composed of a derived HL-93 vehicle that consists of 25% truck load and 100 % of the lane load and 6b, which is composed of a derived HL-93 vehicle that consists of only the truck load were considered for the investigation of girder deflections under live load. An impact factor of 1.33 was applied to the truck load in both load cases 6a and 6b as recommended by AASHTO LRFD Specifications.

In order to simulate load cases 6a and 6b in CSiBridge, derived HL-93 vehicles pertaining to load cases 6a and 6b were defined from the base vehicle used in the general live load case 5. LRFD Simon automatically calculates the live load deflection for load cases 6a and 6b using the distribution factor m^*N_L/N_g and presents the maximum of the two deflections.

4.2.7 Fatigue Live Load

The AASHTO (2017) Specifications Section 3.6.1.4.1 define the vehicle for evaluation of fatigue as follows:

1. The fatigue load shall be one design truck or axle, but with a constant spacing of 30 ft between the 32 kip axles.
2. A dynamic load allowance of 15% (1.15) shall be applied to the static effects of the design truck.

Analysis for fatigue involves positioning the fatigue vehicle in a single lane that spans throughout the bridge length and the roadway width, to obtain the most critical effects. This was achieved in CSiBridge by defining a single lane for fatigue that spans throughout the length and between the rails in the transverse direction. AASHTO LLDF calculation used in the evaluation of fatigue live load response in LGA is as described in Section 2.5.2.

4.3 Consideration of Girder Axial Forces obtained from the CSiBridge 3D FEA Models

The elastic 3D behavior of a bridge depends on the relative stiffness of the composite concrete deck and the steel I-girders which in turn influences the distribution of forces

between the concrete deck and the steel girders. When analyzing composite girders using the long-term elastic modulus of concrete, for sustained superimposed dead loads, and for short term elastic modulus of concrete for vehicular live loads, the portion of slab that acts composite to each steel I-girder is calculated based on the tributary width of the slab for each girder. This assumption has been found to be reasonable and is commonly used in the design of composite bridge girders.

Ideally, in the absence of longitudinally applied axial loads (such as may occur in some cases due to the combination of the bridge skew and specifics of bridge bearing constraints), the axial forces in a composite girder should be zero. In other words, the portion of the slab acting compositely with each girder is such that the axial force on all the girders at a bridge cross-section is zero. This action is captured in a 3D FEA of the concrete deck and the steel I-girders.

The relative distribution of loads and thereby, the participation of the deck with each steel I-girder is also influenced by the type and location of the load. The deformed shape of the concrete deck around each steel I-girder provides an insight into the portion of deck that participates with the steel I-girder. For a uniform pressure load spread over the entire area of the bridge, the portion of deck acting with each steel girder is reasonably well approximated by the tributary widths. However, for a load such as the barrier rail load that is effectively a concentrated load applied at a particular position within the bridge cross-section, the 3D FEA can suggest that the portion of deck that participates with the different girders is different than the tributary width.

CSiBridge uses tributary width of the deck composite with each steel I-girder to report the internal forces of the composite girders. As a result, a measurable net axial force is observed on the composite section in some cases such as the above. It should be noted that the total axial force on the entire bridge system is zero (assuming negligible longitudinal constraints and negligible applied axial loading on the bridge cross-section, which are considered to be appropriate assumptions within the context of this study). However, due to the assumption of tributary widths of deck acting compositely with each steel I-girder, non-zero axial forces are calculated on the individual composite girders. The calculated axial forces on all composite girders of the bridge sum to zero.

Due to the presence of a net girder axial forces, the horizontal axis about which the girder bending moments is calculated becomes important. The neutral axis of the composite girders is at different depths for the non-composite, short term composite and long term composite section. The net effect is that the major axis bending moments and bending stresses are influenced by the presence of the girder axial forces. This effect is more significant for concentrated load cases such as barrier rail load.

CSiBridge, by default reports the internal forces at a horizontal axis passing through the mid-web depth of each section. This entails that the bending moment due to the net axial force must be added to the bending moment resultants obtained from CSiBridge to obtain revised bending moments. The bending stress at the flanges can then be calculated using the revised bending moments and the axial stress due to the axial force can be added to obtain the correct estimates of stress. Of course, the stresses at different locations on the girders is calculated directly by the 3DFEA model and can be output directly, rather than calculating the resultant moments and the back-calculating the stresses from the resultant

moments given the common girder design-analysis cross-section models. A study was conducted to evaluate the effects of axial force on bending moments for girders of Bridge 1. A maximum error of approximately 1 ksi was found for the barrier rail load case. For practical purposes, a maximum error of 1 ksi which is 2% of the material yield strength of 50 ksi, is considered acceptable. Therefore, the effect of the above girder axial forces was ignored in the calculation of the girder major-axis bending moments. However, these axial forces are collected and catalogued in the excel spreadsheets developed in the study of each bridge.

4.4 Presentation of the Results

In this research, results from LRFD Simon and CSiBridge are processed and compiled in a series of excel workbooks. Detailed plots and comparison tables, from these excel workbooks, have been compiled within appendix sections for each of the 26 bridges studied. These 26 sections are contained in Appendix 3. The presentation of the data from the parametric studies, in each Appendix 3 section, is organized so that the results can be readily inspected and understood for the individual bridges studied, as well as for the overall suite of bridges studied. The presentation is predominantly graphical, and organized in the same fashion for each bridge. In each individual appendix section, the most meaningful results addressing the project objectives are presented. Various other data can be examined in the excel worksheets. The workflow of building the analysis models, extracting the results and processing the results will be explained in detail in Section 4.5.

Each Appendix 3 section corresponds to an individual bridge studied, and begins with a summary of the bridge characteristics, girder details and cross-frame details. This is

followed by a synthesis of comparisons between the results from the LGA and from 3D FEA solutions for the selected bridge. Lastly, various detailed plots and tables providing results comparisons are provided. Plots are presented for each of the key response quantities discussed below for each of the following load cases described in Section 4.1:

1a. Steel Dead Load (SDL/SDLF), including the influence of Steel Dead Load Fit (SDLF) effects.

1b. Steel Dead Load (SDL/NLF), not including the influence of Steel Dead Load Fit (SDLF) effects, i.e., based on No-Load Fit.

2a. Concrete Dead Load (CDL), neglecting any influence of prior setup of the concrete during deck placement.

3. Barrier Rail Load (RL).
4. Future Wearing Surface and Utilities Load (DW).
5. Vehicular Live Load (LL).
6. Vehicular Live load for Displacement
7. Fatigue Live Load

For four bridges, as explained in Section 3.5, the following additional load case is considered:

2b. Concrete Dead Load (CDL/SDP), considering the influence of staged deck placement.

These results are presented as sections of Appendix 4, separate from the responses presented in Appendix 3.

The numbering of the appendix sections, which is shown at the top of each of the appendix pages, is as follows:

- The first number corresponds to the Appendix number, i.e., number 3 for the detailed bridge-by-bridge data.
- The number for the second section level corresponds to the bridge being studied, 1 through 26.

The third section level focuses on the different bridge characteristics, responses and contexts listed in Table 11.

Some of the appendix sections have a fourth section level corresponding to attributes such as the girder number, in the sub-sections presenting the girder data, the specific cross-frame response in the sub-sections presenting the cross-frame data, etc.

For a number of the bridges studied, results are presented for three girders – one of the fascia girders, the first interior girder adjacent to this fascia girder, and the central interior girder closest to the mid-width of the bridge. These cases correspond to bridges having parallel skew of their bearing lines and in which there is a symmetry of the geometry about the mid-width of the bridge. In cases where the bearing lines are not parallel to one another, and/or where there is a lack of symmetry about the mid-width of the bridge, four girders are considered in the collection and presentation of the results. From the girders studied, Girder 1 refers to the fascia girder at the top of the plan view, Girder 2 refers to the interior girder adjacent to this fascia girder, and Girder 3 refers to the girder closest to or at the bridge mid-width. Girder 4, if studied, refers to the fascia girder at the bottom of the plan view. For Bridge 1, and for the other bridges where the

results for four girders are presented, Girder 4 refers to the fascia girder at the bottom of the bridge plan. For instance, for Bridge 1, the results are presented for four girders, labeled 1 to 4, because one of the fascia girders has a slightly different bottom flange. Girders G1 and G2 correspond to Girders 1 and 2, Girder G6 corresponds to Girder 3, and Girder G11 is labeled as Girder 4. This is illustrated in Figure 43. Response quantities 1 to 9 (see Table 11) are reported for each of the girders considered. For the major-axis bending moments, vertical deflections and vertical shear forces, the responses obtained from 3D FEA and LGA are shown on the same plots. These comparison plots allow for a direct evaluation of the differences between the 3D FEA and LGA predictions.

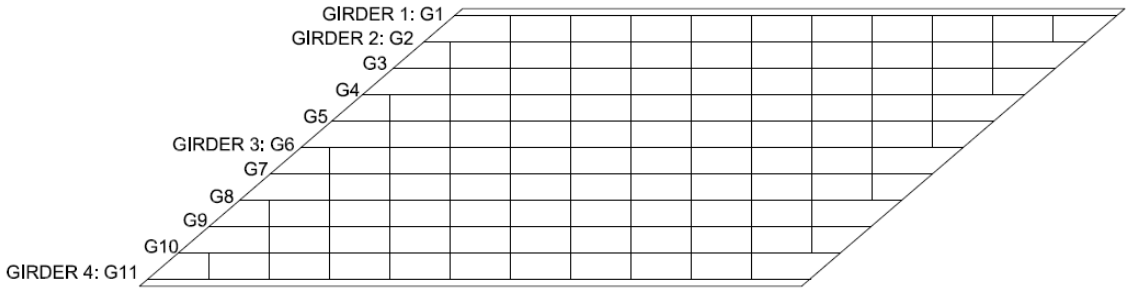

Figure 43. Illustration of Girders 1 to 4 in the presentation of results of Bridge 1.

For the live load vertical deflections, the results presented are based on the maximum values from (1) design truck alone, and (2) 25 % of the design truck taken together with the design lane load, as explained in Section 4.1.6.

Table 11. Organizaton of third section level of Appendix 3.

Third Section Level Number	Focus	Context
1	Summary of bridge characteristics, and synthesis of comparisons between LGA and 3D FEA solutions	
2	Major-Axis bending moments, and fatigue stress range for the top and bottom flanges	Three or more girders
3	Vertical deflections	Three or more girders
4	Layover displacements	Three or more girders
5	Twist rotations	Three or more girders
6	Normalized twist rotations	Three or more girders
7	Vertical shear forces	Three or more girders
8	Top flange lateral bending stresses	Three or more girders (only for 3D FEA)
9	Bottom flange lateral bending stresses	Three or more girders (only for 3D FEA)
10	Cross-frame member axial forces	Cross-frame top chords, bottom chords and diagonal members (only for 3D FEA)
11	Overall cross-frame resultant moments and shears	Overall cross-frame units (only for 3D FEA)
12	Vertical reactions	Each of the individual bridge bearings
13	Lateral displacements	Bridge bearings (only for 3D FEA)
14	Live load distribution factor estimates	Three or more girders
15	Normalized mean differences	Major-axis bending moments, shear forces and vertical displacements for each of the girders considered
16	Detailed hand calculations	Various quantities

Regarding the calculation of girder layover displacements, two different values are presented on the same plot in the third-level 4 listed in Table 11:

1. Transverse displacement of the top flange and
2. Relative displacement of the top flange with respect to the bottom flange.

The related twist rotations are presented in two different ways in the third-levels 5 and 6:

1. Twist rotations in radians in Section 5 and
2. Relative displacement of the top flange with respect to the bottom flange per foot depth of the web, i.e., the relative displacements from Section 4, divided by 12 inches, in Section 6.

A summary table is provided in the third-level 5, providing a comparison of the 3D FEA layovers at the supports to estimates from LGA using procedures recommended by FDOT. The procedure is explained in more detail in Section 5.2.1.2.

The cross-frame forces are reported as the axial forces in the component cross-frame members, as well as the resultant moments and shear forces on the overall cross-frames in the third-level 10 and 11. Cross-frame member axial forces are reported separately for the top chords, the bottom chords and the diagonal members respectively on separate plots in the third-level 10. In addition, the cross-frame resultant moment and resultant shear forces, at a transverse section at the mid-width of each cross-frame, are reported separately in the third-level 11. For loadings in which the bridge is composite, the resultant moments and shears include the contribution from the bridge deck to the cross-frame internal forces.

The cross-frame results are presented as bar charts showing the forces on a cross-frame-by-cross-frame basis moving along the length of the bridge within each “bay” between the girders. The plots start in Bay 1 between Girders 1 and 2 (at the top left of the plan drawing), move toward the top right corner of the plan, then progress downward to the next bay and from left to right again. This is explained in Figure 44 showing a plan view of Bridge 1 that illustrates the girder numbering G1 through G11 as well as the Bays 1 through 10

between these girders. In addition, the specific cross-frames are numbered from 1 to 12 in each bay as we move from left to right in this bridge. All the bays have the same total number of cross-frames in this bridge.

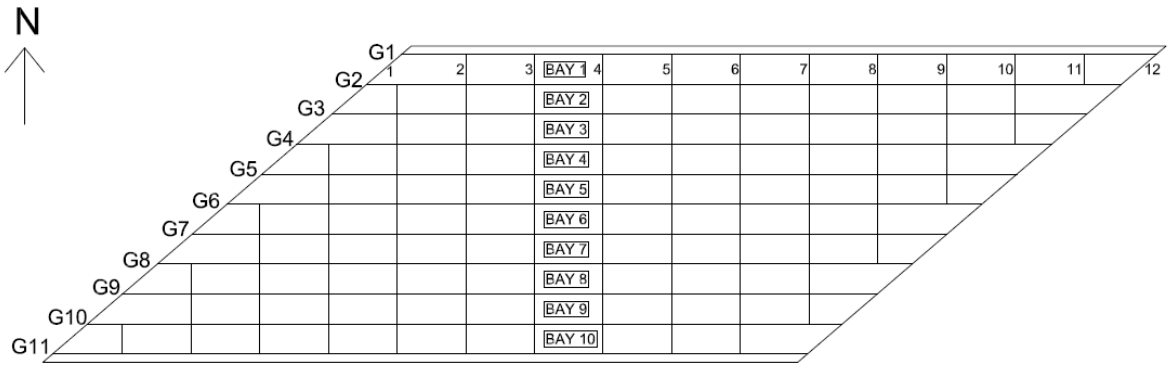

Figure 44. Girder, bay, and cross-frame numbering for Bridge 1.

Figure 45 shows the corresponding plan for Bridge 2, which is the same as Bridge 1 but with an improved alternative cross-frame arrangement involving the use of ample staggers and offsets of the cross-frames throughout the bridge. The development of the alternative cross-frame arrangement was explained in Section 3.3.

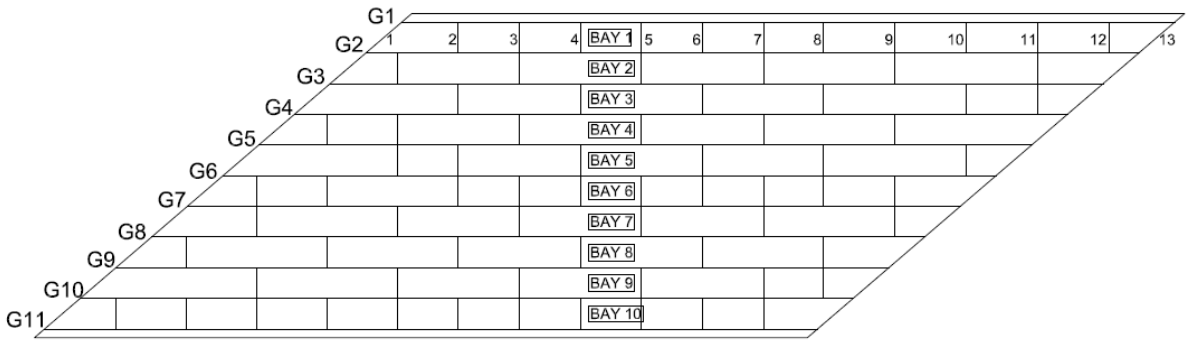

Figure 45. Girder, bay, and cross-frame numbering for Bridge 2.

Figures 46 and 47 show example cross-frame component force results for these two bridges. Specifically, these plots show the top chord forces from 3D FEA, corresponding

to the nominal concrete dead load for these bridges. These plots provide a concise compilation of all the cross-frame component forces throughout these structures. The plots in Figures 46 and 47 are annotated to highlight the cross-frame component member forces corresponding to each of the bays. In Figure 46, 14 forces are shown for each of the bays. Two forces are plotted for the cross-frames at the abutment lines, i.e., for Bay 1, the abutment line cross-frames are labeled as 1 and 12 in Figure 44. These two forces are the forces on each side of the inverted-V attachment of the diagonals to the top chords in the cross-frames at the abutment lines. Otherwise, each bar in the left-most portion of the graph corresponding to Bay 1 corresponds to cross-frames 2 through 12 in Figure 44. The bar graphs for the other bays are similar.

Figure 47 conveys all the CDL top-chord forces in Bridge 2. In this case, there are 15 bar values for Bays 1 and 10, since there are 13 cross-frames in these bays, and the forces on each side of the top chord are shown at the abutment lines. Most of the intermediate bays in Bridge 2 have only eight cross-frames, and therefore 10 bars are shown for each of these bays. Bay 6 has 12 cross-frames and 14 corresponding cross-frame top chord forces.

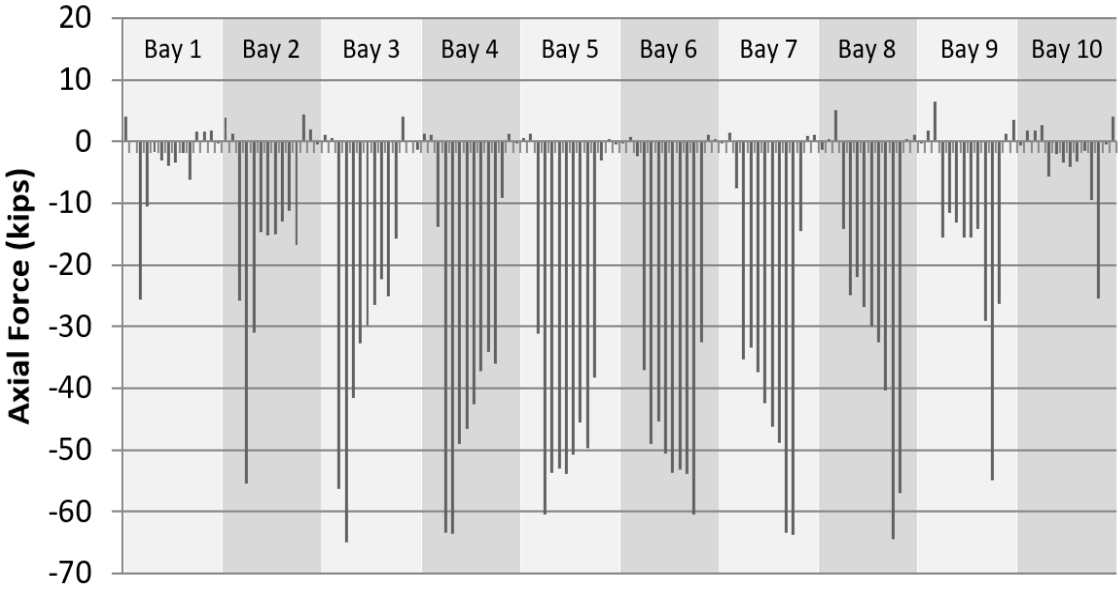

Figure 46. Example cross-frame component force plot (CDL top-chord forces), Bridge 1.

Given these plots various aspects of the cross-frame responses in the different bridges can be readily ascertained. For instance, the development of a transverse load path through the cross-frames in the short direction between the obtuse corners of each of these bridges can be observed. In addition, it's easier to compare the overall relative magnitudes of the cross-frame forces. For instance, comparing Figures 46 and 47, one can observe that the maximum cross-frame forces in Bridge 2 are approximately one-half those in Bridge 1. Bridge 2 has a smaller number of cross-frames, 94 in total, compared to 120 cross-frames in Bridge 1, and yet the cross-frames in Bridge 2 tend to have smaller internal forces. Potential economies may be gained by recognizing the influence of an alternative cross-frame arrangement with ample offsets and staggers.

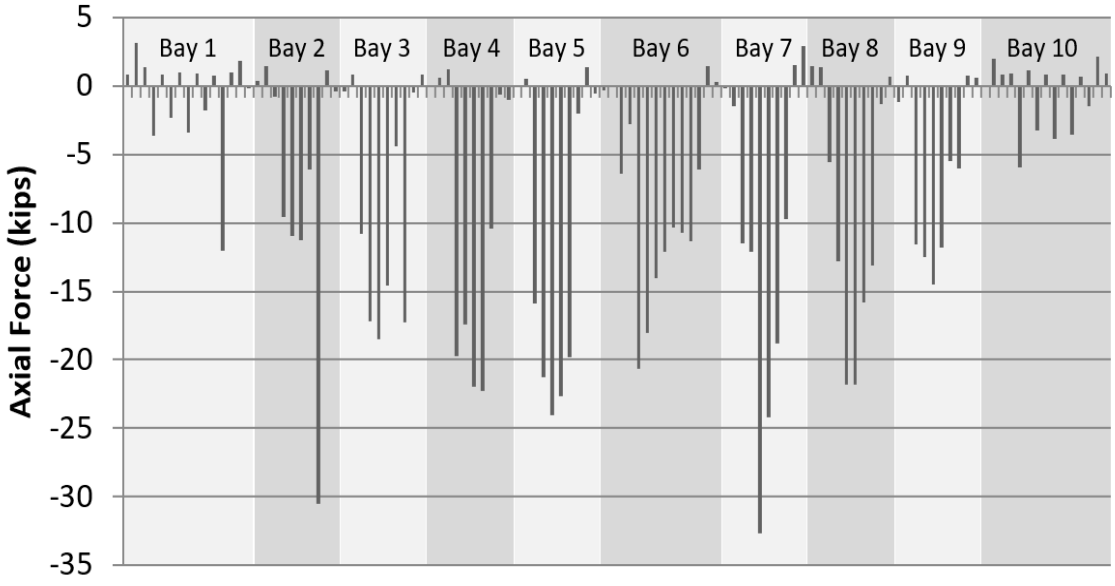

Figure 47. Example cross-frame component force plot (CDL top-chord forces), Bridge 2.

It is known that theoretically (i.e., based on engineering idealization) the girder flange lateral bending stresses and the cross-frame forces are zero for steel dead load fit under steel dead load. Therefore, these plots are not included in the appendix sections. To maintain the same page locations for presentation of the different results, the space that would correspond to these plots is empty. This maintains all the plots at the same locations within all the presentations, making it easier to readily locate and compare the various responses.

In the third-level 12 listed in Table 11, vertical reactions are reported at all the bearing locations using bar charts. These bar charts show the reactions for each bearing. For each support line, these quantities are reported for each bearing as one moves from the top to the bottom of the plan view (i.e., from girders G1 through Gn, where n is the fascia girder number at the bottom of the plan view). For the simple-span bridges, the results are listed starting from the left-most support line and then moving to the right-most support line in

the plan view. For multi-span continuous bridges, the vertical reactions are reported at the left-most support line, then the right-most support line, and finally at the intermediate pier supports. For three- and four-span continuous bridges, the bearing reactions at the pier supports are presented starting from the left-most pier and progressing to the right-most pier.

In addition, in the third-level 13 listed in Table 11, the 3D FEA lateral displacements perpendicular to the girders at all the bearing locations are presented using bar charts. The order of presentation of this data is the same as that described above for the girder vertical reactions. As mentioned in Section 4.1.1, a representative elastomeric bearing shear stiffness of 100 kip/ft is assumed at each of the bearing locations in the bridge models. The corresponding bearing lateral forces can be determined by multiplying the lateral displacements (presented in inches), by (100/12).

Significant differences are observed in the live load responses obtained from 3D FEA and LGA. This is readily apparent by comparison of the live load distribution factors (LLDF) obtained from 3D FEA to the AASHTO live load distribution factors employed with LGA. In the third-level 14, the live load distribution factors obtained from 3D FEA are compared to the LGA LLDF values obtained based on the requirements of Section 4 of the AASHTO LRFD Specifications. LRFD Simon provides live load bending moment envelopes at every tenth point in the spans. If these moment values are divided by the AASHTO LLDF an envelope of the bending moments corresponding to a LLDF = 1.0 is obtained. The ratio of 3D FEA live load envelope bending moments at the tenth points to the corresponding bending moments for LLDF = 1.0 obtained from LRFD Simon, are presented as the 3D FEA LLDF. 3D FEA LLDF are presented for both the positive and

negative moment envelopes. The negative moment LLDF are taken as zero for simple span bridges. Additionally, 3D FEA LLDF are also presented for moments obtained from fatigue live loading on the bridge.

Section 14 also provides plots of the 3D FEA based live load distribution factors (LLDF) for moment and for the shear ranges obtained from analyses considering the AASHTO fatigue load vehicle. These 3D FEA LLDF are somewhat different from the above values. Fatigue shear range is required in the design of shear connectors. Hence, Section 14 also presents 3D FEA LLDF for fatigue shear range. Similar to the LLDF calculation for moments or shears, LLDF for shear range is the ratio of 3D FEA fatigue shear live load shear range at the tenth points to the corresponding shear range for LLDF = 1.0 obtained from LRFD Simon.

For the comparison studies, the normalized mean difference and normalized difference of the maximums are used to quantify the differences between the 3D FEA and 1D LGA results. Additional measures of difference are employed in the evaluation of results from the parametric studies. The additional measures of differences are not presented in the appendix sections and are explained in detail in Section 5.2.3. The measures of differences quantified in the appendix sections are described below.

The normalized mean difference is defined as follows:

$$\varepsilon_{mean} = \frac{\sum_{i=1}^{n} \left| \text{LGA} - \text{3DFEA} \right|}{n \times \left| \text{3DFEA} \right|_{\max}} \tag{14}$$

where,

n = number of data points along a given girder, throughout the length of the bridge (data sampled at the 10th points) for girder moments, shears and vertical displacements, or the total number of bearings, for the bridge vertical reactions

The normalized mean difference is useful as a broad measure of accuracy, particularly for quantities such as displacement, where both underestimating and overestimating may have negative consequences.

The normalized difference of the maximums is defined as:

$$\varepsilon_{\max} = \frac{\left(\left|\mathrm{LGA}\right|_{\max} - \left|\mathrm{3DFEA}\right|_{\max}\right)}{\left|\mathrm{3DFEA}\right|_{\max}} \tag{15}$$

The normalized difference of the maximums is a more demanding measure, indicating the worst-case conservative and unconservative differences, normalized by the corresponding maximum 3D FEA response. The normalized difference of the maximums is computed as the difference between the maximum positive and maximum negative responses. This calculation is conducted without consideration of the specific locations of the responses.

Section 15 presents the summary ε_{mean} and ε_{max} values for the bending moments, vertical shear forces, vertical displacements and support reactions, for comparison of the 3D FEA and LGA responses. For the bending moments and shear forces, ε_{mean} and ε_{max} values are presented for all the load cases (including the fatigue live load case) for each of the considered bridge girders. Additionally, bending moment ε_{mean} and ε_{max} values are presented for the Strength I and Service II load combinations, and shear ε_{mean} and ε_{max}

values are reported for Strength I. For the vertical displacements, ε_{mean} values are reported for SDL, CDL, RL, and DW, and ε_{max} values are reported for all the load cases. Additionally, ε_{mean} and ε_{max} values are reported for the Total Dead Load (Steel Dead Load Fit), TDL (SDLF), load combination. This constitutes the sum of the vertical displacements for the dead load cases SDL (SDLF), CDL, RL and DW. The TDL (SDLF) vertical displacement values are used to determine the camber for the girders.

For the bearing reactions, ε_{mean} values are presented for all the load cases and for the Strength I and Service II load combinations.

Each appendix section concludes with a level three Section 16 presenting the hand calculation of the composite and noncomposite loads, the AASHTO live load distribution factors, including the check on rigid cross-section requirement for the fascia girders, and "exact" live load distribution factors to be applied to the results obtained from LRFD Simon to match the results from CSiBridge.

4.5 Workflow for Parametric Studies

The 26 bridges studied in the parametric studies are existing bridges, for which drawings are available. 3D FEA and LGA models are built from the data obtained from these drawings. Loads are calculated as described in Section 4.2. The process from obtaining data to analyzing the models can be summarized as follows:

1. Extract essential data from bridge drawings:
    a) Define geometry of the bridge: articulation, span lengths, bridge width, overhang lengths, parallel or nonparallel skew, skew angles at each bearing line.

b) Cross-frame layout: arrangement of intermediate cross-frames – contiguous (perpendicular to girders or parallel to skew) or staggered, end cross-frames, intermediate pier cross-frames for continuous span bridges, staggers near end and/or intermediate pier cross-frames.

c) Girder sizes: number of girders, web depth, flange widths, flange and web thicknesses, locations of transition in flange widths and flange and/or web thickness

d) Cross-frame sizes: types of end and intermediate cross-frames, number of cross-frames of each type, sizes of cross-frame members.

e) Deck: structural thickness of deck, sacrificial thickness, haunch depths for girders, reinforcement layout and bar sizes.

2. Calculation of weights and its application in analysis models:

a) The steel dead load is calculated as described in Section 4.2.1.

b) The concrete dead load is calculated as described in Section 4.2.2.

c) For staged deck placement analyses, parts of the deck and the corresponding additional loads are calculated in stages, and the deck in each stage is made composite beginning from the corresponding succeeding stages. It follows that the CDL loads are applied successively in stages in both CSiBridge and LRFD Simon.

d) LRFD Simon internally calculates the weight of the modeled steel girders and applies it as a DC1 load. Additional DC1 load spread uniformly over the length of the bridge can be defined in the Simon user interface. Loads applied in CSiBridge and LRFD Simon must be equivalent. Total DC1 load includes the weights of steel girders, cross-frames, miscellaneous steel, concrete deck, overhang tapers, sacrificial thickness, haunches and SIP forms. Hence, additional DC1 load in LRFD

Simon includes the weight of cross-frames, miscellaneous steel, concrete deck, overhang tapers, sacrificial thickness, haunches and SIP forms applied uniformly over the length of each girder.

e) LRFD Simon provides results for DC1 and "Other DC1" load described in part d). SDL comprises of weights of steel girders, cross-frames and miscellaneous. Adjustment factors for results of DC1 and "Other DC1" obtained from LRFD is modified using factors to obtain results for SDL and CDL cases.

It should be noted that the weight of end cross-frames is not included in the calculations of the SDL and CDL factors. The weight of the end cross-frames are applied at the ends of the girders, which are the points of support for the girders. In LGA, the point loads applied at the support are directly transmitted to the supports. Hence, the weights of end cross-frames are directly added to the LGA support reactions for SDL. Tributary end cross-frame or intermediate pier cross-frame weights are calculated for each girder bearing support and are added to the SDL reactions.

3. Calculation of live load distribution factors (LLDF) for LGA:

a) Calculation of the AASHTO (2017) LLDF for LGA is discussed in Section 2.5.2. The calculation of the longitudinal stiffness parameter K_g involves the use of moment of inertia, I, of the steel girder. A typical steel I-girder in a bridge has a number of section transitions within a span. It is therefore, necessary to obtain an "average" representative estimation of moment of inertia, I, to be used in the calculation of the longitudinal stiffness parameter. Hence, in the parametric studies, "average" moment of inertia, I, of a girder is obtained by averaging the moment of

inertia of the steel section at each 20th point in a given span. The length of the given span is used in estimation of moment live load distribution factors for positive bending. For the estimation of negative bending moment at an interior support of a multi-span continuous bridge, AASHTO (2017) Table 4.6.2.2.1-2 recommends using the average lengths of the two adjacent spans for the estimation of moment live load distribution factor. Similarly, an average moment of inertia, *I*, is calculated as the average of the "average" moment of inertia for the two adjacent spans. Thus, positive moment LLDF is calculated for each span, and negative moment LLDF is calculated for a set of adjacent spans. The LLDF thus estimated are approximately equal to one another. Hence, the maximum of the LLDF estimates calculated is used as the bending moment LLDF in LGA.

b) The shear LLDF, on the other hand, is only dependent on the spacing and hence, is a unique value for each girder.

c) The fatigue LLDF for bending moment is calculated as the bending moment LLDF for a single lane in a) divided by the multiple presence factor of 1.2.

d) The fatigue shear LLDF is similarly calculated as the shear LLDF for a single lane in b) divided by the multiple presence factor of 1.2.

4. Building the 3D FEA analysis model:

a) Aspects of 3D FEA modeling in CSiBridge are described in Section 4.1.1.

b) Dead load cases are simulated in CSiBridge using its "Staged Construction" capabilities. The staged construction sequence in CSiBridge, in a way, simulates the sequence of construction of the bridge and the application of loads on it. For example, the noncomposite DC1 load case consists of the steel dead load and the

wet concrete load applied to the steel superstructure. The definition of the DC1 (with SDL (NLF) load case in CSiBridge consists of the following two stages:

i) Activate the steel superstructure comprising of steel girders and the cross-frames. The self-weight of the superstructure is then applied to the activated steel superstructure. This refers to the condition of SDL (NLF).

ii) The wet concrete load is applied to the steel superstructure.

c) The definition of SDL (SDLF) load case in CSiBridge consists of the following stages:

i) Activate the steel superstructure comprising of steel girders and the cross-frames. Apply a stiffness modifier of 1E-20 to the cross-frames, to "deactivate" the stiffness of the cross-frames. The self-weight of the superstructure is then applied to the active steel I-girders, because the cross-frame stiffness has been deactivated. However, the self-weight of the cross-frames will be applied to the steel structure since the cross-frames are a part of the superstructure. This refers to the condition of SDL (SDLF). For SDL (SDLF), it is important to ensure lateral stability of the girders. Hence, the top flanges of all the girders are restrained at the bearing lines.

ii) The self-weight of the superstructure is then applied to the active steel I-girders, because the cross-frame stiffness has been deactivated. However, the self-weight of the cross-frames will be applied to the steel structure since the cross-frames are a part of the superstructure. This refers to the condition of SDL (SDLF). For SDL (SDLF), it is important to ensure lateral stability of the girders. Hence, the top flanges of all the girders are restrained at the bearing

lines. The results of this stage should theoretically match results from LGA, provided the loads are applied consistently in both LGA and 3D FEA.

d) Staged construction of the bridge can be defined similar to the DC1 load case using the CSiBridge staged construction capabilities. For example, a bridge that is constructed in three stages of deck pour can be defined is CSiBridge using the following:

   i) Activate the steel superstructure comprising of steel girders and the cross-frames. The self-weight of the superstructure is then applied to the activated steel superstructure.

   ii) Apply the wet concrete load pertaining to the first stage of deck pour to the steel superstructure.

   iii) The concrete poured in the previous stage should be simulated to be composite with the steel superstructure. This is achieved by using the feature "Remove Forms". Removing the forms pertaining to the deck pour in the previous stage essentially activates the stiffness of the concrete deck poured in the previous stage. Apply the wet concrete load pertaining to the second stage of deck pour to the partially composite superstructure.

   iv) Remove the forms pertaining to the deck pour in the second stage, and apply the wet concrete pertaining to the second stage of deck pour to the partially composite superstructure.

e) The definition of composite dead load cases in CSiBridge consists of one stage: Activate the bridge structure consisting of the steel superstructure and the concrete deck. Apply a stiffness reduction factor of 1/3 to the concrete deck, to simulate

long-term stiffness of the composite bridge structure. Apply the dead load (barrier rail or wearing surface load) to the composite structure.

f) Aspects of live load modeling in CSiBridge are described in Section 4.2.5. The short-term stiffness of the concrete deck is used in live load analyses. To simulate short-term stiffness, the stiffness of the bridge structure does not need to be modified.

5. Building the LGA analysis model:
   a) Aspects of LGA modeling in LRFD Simon are described in Sections 4.1.2.
   b) Calculation of steel and concrete dead loads is described in are applied to the noncomposite girder by LRFD Simon.
   c) The barrier rail dead load and the wearing surface loads are distributed in the ratios of total lengths of each girder. These loads are applied to the composite girder. Tributary width is the effective width of each girder, as per AASHTO LRFD Specification. The long-term stiffness of the concrete deck is used in used in calculating the properties of the composite girder.
   d) The short-term stiffness is used in calculating the properties of the composite girder, for live load analysis.
6. 3D FEA and LGA and extracting results:
   a) The 3D FEA model is analyzed and the following results are extracted:
      i) Bending moments and shear forces for each load case separately for all girders exported from the CSiBridge interface in the form of excel sheets.
      ii) Displacements and rotations for each load case separately for all girders exported from the CSiBridge interface in the form of excel sheets.

iii) Bearing reactions for each load case exported from the CSiBridge interface in the form of excel sheets.

iv) Bearing displacements for each load case exported from the CSiBridge interface in the form of excel sheets.

v) Cross-frame forces from CSiBridge extracted using an excel VBA script. The excel file is named "VBA Code" and is used in generating bridge appendices as explained later.

b) Girder LGA models for each bridge are analyzed and the following results are extracted: Bending moments, shear forces, vertical displacements and reactions obtained from LRFD Simon files and processed in an excel sheet for each girder.

c) An excel file named "Consolidated Results" assembles results of bending moments and shear forces from 3D FEA for all load cases, for the girders to be studied. Plots for stresses in the top and bottom flanges of each girder are generated. Additionally, fatigue results from LRFD Simon results are obtained and comparison plots for fatigue stress range for girders are plotted.

d) An excel file named "Consolidated Displacements" assembles results of vertical displacements, layover displacements, twist rotations and normalized twist rotations from 3D FEA for all load cases, for the girders to be studied.

e) An excel file named "Comparison 1D vs 3D" assembles LGA and 3D FEA results described in b), c) and d) above. Comparison plots for bending moments, vertical shear forces and vertical displacements are developed. Additionally, data from LGA and 3D FEA results is further processed to calculate ε_{mean}, ε_{max}, layovers and LLDFs.

f) An excel file named “Consolidated Reactions” assembles results of bearing reactions from 3D FEA and LGA. Comparison bar charts for vertical reactions, as well as bar charts showing lateral bearing displacements from 3D FEA are developed.

g) Finally, all of these plots are collected and organized in the order mentioned in Table 11, in a file named “Bridge Appendix”. A pdf developed from this excel file constitutes the appendix section for each bridge.

The processed results in the appendices are further evaluated to develop recommendations for application of LGA for straight skewed bridges having skew index approaching 0.3. CHAPTER 5 describes the synthesis and evaluation of these processed results from LGA and 3D FEA, to develop recommendations for application of LGA.

CHAPTER 5. RECOMMENDED DESIGN GUIDELINES AND DETAILED DISCUSSION OF RESULTS

5.1 Organization of this Chapter

This chapter presents the results from the evaluation and comparison of a wider range of LGA and 3D FEA calculations important to steel I-girder bridge design.

Key responses discussed are:

1. The girder STR I major-axis bending moments
2. The girder STR I vertical shear forces.
3. The girder live load shear forces, focusing in particular on the live load shear forces at the obtuse corners of the bridge spans.
4. The girder STR I bearing reactions.
5. The girder maximum total dead load vertical displacements, including consideration of the effects of Steel Dead Load Fit (SDLF) detailing of the cross-frames.
6. The girder concrete dead load maximum vertical displacements, considering both staged and unstaged deck placement.
7. The girder layovers under the total dead load, which for SDLF detailing of the cross-frames is equal to the girder layovers under the concrete dead load. This is because the layovers are approximately zero under the steel dead load when SDLF detailing is employed. (These responses are estimated indirectly from the LGA results using equations recommended by FDOT; since the calculations are

relatively straightforward, simple, and based fundamentally on structural mechanics, they are considered as a part of the LGA calculations in this work.)

8. The girder fatigue live load vertical shear forces.
9. The girder fatigue live load flexural stresses.

Section 5.2 first summarizes (1) the specific LGA calculation procedures recommended based on this research, (2) the bridge characteristics required for application of these procedures (i.e., the limits of applicability of the recommended LGA procedures). This section then discusses the specific measurement of the differences between the LGA and 3D FEA results upon which the recommended procedures are based. The bridges from the parametric study satisfying the stated requirements are then listed, and key attributes of these bridges are highlighted. Lastly, the bridges from the parametric study that do not satisfy the stated requirements are listed and the requirements they violate are summarized.

Section 5.3 focuses on detailed comparisons between the LGA and 3D FEA results, considering each of the key bridge responses listed above.

Section 5.4 provides a summary of the various results and findings of the studies and presents conclusions based on it.

5.2 Recommendations for Application of LGA

Section 5.2.1 summarizes the specific LGA-based calculation procedures recommended based on this research. Section 5.2.2 then lists and discusses the bridge characteristics required for application of these procedures (i.e., the limits of applicability of the recommended LGA procedures). Section 5.2.3 discusses the specific measurement

of the differences between the LGA and 3D FEA results upon which the recommended procedures are based. Specific comparisons between the LGA and 3D FEA results are presented in Section 5.3. Section 5.2.4 lists the bridges from the parametric study satisfying the stated requirements, and highlights the key attributes of these bridges. Lastly, this section lists the bridges from the parametric study that do not satisfy the stated requirements and summarizes the requirements they violate.

5.2.1 Recommended LGA-Based Procedure

The LGA-based procedures recommended in this research involve routine LGA calculations, as implemented in the LRFD Simon software (NSBA, 2019), as well as the following specific practices and/or adjustments to obtain complete estimates of the forces necessary for design:

1. Distribute the miscellaneous steel dead loads, cross-frame steel dead loads, concrete dead load, rail loads (i.e., barrier loads), and wearing surface and utility loads equally as line loads to all the girders.
2. Employ the FDOT procedures for calculation of girder layovers. These procedures are summarized below in Section 5.2.1.2.
3. Increase the calculated STR I girder vertical reactions at the obtuse corners of bridge simple spans, and at the fascia girders in continuous spans, by a multiplicative factor of 1.15. The background to this factor is summarized in Section 5.2.1.3.
4. Increase the live load shears in the fascia girders from the AASHTO fatigue truck loading by a multiplicative factor of 1.15. This factor may be varied linearly from

this maximum value, at the obtuse corners of the bridge spans, to 1.0 at the mid-spans, similar to the variation in the AASHTO LRFD skew correction factor. The background to this factor is summarized in Section 5.2.1.4.

5. Employ the AASHTO LRFD Article C6.10.1 recommendations for estimating the girder flange lateral bending stresses, with recommended minor modifications/simplifications (see Section 5.2.1.5).
6. In addition to satisfying the base AASHTO LRFD requirements for design of cross-frames and diaphragms, including the consideration of wind load forces, forces from overhang loads during construction, etc., design for the DC1 + DC2, DW and LL cross-frame and diaphragm forces specified below (in Section 5.2.1.6) as a minimum using the appropriate LRFD load combinations.

The detailed considerations associated with these calculations are discussed below.

5.2.1.1 Distribution of Dead Loads

The dead loads are calculated as described in Section 2.5.1. For all the bridges considered in the parametric studies, all the dead loads are distributed equally to all the girders.

5.2.1.2 Calculation of Girder Layovers

Florida DOT (FDOT, 2018) recommends an estimation of the maximum girder layovers at simply-supported girder bearing lines based on the girder vertical deflections from LGA and a fundamental application of compatibility of deformations. The girder layover is defined as the lateral displacement of its top flange relative to its bottom flange as shown in Figure 48.

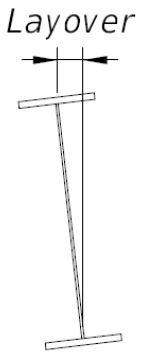

Figure 48. Definition of girder layover.

The steps of the FDOT procedure are as follows:

1. For bridges employing Steel Dead Load Fit (SDLF) detailing of the cross-frames, the layover under the full steel dead load is taken equal to zero. This recognizes that SDLF detailing results in the girder webs being approximately plumb under the full steel dead load.
2. The girder layover at the completion of the deck placement is of primary interest. This layover is calculated by first estimating the girder major-axis bending rotation α, due to the concrete dead load (CDL) associated with the bridge deck self-weight. If this rotation is provided directly by the LGA software, then it is recommended to use the provided value. Alternatively, given the associated CDL vertical displacement at the girder 1/10th point within the span, $\delta_{0.1Ls}$, the girder major-axis bending rotation may be estimated as

$$\alpha = \frac{\delta_{0.1L_s}}{0.1L_s} \tag{16}$$

in radians, where L_s is the span length. This estimate is based on the assumption that α is sufficiently small such that $\alpha \cong \tan(\alpha) \cong \sin(\alpha)$, which is the case for any practical bridge girder end rotations. This estimate is employed with the 1/10 point deflections obtained from LRFD Simon in this research.

3. Another potential estimate is

$$\alpha = \frac{3.2\delta_{\max}}{L_s} \tag{17}$$

where δ_{max} is the maximum CDL girder deflection within the span. This is based on the assumption of a simply-supported prismatic girder loaded by a constant uniformly distributed load. This estimate is not recommended unless the prismatic simply-supported condition is approximately satisfied.

4. Given the girder major-axis bending rotation, α, and the assumption that the cross-frame deformations are small enough such that the cross-frames may be modeled as rigid diaphragms within their own plane, compatibility of deformations between the girders and the cross-frames requires that the girders must twist by an angle

$$\phi = \alpha \tan(\theta) \tag{18}$$

in radians, where θ is the skew angle of the bearing line, equal to zero when the bearing line is perpendicular to the longitudinal axis of the girders.

5. Given the girder twist angle under the CDL, the corresponding layover at the top flange of the girder may be estimated as

$$Layover = D\phi \tag{19}$$

where D is the girder web depth. Similar to the above assumptions for α, this calculation is based on the assumption that ϕ is a small enough angle such that $\phi \cong \tan(\phi) \cong \sin(\phi)$.

5.2.1.3 Calculation of Strength I Girder Vertical Reactions

The STR I reactions from 3D FEA at the bearings on the fascia girders corresponding to obtuse corners of simple spans, and all the bearings on the fascia girders of continuous-span bridges, tend to be significantly larger in many of the bridges that qualify for LGA, compared to the corresponding LGA reactions. This occurs both at end abutments and at pier bearing lines in continuous-span bridges, since the intermediate bearings correspond to an obtuse corner on one of the spans and an acute corner on the other span on both sides of the bridge cross-section. This is due to the tendency to develop a transverse load path in the short direction between the obtuse corners of the span in parallel skew bridges. In addition, the torsional moment induced in the girders by the bearing-line cross-frames forcing a twist (i.e., layover) into the fascia girder tends to increase the end reaction on the fascia girder at the obtuse corner the spans. Based on the bridges studied in this research, it is determined that the STR I bearing reaction on the fascia girder can be predicted accurately to conservatively in all cases, where LGA is permitted, by multiplying the corresponding reaction from LGA, for the fascia girder at the obtuse corners of simple

spans, and at all the bearings in continuous spans, by a factor of 1.15. It should be noted that no modifications are required for the other girder reactions. In addition, it should be noted that even after multiplying the fascia girder reactions by this factor, the largest reaction may still occur at a location other than the fascia girder.

5.2.1.4 Calculation of Fascia Girder Live Load Shears from the AASHTO Fatigue Truck Loading

The results of the research studies indicate that the fascia girder live load shear forces due to the fatigue truck loading generally tend to be underpredicted by LGA in the vicinity of the span obtuse corners. The underlying causes of this behavior are similar to those discussed above for the girder bearing reactions. Based on the bridges studied in this research, it is determined that the live load shear forces on the fascia girder from the AASHTO Fatigue Truck loading can be predicted accurately to conservatively in all cases where LGA is permitted by multiplying the corresponding forces from LGA, for the fascia girders at the obtuse corners of the spans, by a factor of 1.15. This multiplicative factor is in addition to the application of the skew correction factor of AASHTO LRFD Article 4.6.2.2.3c.

It should be noted that the STR I girder shear forces are predicted adequately by the standard AASHTO LRFD procedures, including the LRFD Article 4.6.2.2.3c skew correction factor for the live load shears, for the bridges where LGA is permitted. It appears that the skew correction for the distribution of the AASHTO HL93 live load is different than that for the AASHTO fatigue truck loading.

5.2.1.5 Estimation of Girder Flange Lateral Bending Stresses

In straight skewed bridges, intermediate cross-frames framed perpendicular to the girders connect to the girders at different longitudinal positions within the span. This results in twisting of the girders to maintain compatibility of the girder and cross-frame displacements and rotations. This twisting of the girders produces cross-frame forces and girder flange lateral bending stresses.

AASHTO LRFD Article 6.7.4.2 recommends generous offsets between the intermediate cross-frames and the bearing lines, and generous staggers between the cross-frames within the span, to soften the transverse load path in skewed I-girder bridges. Generous offsets and staggers tend to increase the girder flange lateral bending stresses in most situations, while reducing the magnitude of the cross-frame forces due to the softening of the transverse load path. The cross-frame staggers interrupt and reduce the stiffness of the transverse load path by forcing load transfer via girder flange lateral bending.

In steel girder bridges where the cross-frames are detailed for Steel Dead Load Fit (SDLF), the girder flange lateral bending stresses and the cross-frame forces are theoretically zero under the steel dead load. However, significant flange lateral bending stresses can be induced by other dead loads and by live load effects. The girder top flanges need to be checked considering flange lateral bending when the girders are in their noncomposite condition during construction; however, AASHTO LRFD does not require any further consideration of flange lateral bending in the top flanges once the bridge is in its final composite condition.

Significant girder flange lateral bending stresses may be caused generally by wind, and by torsion from eccentric concrete deck overhang loads acting on cantilever forming brackets placed along fascia girders during construction. In addition, significant girder flange lateral bending can be caused by the above interactions between the cross-frames and the girders in resisting the dead load effects.

Article C6.10.1 provides the following rules for a simple upper-bound estimate of the girder flange lateral bending stresses from the interactions between the cross-frames and the girders in resisting the gravity load effects, when LGA is employed:

1. The total unfactored flange lateral bending stress in a girder flange at a cross-frame or diaphragm, when discontinuous (e.g., staggered) cross-frames or diaphragms are used at or near supports, may be taken as:
    a. 7.5 ksi for exterior girders
    b. 10 ksi for interior girders

    These values are intended as estimates at discontinuous cross-frame lines at or near supports, but not along the entire length of the bridge.
2. In regions of the girders with contiguous cross-frames or diaphragms, these values need not be considered. That is, the flange lateral bending stresses may be taken equal to zero in these regions.
3. The total unfactored flange lateral bending stress in a girder flange, when cross-frames or diaphragms are placed in discontinuous lines (e.g., staggered) throughout the bridge span, may be taken as:
    a. 2.0 ksi for exterior girders.
    b. 10 ksi for interior girders.

It is expected that the reduced flange lateral bending stresses in the exterior girders in these cases are due to the reduced cross-frame or diaphragm forces associated with the interaction between the girders and cross-frames in resisting the vertical (gravity) loads. However, in this research, it is seen that the maximum STR I flange lateral bending stresses in the bottom flange occur at the first intermediate cross-frame in the vicinity of the obtuse corners in bridge spans, which have a contiguous cross-frame arrangement. In most of these cases, the flange lateral bending stresses are larger than the stresses caused by eccentric overhang bracket loads. Hence, it is suggested that the recommendation 3 above for total unfactored flange lateral bending stress in an exterior girder flange be modified as follows:

The total unfactored flange lateral bending stress in a girder flange, when cross-frames or diaphragms are placed in discontinuous lines (e.g., staggered) throughout the bridge span, may be taken as:

a) 7.5 ksi for exterior girders
b) 10 ksi for interior girders

In all of the above cases, AASHTO LRFD Article C6.10.1 recommends that the unfactored values of the flange lateral bending stresses be apportioned to the dead and live load in the same proportion as the unfactored major-axis dead and live load stresses at the girder cross-section under consideration. In this research, it is recommended that a weighted average load factor of 1.6 be assumed in all cases when checking the STR I limit state. As such, the above values are multiplied by 1.6 to determine the upper-bound estimates of the factored flange lateral bending stresses for STR I load combinations. The above stress estimates are extremely coarse values. It is not appropriate to require the

designer to perform large numbers of tedious calculations implying high precision with these estimates, or to imply that the apportionment of these stresses to the different load cases is somehow tied in some precise way to the flexural stresses in the girders at the cross-frame location. Table 2 lists the recommended weighted average load factors for the STR I load combination as well as other load combinations.

These estimated flange lateral bending stresses are to be combined with the flange lateral bending stresses due to other effects. That is, these factored stresses must be calculated separately and added to the appropriate factored stresses from wind, eccentric overhang bracket loads, etc. according to the AASHTO LRFD load combination rules. The recommendations provided in this section only address the calculation of the girder flange lateral bending stresses due to skew effects.

Table 12. Weighted average load factors for AASHTO LRFD Article C6.10.1 estimation of girder flange lateral bending stresses.

Load Combination Limit State	Weighted Average Load Factor Applied to Article C6.10.1 Coarse Estimate of f_ℓ
Strength I	1.6
Strength II	1.3
Strength III	1.25
Strength IV	1.25
Strength V	1.3
Extreme Event I	1.0, γ_p
Extreme Event II	0.7
Service I	1.0
Service II	1.2
Fatigue I	1.75
Fatigue II	0.8

5.2.1.6 Estimation of Cross-Frame of Diaphragm Forces

Similar to girder flange lateral bending stresses, there is no direct way of estimating the cross-frame forces associated with the interactions between the cross-frames and the girders in resisting the dead load effects when LGA is employed. AASHTO LRFD (AASHTO 2017) presently does not provide any guidance for the estimation of the cross-frame forces considering these actions.

Table 13 provides upper-bound estimates of the cross-frame DC1+DC2 (component dead load), DW (wearing surface and utilities) and LL (vehicular live load) member forces (axial force or total cross-frame shear force) due to these dead load effects for bridges that

satisfy the specified requirements for application of LGA, determined from the bridge studies conducted in this research. The upper-bound STR I forces determined from this research are listed in the second to last column. The last column lists the controlling bridge corresponding to the upper-bound STR I cross-frame force. These forces are to be considered as either tension or compression, or positive or negative, in determining the load demands on the cross-frame members. To determine the cross-frame diagonal axial forces, the total cross-frame shears should be apportioned to the individual diagonals as appropriate (equal apportionment for X type cross-frames, and apportionment to a single diagonal for v or inverted-v type cross-frames, and the diagonal axial forces should then be calculated by considering the total shear as one component of the diagonal axial force. In addition, similar to the estimation of the girder flange lateral bending stresses discussed in Section 5.2.1.5, these forces are to be combined with the cross-frame forces determined due to other effects (e.g., wind, eccentric overhang bracket loads, etc.) according to the AASHTO LRFD load combination rules. One can observe that if the DC1+DC2, DW and LL upper-bound estimates are combined using the respective STR I load factors 1.25, 1.50 and 1.75, significantly larger forces are obtained compared to the STR I bounded values. This is because (1) the maximum values for the different load cases do not necessarily occur in the same cross-frame member, and (2) the actual cross-frame forces due to the specific load effects may be of opposite sign at the cross-frame member experiencing the maximum demand under the STR I load combination.

It should be emphasized that the above forces are upper-bound values obtained considering the bridges evaluated in this research and for which LGA is permitted based on the requirements of Section 5.2.2. The actual force demands in a large number of the

cross-frames generally will tend to be significantly smaller than these values. This is the case in general for typical cross-frame design. That is, even if 3D FEA is employed to obtain the cross-frame force demands, one set of cross-frame member sizes will often be selected for the intermediate and the bearing line cross-frames, providing the benefits of repetition of member sizes in the cross-frame fabrication.

Table 13. Upper-bound cross-frame forces, in kips, associated with the interaction between the cross-frames in the girders in resisting vertical loads, applicable for bridges in which LGA is permitted considering the requirements of Section 5.2.2.

Cross-frame (CF) Component Force	DC1+DC2	DW	LL	STR I	Bridge corresponding to STR I CF Force
Intermediate CF Bottom Chord Axial Force	38	3	77	137	22
Intermediate CF/Diaphragm Shear Force	23	1	32	62	17
Intermediate CF Top Chord Axial Force	29	1	34	51	8
Bearing Line CF Bottom Chord Axial Force	17	2	62	128	11
Bearing Line CF/Diaphragm Shear Force	14	1	18	38	22
Bearing Line CF Top Chord Axial Force	17	2	19	40	4

5.2.2 Bridge Characteristics Required for Application of the Recommended LGA Procedures

The recommended LGA procedures detailed in Section 2.1 are subject to the following requirements, or limits of applicability:

1. Straight bridges with parallel skew, or with adjacent bearing line skew angles throughout the bridge differing by less than or equal to 10°.
2. Constant girder spacing along the bridge length (no splay of the girders).
3. Equal spacing between the girders across the bridge width.
4. Deck overhang width from 25 to 45 % of the girder spacing.
5. Bridge framing width, 40 ft < w_g < 130 ft.
6. Cross-frame and/or diaphragm spacing, L_b < 25 ft.
7. Concentrated line loads at the edges of the deck, such as barrier rail loads, less than or equal to 625 plf.
8. In unbraced lengths containing steps in the flanges, smallest flange lateral moment of inertia greater than or equal to one-half of the largest flange lateral moment of inertia within the unbraced length.
9. Ratio of web depth to the width of the girder flanges, D/b_f < 4.5.
10. All cross-frames have top and bottom chords.
11. Cross-frames detailed for steel dead load fit (SDLF).
12. For I_s < 0.3, first intermediate cross-frames or diaphragms offset by a minimum of $4b_f$ from the support, where b_f is the largest girder flange width within the unbraced lengths on either side of the cross-frame or diaphragm under consideration.

13. For $0.3 < I_s < 0.4$, the above offset requirement for the first intermediate cross-frames or diaphragms, plus use of a staggered cross-frame arrangement within the bridge spans in which all girder unbraced lengths between intermediate diaphragms or cross-frame locations are greater than or equal to $4b_f$, where b_f is the largest girder flange width within the unbraced length.
14. If the above offset requirement relative to the support results in an excessive unbraced length on the fascia girder at an acute corner, a cross-frame with top and bottom chords and no diagonal members can be framed from the first interior girder to the fascia girder at a smaller offset from the support.

The following is a commentary on these requirements:

Regarding items 1 through 3, the parametric study bridges having nonparallel skew, splay, and/or non-equal spacing of the girders have noticeably larger differences between the LGA and 3D FEA results, as discussed further in Section 5.3, with the exception of Bridge 22, which has adjacent cross-frame lines that are within 4° of one another.

Items 4 through 6 are largely based on the limits of the parametric study.

Item 7 relates to differences between LGA and 3D FEA results pertaining to the distribution of concentrated line loads at the edge of the deck to the various girders within the bridge cross-section. Results from the parametric studies commonly show that the assumption of uniform distribution of the barrier rail loads to all the girders across the bridge cross-section differs substantially from the 3D FEA predictions for these specific loads. However, the barrier rail loads considered in the parametric studies (430 plf) produce relatively small moments compared to the other bridge loadings. Therefore, the significant

approximation of equal distribution of the barrier rail loads to all the girders is relatively inconsequential in the bridges considered. The 625 plf limit stated in Item 7 accommodates larger concrete barrier rails, and is based on the judgement of the project team, given the parametric results with 430 plf barrier rail loads.

Item 8 is based on the results from one of the FDOT bridges studied, Bridge 15, in which there is a sharp spike in the girder flange lateral bending stresses in one of the girder unbraced lengths. This sharp spike is due to an extreme change in one of the girder flange widths. The AASHTO LRFD Article C6.10.8.2.3 provisions suggest simplifications in the evaluation of lateral-torsional buckling of girders with steps in the flange sizes when the change in the flange lateral bending moments of inertia are no larger than a factor of two at the flange steps. Item 8 is a practical generalization of this AASHTO LRFD requirement.

Item 9 relates most directly to the estimation of the girder flange lateral bending stresses. The recommended D/b_f limit is based on the largest corresponding ratio for the bridges considered in the parametric studies. AASHTO LRFD Article C6.10.1 states that its estimates "are based on a limited examination of refined analysis results for bridges with skews approaching 60° from normal and an average D/b_f ratio of approximately 4.0. Girders with larger D/b_f values will tend to have larger flange lateral bending stresses due to various effects, although for a given girder web depth, smaller b_f tends to give smaller girder torsional stiffness.

Regarding Item 10, although the use of X-type cross-frames without top chords can be an effective way to soften the bridge transverse stiffness for noncomposite loadings, use of V-type cross-frames without top chords introduces a significant loss of cross-frame flexural

stiffness prior to the bridge deck becoming composite (White et al., 2012). All of the bridges considered in the parametric studies have top and bottom chords at the cross-frames. This practice tends to result in smaller cross-frame bottom chord forces.

All of the bridges were assumed to have cross-frames detailed for Steel Dead Load Fit (SDLF) in the project parametric studies. SDLF detailing is an appropriate option for skewed I-girder bridges. This practice results in girders that are approximately plumb at the completion of the steel erection. In addition, the girder flange lateral bending stresses and the cross-frame forces are effectively negligible under the steel self-weight when this detailing practice is employed. SDLF detailing effectively forces the bridge to respond in a manner close to the LGA approximation under the steel self-weight. No-load fit (NLF) detailing of the cross-frames is not recommended for bridges with significant skew of their bearing lines since the girders will layover at these bearing lines under the steel dead load in a manner related to the Concrete Dead Load layovers discussed in Section 5.2.1.2. Also, the girder flange lateral bending stresses and the cross-frame forces are generally significant under the steel dead load if the cross-frames are detailed for NLF.

In some situations, Total Dead Load Fit (TDLF) may be specified, although TDLF is not permitted by FDOT without approval from the Structures Design Office (FDOT, 2019a). The recommended LGA procedures are considered applicable for TDLF detailing of the cross-frames. The girder webs will be approximately plumb, and the total dead load girder flange lateral bending stresses and cross-frame forces will be relatively small when TDLF detailing is employed. Therefore, the girder flange lateral bending estimates discussed in Section 5.2.1.5 and the cross-frame force estimates discussed in Section 5.2.1.6 will tend to be more conservative if TDLF detailing is employed. It should be noted, however, that

TDLF tends to increase the cross-frame forces, girder flange lateral bending stresses, and general fit-up forces within the bridge system during the steel erection stage, compared to SDLF (White et al., 2015; NSBA 2016).

Requirement 12 is necessary to avoid stiff transverse load paths to the bearing lines, resulting in larger cross-frame forces. Development of a stiff transverse load path due to inadequate offsets is seen in Bridge 25, which has noticeably larger differences between the LGA and 3D FEA TDL (SDLF) vertical displacements and large flange lateral bending stresses. Bridges 6 and 17, on the other hand, have offsets that are slightly lower than the recommended limit of $4b_f$, but satisfy all the other required limits for the application of LGA. LGA results are within the tolerances established in Section 5.2.3. Moreover, Bridge 6 has unequal girder spacings. Hence, although Bridges 6 and 17 violate requirement 12, these bridge are taken as exceptions and are considered in the different presentations and evaluations to satisfy the requirements of LGA. Similarly, Bridge 11 has cross-frames along the skewed bearing lines and intermediate cross-frames framing into the bearings, but satisfies all other requirements of LGA. Therefore, Bridge 11 is also considered to satisfy the requirements of LGA. Similarly, the flange lateral bending stress of the central interior girder of Bridge 8 is larger than the AASHTO recommendations, and is considered an exception.

Bridge 5 has a skew index larger than 0.4 with contiguous intermediate cross-frame lines. This bridge satisfies all the requirements of LGA. However, Bridge 5 is considered to be an exception, and as such, Requirement 13 is recommended based on the behavior of other parametric study bridges that have skew indices larger than 0.3.

The Item 14 note avoids this stiff load path effect at acute corners in bridges having significant skew of the corresponding bearing line, and where a cross-frame close to the bearing on the first interior girder may be needed to reduce the lateral unbraced length on the fascia girder at the acute corner.

Requirement 14, or other means such as the use of lean-on bracing systems, is necessary to alleviate stiff transverse load path effect, and corresponding larger cross-frame forces, in bridges with a larger skew index. The use of cross-frame staggers and offsets throughout the bridge plan can be an effective strategy to reduce the overall number of cross-frames in the bridge while concomitantly reducing the forces the cross-frames need to be designed for.

The recommended LGA procedures are useable for bridges with skew indices up to 0.4 as long as a cross-frame framing arrangement is specified that will alleviate large transverse force effects.

5.2.3 Measurement of Differences between LGA and 3D FEA

The recommended LGA procedures discussed in Section 5.2.1, and the requirements that need to be satisfied for the use of these procedures discussed in Section 5.2.2 are based on the following measures of the differences between the calculation results:

1. Professional factor ρmax no larger than 1.11 in all cases for the following responses:
    a. Girder STR I positive major-axis bending moments.
    b. Girder STR I negative major-axis bending moments.

c. Girder STR I positive shear forces.
d. Girder STR I negative shear forces (the maximum negative shear forces commonly occur at opposite end of the girder spans from the maximum positive shear forces).
e. Girder STR I bearing reactions.
f. Girder fatigue live load vertical shear ranges.
g. Girder fatigue live load flexural stress ranges at locations subjected to net tension stresses.

where the professional factor is defined as

$$\rho_{\max} = \frac{\left|3DFEA\right|_{\max}}{\left|LGA\right|_{\max}} \tag{20}$$

$\left|3DFEA\right|_{\max}$ = girder maximum 3D FEA response throughout the bridge length

$\left|LGA\right|_{\max}$ = girder maximum LGA response throughout the bridge length

The professional factor is commonly employed in structural reliability analysis, where the numerator of this ratio is typically the measured strength of a structural component, and the denominator is the predicted strength using a selected engineering approximation. For cases where ρmax is greater than 1.0, this factor gives the ratio by which the approximate calculation would need to be scaled to ensure an accurate prediction of the measured strength. In this work, $\left|3DFEA\right|_{\max}$ and $\left|LGA\right|_{\max}$ are the maximum calculated demands obtained from the benchmark 3D FEA calculations and the demands calculated by the selected LGA analysis approximation.

In the bridge appendices generated in the studies, the accuracy of the LGA solutions are provided for many of the above quantities in terms of the measure

$$\varepsilon_{\max 1} = \frac{\left|LGA\right|_{\max} - \left|3DFEA\right|_{\max}}{\left|3DFEA\right|_{\max}} \tag{21}$$

The above two difference measures are related as follows. Given a value for ρmax, one can calculate

$$\varepsilon_{\max 1} = \frac{1}{\rho_{\max}} - 1 \tag{22}$$

Conversely, given a value for ε_{max1}, the professional factor may be calculated as

$$\rho_{\max} = \frac{1}{\varepsilon_{\max 1} + 1} \tag{23}$$

Therefore, $\rho_{max} = 1.11$ corresponds to an "unconservative" difference of LGA relative to 3D FEA of $\varepsilon_{max1} = -0.10$.

The selection of $\varepsilon_{max1} = -0.10$ as an acceptable tolerance for evaluation of the differences between the LGA and 3D FEA for the above responses is of course subjective. The fact of the matter is that finite differences between the LGA and 3D FEA responses, some being "unconservative," can occur even for a straight I-girder bridge with zero skew. The value of $\varepsilon_{max1} = -0.10$ is selected as a value for which the overall impact on any reduction in the bridge structural reliability

is relatively small. Specifically, the influence of $\varepsilon_{max1} = -0.10$, or $\rho_{max} = 1.11$ is approximately two times the impact on the structural reliability by variations in the load modifier η_i in Article 1.3.2.1 of AASHTO LRFD.

2. A normalized difference $\varepsilon_{max\,2} < 0.0005$ in all cases for the girder total dead load vertical displacements, including the consideration of the effects of steel dead load fit (SDLF) detailing of the cross-frames, where

$$\varepsilon_{max\,2} = \frac{\left(\Delta_{LGA}\right)_{max} - \left(\Delta_{3DFEA}\right)_{max}}{L_s} \tag{24}$$

$\left(\Delta_{LGA}\right)_{max}$ = girder maximum total dead load vertical deflection from LGA, downward deflections taken as negative

$\left(\Delta_{3DFEA}\right)_{max}$ = girder maximum total dead load vertical deflection from 3DFEA, downward deflections taken as negative

This normalized difference is considered to be a more appropriate measure than ρmax when comparing the LGA total dead load vertical displacement predictions to corresponding 3D FEA values. This is because the ρmax values for the LGA total dead load vertical displacement predictions can be larger than 1.11 and smaller than 0.91 (i.e., $\varepsilon_{max1} < -0.10$ or > 0.10). However, depending on the span length, these differences may acceptable. The limit of 0.0005 on $\varepsilon_{max\,2}$ can be related indirectly to typical tolerances on the roadway smoothness, as discussed below.

The girder total dead load (TDL) displacements are used in setting girder cambers. A significant portion of the girder cambers is "taken out" by the girder vertical deflections during the casting of the deck. Thus, approximations in the TDL displacements can ultimately have some influence on the smoothness of the finished deck. Although the smoothness tolerances of the finished deck surface are not directly related to the differences between LGA and 3D FEA, the smoothness tolerances can be used as an assessment of the differences between LGA and 3D FEA in the prediction of the girder TDL displacements.

Deck smoothness tolerances are provided in Section 400-15.2.5.5 of the FDOT Specifications (FDOT, 2019b). This section states the following limit for deviations in the finished deck elevation, measured using a profilograph, longitudinally along the length of the bridge:

"Correct individual bumps or depressions exceeding a cutoff height of 0.3 inch from a chord of 25 feet (see ASTM E1274) on the profilograph trace."

A deviation of 0.3 inch per 25 feet comes out to a limit of 1/1000. Recognizing that the maximum displacement approximately occurs at the mid-span of the girders, and considering an extension of the deck smoothness limit to vertical deviations along the length of the girders due to approximations from the structural analysis, a similar longitudinal "tolerance" on the deviation between the LGA and 3D FEA vertical displacements can be set as $\frac{L_s / 2}{1000} = \frac{L_s}{2000}$, where L_s is the span length.

The tolerance of 0.0005 on ε_{max2} can also be related to the positive camber tolerance of 1.5 inches on a welded girder given in Section 3.5.1.3 of (AWS, 2019a). For a span length of 250 ft, $1.5in / 250\,ft / (12in / ft) = 0.0005$.

3. A normalized difference $\varepsilon_{max3} < 0.001$ in all cases for the girder total dead load vertical displacements, including the consideration of the effects of steel dead load fit (SDLF) detailing of the cross-frame, where

$$\varepsilon_{\max 3} = \max\left\{\begin{array}{l}\dfrac{\left|\left[\left(\Delta_{LGA}\right)_{\max} - \left(\Delta_{3DFEA}\right)_{\max}\right]_{G3} - \left[\left(\Delta_{LGA}\right)_{\max} - \left(\Delta_{3DFEA}\right)_{\max}\right]_{G1}\right|}{w_g}, \\ \dfrac{\left|\left[\left(\Delta_{LGA}\right)_{\max} - \left(\Delta_{3DFEA}\right)_{\max}\right]_{G3} - \left[\left(\Delta_{LGA}\right)_{\max} - \left(\Delta_{3DFEA}\right)_{\max}\right]_{G4}\right|}{w_g}\end{array}\right\} \quad (25)$$

$\left[\left(\Delta_{LGA}\right)_{\max} - \left(\Delta_{3DFEA}\right)_{\max}\right]_{G3}$ = difference between the maximum LGA and 3D FEA displacements for the girder closest to the mid-width of the bridge cross-section.

$\left[\left(\Delta_{LGA}\right)_{\max} - \left(\Delta_{3DFEA}\right)_{\max}\right]_{G1}$ = difference between the maximum LGA and 3D FEA displacements for fascia girder G1.

$\left[\left(\Delta_{LGA}\right)_{\max} - \left(\Delta_{3DFEA}\right)_{\max}\right]_{G3}$ = difference between the maximum LGA and 3D FEA displacements for the other fascia girder, which is labeled as G4 (irrespective of the total number of girders in the bridge cross-section).

w_g = width of the bridge between the fascia girders

Clearly, this measure relates to the difference between the LGA and 3D FEA girder vertical displacements and its variation across the bridge cross-section

width. The limit of 0.001 on this measure can be related indirectly to a second deck smoothness tolerance provided in Section 400-15.2.5.5 of the FDOT Specifications (FDOT, 2019b):

"Ensure that the surface meets a ¼ inch in 10 feet straightedge check made transversely across the deck."

A transverse deviation of 1/4 inch per 10 feet translates to a limit of 1/480, which rounds to 1/500. Recognizing that cross-slopes are generally built across the deck from the median at the center of the bridge to the two transverse edges of the bridge, and considering an extension of the deck smoothness limit to vertical deviations along the length of the girders due to approximations from the structural analysis, a similar transverse "tolerance" on the deviation between the LGA and 3D FEA vertical displacements can be set as $(w_g/2)/500 = w_g/1000$, where w_g is the bridge framing width.

4. Lastly, a maximum difference between LGA estimates of the girder layovers at the simply-supported ends of the bridge under the total dead load, including the consideration of the effects of steel dead load fit (SDLF) detailing of the cross-frames, and the corresponding 3D FEA values, εmax4, less than or equal to 0.25 inches, where

$$\varepsilon_{\max 4} = \left|\left(\Delta_l\right)_{LGA} - \left(\Delta_l\right)_{3DFEA}\right| \tag{26}$$

$\left(\Delta_l\right)_{LGA}$ = total dead load layover displacement at the girder top flange predicted using FDOT recommended calculations and the major-axis bending displacements from LGA, including the consideration of the effects of steel

dead load fit (SDLF) detailing of the cross-frames (girder steel dead load layovers taken equal to zero).

$(\Delta_l)_{3DFEA}$ = total dead load layover displacement at girder top flange obtained from 3D FEA solution, including the consideration of the effects of steel dead load fit (SDLF) detailing of the cross-frames (girder steel dead load layovers approximately equal to zero, based on 3D FEA calculations).

The rationale behind this measure is that the most meaningful parameter pertaining to girder layover is the physical layover itself, i.e., the lateral deflection at the top of the girders relative to the bearings at the simply-supported girder end bearing locations, and that 0.25 inches is a reasonable tolerance on this displacement coming from differences between LGA and 3D FEA solutions.

5.2.4 Summary of Parametric Study Bridges Satisfying and not Satisfying the Requirements for use of LGA

The parametric study bridges that satisfy the stated requirements for use of LGA, and some of their key attributes, are as follows:

- Bridge 4 (3 Alt): two-span continuous bridge; θ = 38.2° and I_s = 0.39; intermediate cross-frames have ample offsets from the bearing lines and have a staggered framing arrangement.
- Bridge 5: simple span bridge; θ = 29.4° and I_s = 0.42; contiguous intermediate cross-frame lines.

- Bridge 18: simple-span bridge; θ = 39.7° and I_s = 0.2; ample offsets and staggers of the intermediate cross-frames.
- Bridge 21: simple-span bridge; θ = 16.2° and I_s = 0.15; contiguous intermediate cross-frame lines arranged parallel to the skewed bearing lines.
- Bridge 26: two-span continuous bridge; θ = 10° and I_s = 0.15; contiguous intermediate cross-frame lines arranged parallel to the skewed bearing lines.

The following bridges come close to satisfying the specified requirements for use of LGA:

- Bridge 6: two-span continuous bridge; θ = 20.7° and I_s = 0.35; with contiguous intermediate cross-frame lines; offset from the bearing line less than $4b_f$ for a small number of the intermediate cross-frames; unequal girder spacing.
- Bridge 8: two-span continuous bridge; θ = 23.4° and I_s = 0.27; intermediate cross-frames arranged at very small offsets, resulting in a response that is nearly the same as a contiguous cross-frame framing arrangement parallel to the bearing lines.
- Bridge 11: cross-frames directly framed into the bearing line at the pier.
- Bridge 17: the offset from the bearing line is slightly less than $4b_f$ for a small number of the intermediate cross-frames. This bridge is a simple span with θ = 41.5° and I_s = 0.28. It has contiguous intermediate cross-frame lines with an offset relative to the abutment bearing lines.
- Bridge 22: nonparallel skew; however, the bearing lines are nearly parallel. This is a two-span continuous bridge with θ = 36.1, 32.1 and 28.4°, and I_s = 0.31. It has contiguous intermediate cross-frame lines with an offset relative to the abutment bearing lines as well as the pier bearing lines.

The bridges studied which do not satisfy the stated requirements, and the requirements they violate, are as follows:

- Bridge 1: skew index larger than 0.4 with contiguous intermediate cross-frame lines.
- Bridge 2: skew index larger than 0.4.
- Bridge 3: cross-frames frame into the bearing lines; skew index larger than 0.3 with contiguous intermediate cross-frame lines.
- Bridge 7: skew index larger than 0.3 with contiguous intermediate cross-frame lines; offset from the bearing line less than $4b_f$ for a small number of the intermediate cross-frames.
- Bridge 9: skew index larger than 0.4 with contiguous intermediate cross-frame lines; cross-frames directly framed into the bearing line at the pier.
- Bridge 10 (9 Alt): skew index larger than 0.4.
- Bridge 12: nonparallel skew; skew index larger than 0.3 with contiguous intermediate cross-frame lines; cross-frames framed directly into bearing lines at the piers.
- Bridge 13: nonparallel skew.
- Bridge 14 (13 Alt): nonparallel skew.
- Bridge 15: nonparallel skew; skew index larger than 0.3 with contiguous intermediate cross-frame lines; offset from the bearing line less than $4b_f$ for a small number of the intermediate cross-frames; smaller flange within an unbraced length having a flange transition has a lateral moment of inertia smaller than one-half of the moment of inertia of the larger flange within this unbraced length.

- Bridge 16 (15 Alt): nonparallel skew; smaller flange within an unbraced length having a flange transition has a lateral moment of inertia smaller than one-half of the moment of inertia of the larger flange within this unbraced length.
- Bridge 19: splayed girder bridge; skew index larger than 0.4 with contiguous intermediate cross-frame lines.
- Bridge 20: splayed girder bridge; skew index larger than 0.4.
- Bridge 23: skew index larger than 0.3 with contiguous intermediate cross-frame lines; cross-frames directly framed into the bearing line at the pier.
- Bridge 24: skew index larger than 0.3 with contiguous intermediate cross-frame lines.
- Bridge 25: offsets from the bearing lines less than $4b_f$ at the abutments; cross-frames framed directly into bearing line at the pier.

5.3 Discussion of the Results of the Parametric Study

5.3.1 Organization of the Discussion

This section presents detailed comparisons of the LGA and 3D FEA solutions from the project parametric studies. The structural behavior of a skewed bridge, is heavily influenced by a number of factors such as the bridge articulation (simple or continuous span), skew index, bridge width, type of skew (parallel or nonparallel skew), skew angle and the cross-frame layout. The behavior of skewed bridges can be explained as that of an orthotropic plate stiffened by cross-frames and diaphragms, delivering loads to the bearing lines. At an intermediate bearing line of a continuous-span bridge, the load path to the bearings from the adjacent spans is complex. The load distribution may occur from one span to another, especially in bridges with unequal spans, to maintain compatibility of the continuous girders within adjacent spans. Observations explaining this behavior are presented in Section 5.3.6. The longitudinal and transverse load paths within the bridge girders are influenced further by the nature of skew, parallel and nonparallel. A key distinction in parallel and nonparallel skew bridges is that all girders in a bridge with parallel skew have equal lengths within a span, whereas girders in a bridge with nonparallel skew have unequal lengths within a span. This affects the stiffness of each girder and influences the apportionment of loads among girders. Furthermore, the obtuse corners within a span in a nonparallel skew bridge may be located at adjacent ends or at the two ends of the shorter diagonal depending on the nature of skew of the bearing lines. Whereas a bridge with parallel skew has a short and long diagonal direction, and a stiff transverse load path tends to form along the short diagonal, bridges with nonparallel skew do not

necessarily have this characteristic. Figure 49 highlights the two possibilities described. This introduces additional complications in the overall bridge behavior.

Considering the above attributes, the behavior of the bridges is presented by dividing the 26 bridges into the following four groups for the evaluation of results of the parametric study:

1. Simple-span bridges with parallel skew,
2. Multi-span continuous bridges with parallel skew,
3. Multi-span continuous bridges with nonparallel skew (note, no nonparallel skew simple-span bridges were identified in the 57 bridges), and
4. Simple-span bridges with splay between the girders (note, no continuous-span splayed I-girder bridges were identified in the 57 bridges).

Table 14 indicates the bridges included in each of these four groups:

Based on the extent of the three-dimensional behavior in a skewed bridge, the different girders – exterior, first interior and the central girders – are subjected to different loads when compared to the loads calculated using the assumptions for LGA. Exterior girders directly receive loads from overhangs and the components supported from overhangs. Hence, establishing appropriate assumptions of distribution of loads transversely among the girders potentially can be critical in ensuring accuracy of LGA.

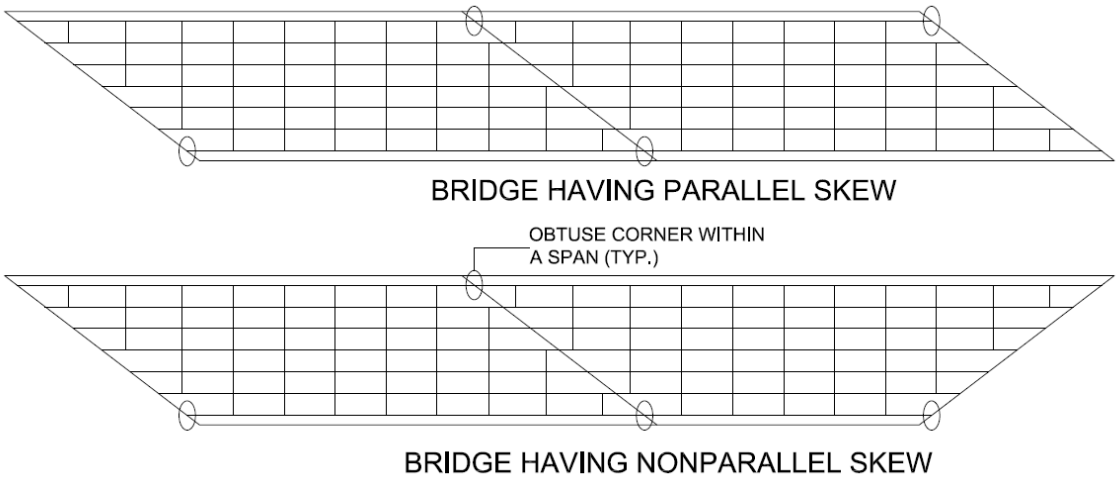

Figure 49. Obtuse corners within spans in a parallel and nonparallel skew bridge.

Table 14. Organization of bridge groups for detailed studies.

Group Number	Articulation	Nature of Skew	Bridges
1	Simple span	Parallel	1, 2, 5, 7, 17, 18, 21
2	Multi-span continuous	Parallel	3, 4, 6, 8, 9, 10, 11, 23, 24, 25, 26
3	Multi-span continuous	Nonparallel	12, 13, 14, 15, 16
4	Simple span splayed girder	Parallel	19, 20

The different assumptions and idealizations employed in this research are enumerated and explained in Chapter 2. To compare 3D FEA and LGA girder responses, the results for exterior girders, first interior girders and the central interior girders are inspected and presented separately for all the bridges studied. The professional factor (ρ_{max}), defined by Equation 20, is employed as the primary summary measure of the differences between the

3D FEA and LGA calculations in the studies. ρ_{max} values are useful in indicating the worst-case conservative and unconservative differences between the calculated responses. Hence, the assessment of accuracy of girder STR I Bending moments, TDL (SDLF) displacements and girder STR I vertical shear forces are based on ρmax values. Differences in 3D FEA and LGA responses are tabulated in the individual bridge appendix sections in terms of normalized mean differences (ε_{mean}) and normalized differences of the maximums, ε_{max1}, defined in Equation 21. Equation 23 shows the relation between ε_{max1} and ρ_{max}.

Key bridge responses that sufficiently quantify the structural behavior of bridges, studied are presented below in the following order:

1. The girder STR I major-axis bending moments.
2. The girder STR I vertical shear forces.
3. The girder live load shear forces, focusing in particular on the live load shear forces at the obtuse corners of the bridge spans.
4. The girder STR I bearing reactions.
5. The girder maximum total dead load vertical displacements, including consideration of the effects of Steel Dead Load Fit (SDLF) detailing of the cross-frames.
6. The girder concrete dead load maximum vertical displacements, considering both staged and unstaged deck placement.
7. The girder layovers under the total dead load, which for SDLF detailing of the cross-frames are equal to the girder layovers under the concrete dead load. This is because the layovers are approximately zero under the steel dead load when

SDLF detailing is employed. (These responses are estimated indirectly from the LGA results using equations recommended by FDOT; since the calculations are relatively straightforward, simple, and based on mechanics, they are considered as a part of the LGA calculations.)

8. The girder fatigue live load vertical shear forces.
9. The girder fatigue live load flexural stresses.
10. Girder flange lateral bending stresses
11. Cross-frame or diaphragm forces
12. Girder live load deflections

5.3.2 Girder STR I Major-axis Bending Moments

3D FEA and LGA girder responses are studied for noncomposite dead load, composite dead and live load cases in the parametric study. The responses from these basic load cases are combined to obtain the response for the STR I load combination. Section 15 of the individual appendix sections of each of the 26 bridges studied contains ε_{max1} values for all the load cases. ρ_{max} values are calculated from the ε_{max1} values using Equation 25. Studying the ρ_{max} or ε_{max1} values for each bridge, it can be seen that 3D FEA solutions and LGA solutions have the largest difference for the rail load and live load cases. Rails are supported on the overhangs of the composite bridge deck. In this research, the center of gravity is assumed to be at 9 in from the outer edge of the rail/overhang. Distribution of the rail load among the bridge girders is complex, and is broadly dependent on the width of the bridge and number of girders in the bridge. In this research, rail loads are distributed equally to all the girders in the bridge in the LGA calculations. This assumption introduces differences

in the rail load responses obtained from 3D FEA and LGA. LGA CDL bending moments are unconservative for a number of bridges when compared 3D FEA CDL bending moments. However, LGA live load responses calculated using the live load distribution factors, as described in Section 2.5.2, is observed to be conservative when compared to 3D FEA responses. This can be attributed to the conservatism associated with AASHTO moment live load distribution factors. Hence, overall, LGA predicts conservative STR I bending moments.

On the contrary, SDL (SDLF) results from LGA and 3D FEA are in close agreement. Theoretically, SDL (SDLF) bending moments should be equal to LGA SDL bending moments. However, the self-weight of the intermediate cross-frames is totaled and applied as equal uniformly distributed load to all the girders in the bridge. Hence, this introduces small differences in the LGA and 3D FEA girder bending moments. The specific cross-frame and diaphragm self-weights tributary to each of the girders may be different for the different girders, and these self-weights are actually applied as concentrated loads at the actual locations of the cross-frames and diaphragms. Therefore, LGA bending moments can be either conservative or unconservative compared to 3D FEA bending moments.

ρ_{max} values greater than unity indicate that the LGA solutions are unconservative compared to 3D FEA solutions, and vice versa if ρ_{max} values are lesser than unity. Figures 50 through 53 show ρ_{max} plots for the STR I positive bending moments for the four groups of bridges.

Figures 54 and 55 show plots of ρ_{max} for the STR I negative bending moments for the second and third groups, respectively. Figures 56 through 61 show plots comparing the

ρ_{max} values for the STR I bending moments for the six pairs of bridges having an original and an alternate cross-frame arrangement. In Figures 50 through 53, the results for the different girders are shown in the same plot. In Figures 56 through 61, separate plots are provided for each of the girder classifications. Tables 15 through 26 list corresponding data values for Figures 50 through 61.

Observations regarding the differences between the LGA and 3D FEA results are listed below:

- A consistent trend in the differences between the LGA and 3D FEA STR I bending moments as a function of the bridge skew index is not observed.
- For the simple span and multi-span continuous bridges with parallel skew (Groups 1 and 2), the results are more conservative as we move inward from the exterior to the interior girders for the STR I positive bending moments. A similar trend is observed for STR I negative bending moments for the multi-span continuous bridges with parallel skew (Group 2). However, the STR I positive and negative bending moments for bridges in Group 3 do not show such a trend. Bridges in Groups 3 are multi-span continuous bridges having nonparallel skew. The span lengths of the girders across the width of the bridge are not the same due to non-parallel skew. One of the exterior girders has the maximum span lengths and the other exterior girder has the minimum span length, when compared to the span length of the interior girders in the bridge. Therefore, this potentially introduces a larger error in the exterior girders. Similar to the non-parallel

skew bridges, for the splayed girder bridges in Group 4, the accuracy of LGA results is highly dependent on the geometry of the bridge.

- For all the simple span bridges with parallel skew (Group 1), the ρ_{max} values for the STR I moments are accurate to conservative. The largest conservative estimates correspond to the smallest values of ρ_{max}. The smallest value of ρ_{max} is 80% for the first interior girder and the central interior girder of Bridge 21. The cross-frames of Bridge 21 are parallel to the skewed bearing lines. In general, the largest conservatism is observed for the central interior girders. The conservatism of the STR I bending moments is smaller as one moves outward from the interior girders to the fascia girders.
- For the two-span continuous bridges with parallel skew (Group 2), the largest value of ρ_{max} for the positive STR I bending moments, 106%, is observed for the exterior girder of Bridge 6. Values of ρ_{max} greater than 100% indicate the LGA estimates are smaller than 3D FEA estimates. Bridge 6 is 112.2 ft wide, has 14 girders and contiguous cross-frames. The spacing between the girders is not constant, introducing additional approximations in the distributions of loads in the LGA.
- For the two-span continuous bridges with parallel skew (Group 2), the smallest ρ_{max} for the STR I bending moments is 67% for the central interior girders of Bridge 23. Bridge 23 has intermediate cross-frames framing into the bearings at the intermediate pier in addition to having cross-frames along the bearing line at this location. The corresponding high transverse

stiffness has a significant effect on the live load distribution among the various girders in the bridge. This is affirmed by the large differences in the maximum live load moments predicted by LGA and 3D FEA. The STR I negative bending moments estimated by LGA are observed to be conservative with respect to 3D FEA for all the Group 2 bridges. The smallest ρ_{max} value is 77% for the central interior girder of Bridge 26, which has cross-frames arranged parallel to the skew. This is followed by a ρ_{max} value of 78% for the central interior girder of Bridge 23.

- ρ_{max} value is unconservative for the splayed exterior girder of Bridge 19. The behavior of the splayed girder bridge is more heavily influenced by changes in the geometry of the bridge compared to parallel skew bridges.
- The parametric study involves the study of six pairs of bridges having the original and an alternative cross-frame arrangement. The alternative cross-frame arrangement reduces the influence of the stiff transverse load path in the short diagonal direction of the spans of bridges having parallel skew. The ρ_{max} values are smaller for the alternative cross-frame arrangement in some cases and larger for other cases. This can be attributed to the fact that the six pairs of bridges consist of two pairs of nonparallel skew bridges and a pair of splayed girder bridges.

Table 15. ρ_{max} values for STR I positive bending moments, simple span bridges, parallel skew.

Bridge	Skew Index	Width (ft)	CF Framing Arrangement Notes	ρ_{maxG1}	ρ_{maxG2}	ρ_{maxG3}	ρ_{maxG4}
1	0.46	87.1	Contiguous	0.96	0.93	0.83	0.96
2	0.46	87.1	Staggered	0.99	0.94	0.86	0.98
5*	0.42	115.4	Contiguous	0.92	0.93	0.87	0.92
7	0.33	54.4	Contiguous	0.90	0.92	0.83	0.90
17*	0.28	71.1	Contiguous	0.90	0.94	0.84	0.90
18*	0.20	58.2	Staggered	0.95	0.96	0.89	0.95
21*	0.15	135.1	Parallel to skew	0.90	0.80	0.79	0.90

* This bridge meets, or nearly meets, the requirements for application of the recommended LGA-based procedures for the bridge design.

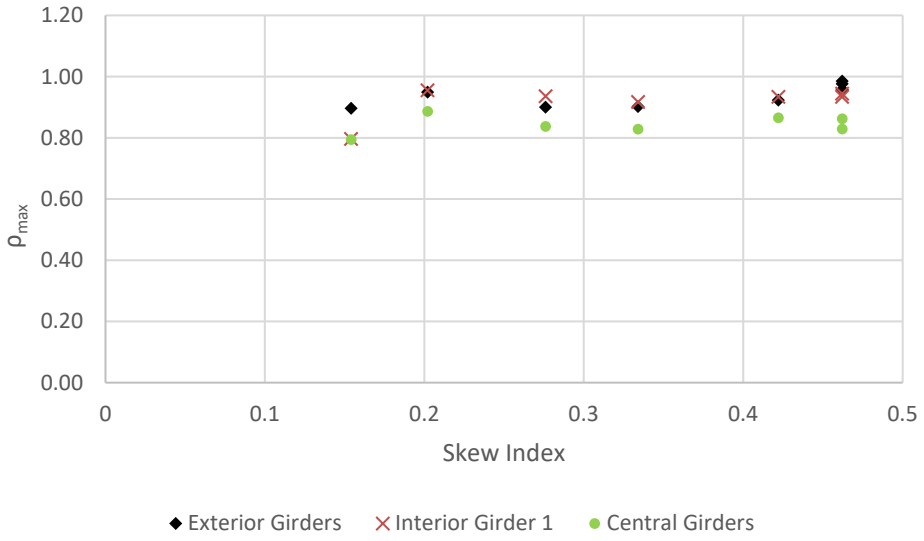

Figure 50. Comparison of ρ_{max} values for STR I positive bending moments, simple span bridges with parallel skew.

Table 16. ρ_{max} values for STR I positive bending moments, multi-span continuous bridges, parallel skew.

Bridge	Skew Index	Width (ft)	CF Framing Arrangement Notes	ρ_{maxG1}	ρ_{maxG2}	ρ_{maxG3}	ρ_{maxG4}
3	0.39	102.1	Contiguous, CF framing into bearing line	0.96	0.94	0.88	0.96
4*	0.39	102.1	Staggered	1.01	0.95	0.92	1.01
6*	0.35	112.2	Contiguous	1.06	0.94	0.84	1.06
8*	0.27	101.1	Staggered	0.95	0.93	0.92	0.95
9	0.47	54.3	Contiguous, CF framing into bearing line	0.93	0.92	0.84	0.91
10	0.47	54.3	Staggered	0.91	0.90	0.85	0.92
11*	0.26	67.1	Contiguous, CF framing into bearing line	0.93	0.91	0.82	0.93
23	0.37	84.2	Contiguous, CF framing into bearing line	0.94	0.74	0.67	0.93
24	0.37	55.3	Contiguous, inadequate offsets near bearing line	0.94	0.94	0.79	0.94
25	0.25	43.1	Contiguous, CF framing into bearing line	0.91	0.96	0.96	0.91
26*	0.15	73.1	Parallel to skew	1.02	0.93	0.82	1.02

* This bridge meets, or nearly meets, the requirements for application of the recommended LGA-based procedures for the bridge design.

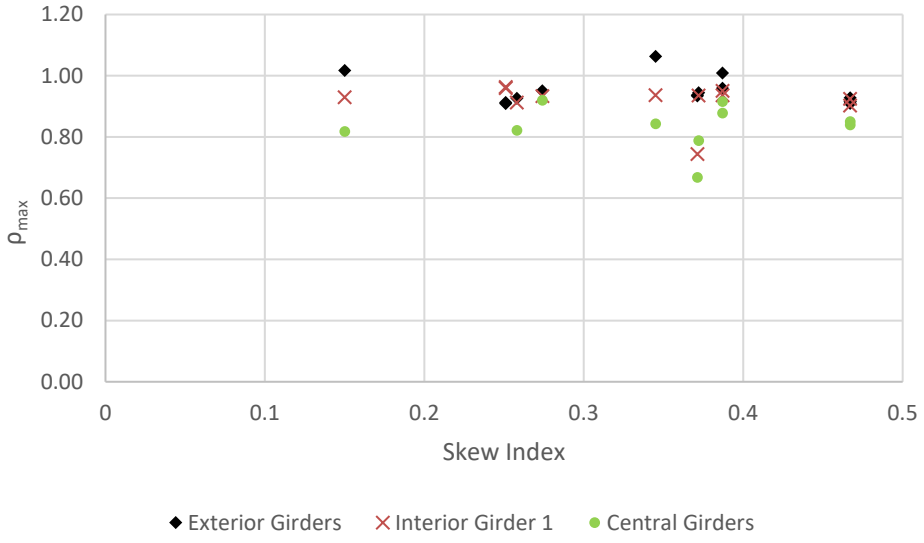

Figure 51. Comparison of ρ_{max} values for STR I positive bending moments, multi-span continuous bridges with parallel skew.

Table 17. ρ_{max} values for STR I positive bending moments, multi-span continuous bridges, nonparallel skew.

Bridge	Skew Index	Width (ft)	CF Framing Arrangement Notes	ρ_{maxG1}	ρ_{maxG2}	ρ_{maxG3}	ρ_{maxG4}
12	0.32	42.5	Contiguous, CF framing into bearing line	0.93	0.92	0.89	0.92
13	0.23	43.1	Contiguous	0.76	0.89	0.92	0.76
14	0.23	43.1	Staggered	0.76	0.89	0.93	0.77
15	0.33	60.2	Contiguous	0.97	0.87	0.74	0.92
16	0.33	60.2	Staggered	0.98	0.88	0.78	0.93
22*	0.31	85.5	Contiguous	0.91	0.91	0.84	0.88

* This bridge meets, or nearly meets, the requirements for application of the recommended LGA-based procedures for the bridge design.

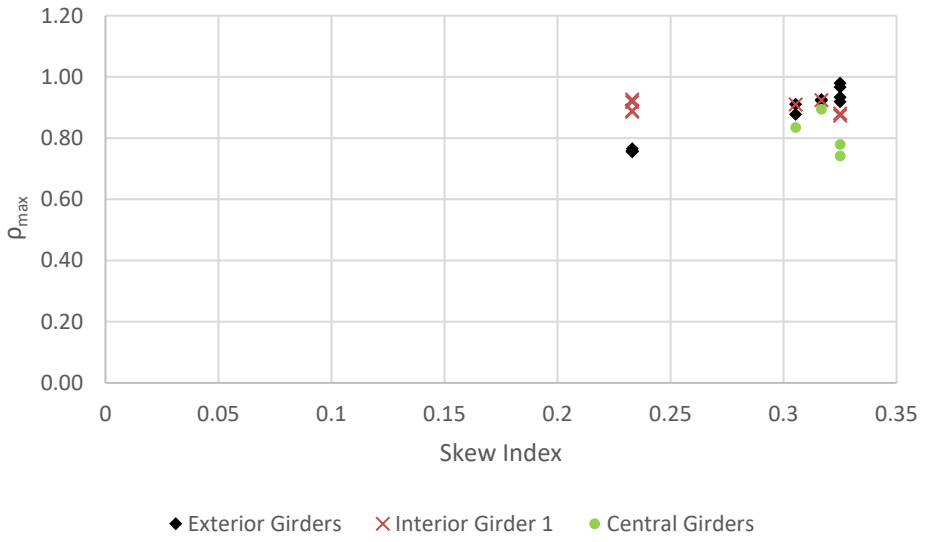

Figure 52. Comparison of ρ_{max} values for STR I positive bending moments, multi-span continuous bridges with nonparallel skew.

Table 18. ρ_{max} values for STR I positive bending moments, splayed girder bridges, parallel skew.

Bridge	Skew Index	Width (ft)	CF Framing Arrangement Notes	ρ_{maxG1}	ρ_{maxG2}	ρ_{maxG3}	ρ_{maxG4}
19	0.448	67.6	Contiguous	1.07	0.76	0.80	0.75
20	0.448	67.6	Staggered	0.98	0.87	0.84	0.79

Figure 53. Comparison of ρ_{max} values for STR I positive bending moments, splayed girder bridges with parallel skew.

Table 19. ρ_{max} values for STR I negative bending moments, multi-span continuous bridges, parallel skew.

Bridge	Skew Index	Width (ft)	CF Framing Arrangement Notes	ρ_{maxG1}	ρ_{maxG2}	ρ_{maxG3}	ρ_{maxG4}
3	0.39	102.1	Contiguous, CF framing into bearing line	0.93	0.88	0.84	0.93
4*	0.39	102.1	Staggered	0.96	0.89	0.86	0.96
6*	0.35	112.2	Contiguous	0.96	0.84	0.80	0.96
8*	0.27	101.1	Staggered	0.92	0.88	0.88	0.92
9	0.47	54.3	Contiguous, CF framing into bearing line	0.96	0.86	0.79	0.87
10	0.47	54.3	Staggered	0.93	0.89	0.84	0.87
11*	0.26	67.1	Contiguous, CF framing into bearing line	0.89	0.89	0.83	0.89
23	0.37	84.2	Contiguous, CF framing into bearing line	0.95	0.78	0.78	0.95
24	0.37	55.3	Contiguous, inadequate offsets near bearing line	0.95	0.89	0.80	0.95
25	0.25	43.1	Contiguous, CF framing into bearing line	0.90	0.92	0.92	0.90
26*	0.15	73.1	Parallel to skew	0.94	0.82	0.77	0.94

* This bridge meets, or nearly meets, the requirements for application of the recommended LGA-based procedures for the bridge design.

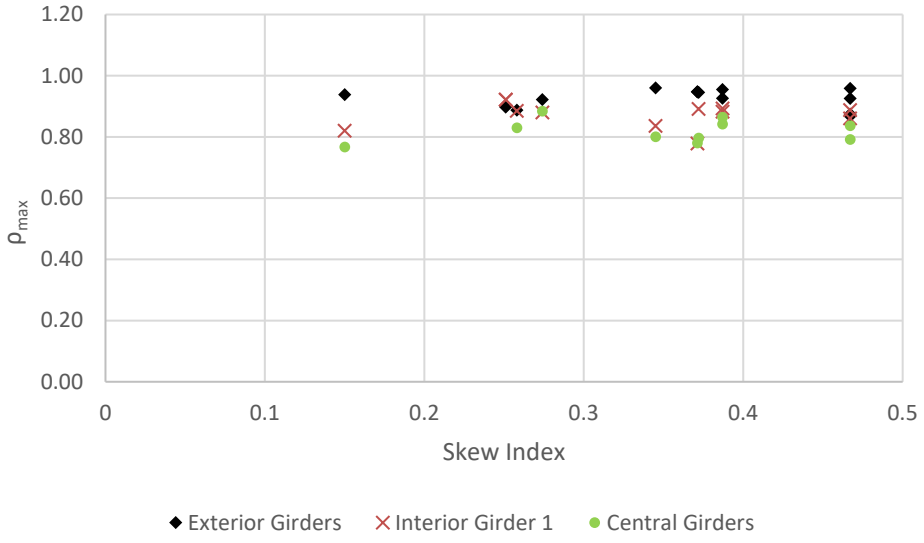

Figure 54. Comparison of ρ_{max} values for STR I negative bending moments, multi-span continuous bridges with parallel skew.

Table 20. ρ_{max} values for STR I negative bending moments, multi-span continuous bridges, nonparallel skew.

Bridge	Skew Index	Width (ft)	CF Framing Arrangement Notes	ρ_{maxG1}	ρ_{maxG2}	ρ_{maxG3}	ρ_{maxG4}
12	0.32	42.5	Contiguous, CF framing into bearing line	0.96	0.89	0.90	0.85
13	0.23	43.1	Contiguous	0.80	0.95	0.96	0.80
14	0.23	43.1	Staggered	0.81	0.95	0.93	0.80
15	0.33	60.2	Contiguous	0.88	0.86	0.85	0.93
16	0.33	60.2	Staggered	0.91	0.86	0.84	0.94
22*	0.31	85.5	Contiguous	0.89	0.86	0.86	0.91

* This bridge meets, or nearly meets, the requirements for application of the recommended LGA-based procedures for the bridge design.

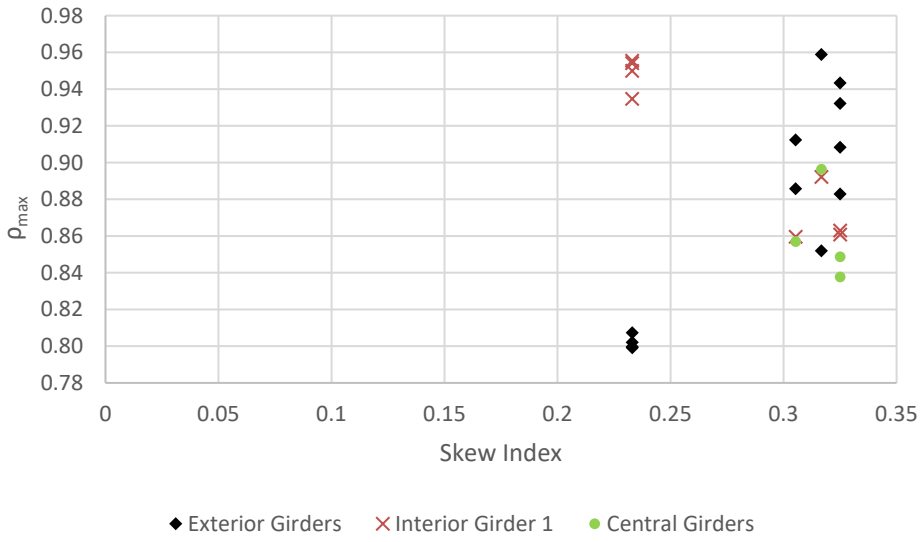

Figure 55. Comparison of ρ_{max} values for STR I negative bending moments, multi-span continuous bridges with nonparallel skew.

Table 21. ρ_{max} values for STR I positive bending moments for exterior girders of bridges with original and alternative cross-frame arrangement.

Bridge	Skew Index	CF Arrangement	Characteristics of Bridge Geometry	ρ_{maxG1}	ρ_{maxG4}
1	0.46	Original	Simple span, parallel skew	0.96	0.96
2		Alternative		0.99	0.98
3	0.47	Original	Two-span continuous, parallel skew	0.96	0.96
4*		Alternative		1.01	1.01
9	0.39	Original	Two-span continuous, parallel skew	0.93	0.91
10		Alternative		0.91	0.92
13	0.33	Original	Four-span continuous, nonparallel skew	0.76	0.76
14		Alternative		0.76	0.77
15	0.23	Original	Four-span continuous, nonparallel skew	0.97	0.92
16		Alternative		0.98	0.93
19	0.45	Original	Simple span, splayed girder, parallel skew	1.07	0.75
20		Alternative		0.98	0.79

* This bridge meets, or nearly meets, the requirements for application of the recommended LGA-based procedures for the bridge design.

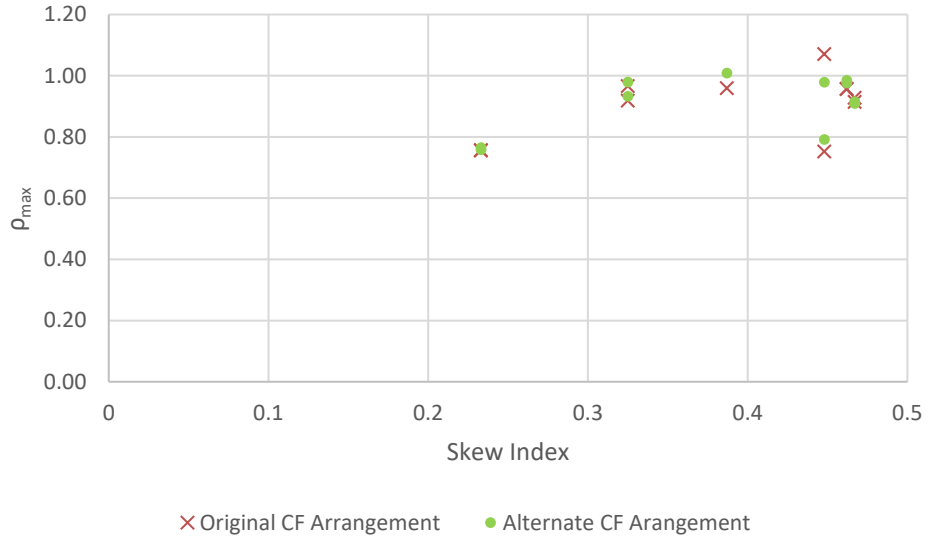

Figure 56. Comparison of ρ_{max} values for STR I positive bending moments, exterior girders in bridges with original and alternate cross-frame arrangements.

Table 22. ρ_{max} values for STR I positive bending moments for first interior girders of bridges with original and alternative cross-frame arrangements.

Bridge	Skew Index	CF Arrangement	Characteristics of Bridge Geometry	ρ_{maxG2}
1	0.46	Original	Simple span, parallel skew	0.93
2		Alternative		0.94
3	0.39	Original	Two-span continuous, parallel skew	0.94
4*		Alternative		0.95
9	0.47	Original	Two-span continuous, parallel skew	0.92
10		Alternative		0.90
13	0.23	Original	Four-span continuous, nonparallel skew	0.89
				0.92
14		Alternative		0.89
				0.93
15	0.33	Original	Four-span continuous, nonparallel skew	0.87
16		Alternative		0.88
19	0.45	Original	Simple span, splayed girder, parallel skew	0.76
20		Alternative		0.87

* This bridge meets, or nearly meets, the requirements for application of the recommended LGA-based procedures for the bridge design.

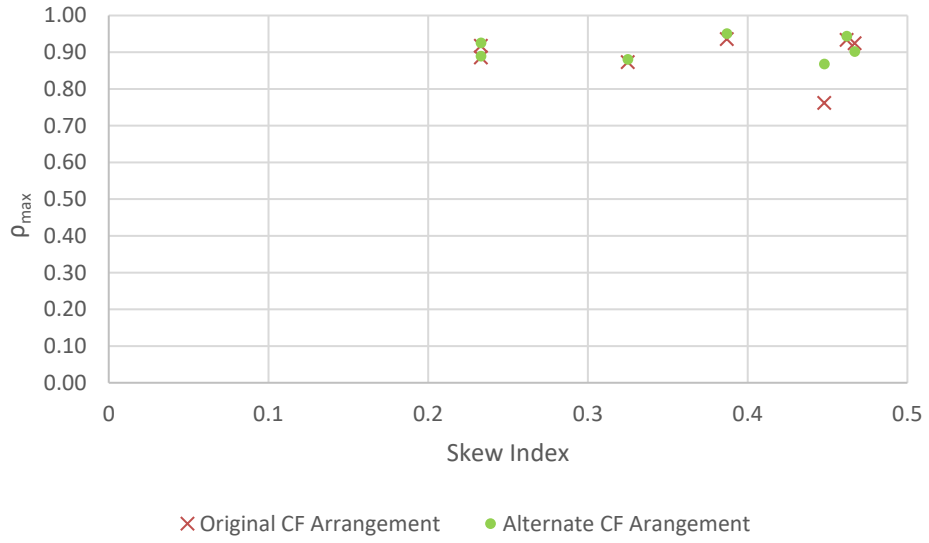

Figure 57. Comparison of ρ_{max} values for STR I positive bending moments, first interior girders in bridges with original and alternate cross-frame arrangements.

Table 23. ρ_{max} values for STR I positive bending moments for central interior girders of bridges with original and alternative cross-frame arrangements.

Bridge	Skew Index	CF Arrangement	Characteristics of Bridge Geometry	ρ_{maxG3}
1	0.46	Original	Simple span, parallel skew	0.83
2		Alternative		0.86
3	0.39	Original	Two-span continuous, parallel skew	0.88
4*		Alternative		0.92
9	0.47	Original	Two-span continuous, parallel skew	0.84
10		Alternative		0.85
15	0.33	Original	Four-span continuous, nonparallel skew	0.74
16		Alternative		0.78
19	0.45	Original	Simple span, splayed girder, parallel skew	0.80
20		Alternative		0.84

* This bridge meets, or nearly meets, the requirements for application of the recommended LGA-based procedures for the bridge design.

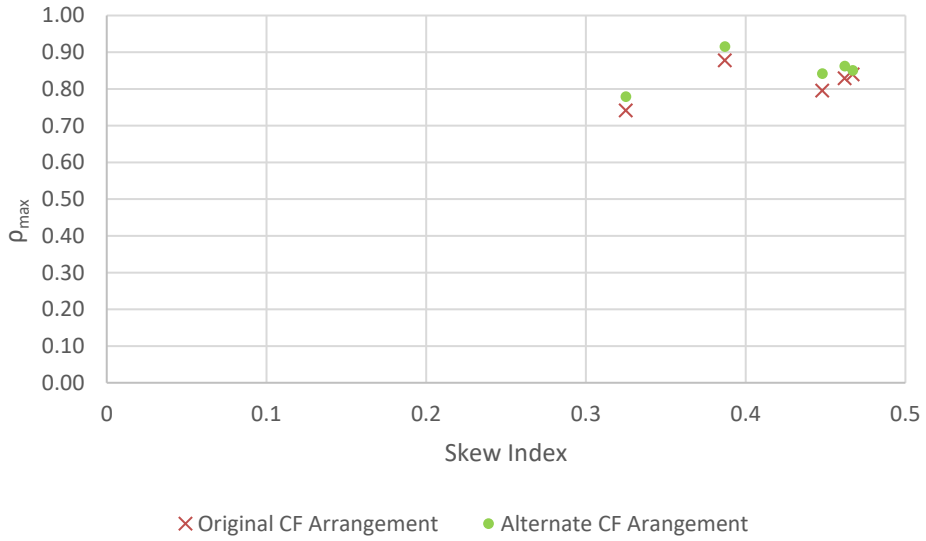

Figure 58. Comparison of ρ_{max} values for STR I positive bending moments, central interior girders in bridges with original and alternate cross-frame arrangements.

Table 24. ρ_{max} values for STR I negative bending moments for exterior girders of bridges with original and alternative cross-frame arrangements.

Bridge	Skew Index	CF Arrangement	Characteristics of Bridge Geometry	ρ_{maxG2}
3	0.39	Original	Two-span continuous, parallel skew	0.88
4*		Alternative		0.89
9	0.47	Original	Two-span continuous, parallel skew	0.86
10		Alternative		0.89
13	0.23	Original	Four-span continuous, nonparallel skew	0.95
				0.96
14		Alternative		0.95
				0.93
15	0.33	Original	Four-span continuous, nonparallel skew	0.86
16		Alternative		0.86

* This bridge meets, or nearly meets, the requirements for application of the recommended LGA-based procedures for the bridge design.

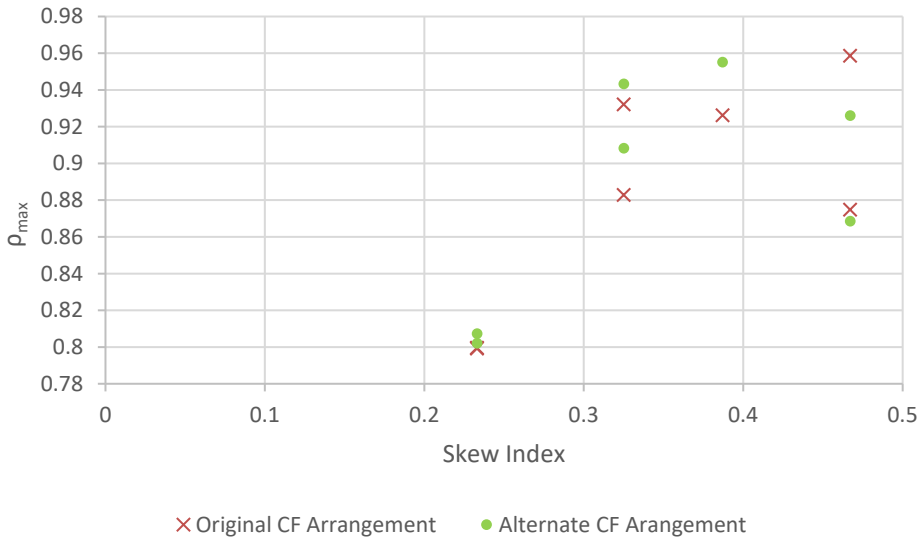

Figure 59. Comparison of ρ_{max} values for STR I negative bending moments, exterior girders in bridges with original and alternate cross-frame arrangements.

Table 25. ρ_{max} values for STR I negative bending moments for first interior girders of bridges with original and alternative cross-frame arrangements.

Bridge	Skew Index	CF Arrangement	Characteristics of Bridge Geometry	ρ_{maxG3}
3	0.39	Original	Two-span continuous, parallel skew	0.84
4*		Alternative		0.86
9	0.47	Original	Two-span continuous, parallel skew	0.79
10		Alternative		0.84
15	0.33	Original	Four-span continuous, nonparallel skew	0.85
16		Alternative		0.84

* This bridge meets, or nearly meets, the requirements for application of the recommended LGA-based procedures for the bridge design.

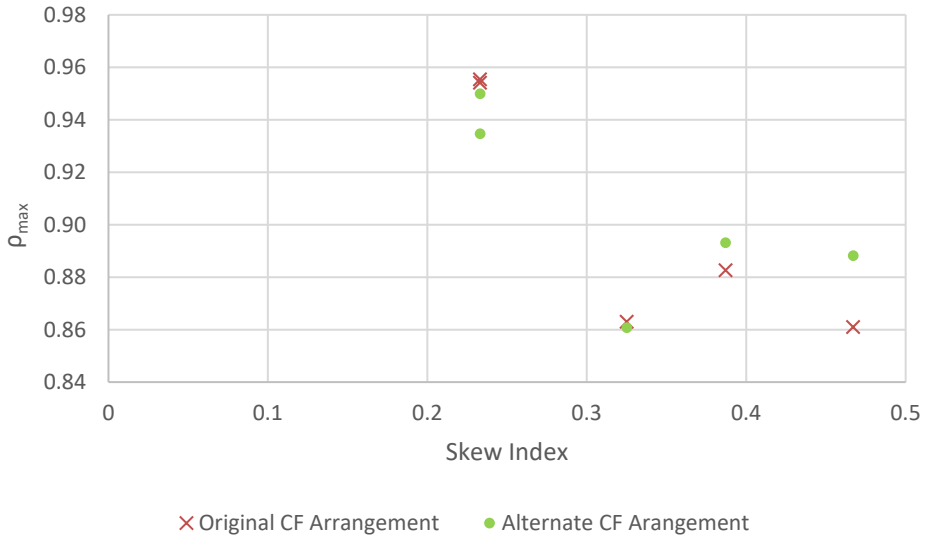

Figure 60. Comparison of ρ_{max} values for STR I negative bending moments, first interior girders in bridges with original and alternate cross-frame arrangements.

Table 26. ρ_{max} values for STR I negative bending moments for first interior girders of bridges with original and alternative cross-frame arrangements.

Bridge	Skew Index	CF Arrangement	Characteristics of Bridge Geometry	ρ_{maxG3}
3	0.39	Original	Two-span continuous, parallel skew	0.84
4*		Alternative		0.86
9	0.47	Original	Two-span continuous, parallel skew	0.79
10		Alternative		0.84
15	0.33	Original	Four-span continuous, nonparallel skew	0.85
16		Alternative		0.84

* This bridge meets, or nearly meets, the requirements for application of the recommended LGA-based procedures for the bridge design.

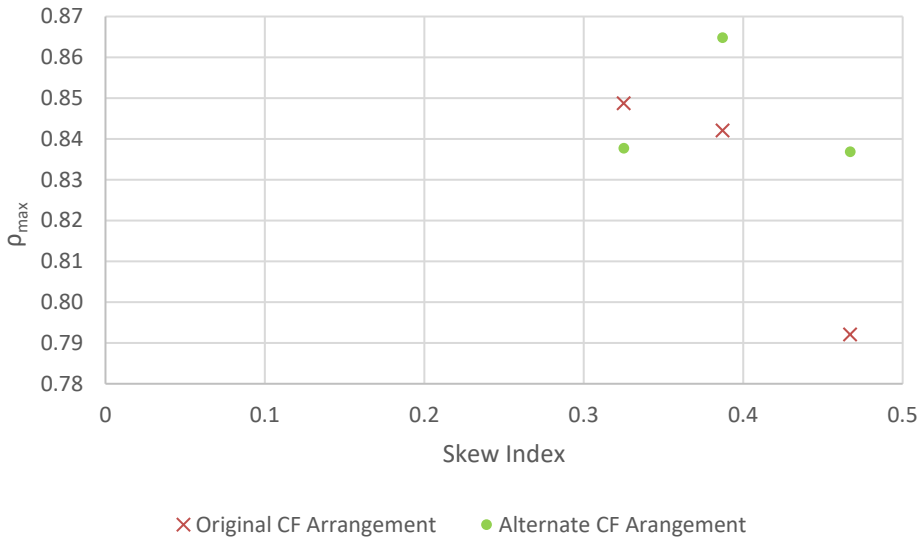

Figure 61. Comparison of ρ_{max} values for STR I negative bending moments, central interior girders in bridges with original and alternate cross-frame arrangements.

5.3.3 Girder STR I Vertical Shear Forces

In a skewed bridge, intermediate cross-frames perpendicular to the girder act to transfer shear forces to the girders at the connecting points. Hence, the shear force diagrams are discontinuous at the locations where the cross-frames connect to the girders. The deck, after hardening, also transfers forces due to its high in-plane rigidity. Additionally, in spans having parallel skew, there is a tendency to form a transverse load path between the obtuse corners. Furthermore, the bearing line cross-frames aligned along the skew tend to twist the girders to maintain system compatibility, thus developing a torsional moment that tends to increase the load transferred at the obtuse corners, and decrease loads at the acute corners. These two effects drive additional shear forces at the ends of girders near the obtuse corners. Hence, larger ρ_{max} values for STR I shear forces are observed compared to STR I bending moments. Furthermore, a greater number of discontinuities are observed in the shear force diagrams when a staggered cross-frame arrangement is used (since stagger may increase the number of points along the girders at which cross-frames are connected). Such discontinuities are difficult to track in LGA, adding to the differences observed in 3D FEA and LGA solutions.

Figures 63 through 66 show ρ_{max} plots for the STR I vertical shear forces for the four groups of bridges. Tables 27 through 30 list the data for the plots shown in Figures 63 through 66, for easy identification of the bridges and the corresponding data in the plots. Figures 67 through 69 show plots comparing the ρ_{max} values for the STR I vertical shear forces for the six pairs of bridges having an original and an alternate cross-frame arrangement. Tables 31 through 33 list the corresponding data values. In Figures 63

through 66, the results for the different girders are shown in the same plot. Figures 67 through 69, separate plots are provided for each of the girder classifications.

The STR I vertical shear forces for the simple span bridges with parallel skew (Group 1) are under-predicted for the exterior girders of Bridges 1, 2, 5, and 18. STR I vertical shear forces for the exterior girders of Bridges 1 and 2 are under-predicted by a magnitude greater than 10%. Cells that do not satisfy this tolerance have a ρ_{max} value larger than 1.11 and are highlighted in Tables 27 through 30. Bridge 1 has a skew index of 0.45, a skew angle of 49° and a contiguous cross-frame arrangement. Hence, a very stiff transverse load path develops between the obtuse corners of the bridge, introducing large differences between the LGA and 3D FEA vertical shear estimates. Bridge 2 is Bridge 1 with an alternate staggered cross-frame arrangement, and generous end offsets. Therefore, while the magnitude of under-predictions are smaller than in Bridge 1, the differences are still greater than 10% due to the development of a transverse load path between the obtuse corners of the bridge. Similarly, the STR I vertical shear forces for the exterior girders of Bridges 6 and 19 are underestimated by more than 10%. Bridge 19 is a splayed girder bridge. However, for Bridge 6, the under-prediction is a numerical anomaly of the 3D FEA solution. This can be seen in Appendix Section 3.6.7.1. A plot of STR I vertical shear forces for the exterior girder (Girder 1) of Bridge 6 is reproduced in Figure 62. As can be seen, if the numerical anomaly is ignored, LGA shear forces are larger than 3D FEA shear forces.

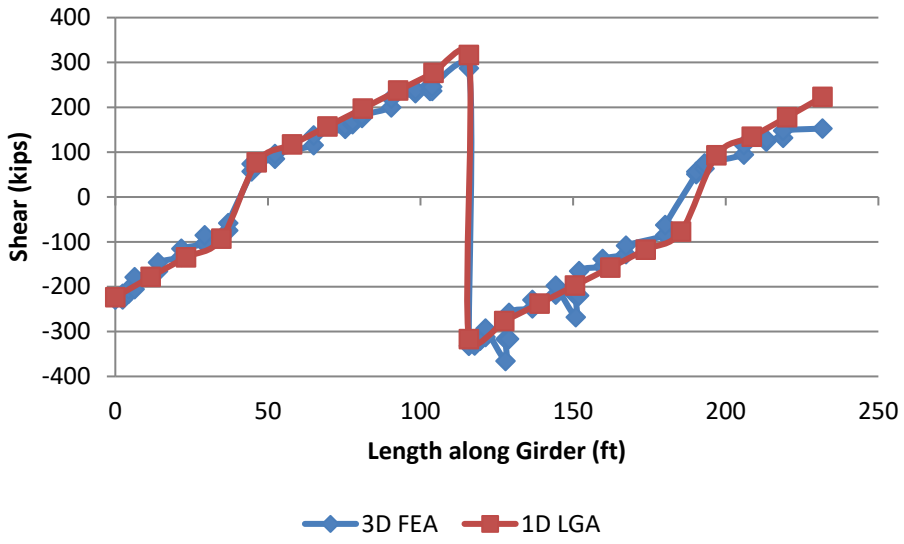

Figure 62. STR I vertical shear forces for Girder 1 of Bridge 6.

Table 27. ρ_{max} values for STR I vertical shear forces, simple span bridges, parallel skew (shaded cells indicate ρ_{max} values that exceed the targeted limits for applicability of LGA).

Bridge	Skew Index	Width (ft)	CF Framing Arrangement Notes	ρ_{maxG1}	ρ_{maxG2}	ρ_{maxG3}	ρ_{maxG4}
1	0.46	87.1	Contiguous	1.31	0.87	0.81	1.30
2	0.46	87.1	Staggered	1.15	0.84	0.88	1.20
5*	0.42	115.4	Contiguous	1.00	0.86	0.86	1.00
7	0.33	54.4	Contiguous	0.96	0.74	0.77	0.96
17*	0.28	71.1	Contiguous	0.73	0.76	0.82	0.73
18*	0.20	58.2	Staggered	1.01	0.85	0.81	1.01
21*	0.15	135.1	Parallel to skew	0.88	0.86	0.85	0.88

* This bridge meets, or nearly meets, the requirements for application of the recommended LGA-based procedures for the bridge design.

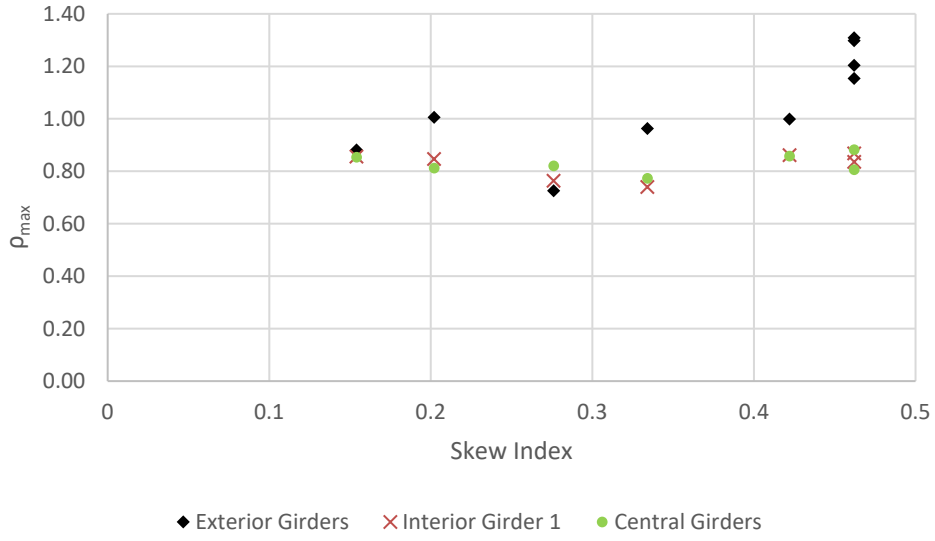

Figure 63. Comparison of ρ_{max} values for STR I vertical shear forces, simple span bridges with parallel skew.

Table 28. ρ_{max} values for STR I vertical shear forces, multi-span continuous bridges, parallel skew (shaded cells indicate ρ_{max} values that exceed the targeted limits for applicability of LGA).

Bridge	Skew Index	Width (ft)	CF Framing Arrangement Notes	ρ_{maxG1}	ρ_{maxG2}	ρ_{maxG3}	ρ_{maxG4}
3	0.39	102.1	Contiguous, CF framing into bearing line	0.96	0.82	0.86	0.96
4*	0.39	102.1	Staggered	0.98	0.85	0.88	0.98
6*	0.35	112.2	Contiguous	1.15	0.81	0.81	1.15
8*	0.27	101.1	Staggered	0.97	0.86	0.87	0.97
9	0.47	54.3	Contiguous, CF framing into bearing line	1.01	0.82	0.85	0.95
10	0.47	54.3	Staggered	0.92	0.84	0.86	0.85
11*	0.26	67.1	Contiguous, CF framing into bearing line	1.00	0.84	0.87	1.00
23	0.37	84.2	Contiguous, CF framing into bearing line	0.75	0.83	0.94	0.99
24	0.37	55.3	Contiguous, inadequate offsets near bearing line	1.01	0.83	0.90	1.01
25	0.25	43.1	Contiguous, CF framing into bearing line	0.95	0.90	0.91	0.94
26*	0.15	73.1	Parallel to skew	1.04	0.85	0.81	1.04

* This bridge meets, or nearly meets, the requirements for application of the recommended LGA-based procedures for the bridge design.

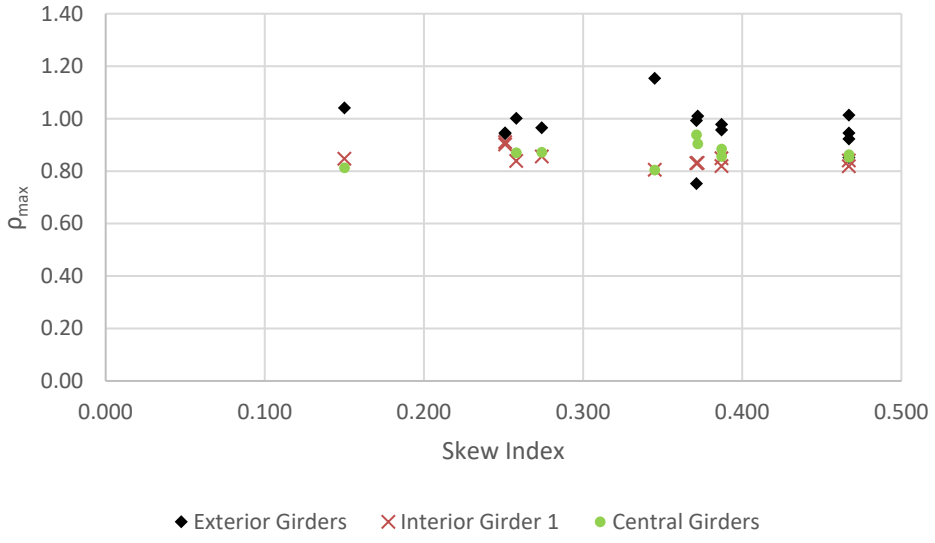

Figure 64. Comparison of ρ_{max} values for STR I vertical shear forces, multi-span continuous bridges with parallel skew.

Table 29. ρ_{max} values for STR I vertical shear forces, multi-span continuous bridges, nonparallel skew.

Bridge	Skew Index	Width (ft)	CF Framing Arrangement Notes	ρ_{maxG1}	ρ_{maxG2}	ρ_{maxG3}	ρ_{maxG4}
12	0.32	42.5	Contiguous, CF framing into bearing line	0.95	0.82	0.97	0.97
13	0.23	43.1	Contiguous	0.82	0.96	0.96	0.82
14	0.23	43.1	Staggered	0.83	0.97	0.94	0.82
15	0.33	60.2	Contiguous	0.88	0.81	0.92	0.98
16	0.33	60.2	Staggered	0.90	0.82	0.89	0.97
22*	0.31	85.5	Contiguous	0.92	0.80	0.85	1.07

* This bridge meets, or nearly meets, the requirements for application of the recommended LGA-based procedures for the bridge design.

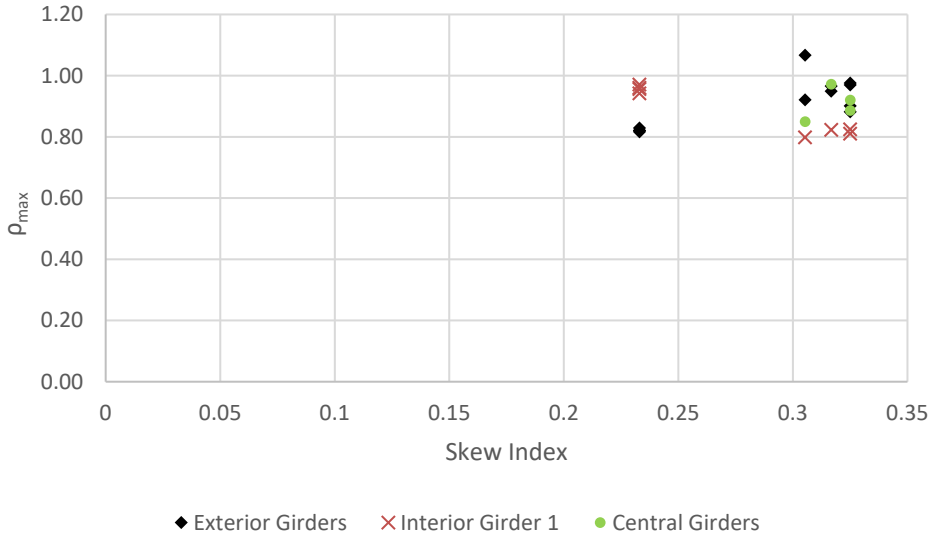

Figure 65. Comparison of ρ_{max} values for STR I vertical shear forces, multi-span continuous bridges with nonparallel skew.

Table 30. ρ_{max} values for STR I vertical shear forces, splayed girder bridges, parallel skew (shaded cells indicate ρ_{max} values that exceed the targeted limits for applicability of LGA).

Bridge	Skew Index	Width (ft)	CF Framing Arrangement Notes	ρ_{maxG1}	ρ_{maxG2}	ρ_{maxG3}	ρ_{maxG4}
19	0.45	67.6	Contiguous	1.19	0.83	0.79	1.23
20	0.45	67.6	Staggered	1.06	0.89	0.84	1.09

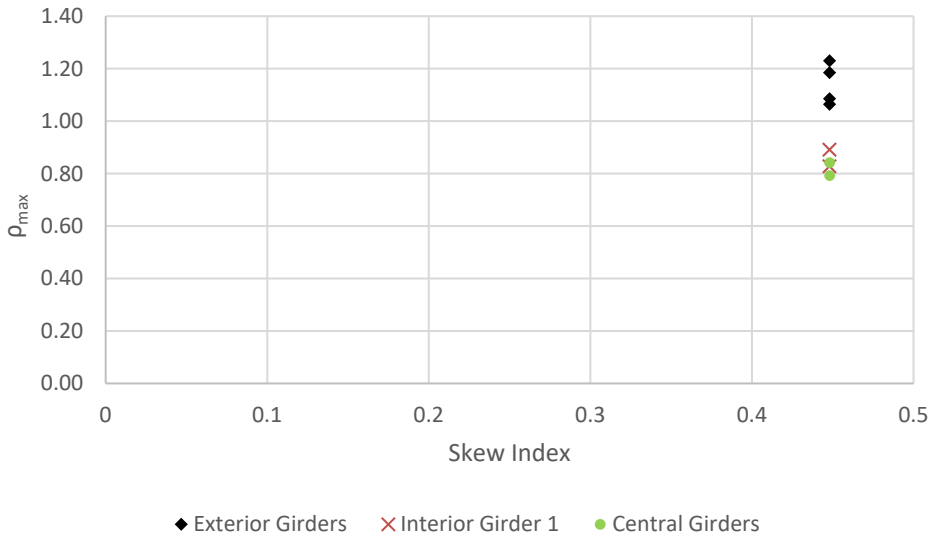

Figure 66. Comparison of ρ_{max} values for STR I vertical shear forces, splayed girder bridges with parallel skew.

Table 31. ρ_{max} values for STR I vertical shear forces for exterior girders of bridges with original and alternative cross-frame arrangements (shaded cells indicate ρ_{max} values that exceed the targeted limits for applicability of LGA).

Bridge	Skew Index	CF Arrangement	Characteristics of Bridge Geometry	ρ_{maxG1}	ρ_{maxG4}
1	0.46	Original	Simple span, parallel skew	1.31	1.30
2		Alternative		1.15	1.20
3	0.39	Original	Two-span continuous, parallel	0.96	0.96
4*		Alternative		0.98	0.98
9	0.47	Original	Two-span continuous, parallel	1.01	0.95
10		Alternative		0.92	0.85
13	0.23	Original	Four-span continuous,	0.82	0.82
14		Alternative		0.83	0.82
15	0.33	Original	Four-span continuous,	0.88	0.98
16		Alternative		0.90	0.97
19	0.45	Original	Simple span, splayed girder,	1.19	1.23
20		Alternative		1.06	1.09

* This bridge meets, or nearly meets, the requirements for application of the recommended LGA-based procedures for the bridge design.

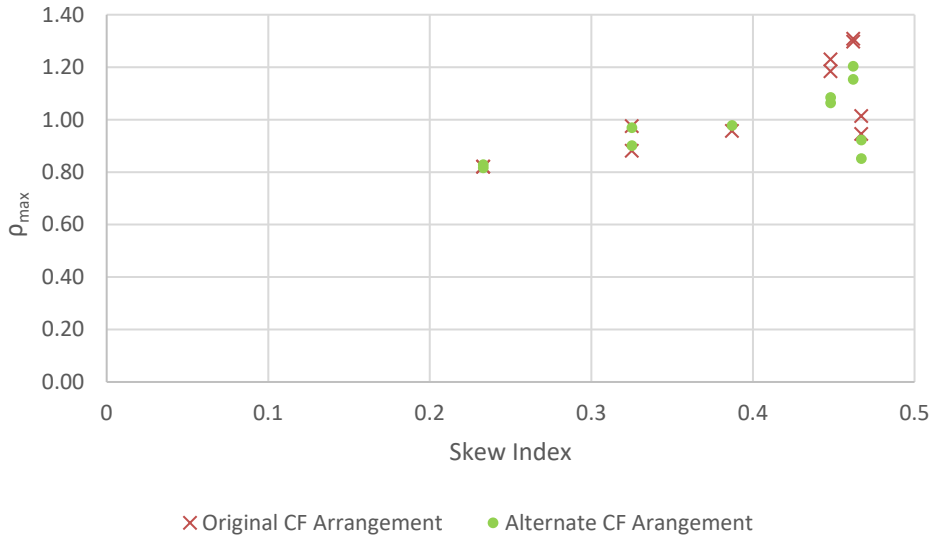

Figure 67. Comparison of ρ_{max} values for STR I vertical shear forces, exterior girders in bridges with original and alternate cross-frame arrangements.

Table 32. ρ_{max} values for STR I vertical shear forces for first interior girders of bridges with original and alternative cross-frame arrangements.

Bridge	Skew Index	CF Arrangement	Characteristics of Bridge Geometry	ρ_{maxG2}
1	0.46	Original	Simple span, parallel skew	0.87
2		Alternative		0.84
3	0.99	Original	Two-span continuous, parallel	0.82
4*		Alternative		0.85
9	0.95	Original	Two-span continuous, parallel	0.82
10		Alternative		0.84
13	0.23	Original	Four-span continuous, nonparallel skew	0.96
				0.96
14		Alternative		0.97
				0.94
15	0.33	Original	Four-span continuous,	0.81
16		Alternative		0.82
19	0.45	Original	Simple span, splayed girder,	0.83
20		Alternative		0.89

* This bridge meets, or nearly meets, the requirements for application of the recommended LGA-based procedures for the bridge design.

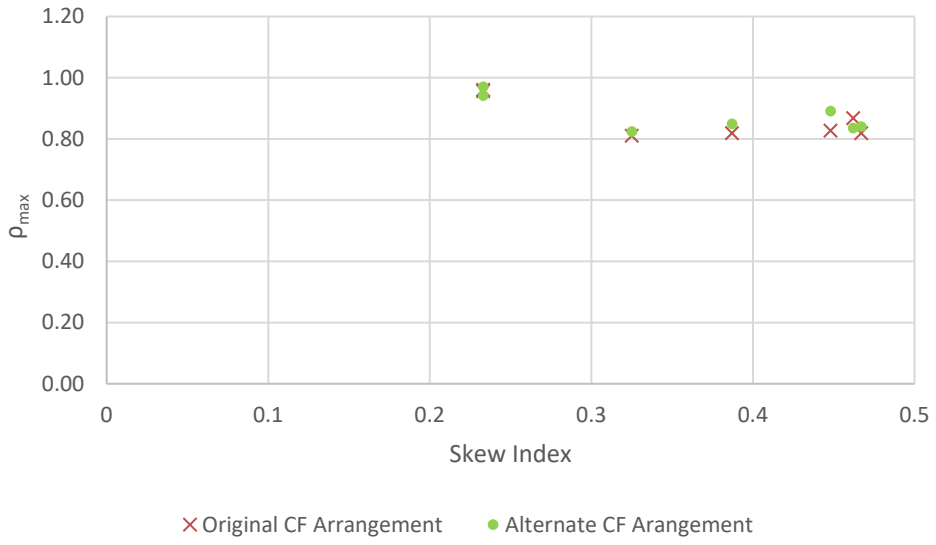

Figure 68. Comparison of ρ_{max} values for STR I vertical shear forces, first interior girders in bridges with original and alternate cross-frame arrangements.

Table 33. ρ_{max} values for STR I vertical shear forces for central interior girders of bridges with original and alternative cross-frame arrangements.

Bridge	Skew Index	CF Arrangement	Characteristics of Bridge Geometry	ρ_{maxG3}
1	0.46	Original	Simple span, parallel skew	0.81
2		Alternative		0.88
3	0.39	Original	Two-span continuous, parallel	0.86
4		Alternative		0.88
9	0.47	Original	Two-span continuous, parallel	0.85
10		Alternative		0.85
15	0.33	Original	Four-span continuous,	0.92
16		Alternative		0.89
19	0.45	Original	Simple span, splayed girder,	0.79
20		Alternative		0.84

* This bridge meets, or nearly meets, the requirements for application of the recommended LGA-based procedures for the bridge design.

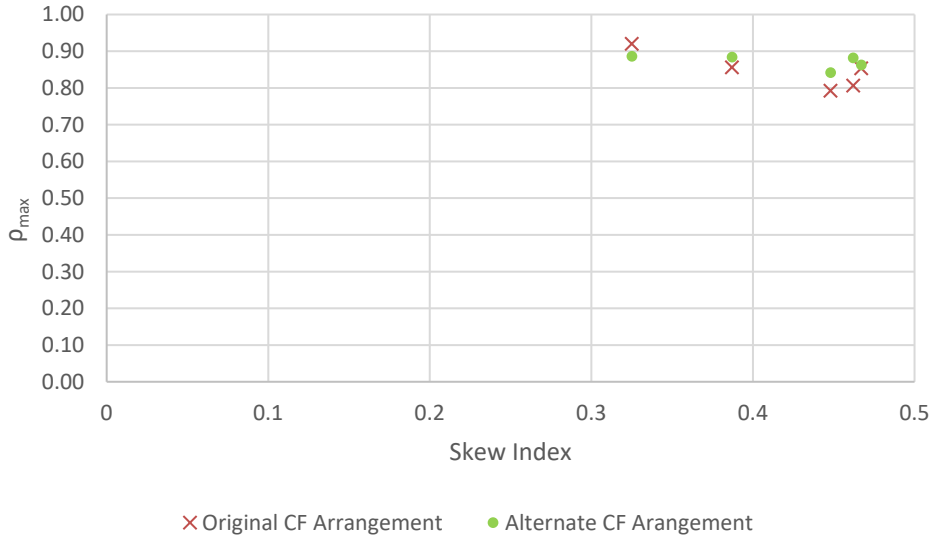

Figure 69. Comparison of ρ_{max} values for STR I vertical shear forces, central interior girders in bridges with original and alternate cross-frame arrangements.

5.3.4 Girder Live Load Shear Forces

Predicting the response of highway bridges to vehicular live load is key in designing for strength and serviceability requirements. 3D FEA solutions typically employ influence surfaces to calculate maximum and minimum envelopes for response quantities, by algorithmically finding the critical location of the vehicle causing the maximum or minimum response. Hence, the problem of estimating live loads is a complex one that involves significant computational demands. The use of live load distribution factors, typically employed in LGA, is a coarse approximation of the live load effects and greatly simplifies the estimation of live loads. The live load distribution factors have been developed to be typically conservative when compared to 3D FEA solutions.

In the parametric study, the behavior of the 26 bridges is studied for the AASHTO HL-93 live load model. As a part of the study, distribution factors using the 3D FEA solutions are calculated and documented in each of the individual bridge appendix sections. LGA results are available from SIMON for the live load envelopes of bending moments and vertical shears at every tenth point in the spans. If these envelope values are divided by the AASHTO live load distribution factor (LLDF) corresponding to the quantity under consideration, an envelope of values corresponding to a LLDF = 1.0 is obtained. The ratio of 3D FEA live load envelope values at the tenth points to the corresponding values for LLDF = 1.0 represents the 3D FEA LLDF. Distribution factors are calculated for the live load girder major-axis bending moments and vertical shear forces.

The distribution factors thus calculated are compared to the empirical distribution factors calculated using the AASHTO recommended expressions. The comparison of

distribution factors provides insight into the general accuracy of LGA with respect to 3D FEA. It is known that the local effects of skew near the bearing lines and the stiff transverse load path that develops between the obtuse corners in a parallel skew bridge span drives larger shear forces at the ends of girders near the obtuse corners. Hence, in a number of cases, the professional factor, ρmax, for the live load shear forces at obtuse corners of bridge spans is observed to be greater than unity. ρ_{max} values, if greater than unity, represent multipliers to be applied to the current AASHTO distribution factors to obtain 3D FEA estimates. Cells that do not satisfy the tolerance established in Section 5.2.2, have a ρ_{max} value larger than 1.11 and are highlighted in the tables in this section. It must be noted that the skew correction factor is included in the AASHTO distribution factors being considered.

Figures 70 and 71 show ρ_{max} values for the exterior girders and first interior girders respectively for simple-span bridges with parallel skew (Group 1). Tables 34 and 35 list the corresponding data. ρ_{max} values for interior girders are smaller than one, implying that the LGA estimates are conservative compared to 3D FEA. The exterior girders of Bridges 1 and 2 have ρ_{max} values greater than 1.2. The LGA estimates are accurate to conservative for the exterior girders of the other simple span bridges studied.

Figures 72 and 74 show ρ_{max} values for the exterior girders and first interior girders respectively, at the obtuse corners corresponding to the end abutments of multi-span continuous bridges with parallel skew (Group 2). Tables 36 and 38 list the corresponding data. A maximum ρ_{max} value of 1.00 is observed for an exterior girder of Bridge 25. A stiff transverse path is developed between the obtuse corners of the spans in Bridge 25 due to

inadequate offsets in the intermediate cross-frames near the end bearing lines. LGA estimates are conservative for the first interior girders of the Group 2 bridges.

Figures 73 and 75 show ρ_{max} values for the exterior girders and first interior girders respectively, at obtuse corners of the spans at the intermediate piers of multi-span continuous bridges with parallel skew (Group 2). Tables 37 and 39 list the corresponding data. LGA estimates are conservative with respect to the 3D FEA values, for all the exterior and first interior girders of the Group 2 bridges.

Figures 76 and 78 show the ratio of 3D FEA to LGA live load shears for the exterior girders and first interior girders respectively, at obtuse corners corresponding to the end abutments of multi-span continuous bridges with nonparallel skew (Group 3). Tables 40 and 42 list the corresponding data values. The maximum ρ_{max} value of 1.1 is observed for an exterior girder of Bridge 22. LGA estimates for the exterior girders of the other bridges studied are conservative with respect to the 3D FEA values. LGA estimates are conservative for the first interior girders of the Group 3 bridges.

Figures 77 and 79 show ρ_{max} values for the exterior girders and first interior girders respectively, at the obtuse corners of the spans at the intermediate piers of multi-span continuous bridges with nonparallel skew (Group 3). Tables 41 and 43 list the corresponding data values. The maximum ρ_{max} value of 1.08 is observed for an exterior girder of Bridge 22.

Figures 80 and 81 show the ρ_{max} values for the exterior girders and first interior girders respectively, at the obtuse corners of the spans corresponding to the end abutments of the splayed girder bridges with parallel skew (Group 4). Tables 44 and 45

list the corresponding data values. LGA estimates are conservative for all the girders of the Group 4 bridges.

Table 34. ρ_{max} values for live load shear forces for exterior girders at the obtuse corners of simple span bridges, parallel skew (shaded cells indicate ρ_{max} values that exceed the targeted limits for applicability of LGA).

Bridge	Skew Index	CF Arrangement Notes	ρ_{maxG1}	ρ_{maxG4}
1	0.46	Contiguous	1.38	1.37
2	0.46	Staggered	1.22	1.31
5*	0.42	Contiguous	0.92	0.92
7	0.33	Contiguous	0.86	0.86
17*	0.28	Contiguous	0.94	0.94
18*	0.20	Staggered	0.97	0.97
21*	0.15	Parallel to skew	0.74	0.74

* This bridge meets, or nearly meets, the requirements for application of the recommended LGA-based procedures for the bridge design.

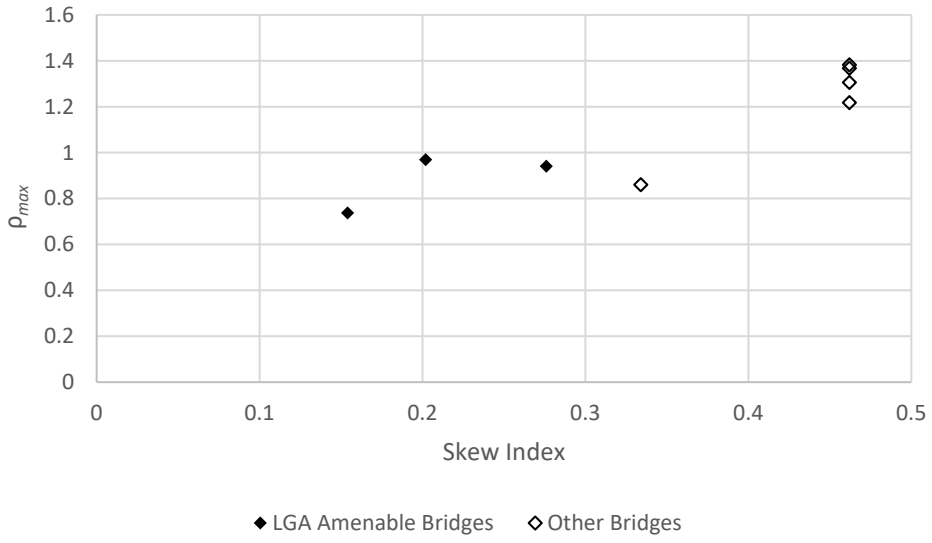

Figure 70. ρ_{max} values for live load shear forces for exterior girders at the obtuse corners of simple span bridges, parallel skew.

Table 35. ρ_{max} values for live load shear forces for first interior girders at the obtuse corners of simple span bridges, parallel skew.

Bridge	Skew Index	CF Arrangement Notes	ρ_{maxG2}
1	0.46	Contiguous	0.72
2	0.46	Staggered	0.68
5*	0.42	Contiguous	0.78
7	0.33	Contiguous	0.68
17*	0.28	Contiguous	0.65
18*	0.20	Staggered	0.74
21*	0.15	Parallel to skew	0.72

* This bridge meets, or nearly meets, the requirements for application of the recommended LGA-based procedures for the bridge design.

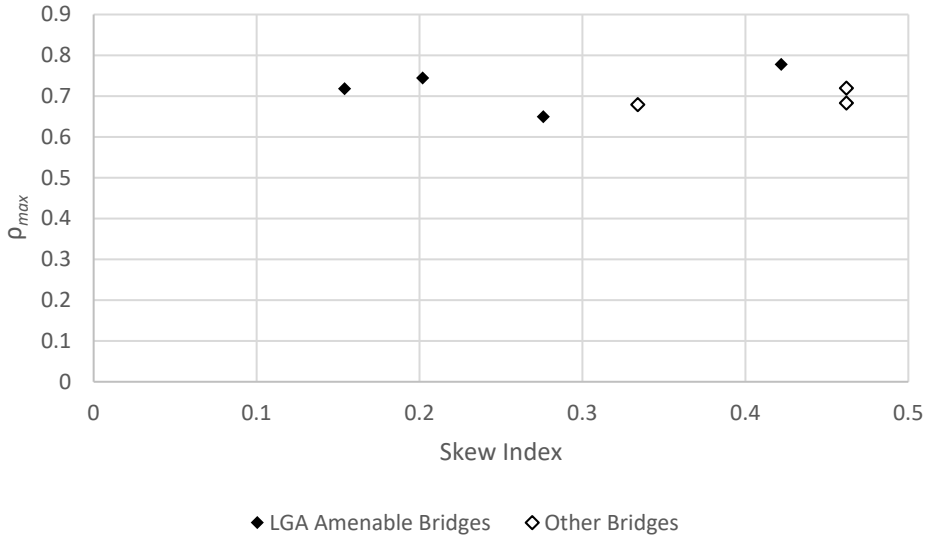

Figure 71. ρ_{max} values for live load shear forces for first interior girders at the obtuse corners of simple span bridges, parallel skew.

Table 36. ρ_{max} values for live load shear forces for exterior girders at obtuse corners corresponding to the end abutments of multi-span continuous bridges, parallel skew.

Bridge	Skew Index	CF Arrangement Notes	ρ_{maxG1}	ρ_{maxG4}
3	0.39	Contiguous, CF framing into bearing line	0.83	0.83
4*	0.39	Staggered	0.85	0.85
6*	0.35	Contiguous	0.97	0.97
8*	0.27	Staggered	0.88	0.88
9	0.47	Contiguous, CF framing into bearing line	0.92	0.99
10	0.47	Staggered	0.73	0.80
11*	0.26	Contiguous	0.99	0.99
23	0.37	Contiguous, CF framing into bearing line	0.96	0.97
24	0.37	Contiguous, inadequate offsets near bearing line	0.98	0.98
25	0.25	Contiguous, CF framing into bearing line	1.00	1.00
26*	0.15	Parallel to skew	0.94	0.94

* This bridge meets, or nearly meets, the requirements for application of the recommended LGA-based procedures for the bridge design.

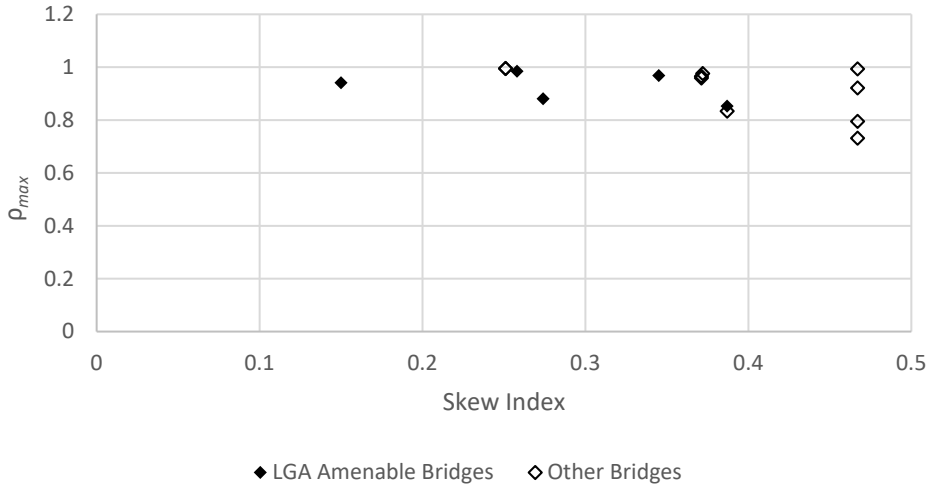

Figure 72. ρ_{max} values for live load shear forces for exterior girders at obtuse corners corresponding to end abutments of multi-span continuous bridges, parallel skew.

Table 37. ρ_{max} values for live load shear forces for exterior girders at obtuse corners of the spans at intermediate piers of multi-span continuous bridges, parallel skew.

Bridge	Skew Index	CF Arrangement Notes	ρ_{maxG1}	ρ_{maxG4}
3	0.39	Contiguous, CF framing into bearing line	0.83	0.83
4*	0.39	Staggered	0.85	0.85
6*	0.35	Contiguous	0.98	0.98
8*	0.27	Staggered	0.93	0.93
9	0.47	Contiguous, CF framing into bearing line	0.97	0.87
10	0.47	Staggered	0.81	0.68
11*	0.26	Contiguous	0.98	0.98
23	0.37	Contiguous, CF framing into bearing line	0.96	0.96
24	0.37	Contiguous, inadequate offsets near bearing line	0.95	0.95
25	0.25	Contiguous, CF framing into bearing line	0.90	0.89
26*	0.15	Parallel to skew	0.97	0.97

* This bridge meets, or nearly meets, the requirements for application of the recommended LGA-based procedures for the bridge design.

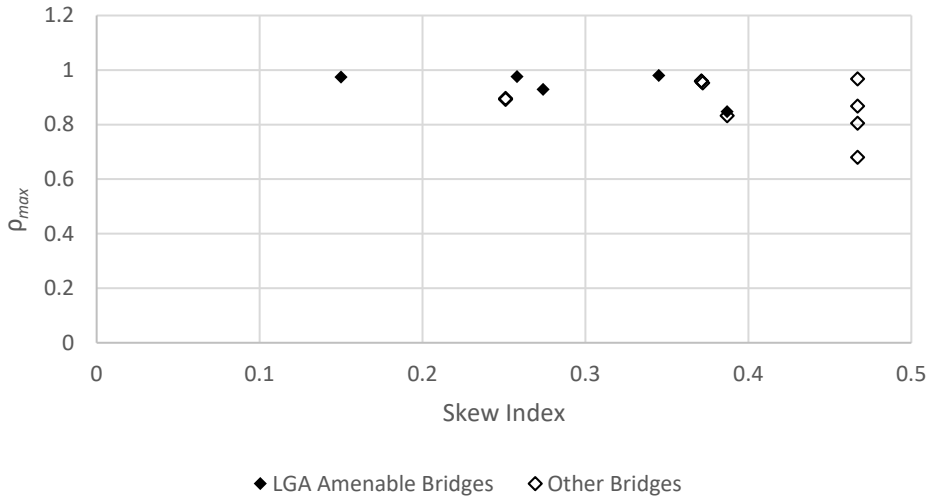

Figure 73. ρ_{max} values for live load shear forces for exterior girders at obtuse corners of the spans at intermediate piers of multi-span continuous bridges, parallel skew.

Table 38. ρ_{max} values for live load shear forces for first interior girders at obtuse corners of the spans at end abutments of multi-span continuous bridges, parallel skew.

Bridge	Skew Index	CF Arrangement Notes	ρ_{maxG2}
3	0.39	Contiguous, CF framing into bearing line	0.62
4*	0.39	Staggered	0.70
6*	0.35	Contiguous	0.67
8*	0.27	Staggered	0.73
9	0.47	Contiguous, CF framing into bearing line	0.67
10	0.47	Staggered	0.69
11*	0.26	Contiguous	0.72
23	0.37	Contiguous, CF framing into bearing line	0.74
24	0.37	Contiguous, inadequate offsets near bearing line	0.69
25	0.25	Contiguous, CF framing into bearing line	0.75
26*	0.15	Parallel to skew	0.79

* This bridge meets, or nearly meets, the requirements for application of the recommended LGA-based procedures for the bridge design.

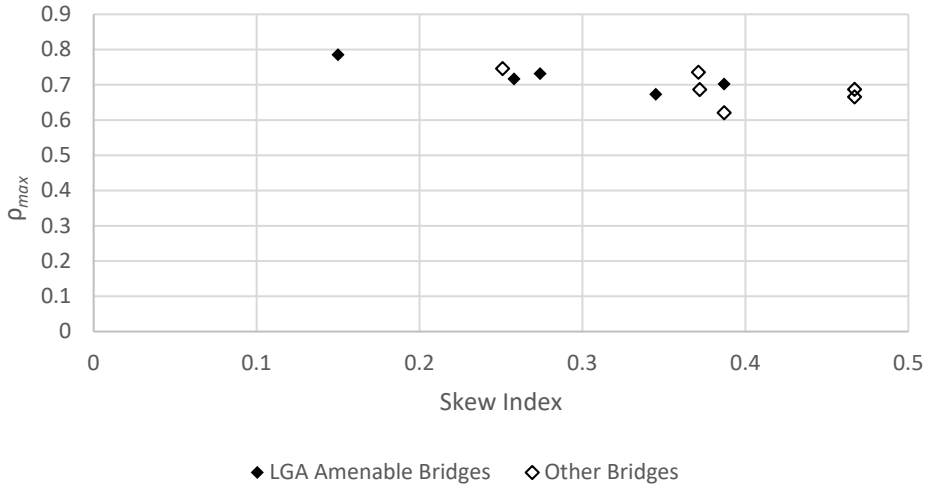

Figure 74. ρ_{max} values for live load shear forces for first interior girders at obtuse corners of the spans at end abutments of multi-span continuous bridges, parallel skew.

Table 39. ρ_{max} values for live load shear forces for first interior girders at obtuse corners of the spans at intermediate piers of multi-span continuous bridges, parallel skew.

Bridge	Skew Index	CF Arrangement Notes	ρ_{maxG2}
3	0.39	Contiguous, CF framing into bearing line	0.69
4*	0.39	Staggered	0.73
6*	0.35	Contiguous	0.71
8*	0.27	Staggered	0.76
9	0.47	Contiguous, CF framing into bearing line	0.66
10	0.47	Staggered	0.72
11*	0.26	Contiguous	0.72
23	0.37	Contiguous, CF framing into bearing line	0.70
24	0.37	Contiguous, inadequate offsets near bearing line	0.70
25	0.25	Contiguous, CF framing into bearing line	0.80
26*	0.15	Parallel to skew	0.80

* This bridge meets, or nearly meets, the requirements for application of the recommended LGA-based procedures for the bridge design.

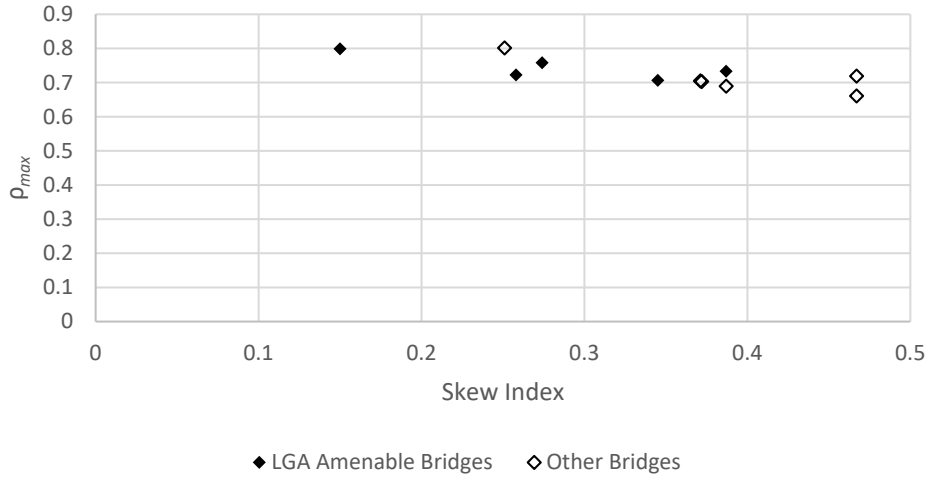

Figure 75. ρ_{max} values for live load shear forces for first interior girders at obtuse corners of the spans at intermediate piers of multi-span continuous bridges, parallel skew.

Table 40. ρ_{max} values for live load shear forces for exterior girders at obtuse corners of the spans at end abutments of multi-span continuous bridges, nonparallel skew.

Bridge	Skew Index	CF Arrangement Notes	ρ_{maxG1}	ρ_{maxG4}
12	0.32	Contiguous, CF framing into bearing line	0.99	0.99
13	0.23	Contiguous	0.57	0.57
14	0.23	Staggered	0.57	0.57
15	0.33	Contiguous	0.92	0.60
16	0.33	Staggered	0.90	0.63
22*	0.31	Contiguous	1.10	1.00

* This bridge meets, or nearly meets, the requirements for application of the recommended LGA-based procedures for the bridge design.

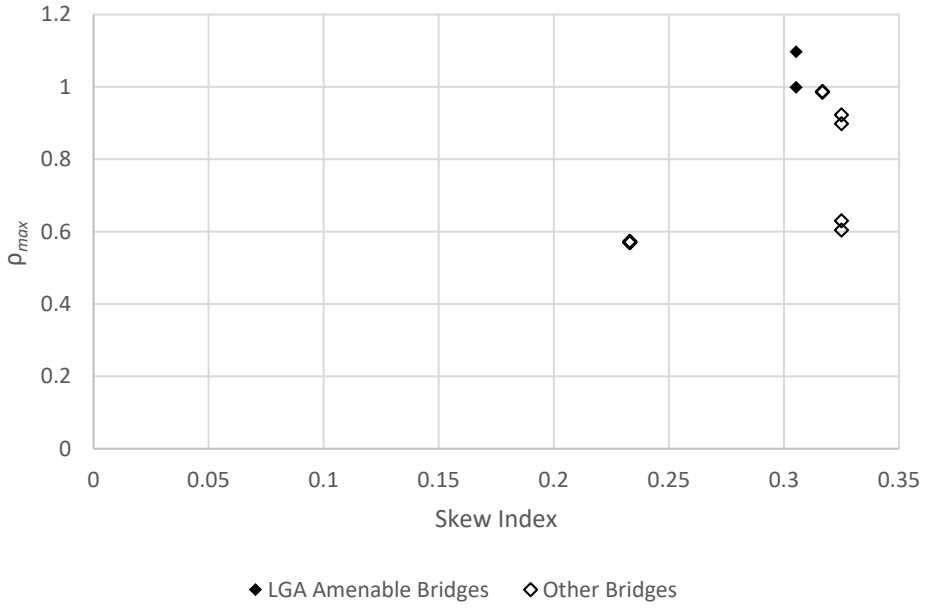

Figure 76. ρ_{max} values for live load shear forces for exterior girders at obtuse corners of the spans at end abutments of multi-span continuous bridges, nonparallel skew.

Table 41. ρ_{max} values for live load shear forces for exterior girders at obtuse corners of the spans at intermediate piers of multi-span continuous bridges, nonparallel skew.

Bridge	Skew Index	CF Arrangement Notes	ρ_{maxG1}	ρ_{maxG4}
12	0.32	Contiguous, CF framing into bearing line	0.89	0.88
13	0.23	Contiguous	0.72	0.71
14	0.23	Staggered	0.72	0.67
15	0.33	Contiguous	0.85	0.90
16	0.33	Staggered	0.82	0.86
22*	0.31	Contiguous	1.04	1.08

* This bridge meets, or nearly meets, the requirements for application of the recommended LGA-based procedures for the bridge design.

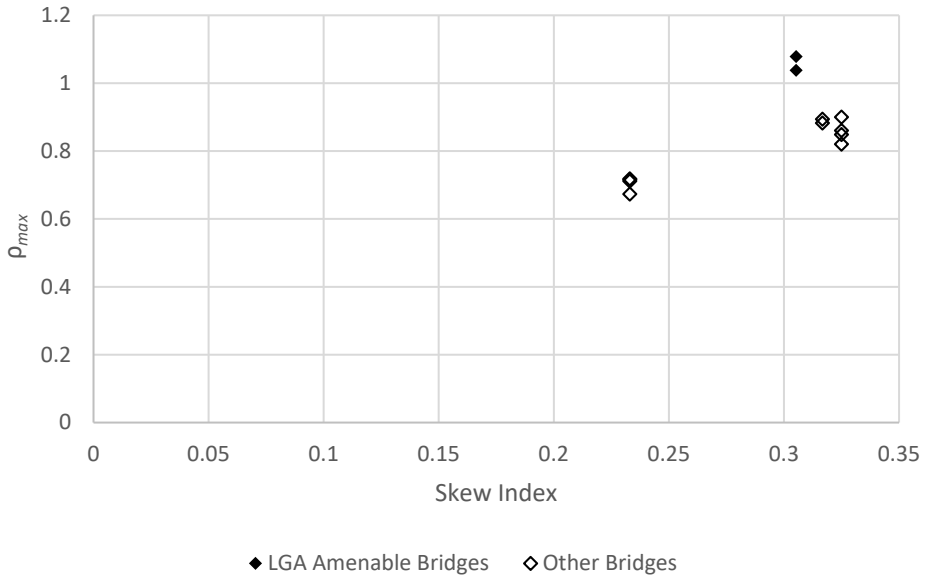

Figure 77. ρ_{max} values for live load shear forces for exterior girders at obtuse corners of the spans at intermediate piers of multi-span continuous bridges, nonparallel skew.

Table 42. ρ_{max} values for live load shear forces for first interior girders at obtuse corners of the spans at end abutments of multi-span continuous bridges, nonparallel skew.

Bridge	Skew Index	CF Arrangement Notes	ρ_{maxG2}
12	0.32	Contiguous, CF framing into bearing line	0.66
13	0.23	Contiguous	0.67
14	0.23	Staggered	0.68
15	0.33	Contiguous	0.66
16	0.33	Staggered	0.73
22*	0.31	Contiguous	0.67

* This bridge meets, or nearly meets, the requirements for application of the recommended LGA-based procedures for the bridge design.

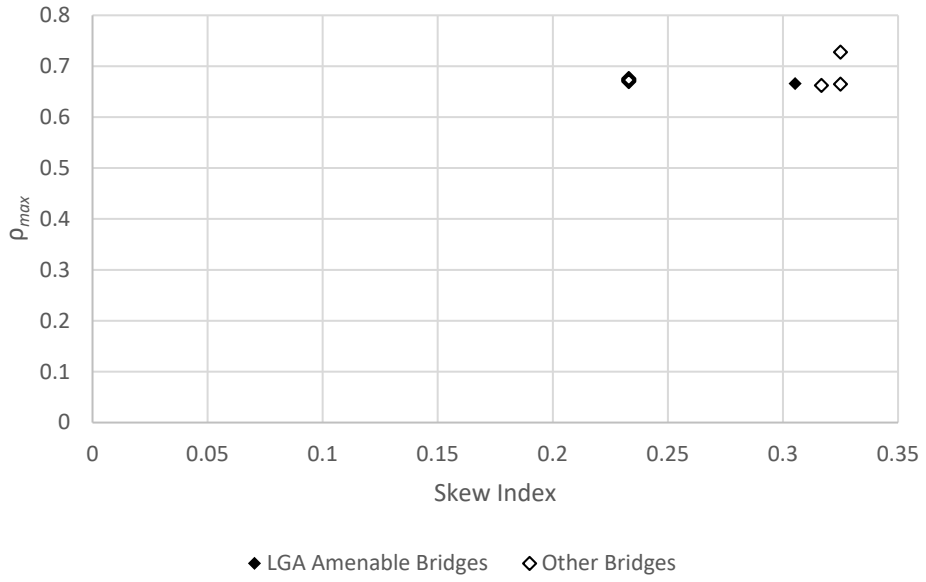

Figure 78. ρ_{max} values for live load shear forces for first interior girders at obtuse corners of the spans at end abutments of multi-span continuous bridges, nonparallel skew.

Table 43. ρ_{max} values for live load shear forces for first interior girders at obtuse corners of the spans at intermediate piers of multi-span continuous bridges, nonparallel skew.

Bridge	Skew Index	CF Arrangement Notes	ρ_{maxG2}
12	0.32	Contiguous, CF framing into bearing line	0.74
13	0.23	Contiguous	0.84
14	0.23	Staggered	0.83
15	0.33	Contiguous	0.69
16	0.33	Staggered	0.73
22*	0.31	Contiguous	0.67

* This bridge meets, or nearly meets, the requirements for application of the recommended LGA-based procedures for the bridge design.

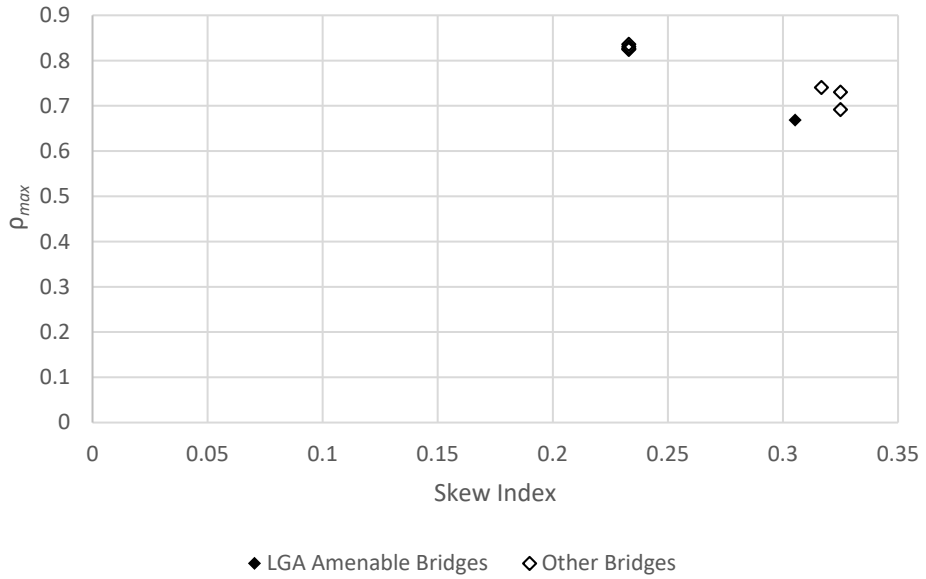

Figure 79. ρ_{max} values for live load shear forces for first interior girders at obtuse corners of the spans at intermediate piers of multi-span continuous bridges, nonparallel skew.

Table 44. ρ_{max} values for live load shear forces for exterior girders at the obtuse corners of simple-span splayed girder bridges, parallel skew.

Bridge	Skew Index	CF Arrangement Notes	ρ_{maxG1}	ρ_{maxG4}
19	0.45	Contiguous	0.88	0.96
20	0.45	Staggered	0.80	0.85

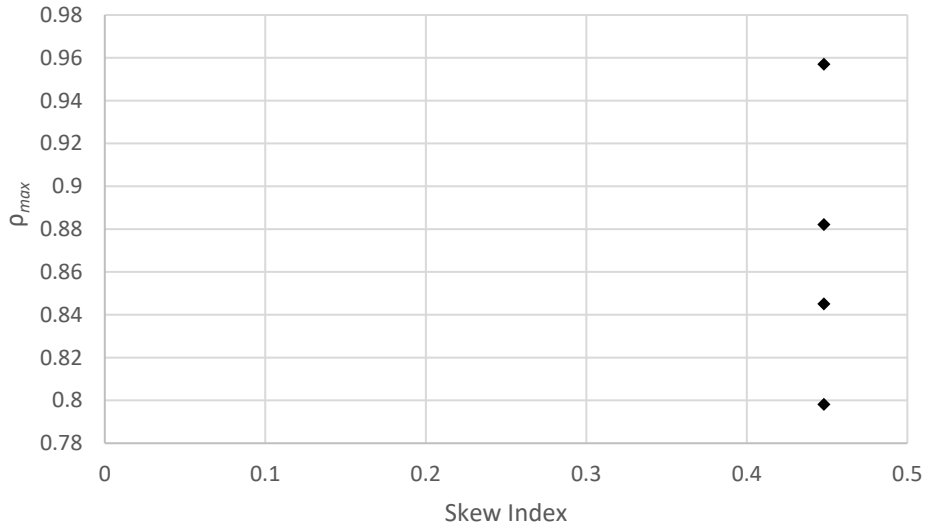

Figure 80. ρ_{max} values for live load shear forces for exterior girders at the obtuse corners of simple-span splayed girder bridges, parallel skew.

Table 45. ρ_{max} values for live load shear forces for first interior girders at the obtuse corners of simple-span splayed girder bridges, parallel skew.

Bridge	Skew Index	CF Arrangement Notes	ρ_{maxG2}
19	0.45	Contiguous	0.64
20	0.45	Staggered	0.79

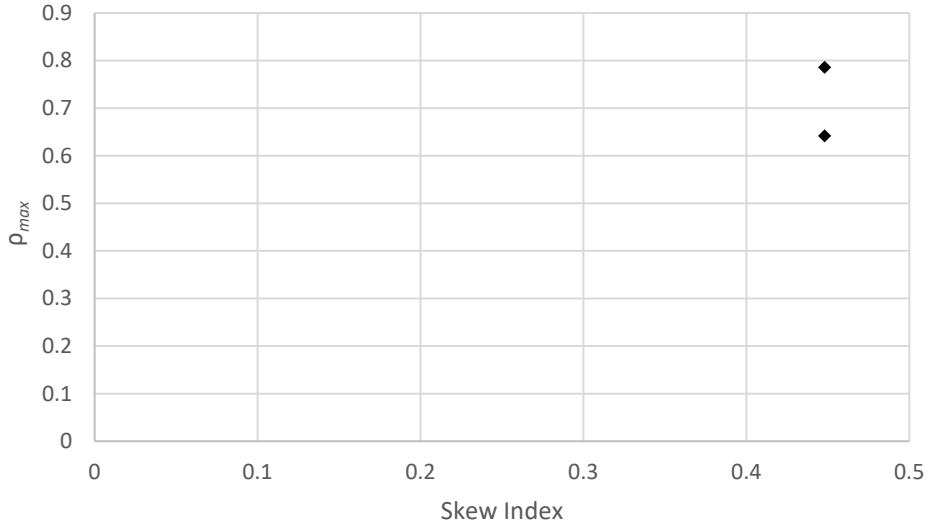

Figure 81. ρ_{max} values for live load shear forces for first interior girders at the obtuse corners of simple-span splayed girder bridges, parallel skew.

5.3.5 Girder Strength I Bearing Reactions

Bearing reactions include the contributions from the girders through girder shear forces and bearing line cross-frames through cross-frame shear forces. Some of the study bridges do not have cross-frames at intermediate pier bearing lines, but have intermediate cross-frames framing into the intermediate bearings. In such cases, bearing reactions include contributions from the intermediate cross-frames framing into the bearing. Similar to the Strength I (STR I) shear forces, the ρ_{max} values for the STR I bearing reactions at obtuse corners of bridge simple spans, and the fascia girders at intermediate pier locations of bridge continuous spans, are observed to be greater than unity. ρ_{max} values for STR I bearing reactions, if greater than unity serve as a correction factor to be applied to the LGA reaction estimates at the above locations to obtain 3D FEA reactions estimates. Cells that do not satisfy the tolerance established in Section5.2.2, have a ρ_{max} value larger than 1.11 and are highlighted in the tables in this section.

Figures 82 through 85 show plots of the largest STR I bearing reactions ρ_{max} values at simple span obtuse corners and on the fascia girders of continuous spans. Tables 46 through 49 list the corresponding data. Typically, the maximum difference between LGA and 3D FEA downward reactions occurs at the obtuse corners of the bridge plans (i.e., at the abutments). It must be noted that while the ρ_{max} values for the STR I bearing reactions are the largest at these locations, the magnitude of the LGA reaction at the obtuse corner may not be the largest when compared to LGA reactions at the other bearings. Additionally, the sum total of the STR I bearing reactions from LGA is not equal to the 3D FEA reactions because of differences in the 3D FEA and LGA live load reaction envelopes. For the 26 bridges studied, uplift is not observed in any of the bridges.

However, the trend in the ρ_{max} values for the STR I reaction is not observed for the STR I uplift case. The 3D FEA reactions are typically smaller than the LGA reactions for the STR I uplift load combination (i.e., greater tendency for uplift) at the acute corners, and larger at the obtuse corners. The differences are due to the use of conservative AASHTO live load distribution factors. Additional differences are introduced by the use of the minimum envelope of the live load bearing reactions in the STR I uplift combination.

Table 46. ρ_{max} values for STR I bearing reactions at obtuse corners for simple span bridges, parallel skew (shaded cells indicate ρ_{max} values that exceed the targeted limits for applicability of LGA).

Bridge	Skew Index	ρ_{max}
1	0.46	1.34
2	0.46	1.23
5*	0.42	1.02
7	0.33	1.12
17*	0.28	1.03
18*	0.20	1.02
21*	0.15	0.90

* This bridge meets, or nearly meets, the requirements for application of the recommended LGA-based procedures for the bridge design.

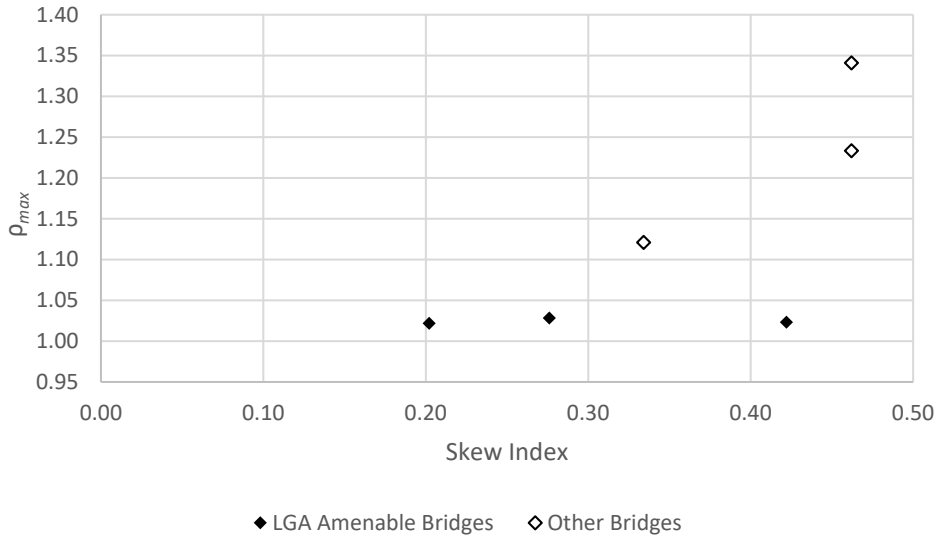

Figure 82. ρ_{max} values for STR I bearing reactions at obtuse corners for simple span bridges, parallel skew.

Table 47. ρ_{max} values for STR I bearing reactions at obtuse corners of the bridge (at the abutments) for multi-span continuous bridges, parallel skew (shaded cells indicate ρ_{max} values that exceed the targeted limits for applicability of LGA).

Bridge	Skew Index	ρ_{max}
3	0.39	1.02
4*	0.39	0.98
6*	0.35	1.08
8*	0.27	0.99
9	0.47	1.06
10	0.47	0.94
11*	0.26	1.11
23	0.37	1.04
24	0.37	0.93
25	0.25	1.03
26*	0.15	1.11

* This bridge meets, or nearly meets, the requirements for application of the recommended LGA-based procedures for the bridge design.

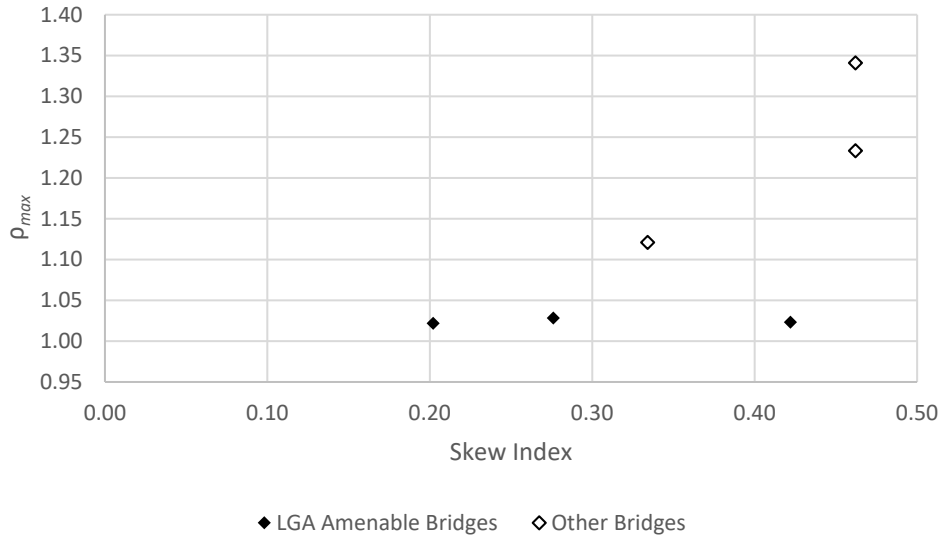

Figure 83. ρ_{max} values for STR I bearing reactions at obtuse corners of the bridge (at the abutments) for multi-span continuous bridges, parallel skew.

Table 48. ρ_{max} values for STR I bearing reactions at obtuse corners of the bridge (at the abutments) for multi-span continuous bridges, nonparallel skew.

Bridge	Skew Index	ρ_{max}
12	0.32	1.09
13	0.23	0.96
14	0.23	0.97
15	0.33	1.03
16	0.33	1.02
22*	0.31	1.11

* This bridge meets, or nearly meets, the requirements for application of the recommended LGA-based procedures for the bridge design.

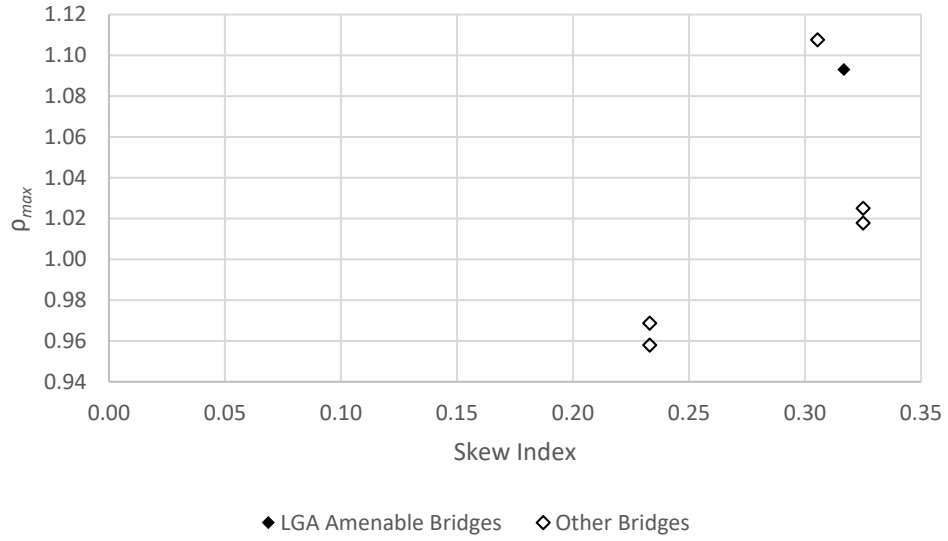

Figure 84. ρ_{max} values for STR I bearing reactions at obtuse corners of the bridge (at the abutments) for multi-span continuous bridges, nonparallel skew.

Table 49. ρ_{max} values for STR I bearing reactions at obtuse corners for simple-span splayed girder bridges, parallel skew (shaded cells indicate ρ_{max} values that exceed the targeted limits for applicability of LGA).

Bridge	Skew Index	ρ_{max}
19	0.448	1.17
20	0.448	1.03

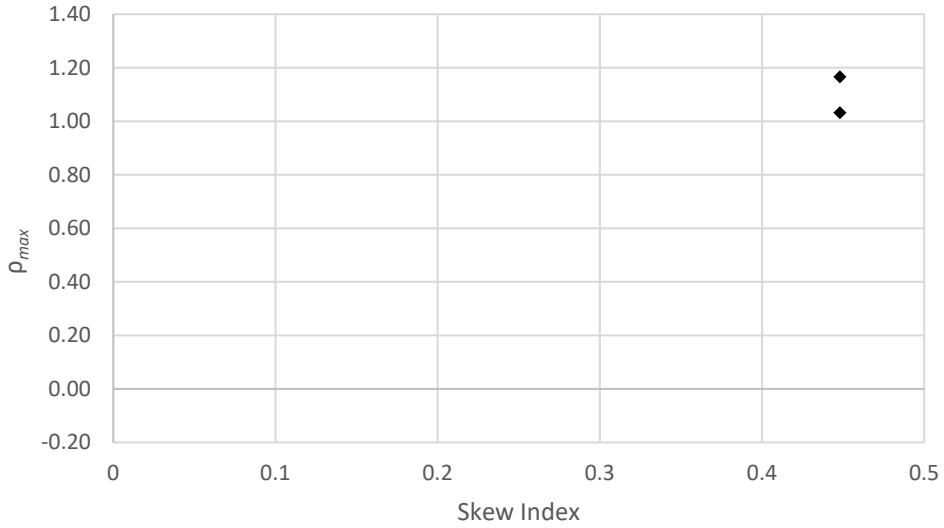

Figure 85. ρ_{max} values for STR I bearing reactions at obtuse corners for simple-span splayed girder bridges, parallel skew.

5.3.6 Girder Maximum TDL Vertical Displacements, Considering the Effects of SDLF Detailing of the Cross-Frames

In a skewed bridge, intermediate cross-frames that are perpendicular to the girders connect to the girders at different longitudinal positions within the span. At such cross-frames, the girders do not deflect by the same amount vertically. Cross-frames employed in the 26 bridges studied are primarily V or inverted V shaped truss-like assemblies. All the cross-frames considered in the studies have a top chord. Such cross-frames have a high in-plane stiffness. Hence, the cross-frames tend to twist the girders such that they essentially have an equal layover at the cross-frame ends due to the differential displacements in the girders. This interaction between the cross-frames and girders influences the overall vertical displacement profile of girders in a skewed bridge. After the concrete deck hardens, a similar participation of the deck is observed in maintaining overall compatibility in the structural system of the bridge deck, cross-frames and girders. Additionally, load distribution may be observed from one span to another, especially in bridges with unequal spans, to maintain compatibility of the continuous girders within adjacent spans. The 3D structural behavior observed in a skewed bridge is a main source of differences in the vertical displacement estimates from LGA and 3D FEA. For LGA, in this research, wet concrete loads, barrier rail loads and wearing surface and utilities loads are distributed equally to the girders in the bridge under consideration. However, the complex 3D action in skewed bridges includes transverse distribution of loads among the girders via cross-frames and the bridge deck for composite loads. Hence, in the bridges that exhibit significant 3D behavior, large differences are observed in the vertical displacements for all load cases, except for SDL (SDLF) load case.

Figure 86 shows a comparative plot of the LGA and 3D FEA displacements for Girder 1 of the nonparallel skew four-span continuous Bridge 13. The 3D FEA vertical displacements in Span 3 are larger than the LGA vertical displacements. On the other hand, the 3D FEA vertical displacements in Span 4 are larger than the LGA vertical displacements. This behavior indicates a load transfer between Spans 3 and 4 that increases the girder vertical displacements in Span 3 and reduces it in Span 4.

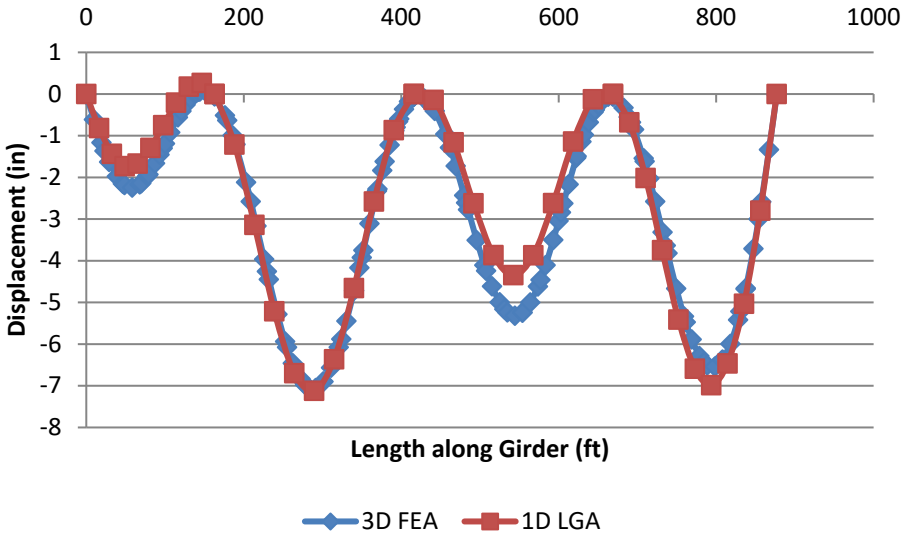

Figure 86. TDL (SDLF) vertical displacements for Girder 1 of Bridge 13.

Measures of differences ε_{max2} and ε_{max3} are used in the comparison of LGA and 3D FEA vertical displacement estimates. ε_{max2}, and ε_{max3} are calculated using the maximum TDL (SDLF) vertical displacement estimates, as indicated in Equation 25 and Equation 26 respectively.

Tables 50 through 53 show the differences in the maximum TDL (SDLF) displacements between the LGA and 3D FEA values for the various girders of the four groups of bridges. These values for each girder studied are compared to the longitudinal

"tolerance" established in Section 5.2.3. Additionally, differences in the differences in the maximum LGA and 3D FEA displacements in the representative central interior girder and an exterior girder for each bridge are compared to the transverse "tolerance" established in Section 5.2.3. Cells that do not satisfy the established "tolerances" are highlighted in the tables.

Table 50. Maximum TDL (SDLF) displacement differences in maximums (inches) between LGA and 3D FEA for bridge girders, simple span bridges, parallel skew (shaded cells indicate values that exceed the targeted limits for applicability of LGA).

Bridge	Skew Index	Width (ft)	Span Length (ft)	CF Framing Arrangement Notes	$[\Delta_{LGAmax} - \Delta_{3DFEAmax}]_{G1}$ (in)	$[\Delta_{LGAmax} - \Delta_{3DFEAmax}]_{G2}$ (in)	$[\Delta_{LGAmax} - \Delta_{3DFEAmax}]_{G3}$ (in)	$[\Delta_{LGAmax} - \Delta_{3DFEAmax}]_{G4}$ (in)	ε_{max3} w_g	ε_{max2}	ε_{max3}
1	0.46	87.1	208	Contiguous	-1.14	-0.66	0.88	-1.10	2.02	0.00045	0.0019
2	0.46	87.1	208	Staggered	-0.31	-0.10	0.34	-0.25	0.66	0.00014	0.0006
5	0.42	115.4	144	Contiguous	-0.47	-0.29	-0.07	-0.47	0.40	0.00027	0.0003
7	0.33	54.4	96	Contiguous	-0.64	0.08	0.34	-0.64	0.98	0.00055	0.0015
17*	0.28	71.1	202	Contiguous	-0.69	-0.39	-0.04	-0.69	0.64	0.00028	0.0008
18*	0.20	58.2	212	Staggered	-0.40	-0.29	-0.20	-0.40	0.20	0.00016	0.0003
21*	0.15	135.1	241	Parallel to skew	-0.07	-0.27	-0.49	-0.07	0.42	0.00017	0.0003

* This bridge meets, or nearly meets, the requirements for application of the recommended LGA-based procedures for the bridge design.

Table 51. Maximum TDL (SDLF) displacement differences in maximums (inches) between LGA and 3D FEA for bridge girders, multi-span continuous bridges, parallel skew (shaded cells indicate values that exceed the targeted limits for applicability of LGA).

Bridge	Skew Index	Width (ft)	Span Length (ft)	CF Framing Arrangement Notes	$[\Delta_{LGAmax} - \Delta_{3DFEAmax}]_{G1}$ (in)	$[\Delta_{LGAmax} - \Delta_{3DFEAmax}]_{G2}$ (in)	$[\Delta_{LGAmax} - \Delta_{3DFEAmax}]_{G3}$ (in)	$[\Delta_{LGAmax} - \Delta_{3DFEAmax}]_{G4}$ (in)	ε_{max3} w_g	ε_{max2}	ε_{max3}
3	0.39	102.1	185	Contiguous, CF framing into bearing line	-1.20	-0.63	-0.17	-1.20	1.03	0.00054	0.0008
4*	0.39	102.1	185	Staggered	-0.91	-0.42	-0.39	-0.91	0.53	0.00041	0.0004
6	0.35	112.2	116	Contiguous	-0.33	-0.24	-0.25	-0.33	0.08	0.00023	0.0001
8*	0.27	84.2	173	Staggered	-0.19	-0.34	-0.48	-0.19	0.28	0.00023	0.0003
9	0.47	54.3	202	Contiguous, CF framing into bearing line	-1.56	-0.71	0.00	-0.19	1.56	0.00064	0.0024
10	0.47	54.3	202	Staggered	-1.07	-0.46	-0.08	-0.53	0.99	0.00044	0.0015
11	0.26	67.1	188	Contiguous, CF framing into bearing line	-0.25	-0.12	-0.03	-0.25	0.22	0.00011	0.0003
23	0.37	84.2	252	Contiguous, CF framing into bearing line	-2.09	-1.11	0.12	-2.10	2.20	0.00070	0.0022
24	0.37	55.3	170	Contiguous, inadequate offsets near bearing line	-0.79	-0.38	0.08	-0.79	0.87	0.00039	0.0013
25	0.25	43.1	196	Contiguous, CF framing into bearing line	-0.99	-0.26	-0.26	-0.99	0.73	0.00042	0.0014
26*	0.15	73.1	92	Parallel to skew	-0.17	-0.09	-0.02	-0.17	0.15	0.00016	0.0002

* This bridge meets, or nearly meets, the requirements for application of the recommended LGA-based procedures for the bridge design.

Table 52. Maximum TDL (SDLF) displacement differences in maximums (inches) between LGA and 3D FEA for bridge girders, multi-span continuous bridges, nonparallel skew (shaded cells indicate values that exceed the targeted limits for applicability of LGA).

Bridge	Skew Index	Width (ft)	Span Length (ft)	CF Framing Arrangement Notes	$[\Delta_{LGAmax} - \Delta_{3DFEAmax}]_{G1}$ (in)	$[\Delta_{LGAmax} - \Delta_{3DFEAmax}]_{G2}$ (in)	$[\Delta_{LGAmax} - \Delta_{3DFEAmax}]_{G3}$ (in)	$[\Delta_{LGAmax} - \Delta_{3DFEAmax}]_{G4}$ (in)	ε_{max3} w_g	ε_{max2}	ε_{max3}
12	0.32	42.5	202	Contiguous, CF framing into bearing line	-0.78	-0.01	-0.10	-0.78	0.68	0.00032	0.0013
13	0.23	43.1	253	Contiguous	0.06	0.09	-0.03	0.26	0.30	0.00009	0.0006
14	0.23	43.1	253	Staggered	-0.15	0.04	-0.06	0.16	0.22	0.00005	0.0004
15	0.33	60.2	188	Contiguous	-1.03	0.32	0.34	-1.22	1.57	0.00054	0.0022
16	0.33	60.2	188	Staggered	-1.04	0.30	0.22	-1.14	1.36	0.00050	0.0019
22*	0.31	85.5	204	Contiguous	-0.28	-0.14	0.01	-0.61	0.63	0.00025	0.0006

* This bridge meets, or nearly meets, the requirements for application of the recommended LGA-based procedures for the bridge design.

Table 53. Maximum TDL (SDLF) displacement differences in maximums (inches) between LGA and 3D FEA for bridge girders, splayed girder bridges, parallel skew (shaded cells indicate values that exceed the targeted limits for applicability of LGA).

Bridge	Skew Index	Width (ft)	Span Length (ft)	CF Framing Arrangement Notes	$[\Delta_{LGAmax} - \Delta_{3DFEAmax}]_{G1}$ (in)	$[\Delta_{LGAmax} - \Delta_{3DFEAmax}]_{G2}$ (in)	$[\Delta_{LGAmax} - \Delta_{3DFEAmax}]_{G3}$ (in)	$[\Delta_{LGAmax} - \Delta_{3DFEAmax}]_{G4}$ (in)	$\varepsilon_{max3} * w_g$	ε_{max2}	ε_{max3}
19	0.31	67.6	196	Contiguous	-2.19	0.16	1.13	-1.67	3.32	0.00093	0.0041
20	0.31	67.6	196	Staggered	-1.61	0.32	0.61	-1.55	2.22	0.00069	0.0027

5.3.7 Girder Maximum TDL Vertical Displacements, Considering the Effects of Staged and Unstaged Deck Placement

Analyses for concrete dead load often assume unstaged deck placement. The implicit assumption in unstaged deck placement is that the entire concrete deck is cast before any part of the deck cast at a previous point of time hardens. In this case, the bare steel structure consisting of I-girders and cross-frames resists resist their own self-weight and the weight of the wet concrete deck slab, deck forms and construction equipment. The deck becomes composite with the steel I-girders once the deck hardens. Depending on the length of the bridge, casting of the deck in stages may be required. If the deck is cast in stages, some portions of the deck become composite with the girders before other portions. As a result, the behavior of the bridge changes during staged deck placement. For simply-supported bridges, casting may proceed from both ends of the bridge. For continuous span bridges, the deck in the positive moment regions is typically placed before the negative moment regions over the intermediate supports in order to minimize cracking of the deck within the negative moment regions. (NHI 2011).

Staged deck placement is studied for four bridges in this research – the two-span continuous Bridges 3 and 4, the three-span continuous Bridge 12 and four-span continuous Bridge 15. Bridges 3, 4 and 12 have parallel skew whereas Bridge 15 has nonparallel skew. Tabls 54 through 56 show the concrete dead load (CDL) displacements for staged and unstaged deck placement, for the exterior, first interior and central interior girders. The differences in the bending moments due to staged and unstaged deck placement are not found to be significant, and can be ignored for all practical purposes in these bridges. However, the differences between the unstaged and staged deck placement vertical

displacements are not insignificant, and cannot be ignored. Staged deck placement displacements are larger than unstaged deck placement displacements. This is generally due to the fact that the vertical displacements associated with the loading from the early stage(s) are larger within the span(s) where the deck concrete is being placed, and the concrete is assumed to set-up in this stage or stages, resulting in larger final vertical displacement than if the deck did not set-up until the entire deck were placed. For exterior girders, the ρ_{max} values reduce for Bridges 3, 4 and 15. The ρ_{max} values increase for the exterior girder of Bridge 12, but the LGA staged deck placement displacement is larger than 3D FEA staged deck placement displacement. The differences between the maximums of LGA and 3D FEA staged deck displacements are larger than the differences between the maximums of LGA and 3D FEA unstaged deck displacements. However, as seen earlier, exterior girder TDL (SDLF) displacements are more critical and the staged deck placement results can potentially improve LGA estimates compared to 3D FEA estimates.

Table 54. Comparison of CDL displacements for staged and unstaged deck placement for exterior girders (shaded cells indicate ρ_{max} values that exceed the targeted limits for applicability of LGA).

Bridge	Deck Construction	LGA (in)	3D FEA (in)	LGA - 3D FEA (in)	ρ_{maxG1}	ρ_{maxG4}
3	Unstaged	4.87	5.76	-0.88	1.18	1.18
3	Staged	5.40	5.83	-0.43	1.08	1.08
4*	Unstaged	4.87	5.33	-0.47	1.10	1.10
4*	Staged	5.36	5.73	-0.37	1.07	1.07
12	Unstaged	6.47	6.58	-0.11	1.02	1.02
12	Staged	7.86	7.01	0.85	0.89	0.89
15	Unstaged	6.50	7.35	-0.85	1.13	1.15
15	Staged	6.83	7.61	-0.79	1.12	1.08

* This bridge meets, or nearly meets, the requirements for application of the recommended LGA-based procedures for the bridge design.

Table 55. Comparison of CDL displacements for staged and unstaged deck placement for first interior girders.

Bridge	Deck Construction	LGA (in)	3D FEA (in)	LGA - 3D FEA (in)	ρ_{maxG2}
3	Unstaged	4.87	5.35	-0.48	1.10
3	Staged	5.41	5.64	-0.22	1.04
4*	Unstaged	4.87	5.14	-0.27	1.06
4*	Staged	5.37	5.69	-0.32	1.06
12	Unstaged	6.47	6.46	0.01	1.00
12	Staged	7.82	6.91	0.91	0.88
15	Unstaged	7.59	7.17	0.42	0.94
15	Staged	8.10	7.53	0.57	0.93

* This bridge meets, or nearly meets, the requirements for application of the recommended LGA-based procedures for the bridge design.

Table 56. Comparison of CDL displacements for staged and unstaged deck placement for central interior girders (shaded cells indicate ρ_{max} values that exceed the targeted limits for applicability of LGA).

Bridge	Deck Construction	LGA (in)	3D FEA (in)	LGA - 3D FEA (in)	ρ_{maxG3}
3	Unstaged	4.87	5.06	-0.19	1.04
3	Staged	5.41	5.63	-0.22	1.04
4*	Unstaged	4.87	5.35	-0.48	1.10
4*	Staged	5.37	5.97	-0.59	1.11
12	Unstaged	6.47	6.46	0.00	1.00
12	Staged	8.19	6.91	1.28	0.84
15	Unstaged	7.62	7.24	0.38	0.95
15	Staged	8.27	7.67	0.60	0.93

* This bridge meets, or nearly meets, the requirements for application of the recommended LGA-based procedures for the bridge design.

5.3.8 Girder Layover under TDL (SDLF)

At skewed bearing lines, the cross-frames connect to the girders along the skew angle. The girders cannot displace vertically, but can rotate at the bearings. End bearing cross-frames typically have a high in-plane stiffness. To maintain compatibility with the major-axis bending rotations associated with girders, the skewed end-bearing cross-frames twist the girders. In parallel skew bridges, the girders twist in opposite direction at the two ends of the bridge. The twist at the bridge ends are reported as layover in radians and additionally as the displacement of the top flange relative to the bottom flange in this research.

Girder layovers, calculated by the FDOT recommended procedure described in Section 5.2.1.2 are considered LGA estimates, and are compared to 3D FEA estimates. Figures 87 through 90 show layover estimates from 3D FEA, LGA, and the difference in the layover estimates between LGA and 3D FEA for the girders that have the maximum differences, for the four groups of bridges. Plots of layovers in radians and layovers in terms of the relative movement of the top flange with respect to the bottom flange in inches are placed next to each other in the same figure for easy comparison. The X axis of the plots indicates the bridge number followed by the angle of skew at the abutment. These plots are preceded by Tables 57 through 60, listing the corresponding data values. The girder number for which the difference in LGA and 3D FEA layovers is maximum is indicated in the tables for each bridge

The layovers for parallel skew bridges are largest for the exterior girders and decrease as one moves toward the interior girders. The small angle approximation where $\tan(\theta) = \theta$ is used, in the estimation of the layovers. The largest CDL layover is approximately 0.02

radians, which amounts to 1.15°. The tangent of this angle is 0.02003. Therefore, the layover estimates are theoretically accurate to the fifth decimal, to the extent that the accuracy depends on the small angle approximation. The largest difference in the layover estimates between LGA and 3D FEA is observed for Bridges 3, 6, 9 and 24. The cross-frame layouts for all these bridges is such that either the intermediate cross-frames frame into the bearing lines or have very small offsets relative to the bearing lines. This introduces significant 3D action through deformation of end cross-frames in the bridge, resulting in larger differences between the LGA and 3D FEA layover estimates. The fact that layover differences are smaller for the bridges having alternative cross-frame arrangements reinforces this observation.

Table 57. Maximum differences in LGA and 3D FEA CDL girder layovers at left abutment for simple span bridges, parallel skew.

Bridge	Skew Index	Skew Angle	Web Depth	Girder	LGA (rad)	3D FEA (rad)	LGA - 3D FEA (rad)	LGA (in)	3D FEA (in)	LGA - 3D FEA (in)
21*	0.15	16.2	102	3	0.0029	0.0031	-0.0002	0.3007	0.3206	-0.0199
5*	0.42	29.4	60.0	3	0.0039	0.0054	-0.0015	0.2353	0.3226	-0.0873
7	0.33	35.5	39.4	1	0.0083	0.0100	-0.0016	0.3273	0.3920	-0.0647
18*	0.20	39.7	84.3	3	0.0096	0.0100	-0.0004	0.8077	0.8387	-0.0310
17*	0.28	41.5	90	1	0.0094	0.0105	-0.0011	0.8421	0.9454	-0.1033
1	0.46	49.4	62	1	0.0184	0.0209	-0.0025	1.1392	1.2928	-0.1536
2	0.46	49.4	62	4	0.0186	0.0181	0.0004	1.1510	1.1247	0.0262

* This bridge meets, or nearly meets, the requirements for application of the recommended LGA-based procedures for the bridge design.

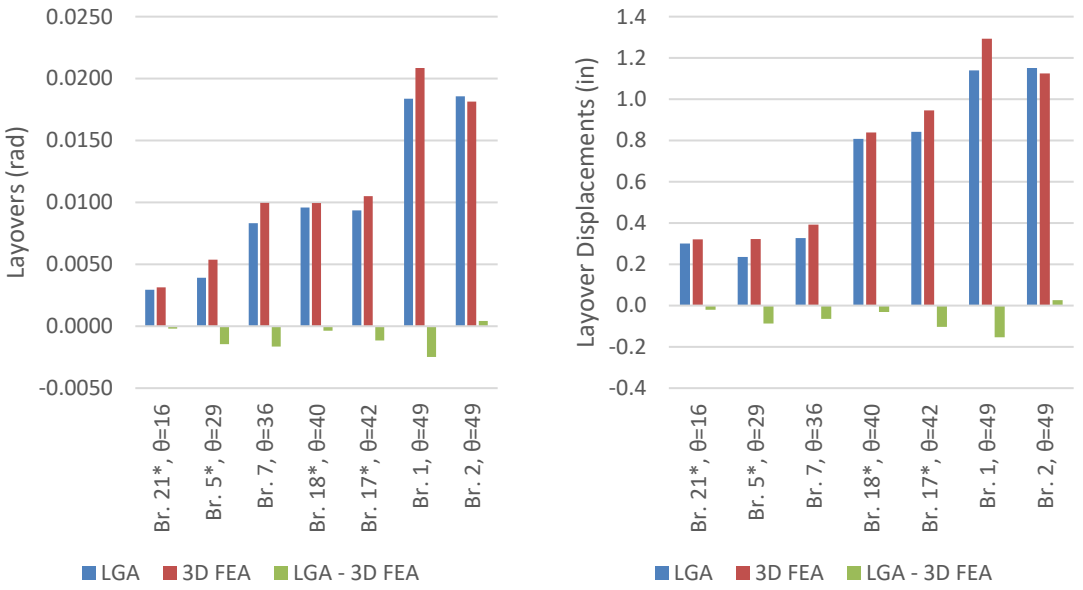

* This bridge meets, or nearly meets, the requirements for application of the recommended LGA-based procedures for the bridge design.

Figure 87. Maximum differences in LGA and 3D FEA CDL girder layovers at left abutment for simple span bridges, parallel skew.

Table 58. Maximum differences in LGA and 3D FEA CDL girder layovers at left abutment for multi-span continuous bridges, parallel skew.

Bridge	Skew Index	Skew Angle	Web Depth	Girder	LGA (rad)	3D FEA (rad)	LGA - 3D FEA (rad)	LGA (in)	3D FEA (in)	LGA - 3D FEA (in)
26*	0.15	10.0	34.0	1	0.0004	0.0003	0.0001	0.0143	0.0104	0.0039
6*	0.35	20.7	39	3	0.0034	0.0038	-0.0003	0.1336	0.1470	-0.0134
8*	0.27	23.4	72	3	0.0018	0.0020	-0.0003	0.1276	0.1472	-0.0197
11*	0.26	38.1	74	1	0.0085	0.0089	-0.0004	0.6282	0.6573	-0.0290
3	0.39	38.2	79	1	0.0071	0.0075	-0.0004	0.5637	0.5964	-0.0327
4*	0.39	38.2	79	3	0.0071	0.0080	-0.0008	0.5630	0.6286	-0.0655
23	0.37	50.7	94	4	0.0124	0.0149	-0.0026	1.1619	1.4026	-0.2407
24	0.37	52.7	70	1	0.0078	0.0092	-0.0014	0.5430	0.6427	-0.0997
25	0.25	54.5	90	1	0.0114	0.0131	-0.0017	1.0284	1.1778	-0.1494
9	0.47	57.2	71	1	0.0148	0.0174	-0.0026	1.0483	1.2364	-0.1881
10	0.47	57.2	71	1	0.0148	0.0164	-0.0016	1.0491	1.1639	-0.1149

* This bridge meets, or nearly meets, the requirements for application of the recommended LGA-based procedures for the bridge design.

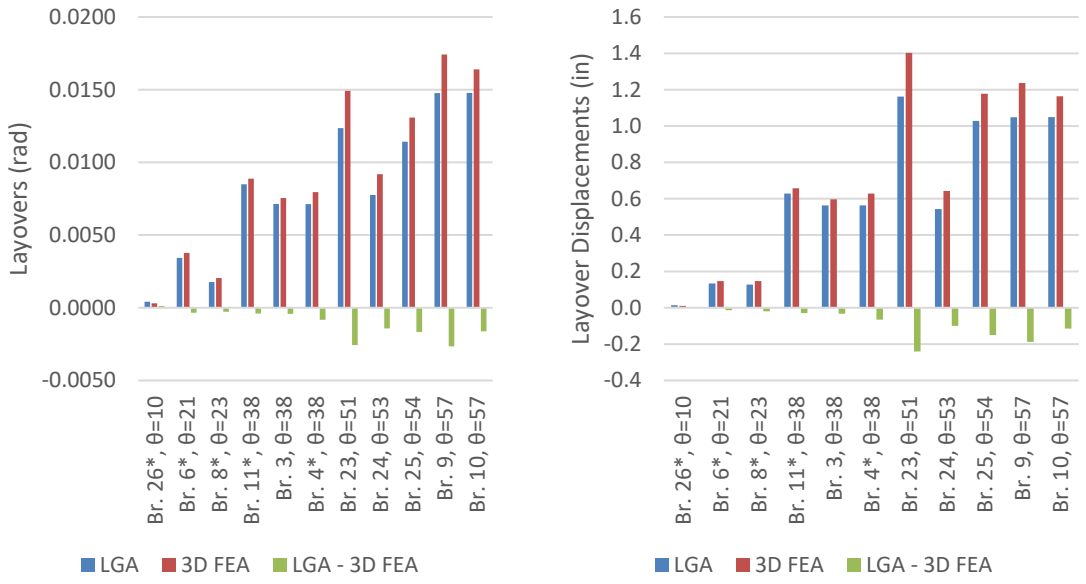

* This bridge meets, or nearly meets, the requirements for application of the recommended LGA-based procedures for the bridge design.

Figure 88. Maximum differences in LGA and 3D FEA CDL girder layovers at left abutment for multi-span continuous bridges, parallel skew.

Table 59. Maximum differences in LGA and 3D FEA CDL girder layovers at left abutment for multi-span continuous bridges, nonparallel skew.

Bridge	Skew Index	Skew Angle	Web Depth	Girder	LGA (rad)	3D FEA (rad)	LGA - 3D FEA (rad)	LGA (in)	3D FEA (in)	LGA - 3D FEA (in)
13	0.23	0	96	4	0.0000	0.0001	-0.0001	0.0000	0.0112	-0.0112
14	0.23	0	96	4	0.0000	0.0001	-0.0001	0.0000	0.0114	-0.0114
22*	0.31	28.36	86	4	0.0059	0.0062	-0.0004	0.5039	0.5355	-0.0316
12	0.32	58.73	71	4	0.0112	0.0122	-0.0010	0.7951	0.8663	-0.0712
15	0.33	45.29	102	4	0.0118	0.0143	-0.0025	1.2037	1.4636	-0.2599
16	0.33	45.29	102	4	0.0118	0.0138	-0.0021	1.2040	1.4144	-0.2105

* This bridge meets, or nearly meets, the requirements for application of the recommended LGA-based procedures for the bridge design.

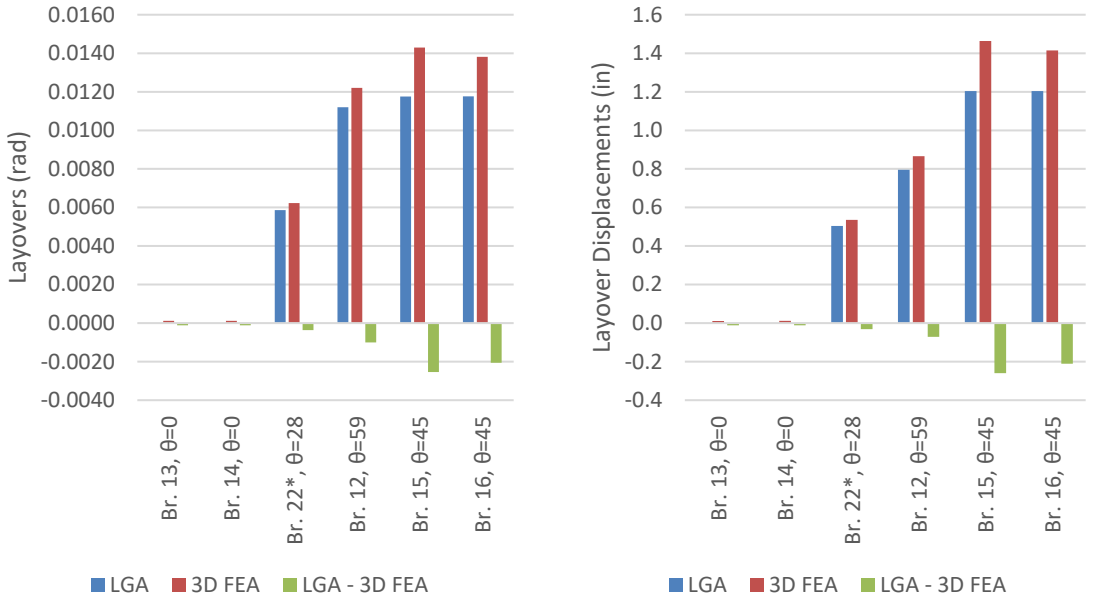

* This bridge meets, or nearly meets, the requirements for application of the recommended LGA-based procedures for the bridge design.

Figure 89. Maximum differences in LGA and 3D FEA CDL girder layovers at left abutment for multi-span continuous bridges, nonparallel skew.

Table 60. Maximum differences in LGA and 3D FEA CDL girder layovers at left abutment for splayed girder bridges, parallel skew.

Bridge	Skew Index	Skew Angle	Web Depth	Girder	LGA (rad)	3D FEA (rad)	LGA - 3D FEA (rad)	LGA (in)	3D FEA (in)	LGA - 3D FEA (in)
19	0.31	52.2	78	4	0.0113	0.0189	-0.0076	0.8802	1.4747	-0.5944
20	0.31	52.2	78	4	0.0091	0.0147	-0.0057	0.7061	1.1501	-0.4440

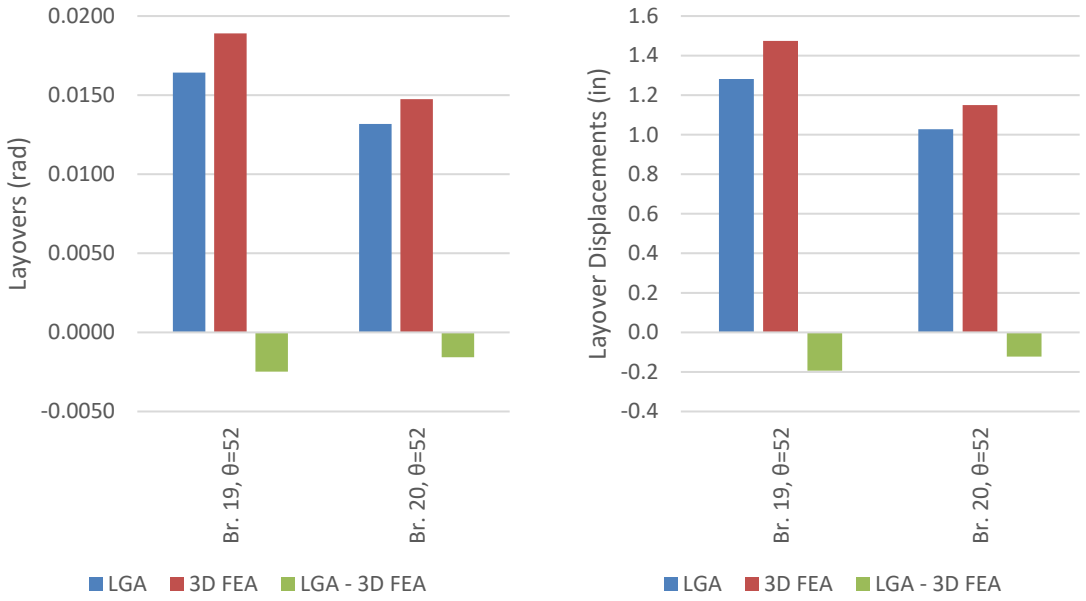

* This bridge meets, or nearly meets, the requirements for application of the recommended LGA-based procedures for the bridge design.

Figure 90. Maximum differences in LGA and 3D FEA CDL girder layovers at left abutment for splayed girder bridges, parallel skew.

5.3.9 Girder Fatigue Live Load Shear Forces

Design of the girder shear connectors is typically governed by the fatigue shear range. Therefore, the distribution factors for the fatigue shear range are calculated and presented at each tenth point of the spans in the individual bridge appendices. The fatigue shear range value at each tenth point is calculated as the difference between the maximum and minimum fatigue shear envelope values. ρ_{max} values for the fatigue shear range at the obtuse corners of bridge spans for a number of bridges are observed to be greater than unity. ρ_{max} values, if greater than unity, represent multipliers to be applied to the current AASHTO estimates. Cells that do not satisfy the tolerance established in Section 5.2.2, have a ρ_{max} value larger than 1.11 and are highlighted in the tables in this section. It should be noted that, in the 3D FEA solutions, the back-calculated distribution factors for the maximum shear envelope values, the minimum shear envelope values, and the shear range values are generally all different. The 3D FEA live load distribution factors are calculated by dividing the shear range obtained from the 3D FEA solution by the shear range obtain from LGA using a live load distribution factor of 1.0. In the LGA solutions, the live load distribution factors from AASHTO Article 4.6.2.2.3 are employed.

Figures 91 and 92 show the ρ_{max} values for exterior girders and first interior girders respectively for simple span bridges with parallel skew (Group 1). Tables 61 and 62 list the corresponding data values. The ρ_{max} values for the interior girders are smaller than one, implying that the LGA estimates are conservative compared to 3D FEA. The exterior girders of Bridges 1 and 2 have ρ_{max} values greater than 1.15. Bridge 5 has the lowest ρ_{max} of 0.86 for the exterior girders.

Figures 93 and 95 show the ρ_{max} values for exterior girders and first interior girders respectively, at the obtuse corners of the spans corresponding to the end abutments in multi-span continuous bridges with parallel skew (Group 2). Tables 63 and 65 list the corresponding data values. The maximum ρ_{max} value of 1.01 is observed for the exterior girders of Bridge 25. A stiff transverse path is developed between the obtuse corners of the spans in Bridges 9 due to cross-frames framing into the bearing line at the intermediate pier and/or inadequate offsets in the intermediate cross-frames near the end bearing lines. The LGA estimates are conservative for the exterior girders of other Group 2 bridges and first interior girders of Group 2 bridges.

Figures 94 and 96 show the ρ_{max} values for exterior girders and first interior girders respectively, at the obtuse corners of the spans at the intermediate piers of multi-span continuous bridges with parallel skew (Group 2). Tables 64 and 66 list the corresponding data values. The maximum ρ_{max} value of 1.07 is observed for the exterior girders of Bridges 9 and 24, followed by a ρ_{max} value of 1.04 for Bridge 25. A stiff transverse path is developed between the obtuse corners of the spans in Bridges 9, 24 and 25 due to cross-frames framing into the bearing line at the intermediate pier and/or inadequate offsets in the intermediate cross-frames near the end bearing lines. The LGA estimates are conservative for the first interior girders of Group 2 bridges.

Figures 97 and 99 show the ρ_{max} values for exterior girders and first interior girders respectively, at the obtuse corners of the spans corresponding to the end abutments of multi-span continuous bridges with nonparallel skew (Group 3). Tables 67 and 69 list the corresponding data values. The maximum ρ_{max} value of 1.06 is observed for an exterior girder of Bridge 12, followed by a ρ_{max} value of 1.03 for an exterior girder of Bridge 22.

The LGA estimates for the exterior girders of the other bridges studied are conservative with respect to the 3D FEA values. The LGA estimates are conservative for the first interior girders of the Group 4 bridges.

Figures 98 and 100 show the ρ_{max} values for exterior girders and first interior girders respectively, at the obtuse corners of the spans at the intermediate piers of multi-span continuous bridges with nonparallel skew (Group 3). Tables 68 and 70 list the corresponding data values. The maximum ratio of 1.18 is observed for an exterior girder of Bridge 12.

Figures 101 and 102 show the ρ_{max} values for exterior girders and first interior girders respectively, at the obtuse corners of the spans at the end abutments of the splayed girder bridges with parallel skew (Group 4). Tables 71 and 72 list the corresponding data values. LGA estimates are conservative for all the girders of Group 4 bridges.

Table 61. ρ_{max} values for fatigue live load shear force ranges for exterior girders at the obtuse corners of simple span bridges, parallel skew (shaded cells indicate ρ_{max} values that exceed the targeted limits for applicability of LGA).

Bridge	Skew Index	CF Arrangement Notes	ρ_{maxG1}	ρ_{maxG4}
1	0.46	Contiguous	1.30	1.28
2	0.46	Staggered	1.15	1.23
5*	0.42	Contiguous	0.86	0.86
7	0.33	Contiguous	0.87	0.87
17*	0.28	Contiguous	0.98	0.98
18*	0.20	Staggered	1.02	1.02
21*	0.15	Parallel to skew	0.91	0.91

* This bridge meets, or nearly meets, the requirements for application of the recommended LGA-based procedures for the bridge design.

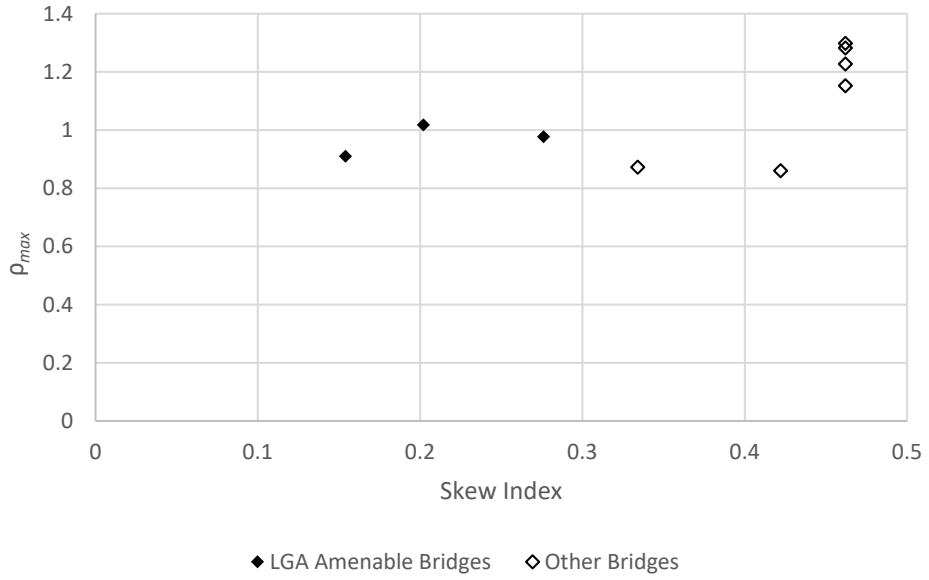

Figure 91. ρ_{max} values for fatigue live load shear force ranges for exterior girders at the obtuse corners of simple span bridges, parallel skew.

Table 62. ρ_{max} values for fatigue live load shear force ranges for first interior girders at the obtuse corners of simple span bridges, parallel skew.

Bridge	Skew Index	CF Arrangement Notes	ρ_{maxG2}
1	0.46	Contiguous	0.66
2	0.46	Staggered	0.64
5*	0.42	Contiguous	0.82
7	0.33	Contiguous	0.80
17*	0.28	Contiguous	0.75
18*	0.20	Staggered	0.81
21*	0.15	Parallel to skew	0.70

* This bridge meets, or nearly meets, the requirements for application of the recommended LGA-based procedures for the bridge design.

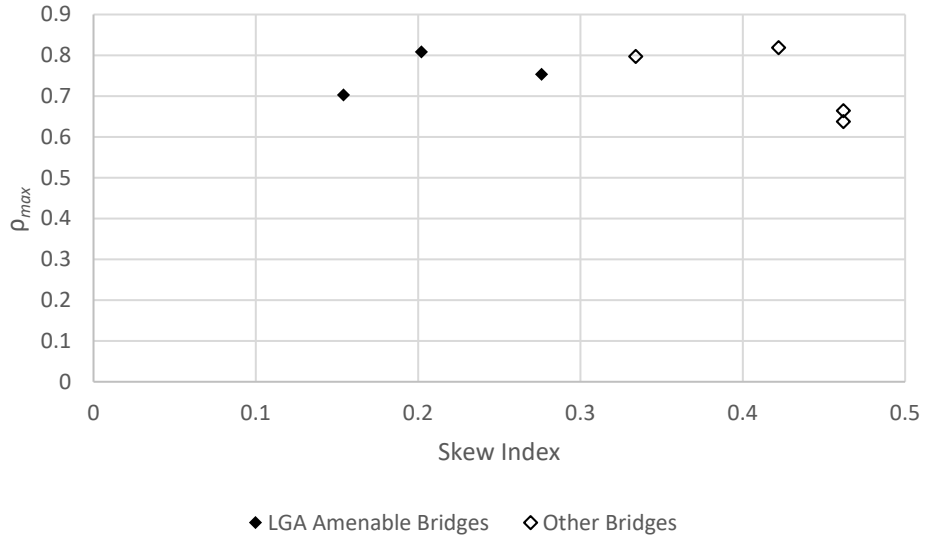

Figure 92. ρ_{max} values for fatigue live load shear force ranges for first interior girders at the obtuse corners of simple span bridges, parallel skew.

Table 63 ρ_{max} values for fatigue live load shear force ranges for exterior girders at the obtuse corners of the spans corresponding to the end abutments of multi-span continuous bridges, parallel skew (shaded cells indicate ρ_{max} values that exceed the targeted limits for applicability of LGA).

Bridge	Skew Index	CF Arrangement Notes	ρ_{maxG1}	ρ_{maxG4}
3	0.39	Contiguous, CF framing into bearing line	0.69	0.69
4*	0.39	Staggered	0.74	0.74
6*	0.35	Contiguous	0.86	0.86
8*	0.27	Staggered	0.77	0.77
9	0.47	Contiguous, CF framing into bearing line	0.76	0.95
10	0.47	Staggered	0.77	0.86
11*	0.26	Contiguous	0.90	0.90
23	0.37	Contiguous, CF framing into bearing line	0.80	0.82
24	0.37	Contiguous, inadequate offsets near bearing line	0.92	0.92
25	0.25	Contiguous, CF framing into bearing line	1.01	1.01
26*	0.15	Parallel to skew	0.90	0.90

* This bridge meets, or nearly meets, the requirements for application of the recommended LGA-based procedures for the bridge design.

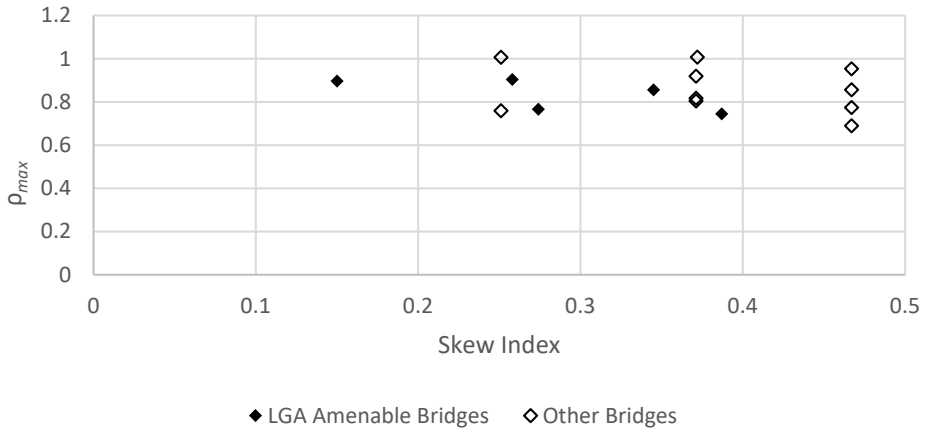

Figure 93. ρ_{max} values for fatigue live load shear force ranges for exterior girders at the obtuse corners of the spans corresponding to the end abutments of multi-span continuous bridges, parallel skew.

Table 64. ρ_{max} values for fatigue live load shear force ranges for exterior girders at the obtuse corners of the spans corresponding to the intermediate piers of multi-span continuous bridges, parallel skew (shaded cells indicate ρ_{max} values that exceed the targeted limits for applicability of LGA).

Bridge	Skew Index	CF Arrangement Notes	ρ_{maxG1}	ρ_{maxG4}
3	0.39	Contiguous, CF framing into bearing line	0.80	0.80
4*	0.39	Staggered	0.83	0.83
6*	0.35	Contiguous	0.97	0.97
8*	0.27	Staggered	0.88	0.88
9	0.47	Contiguous, CF framing into bearing line	1.07	0.95
10	0.47	Staggered	1.01	0.90
11*	0.26	Contiguous	1.02	1.02
23	0.37	Contiguous, CF framing into bearing line	1.00	1.00
24	0.37	Contiguous, inadequate offsets near bearing line	1.07	1.07
25	0.25	Contiguous, CF framing into bearing line	1.03	1.04
26*	0.15	Parallel to skew	0.98	0.98

* This bridge meets, or nearly meets, the requirements for application of the recommended LGA-based procedures for the bridge design.

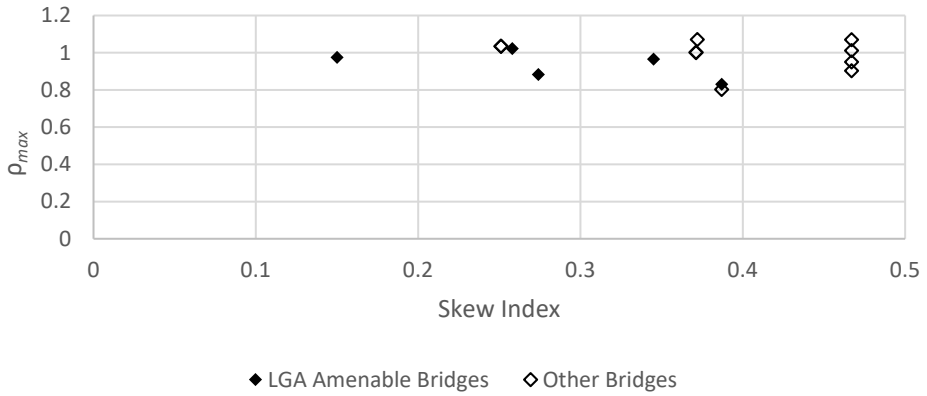

Figure 94. ρ_{max} values for fatigue live load shear force ranges for exterior girders at the obtuse corners of the spans at the intermediate piers of multi-span continuous bridges, parallel skew.

Table 65. ρ_{max} values for fatigue live load shear force ranges for first interior girders at obtuse corners of the spans corresponding to the end abutments of multi-span continuous bridges, parallel skew.

Bridge	Skew Index	CF Arrangement Notes	ρ_{maxG2}
3	0.39	Contiguous, CF framing into bearing line	0.67
4*	0.39	Staggered	0.75
6*	0.35	Contiguous	0.61
8*	0.27	Staggered	0.62
9	0.47	Contiguous, CF framing into bearing line	0.63
10	0.47	Staggered	0.71
11*	0.26	Contiguous	0.67
23	0.37	Contiguous, CF framing into bearing line	0.88
24	0.37	Contiguous, inadequate offsets near bearing line	0.71
25	0.25	Contiguous, CF framing into bearing line	0.73
26*	0.15	Parallel to skew	0.69

* This bridge meets, or nearly meets, the requirements for application of the recommended LGA-based procedures for the bridge design.

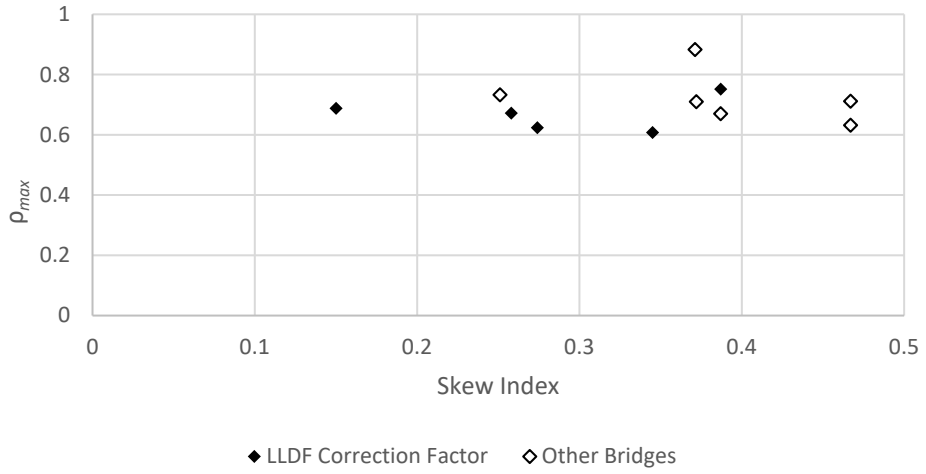

Figure 95. ρ_{max} values for fatigue live load shear force ranges for the first interior girder at the obtuse corners of the spans corresponding to the end abutments of multi-span continuous bridges, parallel skew.

Table 66. ρ_{max} values for the fatigue live load shear force range for the first interior girder at the obtuse corners of the spans at the intermediate piers of multi-span continuous bridges, parallel skew.

Bridge	Skew Index	CF Arrangement Notes	ρ_{maxG2}
3	0.39	Contiguous, CF framing into bearing line	0.92
4*	0.39	Staggered	1.01
6*	0.35	Contiguous	0.73
8*	0.27	Staggered	0.76
9	0.47	Contiguous, CF framing into bearing line	0.76
10	0.47	Staggered	0.84
11*	0.26	Contiguous	0.72
23	0.37	Contiguous, CF framing into bearing line	0.98
24	0.37	Contiguous, inadequate offsets near bearing line	0.85
25	0.25	Contiguous, CF framing into bearing line	0.94
26*	0.15	Parallel to skew	0.74

* This bridge meets, or nearly meets, the requirements for application of the recommended LGA-based procedures for the bridge design.

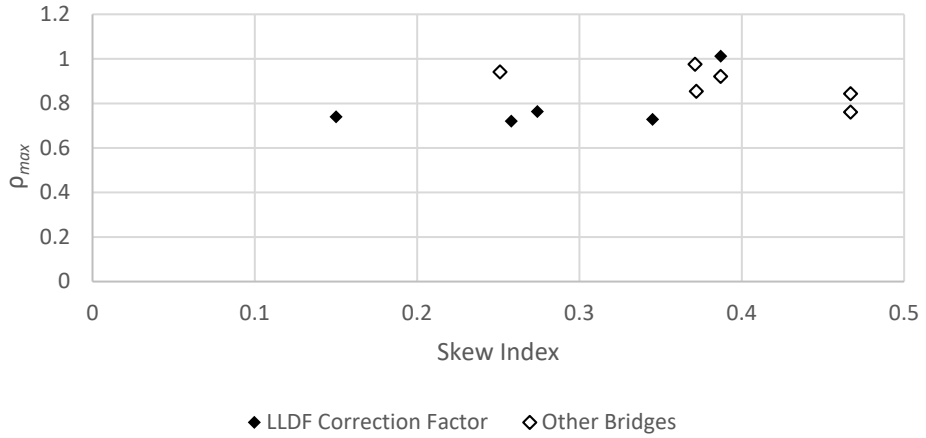

Figure 96. ρ_{max} values for the fatigue live load shear force range for the first interior girder at the obtuse corners of spans at the intermediate piers of multi-span continuous bridges, parallel skew.

Table 67. ρ_{max} values for the fatigue live load shear force range for the exterior girder at the obtuse corners of the span corresponding to the end abutments of multi-span continuous bridges, nonparallel skew (shaded cells indicate ρ_{max} values that exceed the targeted limits for applicability of LGA).

Bridge	Skew Index	CF Arrangement Notes	ρ_{maxG1}	ρ_{maxG4}
12	0.32	Contiguous, CF framing into bearing line	1.06	0.90
13	0.23	Contiguous	0.67	0.67
14	0.23	Staggered	0.67	0.67
15	0.33	Contiguous	0.88	0.54
16	0.33	Staggered	0.84	0.57
22*	0.31	Contiguous	1.03	0.93

* This bridge meets, or nearly meets, the requirements for application of the recommended LGA-based procedures for the bridge design.

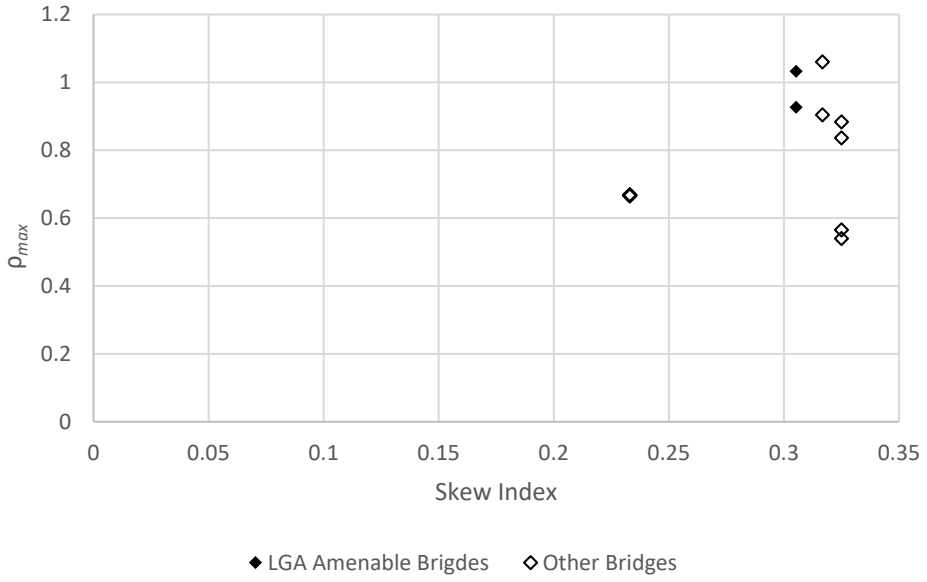

Figure 97. ρ_{max} values for the fatigue live load shear force range for the exterior girder at the obtuse corner of the span corresponding to the end abutments of multi-span continuous bridges, nonparallel skew.

Table 68. ρ_{max} values for the fatigue live load shear force range for first exterior girder at the obtuse corners of the spans at the intermediate piers of multi-span continuous bridges, nonparallel skew (shaded cells indicate ρ_{max} values that exceed the targeted limits for applicability of LGA).

Bridge	Skew Index	CF Arrangement Notes	ρ_{maxG1}	ρ_{maxG4}
12	0.32	Contiguous, CF framing into bearing line	1.07	0.99
13	0.23	Contiguous	1.10	1.09
14	0.23	Staggered	1.07	1.00
15	0.33	Contiguous	0.90	0.95
16	0.33	Staggered	0.81	0.88
22*	0.31	Contiguous	1.16	1.18

* This bridge meets, or nearly meets, the requirements for application of the recommended LGA-based procedures for the bridge design.

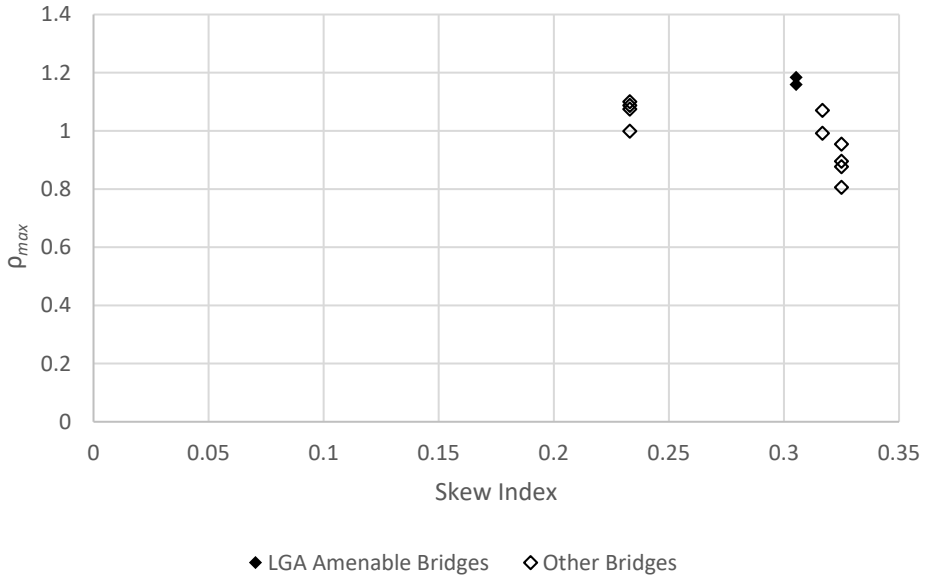

Figure 98. ρ_{max} values for the fatigue live load shear force range for first exterior girder at the obtuse corners of the spans at intermediate piers of multi-span continuous bridges, nonparallel skew.

Table 69. ρ_{max} values for the fatigue live load shear force range for first interior girder at the obtuse corners of the spans at the end abutments of multi-span continuous bridges, nonparallel skew.

Bridge	Skew Index	CF Arrangement Notes	ρ_{maxG2}
12	0.32	Contiguous, CF framing into bearing line	0.72
13	0.23	Contiguous	0.65
14	0.23	Staggered	0.65
15	0.33	Contiguous	0.77
16	0.33	Staggered	0.89
22*	0.31	Contiguous	0.52

* This bridge meets, or nearly meets, the requirements for application of the recommended LGA-based procedures for the bridge design.

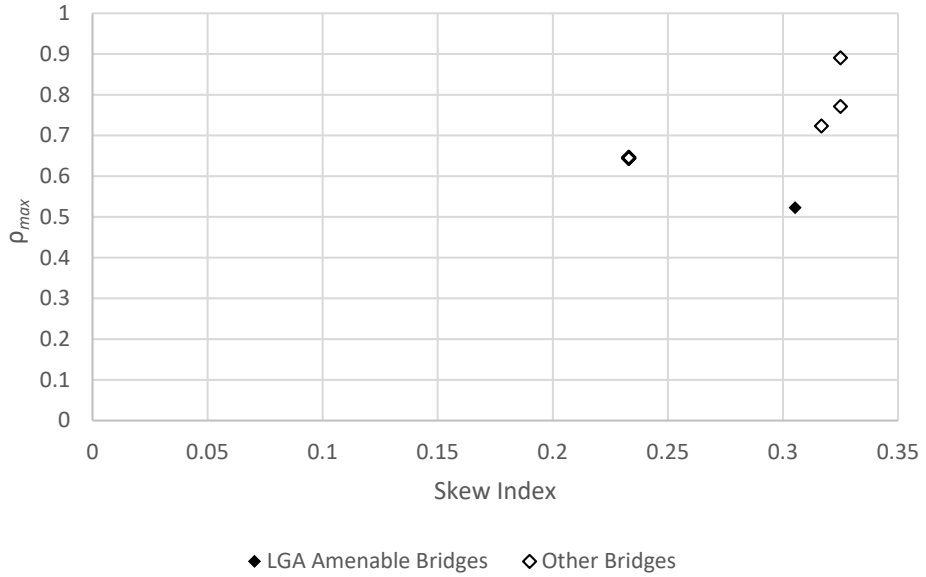

Figure 99. ρ_{max} values for the fatigue live load shear force range for first interior girder at the obtuse corners of the span corresponding to the end abutments of multi-span continuous bridges, nonparallel skew.

Table 70. ρ_{max} values for the fatigue live load shear force range for the first interior girder at the obtuse corners of the spans at the intermediate piers of multi-span continuous bridges, nonparallel skew.

Bridge	Skew Index	CF Arrangement Notes	ρ_{maxG2}
12	0.32	Contiguous, CF framing into bearing line	0.85
13	0.23	Contiguous	0.94
14	0.23	Staggered	0.97
15	0.33	Contiguous	0.88
16	0.33	Staggered	0.96
22*	0.31	Contiguous	0.63

* This bridge meets, or nearly meets, the requirements for application of the recommended LGA-based procedures for the bridge design.

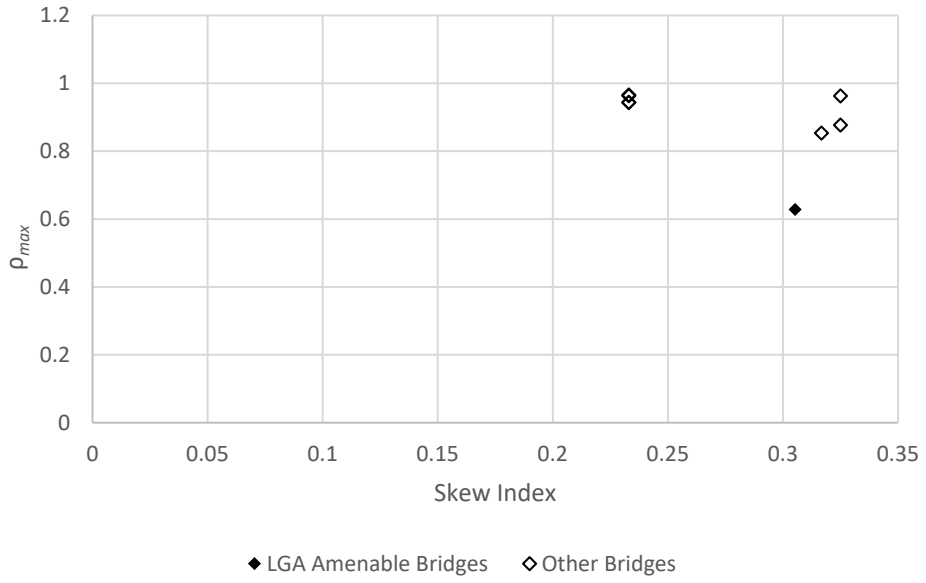

Figure 100. ρ_{max} values for the fatigue live load shear force range for first interior girder at the obtuse corners of the spans at the intermediate piers of multi-span continuous bridges, nonparallel skew.

Table 71. ρ_{max} values for the fatigue live load shear force range for the exterior girders at the obtuse corners of simple-span splayed girder bridges, parallel skew (shaded cells indicate ρ_{max} values that exceed the targeted limits for applicability of LGA).

Bridge	Skew Index	CF Arrangement Notes	ρ_{maxG1}	ρ_{maxG4}
19	0.45	Contiguous	0.86	0.93
20	0.45	Staggered	0.76	0.78

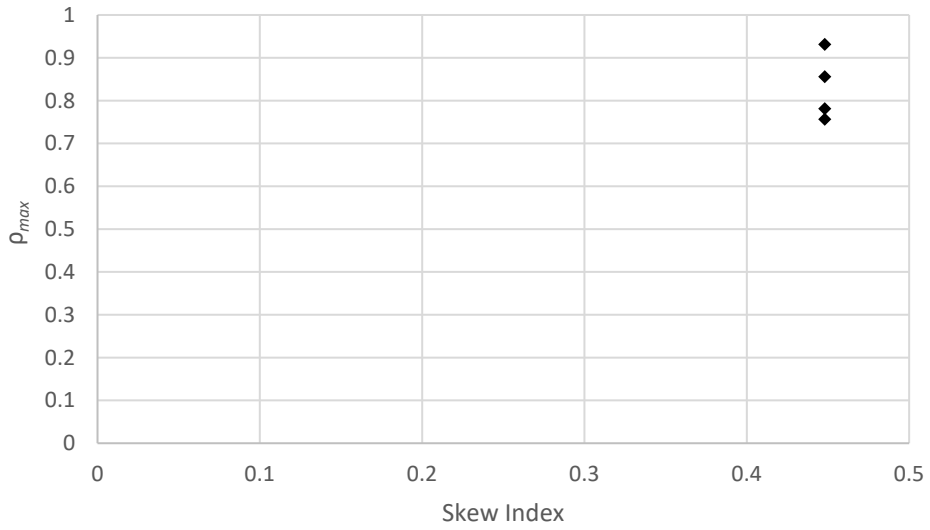

Figure 101. ρ_{max} values for the fatigue live load shear force range for the exterior girders at the obtuse corners of simple-span splayed girder bridges, parallel skew.

Table 72. ρ_{max} values for the fatigue live load shear force range for the first interior girder at the obtuse corners of simple-span splayed girder bridges, parallel skew.

Bridge	Skew Index	CF Arrangement Notes	ρ_{maxG2}
19	0.45	Contiguous	0.75
20	0.45	Staggered	0.93

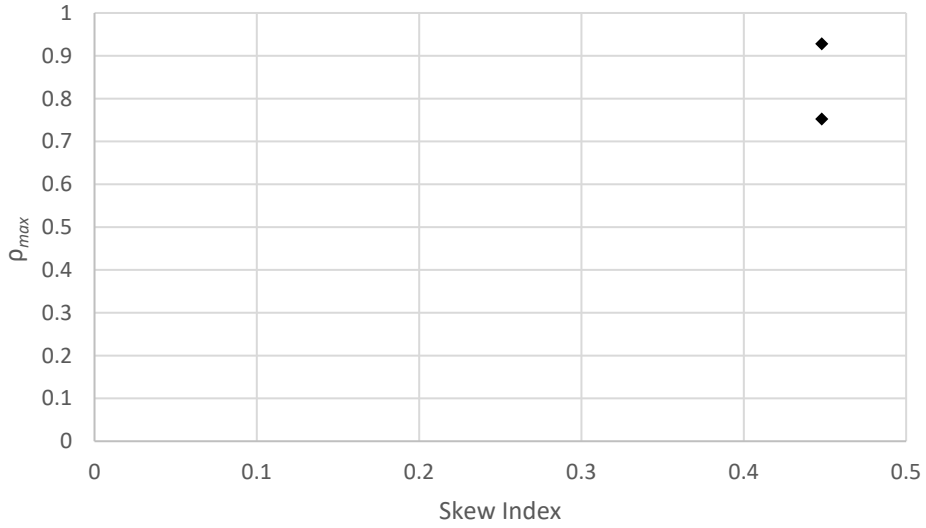

Figure 102. ρ_{max} values for the fatigue live load shear force rang for the first interior girder at the obtuse corners of simple-span splayed girder bridges, parallel skew.

5.3.10 Girder Fatigue Live Load Flexural Stresses

The fatigue flexural stress range can be critical in the design of girder connection plates in certain cases. The 3D FEA and LGA methods used in the study do not provide fatigue live load flexural stresses directly. Maximum and minimum envelopes for fatigue live load bending moment can be obtained from both the 3D FEA and the LGA solutions. By convention, the maximum envelope provides an estimate of the maximum positive bending moment and the minimum envelope provides an estimate of the maximum negative bending moment. Flexural stresses are calculated from the bending moment envelopes given the girder composite cross-section properties.

For continuous-span bridges, the corresponding LGA estimates are typically conservative compared to the 3D FEA estimates. However, larger differences are observed between the LGA and 3D FEA estimates for simple span bridges. The LGA procedures employ a line element idealization in analysis. On the other hand, the 3D FEA procedures involve modeling of the girders, cross-frames, diaphragms, bridge deck, bearings and other structural components at their specific locations in three-dimensional space. For a girder of a simple span bridge, the LGA idealizations are not capable of capturing negative bending moment effects due from the live load on the skewed bridge. The negative bending effects are captured by 3D FEA. Section 1a of the appendices for the 26 bridges show comparative plots of fatigue live load bending moment envelopes. Representative plots for the exterior girder of Bridge 17 are shown in Figures 103 and 104.

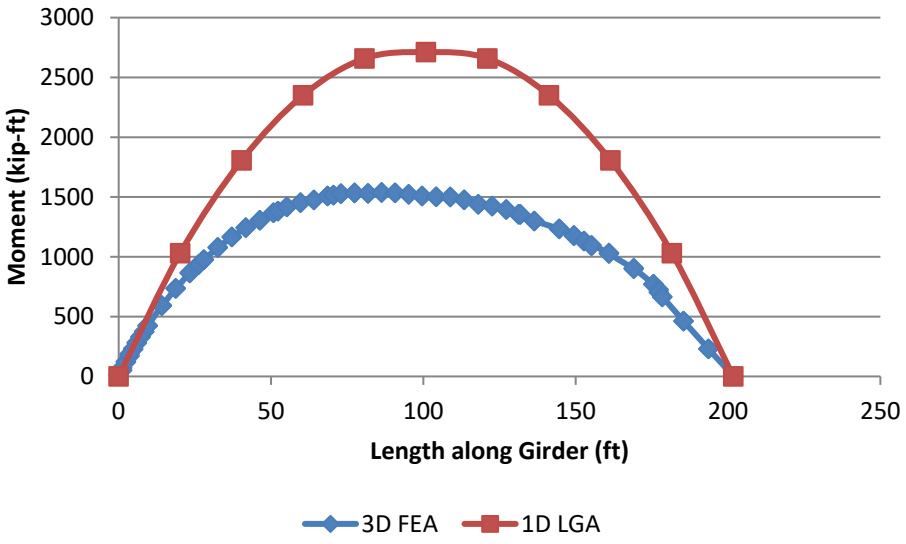

Figure 103. Envelope of maximum major-axis bending moments due to fatigue live loads in Girder 1 of Bridge 17.

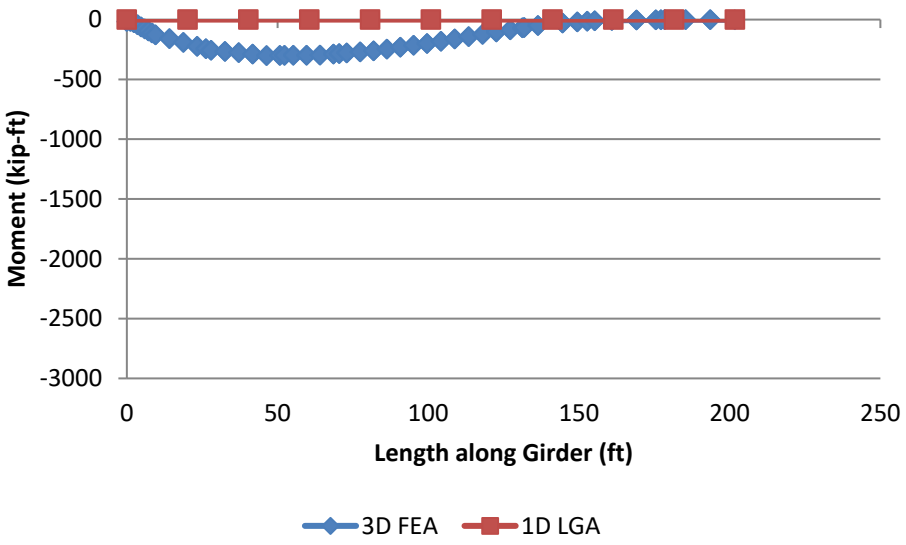

Figure 104. Envelope of minimum major-axis bending moments due to fatigue live loads in Girder 1 of Bridge 17.

Figure 103 indicates that LGA estimates for the maximum envelope of the major-bending moments are conservative compared to the 3D FEA estimates. Negative moment

estimates obtained from 3D FEA are significant in exterior girders near the obtuse corners of simple-span skewed bridges, and are reflected in Figure 104. The flexural stress ranges for the top and bottom flanges are calculated using the maximum and minimum envelopes of the bending moments. Figure 105 shows the major-axis bending stress range due to fatigue live load calculated for the top flange of Girder 1 of Bridge 17. Figure 106 shows the major-axis bending stress range due to fatigue live load calculated for the bottom flange of Girder 1 of Bridge 17. 3D FEA estimates of the stress range are larger than the LGA estimates, until approximately the mid-span of the girder. This is because of the significant negative bending moment caused due to skew near the obtuse corner. A similar increase in fatigue stress range for the top flange of the exterior girder is observed in Girder 1 of Bridge 18.

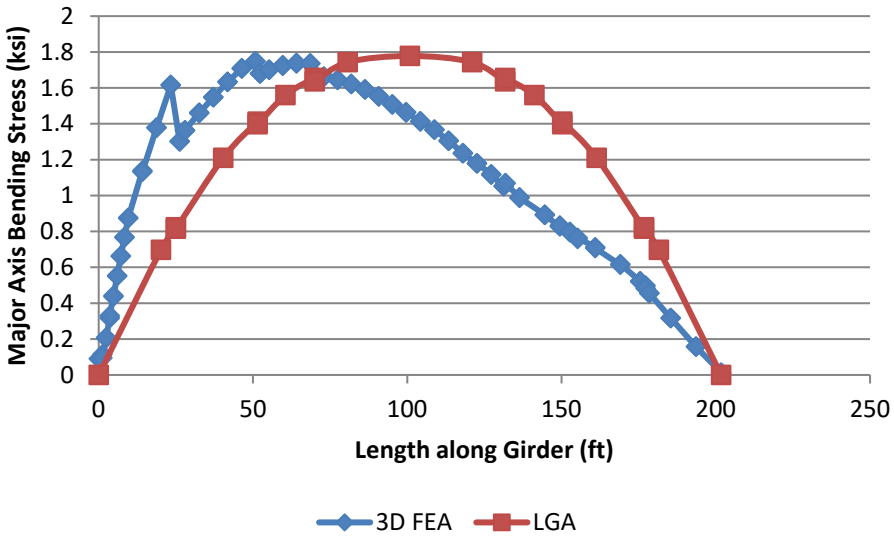

Figure 105. Major-axis bending stress range due to fatigue live loads in the top flange of Girder 1 of Bridge 17.

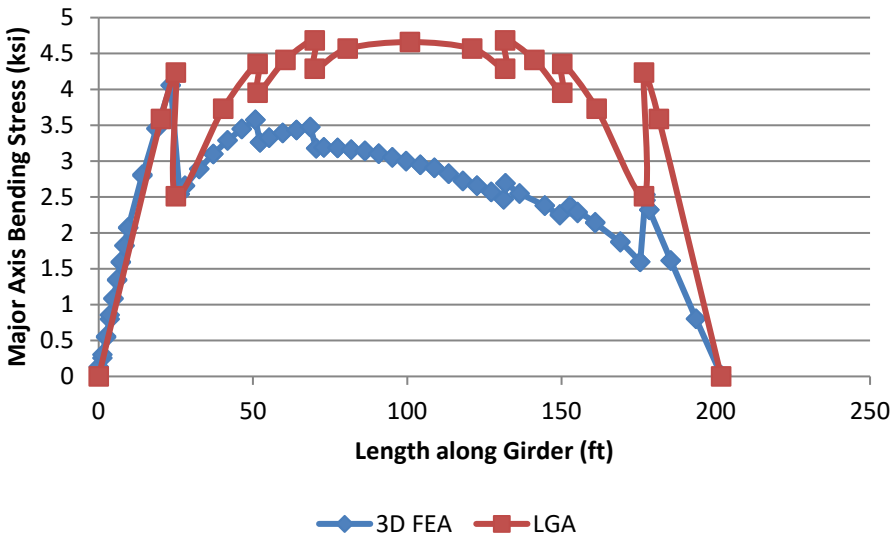

Figure 106. Major-axis bending stress range due to fatigue live loads in the bottom flange of Girder 1 of Bridge 17.

Fatigue design of components and details are required if the components or details are subjected to a net tensile stress. Figure 101 indicates that LGA under-predicts the fatigue stress range for the top flange by a maximum of 1 ksi. However, the top flange is subjected to compression under the dead load cases for this simple-span bridge. Hence, it is highly improbable that the top flange is subjected to a net tensile stress. The bottom flange, on the other hand, is subjected to tensile stresses under dead load. Figure 102 indicates that the maximum under-prediction by LGA is too small to be significant in the fatigue design of the bottom flange and its connections.

5.3.11 Girder Flange Lateral Bending Stresses

As explained in Section 5.2.1.5, twisting of the girders to maintain compatibility of the girder and cross-frame displacements and rotations produces girder flange lateral bending stresses. The stresses developed are influenced by the cross-frame arrangements employed in the bridges: contiguous, staggered and parallel to the skew. AASHTO LRFD Article C6.10.1 recognizes this and suggests estimates for the flange lateral bending stresses based on the cross-frame arrangement used. Generous offsets near the skewed bearing lines are required to mitigate the effects of a stiff transverse load path and reduce the flange lateral bending stresses.

The 3D FEA solutions employed in the parametric study account for flange lateral bending stresses due to overhang bracket loads on the exterior girder in a coarse fashion. CSiBridge models are set up to provide basic estimates of flange lateral bending stresses due to overhang bracket loads on the exterior girder, neglecting the elastic rebounding of the deck and girders when the brackets are removed. CSiBridge, in essence, simulates the torsional effects of overhang bracket loads on the exterior girders by applying equivalent equal and opposite uniformly distributed loads at the top and bottom flange-web junctions. Flange lateral bending stresses due to overhang loads on exterior girders are calculated consistently for LGA using AASHTO LRFD Equation C6.10.3.4.1-2 and the factored estimates based on a load factor of 1.25 for concrete dead loads are added to the recommended estimates in Section 5.2.1.5. These estimated stresses are added to the upper-bound estimated flange lateral bending stresses due to the bridge skew effects, which are discussed in Section 5.2.1.5.

Tables 73 through 76 show comparisons of the maximum STR I bottom flange f_ℓ obtained from 3D FEA to the approximate recommended AASHTO estimates, for all girders for the four groups of bridges. The difference between the AASHTO f_ℓ estimates and the 3D FEA f_ℓ estimates are shown in the tables, and highlighted where this ratio is negative (i.e., where 3D FEA f_ℓ estimates are larger than AASHTO f_ℓ estimates). The AASHTO estimates are accurate to conservative for all girders of the simple-span bridges. The maximum 3D FEA f_ℓ is observed in the left exterior girder of Bridge 17. The maximum f_ℓ occurs at a distance of 9.6 ft. from the bearing supporting the girder on the start abutment, in the vicinity of the obtuse corner of the bridge. This is likely due to the transverse load path that develops between the obtuse corners of Bridge 17.

The f_ℓ values determined using the AASHTO recommendations are underestimated for the central interior girder of Bridge 8, and all the four girders studied for Bridge 25. The cross-frame arrangement of Bridge 8 is staggered. However, the staggers do not satisfy the current AASHTO recommendation, of taking out every other cross-frame from a contiguous arrangement. This aspect is explained further in Section 5.3.12. Combined with the fact that the central girder of a bridge with a staggered arrangement attracts the largest lateral bending, and a stiff transverse path developing between the obtuse corners, the maximum f_ℓ occurs at a location near the mid-length of Span 2. This is shown in Figure 107. On the other hand, the cross-frame arrangement of Bridge 25 is contiguous. However,

the offsets near the abutment bearing lines do not satisfy current AASHTO recommendations, and as well intermediate cross-frames frame into the bearing lines. As a result, the maximum f_ℓ for the girders is observed in the vicinity of the obtuse corners.

The locations of maximum f_ℓ for all the girders of Bridge 25 are shown in Figure 108.

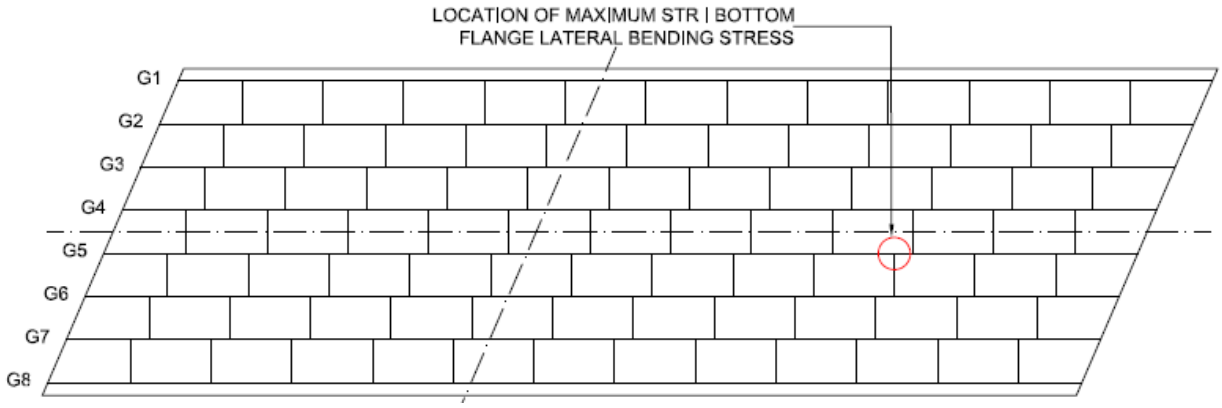

Figure 107. Maximum STR I bottom flange f_ℓ in Girder 3 of Bridge 8.

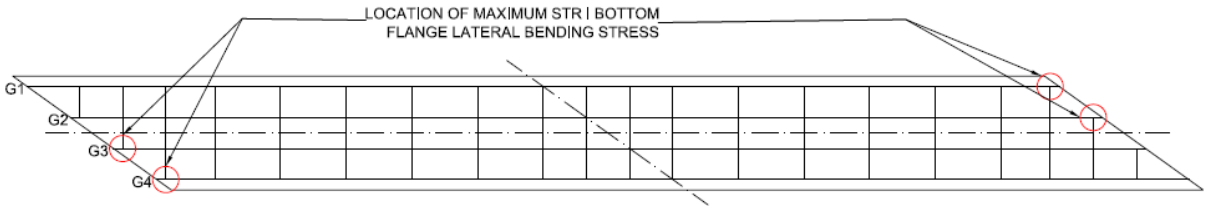

Figure 108. Maximum STR I bottom flange f_ℓ in girders of Bridge 25.

An unusually large f_ℓ of 32 ksi is observed in the central interior girder of Bridge 16.

The maximum stress occurs at a transition of the section in Span 3 where the bottom flange lateral section modulus reduces by a factor of about 10. The location is indicated in Figure 109. Such an abrupt transition is not recommended by AASHTO LRFD Specifications (AASHTO, 2017), and is not common practice. The AASHTO estimates are unconservative ranging up to 10% for many on the girders studied in the 26 bridges.

However, the effect of this unconservative estimate is effectively reduced by a factor of three via the application of the AASHTO LRFD 1/3rd rule.

Hence, it is concluded that AASHTO estimates for f_ℓ are accurate to conservative, provided that AASHTO recommendations for cross-frame arrangement and girder transition as detailed in Section 2, are satisfied.

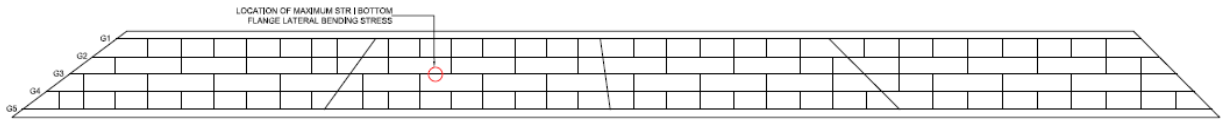

Figure 109. Maximum STR I bottom flange f_ℓ in Girder 3 of Bridge16.

Table 73. Comparison of maximum STR I 3D FEA bottom flange lateral bending stress with AASHTO estimates for LGA for simple span bridges, parallel skew.

			STR I Bottom Flange f_ℓ											
			Left Exterior Girder			Right Exterior Girder			First Interior Girder			Central Interior Girder		
Bridge	Skew Index	CF Arrangement Notes	LGA (ksi)	3D FEA (ksi)	LGA - 3D FEA	LGA (ksi)	3D FEA (ksi)	LGA - 3D FEA	LGA (ksi)	3D FEA (ksi)	LGA - 3D FEA	LGA (ksi)	3D FEA (ksi)	LGA - 3D FEA
1	0.46	Contiguous	12.17	4.14	8.02	12.17	4.11	8.07	16.00	6.78	9.22	16.00	7.53	8.47
2	0.46	Staggered	12.12	3.12	9.00	12.13	5.28	6.85	16.00	5.52	10.48	16.00	8.05	7.95
5*	0.42	Contiguous	12.77	2.12	10.65	12.77	2.12	10.65	16.00	3.20	12.80	16.00	3.21	12.79
7	0.33	Contiguous	17.97	5.48	12.49	17.97	5.48	12.49	16.00	2.22	13.78	16.00	5.16	10.84
17*	0.28	Contiguous	12.95	10.75	2.20	12.95	10.75	2.20	16.00	2.32	13.68	16.00	3.05	12.95
18*	0.20	Staggered	12.41	3.20	9.20	12.41	3.20	9.20	16.00	5.56	10.44	16.00	6.12	9.88
21*	0.15	Parallel to skew	12.27	0.97	11.31	12.27	0.97	11.31	16.00	0.69	15.31	16.00	0.48	15.52
				Mean	8.98		Mean	8.68		Mean	12.24		Mean	11.20
				SD	3.35		SD	3.45		SD	2.22		SD	2.71
				COV	0.37		COV	0.40		COV	0.18		COV	0.24

* This bridge meets, or nearly meets, the requirements for application of the recommended LGA-based procedures for the bridge design.

Table 74. Comparison of maximum STR I 3D FEA bottom flange lateral bending stress with AASHTO estimate for LGA for multi-span continuous bridges, parallel skew (shaded cells indicate values that violate the targeted limits for applicability of LGA).

			STR I Bottom Flange f_ℓ											
			Left Exterior Girder			Right Exterior Girder			First Interior Girder			Central Interior Girder		
Bridge	Skew Index	CF Arrangement Notes	LGA (ksi)	3D FEA (ksi)	LGA - 3D FEA	LGA (ksi)	3D FEA (ksi)	LGA - 3D FEA	LGA (ksi)	3D FEA (ksi)	LGA - 3D FEA	LGA (ksi)	3D FEA (ksi)	LGA - 3D FEA
3	0.39	Contiguous, CF framing into bearing line	10.46	3.11	7.35	10.46	3.11	7.35	16.00	4.56	11.44	16.00	4.67	11.33
4*	0.39	Staggered	10.51	5.38	5.13	10.51	5.38	5.13	16.00	7.47	8.53	16.00	12.67	3.33
6*	0.35	Contiguous	11.24	3.23	8.01	11.24	3.23	8.01	16.00	1.71	14.29	16.00	1.62	14.38
8*	0.27	Staggered	11.12	2.87	8.24	11.12	2.87	8.24	16.00	12.35	3.65	16.00	22.96	-6.96
9	0.47	Contiguous, CF framing into bearing line	11.24	3.35	7.89	10.43	5.67	4.76	16.00	8.22	7.78	16.00	9.13	6.87
10	0.47	Staggered	10.43	5.67	4.76	10.51	4.59	5.92	16.00	8.55	7.45	16.00	12.60	3.40
11*	0.26	Contiguous	10.79	3.26	7.53	10.79	3.26	7.53	16.00	6.92	9.08	16.00	7.90	8.10
23	0.37	Contiguous, CF framing into bearing line	10.75	3.62	7.13	10.75	3.62	7.13	16.00	6.35	9.65	16.00	3.26	12.74
24	0.37	Contiguous, inadequate offsets near bearing line	10.47	6.65	3.82	10.47	6.65	3.82	16.00	9.06	6.94	16.00	11.05	4.95
25	0.25	Contiguous, CF framing into bearing line	10.90	18.51	-7.61	10.90	18.60	-7.71	16.00	16.75	-0.75	16.00	17.12	-1.12
26*	0.15	Parallel to skew	10.79	2.68	8.11	10.79	2.68	4.03	16.00	0.95	16.89	16.00	0.61	26.10
				Mean	5.49		Mean	4.93		Mean	8.63		Mean	7.56
				SD	4.60		SD	4.48		SD	4.77		SD	8.72
				COV	0.84		COV	0.91		COV	0.55		COV	1.15

* This bridge meets, or nearly meets, the requirements for application of the recommended LGA-based procedures for the bridge design.

Table 75. Comparison of maximum STR I 3D FEA bottom flange lateral bending stress with AASHTO estimate for LGA for multi-span continuous bridges, nonparallel skew (shaded cells indicate values that violate the targeted limits for applicability of LGA).

			STR I Bottom Flange f_ℓ											
			Left Exterior Girder			Right Exterior Girder			First Interior Girder			Central Interior Girder		
Bridge	Skew Index	CF Arrangement Notes	LGA (ksi)	3D FEA (ksi)	LGA - 3D FEA	LGA (ksi)	3D FEA (ksi)	LGA - 3D FEA	LGA (ksi)	3D FEA (ksi)	LGA - 3D FEA	LGA (ksi)	3D FEA (ksi)	LGA - 3D FEA
12	0.32	Contiguous, CF framing into bearing line	9.85	9.19	0.66	10.89	9.80	1.09	16.00	9.11	6.89	16.00	9.56	6.44
13	0.23	Contiguous	10.07	8.87	1.20	10.76	8.64	2.13	16.00	9.40	6.60	16.00	9.64	6.36
14	0.23	Staggered	9.86	9.66	0.20	9.87	5.42	4.45	16.00	13.60	2.40	16.00	13.85	2.15
15	0.33	Contiguous	11.78	8.81	2.97	11.34	8.60	2.74	16.00	10.25	5.75	16.00	10.99	5.01
16	0.33	Staggered	11.85	9.61	2.24	11.71	9.58	2.14	16.00	12.41	3.59	16.00	31.32	-15.32
22*	0.31	Contiguous	10.91	3.04	7.87	9.62	2.49	7.14	16.00	2.14	13.86	16.00	1.43	14.57
				Mean	2.52		Mean	3.28		Mean	6.51		Mean	3.20
				SD	2.81		SD	2.19		SD	4.00		SD	9.97
				COV	1.11		COV	0.67		COV	0.61		COV	3.11

* This bridge meets, or nearly meets, the requirements for application of the recommended LGA-based procedures for the bridge design.

Table 76. Comparison of maximum STR I 3D FEA bottom flange lateral bending stress with AASHTO estimate for LGA for splayed girder bridges, parallel skew (shaded cells indicate values that violate the targeted limits for applicability of LGA).

			STR I Bottom Flange f_ℓ											
			Left Exterior Girder			Right Exterior Girder			First Interior Girder			Central Interior Girder		
Bridge	Skew Index	CF Arrangement Notes	LGA (ksi)	3D FEA (ksi)	LGA - 3D FEA	LGA (ksi)	3D FEA (ksi)	LGA - 3D FEA	LGA (ksi)	3D FEA (ksi)	LGA - 3D FEA	LGA (ksi)	3D FEA (ksi)	LGA - 3D FEA
19	0.31	Contiguous	10.59	5.54	5.05	10.58	11.13	-0.56	16.00	5.95	10.05	16.00	8.33	7.67
20	0.31	Staggered	10.63	3.73	6.89	10.62	6.90	3.72	16.00	7.23	8.77	16.00	14.97	1.03
				Mean	5.97		Mean	1.58		Mean	9.41		Mean	4.35
				SD	1.30		SD	3.03		SD	0.90		SD	4.70
				COV	0.22		COV	1.91		COV	0.10		COV	1.08

5.3.12 Estimation of Cross-Frame or Diaphragm Forces

Cross-frames and diaphragms are used to provide bracing to the girders. In skewed bridges, the cross-frames also distribute the dead and live loads within the superstructure system. In addition, they transfer loads in the transverse direction of the bridge. The behavior of a skewed bridge is complex, and forces in the cross-frames are influenced by a number of factors including the skew index, cross-frame framing arrangement, offsets near the skewed bearing lines and types of cross-frames used.

End cross-frames or diaphragms in a skewed bridge are typically aligned along the skew. Intermediate cross-frames are typically oriented perpendicular to the longitudinal axes of the girders for bridges that have a skew angle greater than 20°. For bridges that have a skew angle less than 20°, the cross-frames can be oriented parallel to the skew according to the AASHTO LRFD provisions. Bridges 21 and 26 have skew angles less than 20° and have intermediate cross-frames oriented parallel to the skew. In all other bridges studied, the intermediate cross-frame are oriented perpendicular to the longitudinal axis of girders. The end bearing line members in Bridge 7, and the end and intermediate

pier bearing line members in Bridge 26 are solid diaphragms. All other cross-frames in the bridges studied are V or inverted V assemblies.

Bridges 8 and 18 of the 26 bridges studied have a staggered cross-frame arrangement. However, the staggers are such that, if one connects the ends of cross-frames, the line thus formed is parallel to the skew. This is illustrated in Figure 110, where the lines in the dash-dot format connecting the left upper ends of the cross-frames are oriented parallel to the skew. This results in relatively small offsets that do not satisfy the recommendation of AASHTO LRFD C6.7.4.2, i.e., $L_b > 4b_f$ where b_f is the larger flange width within the unbraced length. AASHTO LRFD Article C6.7.4.2 recommends placing the intermediate cross-frames at a constant spacing along the span length to satisfy the flange resistance requirements and then omitting every other cross-frame as one option. Such a modified arrangement for Bridge 18 is shown in Figure 111.

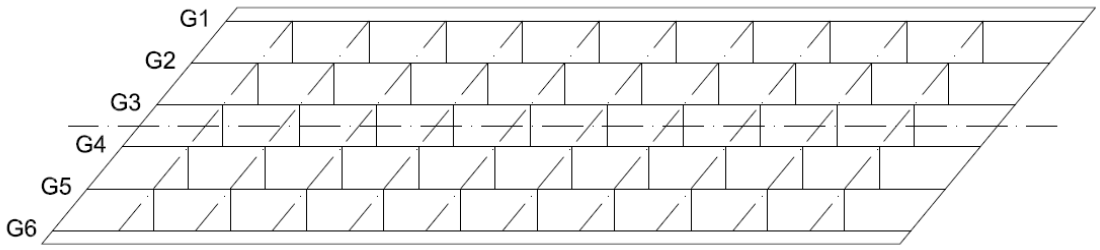

Figure 110. Staggered cross-frame arrangement of Bridge 18.

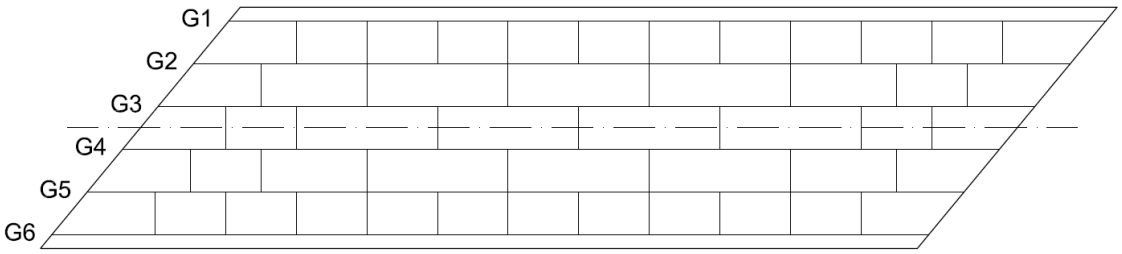

Figure 111. Modified staggered cross-frame arrangement of Bridge 18 satisfying AASHTO LRFD C6.7.4.2 recommendations.

In all the other Bridges 1-7, 9-20, 22-25, the cross-frames are contiguous and the intermediate cross-frames are oriented perpendicular to the longitudinal axis of girders.

Figures 16 through 41 the superstructure layout for all the 26 bridges. Six Bridges, 1, 3, 9, 13, 15 and 19, are studied with an alternative cross-frame framing arrangement. Bridges 2, 4, 10, 14, 16 and 20 are the respective bridges with the alternative cross-frame framing arrangements. The alternative cross-frame framing arrangement is developed using the following recommendations of AASHTO LRFD Article C6.7.4.2:

1. Cross-frames should be placed along the skewed bearing lines at the intermediate piers in continuous-span bridges.
2. The first intermediate cross-frames or diaphragms should be offset by a minimum of $4b_f$ from the support, where bf is the largest girder flange width within the unbraced lengths on either side of the cross-frame or diaphragm under consideration.
3. Use a staggered cross-frame arrangement within the bridge spans in which all girder unbraced lengths between intermediate diaphragms or cross-frame locations are greater than or equal to $4b_f$, where b_f is the largest girder flange width within the unbraced length.
4. If the above offset requirement relative to the support results in an excessive unbraced length on the fascia girder at an acute corner, a cross-frame with top and bottom chords and no diagonal members can be framed from the first interior girder to the fascia girder at a smaller offset from the support.

A modified staggered cross-frame framing arrangement for Bridge 18 is developed and illustrated in Figure 111. Alternative cross-frame framing arrangements are developed using the recommendations listed for the six bridges. Figure 112 illustrates the development of an alternative cross-frame framing arrangement for Bridge 1. Bridge 1 has a high skew index of 0.46. The first intermediate cross-frames are offset by a distance greater than $4b_f$ from the support, where b_f is the largest girder flange width within the unbraced lengths on either side of the cross-frame. Such intermediate cross-frames are placed near the skewed bearing line in every bay. A staggered intermediate cross-frame arrangement is then developed in accordance with Recommendation 3 mentioned above.

Figure 113 illustrates the cross-frame framing arrangement for Bridge 9. The original cross-frame framing arrangement did not have cross-frames placed along the bearing line at the intermediate pier. Instead, intermediate cross-frames near the skewed intermediate pier bearing line were framed into the bearings. In the alternative cross-frame framing arrangements, cross-frames were placed along the bearing line at the intermediate pier. Adequate offsets were provided in accordance with Recommendation 2 above. A staggered intermediate framing arrangement was then developed in accordance with Recommendation 3 above. Figure 114 illustrates the use of Recommendation 4, in developing the alternative cross-frame framing arrangement for Bridge 3.

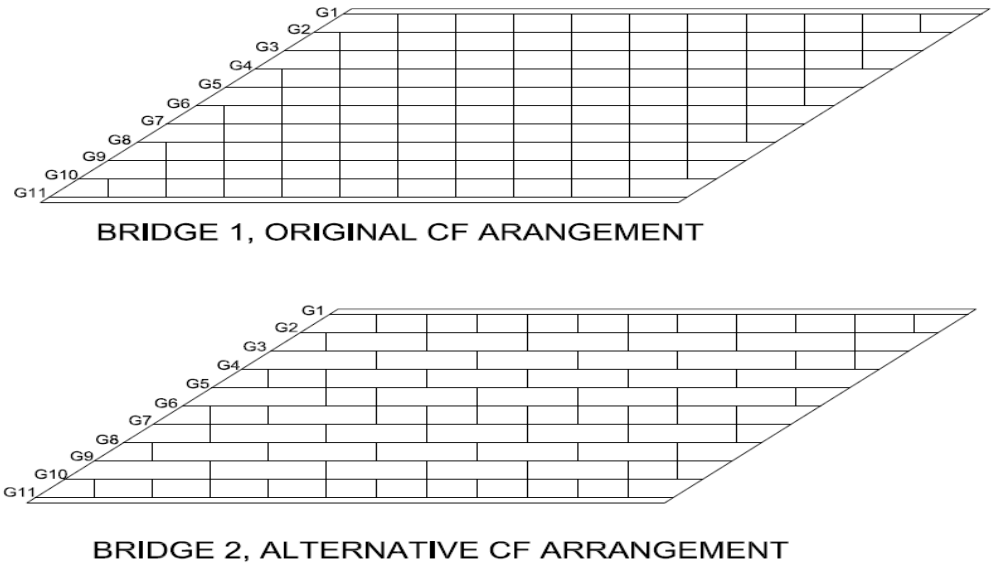

Figure 112. Illustration of development of alternative cross-frame framing arrangement, Bridge 1: original, Bridge 2: alternative.

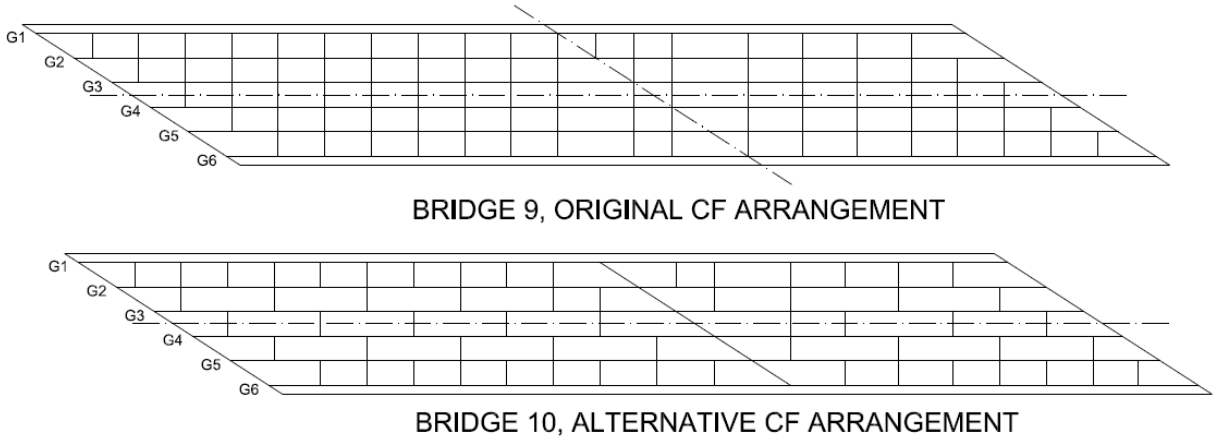

Figure 113. Illustration of development of alternative cross-frame framing arrangement, Bridge 9: original, Bridge 10: alternative.

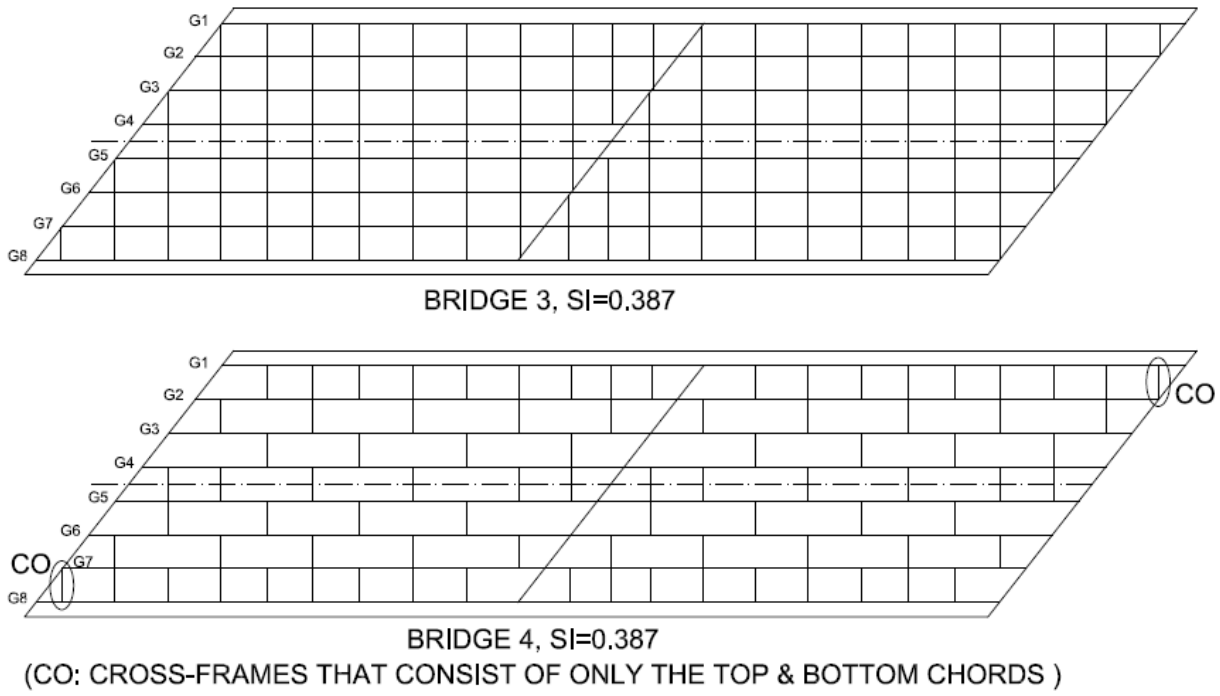

Figure 114. Illustration of development of alternative cross-frame framing arrangement, Bridge 3: original, Bridge 4: alternative.

A study of the cross-frame forces for a total of 19 bridges is performed to obtain upper-bound estimates for design of cross-frame members. Section 5.2 lists and explains the recommendations for application of LGA in lieu of 3D FEA. Bridges with nonparallel skew and splays are not amenable to application of LGA since the behavior of such bridges are heavily influenced by the geometry of each bridge. Hence, in the study, nonparallel skew bridges 12-16, and splayed girder bridges 19-20 are not considered. Bridge 22 has nonparallel skew, however, the differences in the skew angles in this bridge are relatively small and the effects of nonparallel skew on cross-frame forces are observed to very small. Hence, Bridge 22 is considered in the study of cross-frame forces.

Figure 115 shows a plot of maximum tension forces and Figure 116 shows a plot of maximum compression forces in bottom chords of intermediate cross-frames of the 19 bridges studied. Table 77 shows the corresponding data values.

Figure 117 shows a plot of shear forces or the vertical components of the maximum tension forces and Figure 118 shows a plot of shear forces or the vertical components of the maximum compression forces in bottom chords of intermediate cross-frames of the 19 bridges studied. Table 78 shows the corresponding data values.

Figure 119 shows a plot of maximum tension forces and Figure 120 shows a plot of maximum compression forces in top chords of intermediate cross-frames of the 19 bridges studied. Table 79 shows the corresponding data values.

Figure 121 shows a plot of maximum tension forces and Figure 122 shows a plot of maximum compression forces in bottom chords of end bearing and intermediate-pier cross-frames of the 19 bridges studied. Table 80 shows the corresponding data values.

Figure 123 shows a plot of shear forces or the vertical components of the maximum tension forces and Figure 124 shows a plot of shear forces or the vertical components of the maximum compression forces in bottom chords of end bearing and intermediate-pier cross-frames of the 19 bridges studied. Table 81 shows the corresponding data values.

Figure 125 shows a plot of maximum tension forces and Figure 126 shows a plot of maximum compression forces in bottom chords of end bearing and intermediate-pier cross-frames of the 19 bridges studied. Table 82 shows the corresponding data values.

The end bearing line members in Bridge 7, and the end and intermediate pier bearing line members in Bridge 26 are solid-web diaphragms. These are shown in the tables and the corresponding plots as top chords. Hence, the diagonals and bottom chords corresponding to these cross-frames do not have entries. The top chords of the intermediate cross-frames in Bridges 18 and 21 are not subjected to tension under the STR I load combination. Similarly, bottom chords of end cross-frames in Bridge 17 are not subjected to tension under the STR I load combination. Hence, the maximum tension for these cross-frame members are shown as zero in the tables.

Bridges 4, 8, 18, 21 and 26 are amenable to the application of LGA in lieu of 3D FEA. Hence, the maximum forces observed in the cross-frame member components should form the basis of the upper bound forces recommended for design of various cross-frame component members in Section 2.1.6. Bridge 17 satisfies all the requirements of Section 5.2 except the offset of the intermediate cross-frames near the bearing lines are lesser than the recommended offset of 4bf. Similarly, Bridge 22 has a minor nonparallel skew, but it satisfies all other requirements for the application of LGA. In spite of the violations, Bridges 17 and 22 have similar cross-frame forces as the bridges that satisfy LGA applicability requirements of Section 5.2.1.6.

The force requirements specified in Section 5.2.1.6 are upper bound forces based on the results for the bridges that satisfy the requirements of Section 2.2 for the use of LGA. In the tables below, the cross-frame forces for Bridges 4, 8, 18, 21, 26, 11 and 26 are shaded. The same are shown and highlighted in the plots, along with forces in cross-frames of other bridges. The plots help in examining the trends in cross-frame forces in bridges for which LGA is applicable.

Table 77. Maximum tension and compression forces in bottom chords of intermediate cross-frames (shaded values indicate cross-frame forces for bridges that meet or nearly meet the requirements for application of the recommended LGA-based procedures for the bridge design).

Bridge	Skew Index	STR I Max Tension (kip)	STR I Max Compression (kip)
1	0.46	324	171
2	0.46	204	158
3	0.39	102	106
4*	0.39	55	75
5*	0.42	115	77
6	0.35	132	83
7	0.33	NA**	NA**
8*	0.27	57	45
9	0.47	112	214
10	0.47	66	147
11*	0.26	110	117
17*	0.28	113	84
18*	0.20	41	37
21*	0.15	80	15
22*	0.31	137	121
23	0.37	180	261
24	0.37	71	117
25	0.25	58	151
26*	0.15	65	41

* This bridge meets, or nearly meets, the requirements for application of the recommended LGA-based procedures for the bridge design.

** This bridge has solid-web diaphragms rather than cross-frames.

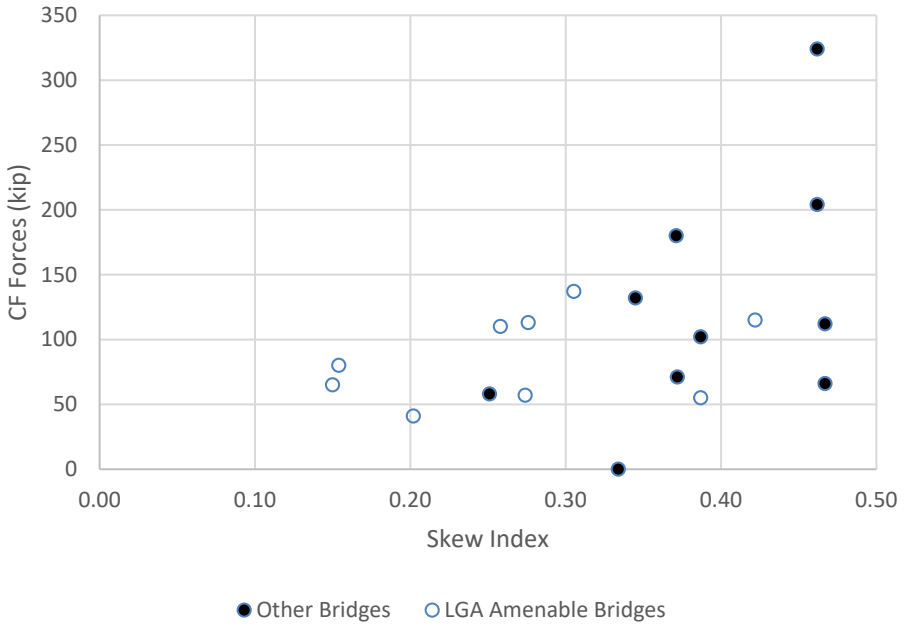

Figure 115. Maximum tension forces in bottom chords of intermediate cross-frames.

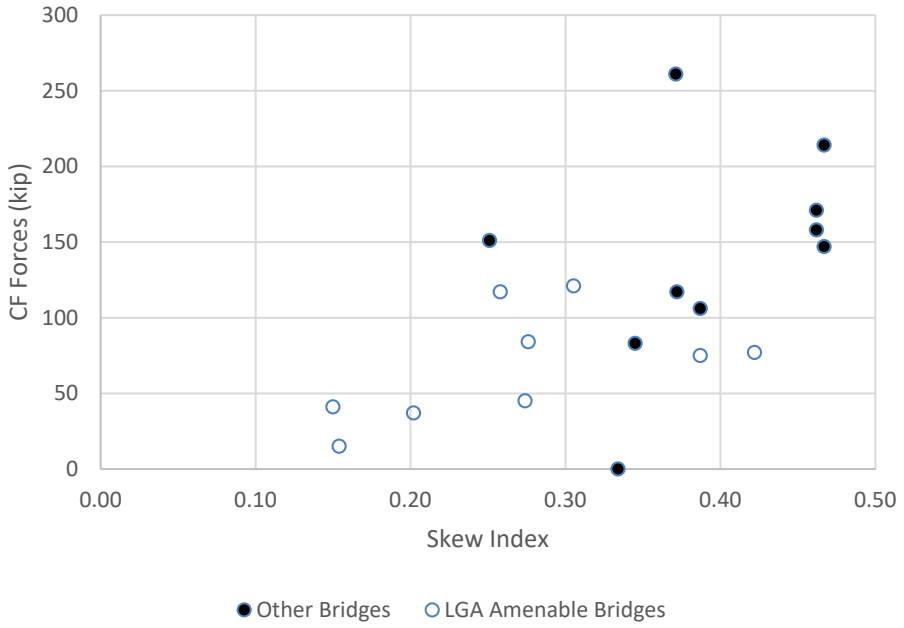

Figure 116. Maximum compression forces in bottom chords of intermediate cross-frames.

Table 78. Maximum tension and compression forces in diagonals of intermediate cross-frames (shaded values indicate cross-frame forces for bridges that meet or nearly meet the requirements for application of the recommended LGA-based procedures for the bridge design).

Bridge	Skew Index	STR I Max Tension (kip)	STR I Max Compression (kip)
1	0.46	113	113
2	0.46	72	72
3	0.39	22	22
4*	0.39	22	22
5*	0.42	7	9
6	0.35	18	18
7	0.33	NA**	NA**
8*	0.27	17	16
9	0.47	38	38
10	0.47	31	31
11*	0.26	36	35
17*	0.28	47	48
18*	0.20	15	15
21*	0.15	25	16
22*	0.31	38	38
23	0.37	76	77
24	0.37	25	25
25	0.25	61	61
26*	0.15	12	12

* This bridge meets, or nearly meets, the requirements for application of the recommended LGA-based procedures for the bridge design.

** This bridge has solid-web diaphragms rather than cross-frames.

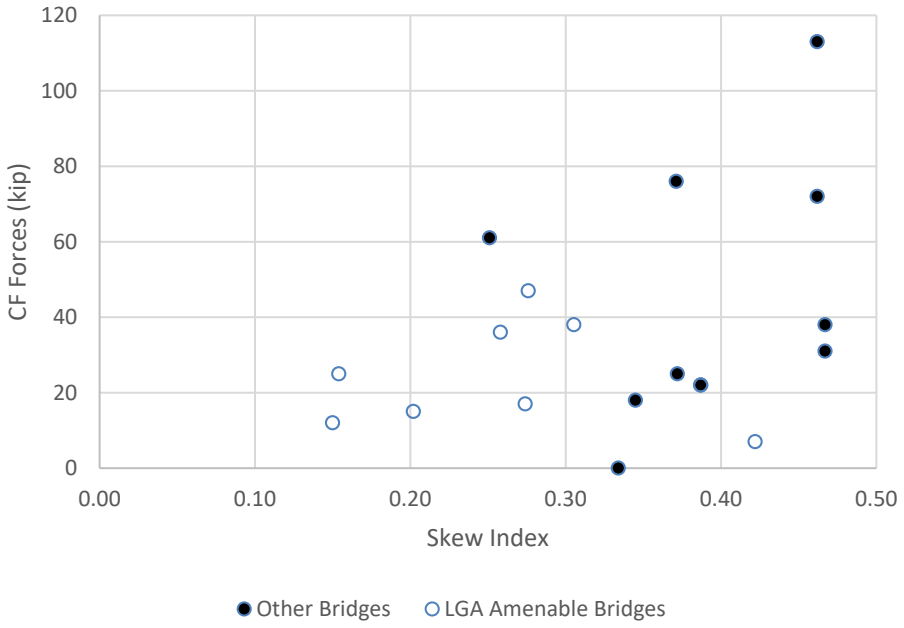

Figure 117. Maximum tension forces in diagonals of intermediate cross-frames.

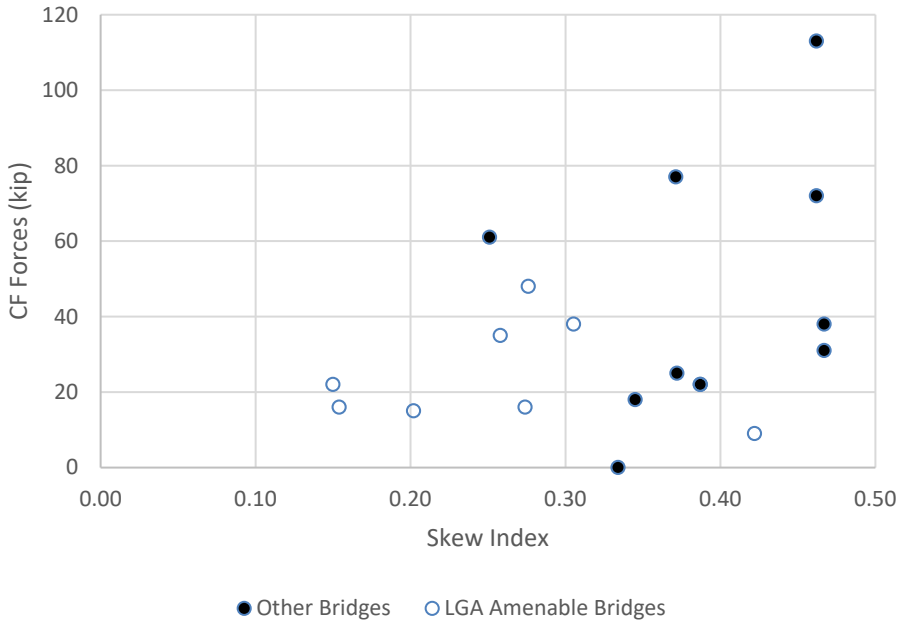

Figure 118. Maximum compression forces in diagonals of intermediate cross-frames.

Table 79. Maximum tension and compression forces in top chords of intermediate cross-frames (shaded values indicate cross-frame forces for bridges that meet or nearly meet the requirements for application of the recommended LGA-based procedures for the bridge design).

Bridge	Skew Index	STR I Max Tension (kip)	STR I Max Compression (kip)
1	0.46	22	105
2	0.46	51	67
3	0.39	37	42
4*	0.39	50	32
5*	0.42	37	37
6	0.35	29	37
7	0.33	NA**	NA**
8*	0.27	51	45
9	0.47	62	38
10	0.47	39	37
11*	0.26	31	30
17*	0.28	10	29
18*	0.20	0	17
21*	0.15	0	24
22*	0.31	26	39
23	0.37	145	95
24	0.37	30	25
25	0.25	93	84
26*	0.15	33	22

* This bridge meets, or nearly meets, the requirements for application of the recommended LGA-based procedures for the bridge design.

** This bridge has solid-web diaphragms rather than cross-frames.

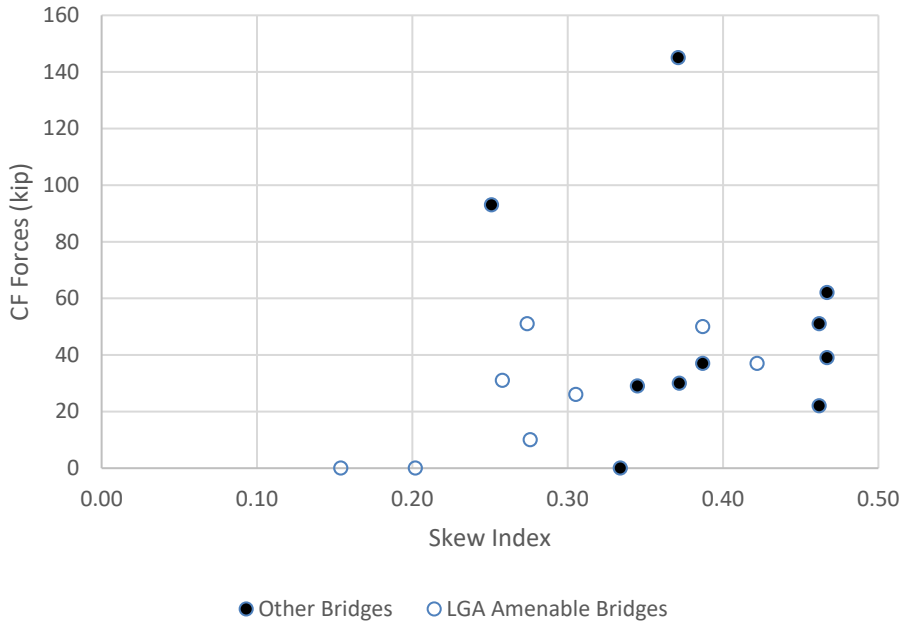

Figure 119. Maximum tension forces in top chords of intermediate cross-frames.

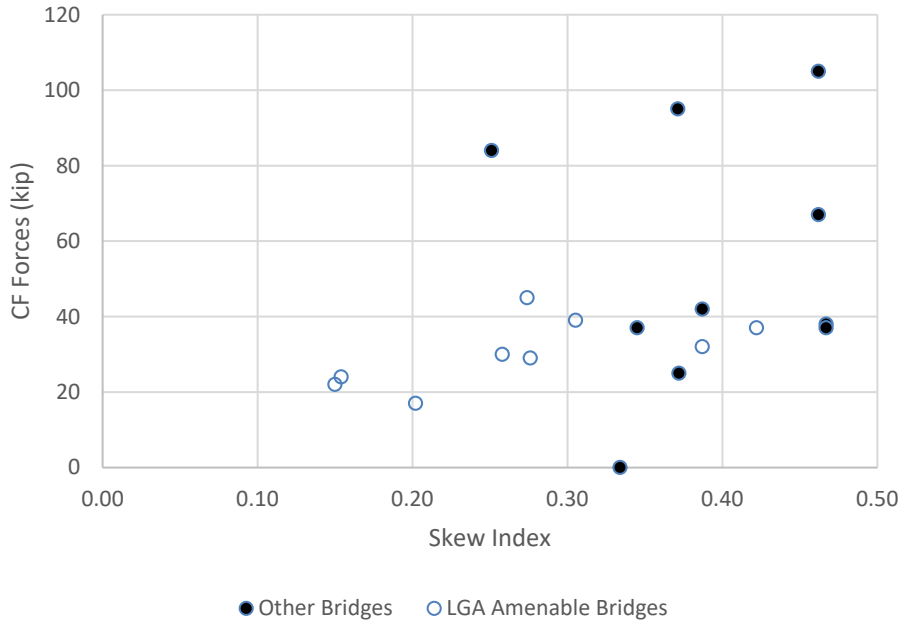

Figure 120. Maximum compression forces in top chords of intermediate cross-frames.

Table 80. Maximum tension and compression forces in bottom chords bearing line cross-frames at abutments and intermediate piers (shaded values indicate cross-frame forces for bridges that meet or nearly meet the requirements for application of the recommended LGA-based procedures for the bridge design).

Bridge	Skew Index	STR I Max Tension (kip)	STR I Max Compression (kip)
1	0.46	5	17
2	0.46	21	16
3	0.39	66	109
4*	0.39	38	35
5*	0.42	6	4
6	0.35	8	9
7	0.33	NA**	NA**
8*	0.27	5	3
9	0.47	7	24
10	0.47	36	33
11*	0.26	53	128
17*	0.28	0	13
18*	0.20	4	10
21*	0.15	6	3
22*	0.31	23	9
23	0.37	8	7
24	0.37	20	15
25	0.25	8	33
26*	0.15	NA	NA

* This bridge meets, or nearly meets, the requirements for application of the recommended LGA-based procedures for the bridge design.

** This bridge has solid-web diaphragms rather than cross-frames.

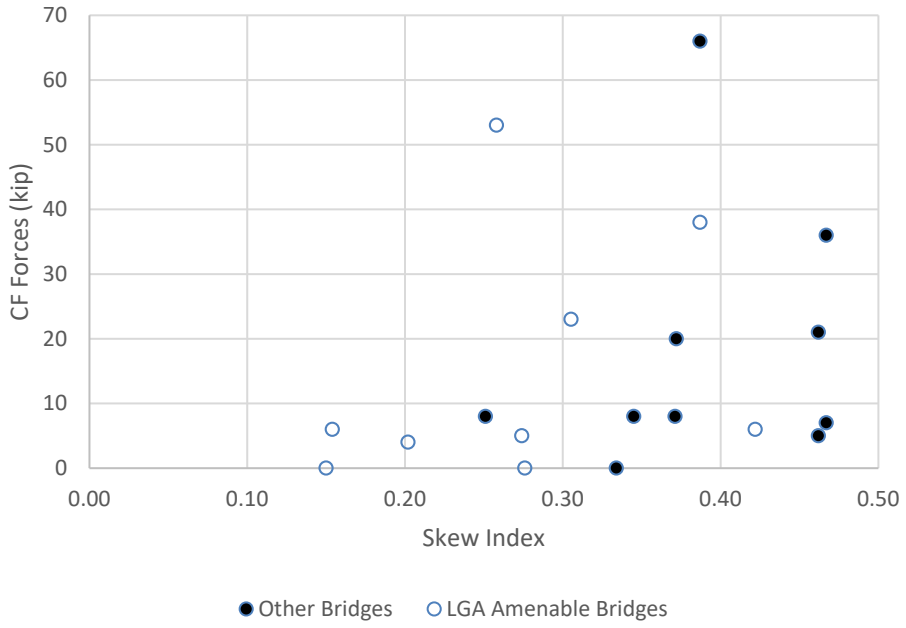

Figure 121. Maximum tension forces in bottom chords of bearing line cross-frames at abutments and intermediate piers.

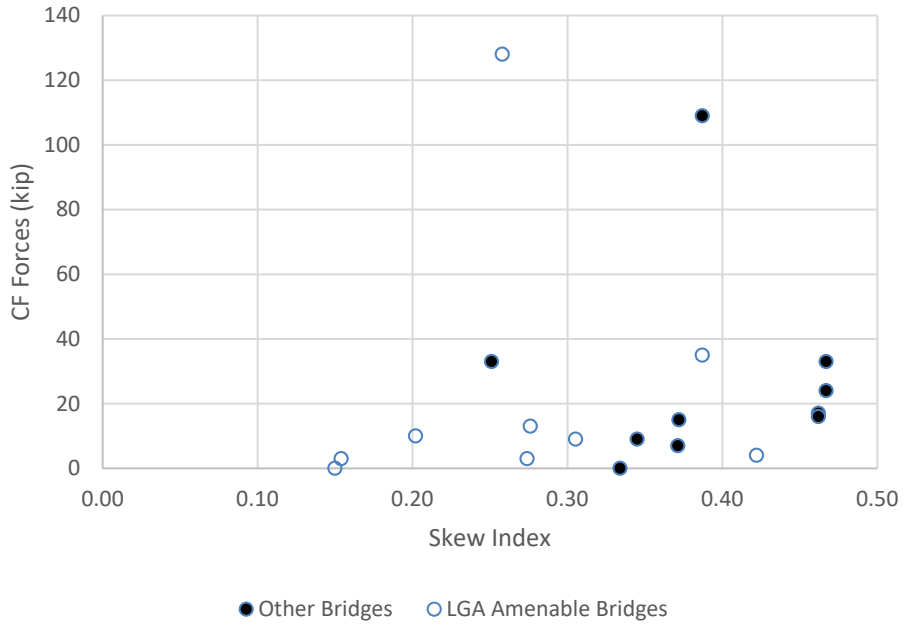

Figure 122. Maximum compression forces in bottom chords of bearing line cross-frames at abutments and intermediate piers.

Table 81. Maximum tension and compression forces in diagonals of end and intermediate-pier cross-frames (shaded values indicate cross-frame forces for bridges that meet or nearly meet the requirements for application of the recommended LGA-based procedures for the bridge design).

Bridge	Skew Index	STR I Max Tension (kip)	STR I Max Compression (kip)
1	0.46	12	14
2	0.46	13	14
3	0.39	18	20
4*	0.39	8	9
5*	0.42	1	1
6	0.35	5	5
7	0.33	NA**	NA**
8*	0.27	2	3
9	0.47	6	6
10	0.47	9	9
11*	0.26	18	21
17*	0.28	6	7
18*	0.20	3	3
21*	0.15	3	3
22*	0.31	21	23
23	0.37	9	11
24	0.37	17	17
25	0.25	20	20
26*	0.15	NA**	NA**

* This bridge meets, or nearly meets, the requirements for application of the recommended LGA-based procedures for the bridge design.

** This bridge has solid-web diaphragms rather than cross-frames.

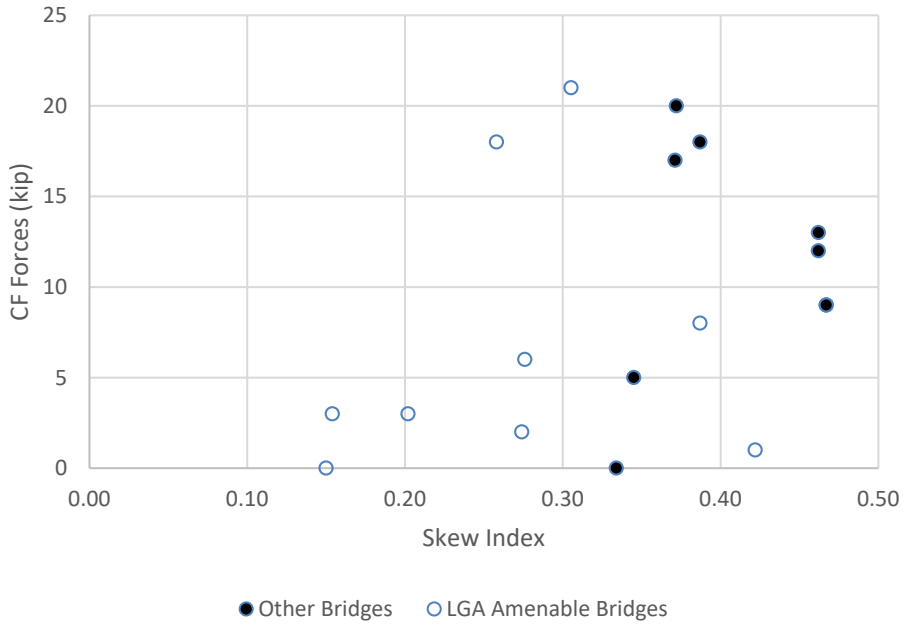

Figure 123. Maximum tension forces in diagonals of end and intermediate-pier cross-frames.

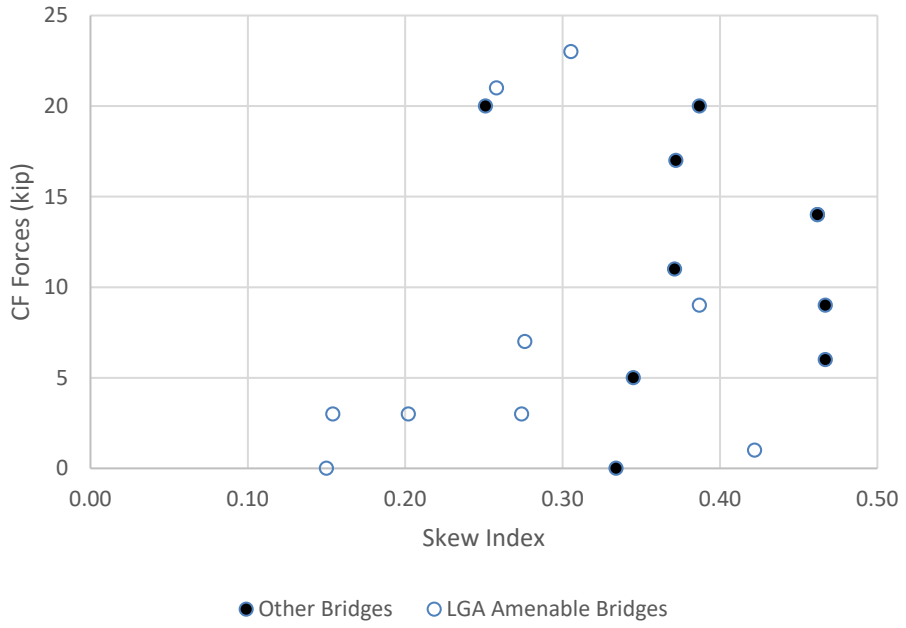

Figure 124. Maximum compression forces in diagonals of end and intermediate-pier cross-frames.

Table 82. Maximum tension and compression forces in top chords of end and intermediate-pier cross-frames (shaded values indicate cross-frame forces for bridges that meet or nearly meet the requirements for application of the recommended LGA-based procedures for the bridge design).

Bridge	Skew Index	STR I Max Tension (kip)	STR I Max Compression (kip)
1	0.46	23	20
2	0.46	26	20
3	0.39	29	44
4*	0.39	27	40
5*	0.42	5	9
6	0.35	15	17
7	0.33	NA**	NA**
8*	0.27	23	15
9	0.47	0	23
10	0.47	22	17
11*	0.26	17	17
17*	0.28	16	38
18*	0.20	16	15
21*	0.15	18	16
22*	0.31	34	27
23	0.37	24	28
24	0.37	38	53
25	0.25	30	43
26*	0.15	NA**	NA**

* This bridge meets, or nearly meets, the requirements for application of the recommended LGA-based procedures for the bridge design.

** This bridge has solid-web diaphragms rather than cross-frames.

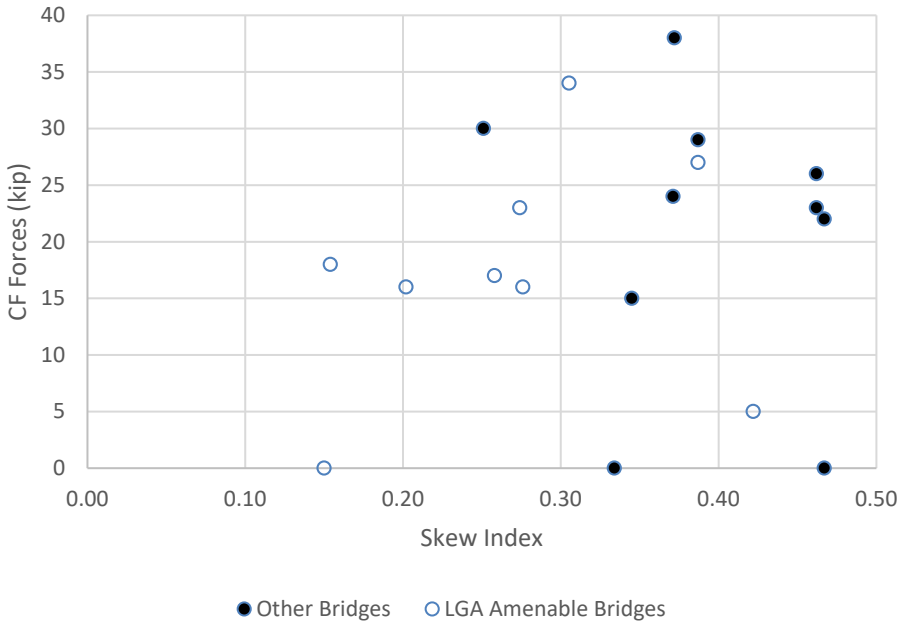

Figure 125. Maximum tension forces in top chords of end and intermediate-pier cross-frames.

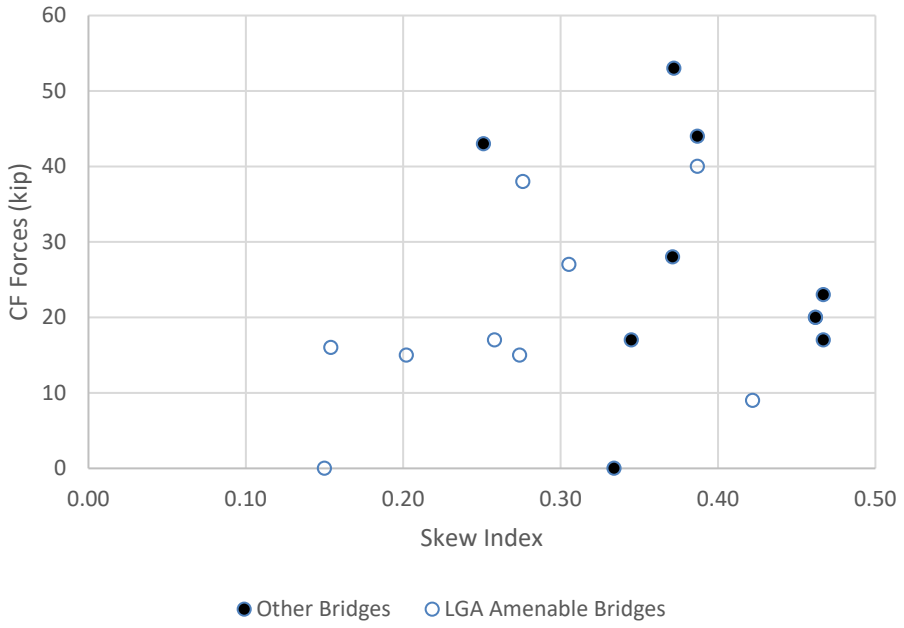

Figure 126. Maximum compression forces in top chords of end and intermediate-pier cross-frames.

It is interesting to note that in all of the above plots, the cross-frame forces tend to be smaller for the bridges that satisfy the requirements for use of the recommended LGA-based procedures.

5.3.13 Girder Live Load Deflections

For optional live load deflection evaluation, AASHTO LRFD Specification (AASHTO, 2017) Article 3.6.1.3.2 states:

If the owner invokes the optional live load deflection criteria specified in Article 2.5.6.2, the deflection should be taken as the larger of:

1. That resulting from the design truck alone, or
2. That resulting from 25% of the design truck taken together with the design lane load

Further, the AASHTO LRFD Specification (AASHTO, 2017) Article 2.5.2.6.2 states:

1. The vehicular load shall include the dynamic allowance
2. When investigating the maximum absolute deflection for straight girder systems, all design lanes shall be loaded, and all supporting components should be assumed to deflect equally
3. For composite design, the stiffness of the design cross-section used for the determination of deflection should include the entire width of the roadway and the structurally continuous portion of the railings, sidewalks and median barriers (we are assuming none of these are structurally continuous in our calculations).
4. For straight girder systems, the composite bending stiffness may be taken as the stiffness determined as specified above, divided by the number of girders

5. The live load portion of Load Combination Service I of Table 3.4.1-1 should be used including the dynamic load allowance, IM. Basically a live load multiplier of (1.0*1.33) should be used. In addition, the reference to Table 3.4.1-1 indirectly brings in the consideration of the multiple presence factor, since Article 3.4.1 indicates calls out the use of the multiple presence factor with Table 3.4.1-1.
6. The live load shall be taken from Article 3.6.1.3.2, which brings in the requirement of 25 % of the HL-93 truck with the lane load, or the HL-93 truck alone.

In summary, all of the above gives the live load distribution factor given by:

$$DF_{\Delta(LGA)} = m\left(\frac{N_L}{N_g}\right) \tag{27}$$

applied with 25 % of the HL-93 truck plus the lane load, or the HL-93 truck alone,

where

m is the multiple presence factor,

N_L is the maximum number of lanes that can be accommodated on the bridge

N_g is the number of girders in the bridge.

LGA live load displacements are obtained as the larger of displacements obtained from the application of 25 % of the HL-93 truck plus the lane load, and the HL-93 truck alone. On the other hand, in 3D FEA models, live load vehicles pertaining to 25 % of the HL-93 truck

plus the lane load, and the HL-93 truck alone are defined. The live load envelopes thus calculated are obtained by influence surface diagrams for displacements by positioning the lanes to obtain the maximum displacement. On comparison to the maximum LGA displacements, maximum 3D FEA live load displacements are always greater than the maximum LGA displacements. This is because LGA maximum displacements are obtained by the assumption that all the girders deflect equally. In a skewed bridge, such a condition will never represent the critical position of lanes obtained from an influence surface for girder vertical displacement.

Table 83 shows a comparison of the maximum live load displacements obtained from LGA and 3D FEA for exterior girders of simple span bridges with parallel skew (Group 1). DF3DFEA represents a distribution factor calculated for the maximum 3D FEA displacements. This distribution factor is compared to AASHTO live load distribution factor for bending moment, $DF_{M(LGA)}$. AASHTO LLDF for bending moment work better than the distribution factor of $DF_{A(LGA)}$ used in LGA. However, a clear correlation does not exist between the distribution factor calculated for the maximum 3D FEA displacements and the AASHTO LLDF for bending moment.

Table 84 shows a comparison of the maximum live load displacements obtained from LGA and 3D FEA for exterior girders of multi-span bridges with parallel skew (Group 2). Similar results as exterior girders of simple span bridges with parallel skew are observed. Similar results are observed for other girders studied, and hence comparison tables are not shown.

Table 83. Comparison of maximum live load displacements obtained from LGA and 3D FEA for exterior girders of simple span bridges, parallel skew (shaded cells indicate values that violate the targeted limits for applicability of LGA).

Bridge	Girder	N_L	N_g	m	$DF_{\Delta(LGA)}$	Δ_{3DFEA}	Δ_{LGA}	Δ_{LGA} / Δ_{3DFEA}	ρ_{max}	$DF_{\Delta(3DFEA)}$	$DF_{M(LGA)}$	$DF_{M(LGA)}$ / $DF_{\Delta(3DFEA)}$
17*	G1	5	7	0.65	0.46	1.71	1.08	0.63	1.58	0.74	0.91	1.24
18*	G1	4	6	0.65	0.43	2.10	1.21	0.57	1.74	0.75	0.82	1.09
21*	G1	11	12	0.65	0.60	1.92	1.58	0.83	1.21	0.72	0.89	1.23
1	G1	7	11	0.65	0.41	2.40	2.31	0.96	1.04	0.43	0.58	1.35
1	G4	7	11	0.65	0.41	2.40	2.04	0.85	1.18	0.49	0.58	1.19
2	G1	7	11	0.65	0.41	2.71	2.36	0.87	1.15	0.47	0.58	1.23
2	G4	7	11	0.65	0.41	2.70	2.08	0.77	1.30	0.54	0.58	1.08
5	G1	9	12	0.65	0.49	1.45	0.99	0.68	1.47	0.72	0.83	1.16
7	G1	9	12	0.65	0.49	1.28	0.68	0.53	1.90	0.93	0.94	1.02

* This bridge meets, or nearly meets, the requirements for application of the recommended LGA-based procedures for the bridge design.

Table 84. Comparison of maximum live load displacements obtained from LGA and 3D FEA for exterior girders of multi-span continuous bridges, parallel skew (shaded cells indicate values that violate the targeted limits for applicability of LGA).

Bridge	Girder	N_L	N_g	m	$DF_{\Delta(LGA)}$	Δ_{3DFEA}	Δ_{LGA}	Δ_{LGA} / Δ_{3DFEA}	$DF_{\Delta(3DFEA)}$	$DF_{M(LGA)}$	$DF_{M(LGA)}$ / $DF_{\Delta(LGA)}$
23	G2	6	7	0.65	0.56	2.45	1.88	0.77	0.73	0.87	1.20
23	G2	6	7	0.65	0.56	2.45	1.88	0.77	0.73	0.87	1.20
8	G2	8	8	0.65	0.65	1.77	1.28	0.72	0.90	0.91	1.01
24	G2	4	7	0.65	0.37	1.47	0.86	0.59	0.63	0.69	1.09
25	G2	3	4	0.65	0.49	1.74	1.38	0.79	0.62	0.94	1.53
25	G2	3	4	0.65	0.49	1.71	1.38	0.81	0.60	0.94	1.55
9	G2	4	6	0.65	0.43	1.94	1.25	0.64	0.67	0.77	1.14
9	G2	4	6	0.65	0.43	1.76	1.25	0.71	0.61	0.77	1.27
10	G2	4	6	0.65	0.43	1.88	1.25	0.67	0.65	0.77	1.19
10	G2	4	6	0.65	0.43	1.77	1.25	0.71	0.61	0.77	1.26
3	G2	8	8	0.65	0.65	1.50	1.07	0.71	0.91	1.00	1.10
4	G2	8	8	0.65	0.65	1.60	1.07	0.67	0.97	1.00	1.03
6	G2	9	14	0.65	0.42	1.63	1.06	0.65	0.64	0.57	0.88
26	G2	5	10	0.65	0.33	0.96	0.50	0.52	0.63	0.59	0.94
11	G2	5	7	0.65	0.46	1.78	1.24	0.70	0.67	0.77	1.15

* This bridge meets, or nearly meets, the requirements for application of the recommended LGA-based procedures for the bridge design.

CHAPTER 6. CONCLUSIONS

The objective of this research is to understand more fully the behavior of steel I-girder bridges with skew indices approaching 0.3, and to determine when, for skewed bridges having skew indices approaching 0.3, Line Girder Analysis (LGA) will yield results that are very similar to those obtained from more complex modeling. To achieve this, a parametric study was carried out for 26 bridges. Twenty of the bridges studied were selected from the 57 FDOT screened bridges. Six bridges out of the 20 bridges that were estimated to exhibit the largest skew effects were identified and studied with an alternative cross-frame arrangement.

Section 5.2 summarizes the recommended LGA-based calculation procedures for straight skewed I-girder bridges with small to moderate skew. The LGA-based calculations involve equal distribution of dead loads and use of AASHTO live load distribution factors for the calculation of live load effects.

Assumptions involved in load distribution to girders influences the accuracy of LGA. Additionally, the behavior of skew bridges is influenced by numerous structural attributes. A few of the observed qualitative aspects of structural behavior of skewed bridges are:

1. STR I bending moments predicted by LGA are conservative for all girders of all bridges compared to 3D FEA. This is because of the conservatism associated with the AASHTO live load distribution factors used in LGA. Hence, although LGA underpredicts CDL bending moments for a number of bridges, the overall STR I bending moment predictions are conservative compared to 3D FEA.

2. The presence of cross-frames in skewed bridges tends to engage all the girders and the tributary CDL and DW loads tend to be approximately equal on all the girders. Hence, the assumption of equal distribution of CDL and DW loads to all the girders in the bridge cross-section is observed to be a reasonable one. However, for barrier rails, the exterior girders attract most of the load. In very wide bridges, barrier rail load tends to induce an upward force on the central interior girders.
3. The accuracy of LGA estimates of the TDL (SDLF) displacements depends critically on the accuracy of LGA for prediction of the dead load responses. Large differences between the LGA and 3D FEA predictions are observed in a number of bridges. This is because the criteria in Section 5.2.3 for application of LGA are violated. The maximum differences are observed in the exterior girders.
4. The cross-frame framing arrangement significantly influences the behavior of straight skewed bridges. Some of the observed qualitative effects are:
    a) Comparison of a contiguous and an alternative staggered cross-frame arrangement shows that exterior girders attract more load when the cross-frame framing arrangement is contiguous.
    b) The maximum flange lateral bending stress is generally found to occur at the location of the first intermediate cross-frame for a contiguous cross-frame framing arrangement. On the other hand, if a staggered cross-frame framing arrangement is employed, the maximum flange lateral bending stress in generally observed in the central interior girder near the center of the bridge span.

c) The mitigation of a stiff transverse load path achieved by using a staggered cross-frame framing arrangement reduces the transfer of load to the obtuse corners, in turn reducing the vertical reactions and girder end shears.
d) The girder layovers are smaller for alternative staggered cross-frame arrangements.

Hence, it can be concluded that the key variables affecting the behavior of straight I-girder skewed bridges are:

1. The skew index,
2. The nature of the skew (parallel or nonparallel skew),
3. The actual skew angle at the bearing lines, and
4. The framing arrangement of the cross-frames.

It is concluded that LGA is not applicable for nonparallel skewed and splayed girder bridges. This is because additional complications are introduced in the behavior of nonparallel skewed and splayed girder bridges that are difficult to be captured by LGA

Another potential way of looking at parallel skewed bridges is to classify them broadly into three categories:

1. Bridges having skew index, $I_s \leq 0.15$ and skew angle, $\theta \leq 20°$. Generally, for the bridges in this category, cross-frames are oriented parallel to skew.
2. Bridges having skew index, $I_s \leq 0.3$ and skew angle, $\theta > 20°$.The bridges in this category may have a contiguous or staggered cross-frame arrangement.

3. Bridges having skew index, $I_s > 0.3$ and skew angle, $\theta > 20°$.The bridges in this category may have a contiguous or staggered cross-frame arrangement.

Bridges 21 and 26 from the parametric study fall into Category 1. LGA is applicable to both of these bridges.

Bridges 8, 11, 17, 18 and 25 fall into Category 2. LGA is applicable to Bridges 8, 11, 17 and 18. LGA is not applicable to Bridge 25 because its cross-frame arrangement does not satisfy the recommended requirements.

The remaining parallel skewed bridges fall into Category 3. LGA is applicable to Bridges 4 and 5. The bridges in this category exhibit larger three-dimensional effects than the bridges in Category 2. Hence, it is recommended that LGA is applicable to bridges belonging to this category only if a staggered cross-frame arrangement is employed to mitigate the transverse load path effects.

In conclusion, the synthesized results from this research project provide detailed insights into the various structural attributes influencing the behavior of straight skewed I-girder bridges. Based on the understanding of the overall behavior, recommended guidelines for application of LGA have been developed.

APPENDIX 1. DATA SUMMARY OF 57 SELECTED BRIDGES

Tables 85 to 88 summarize the cross-frame details of all bridges, in the order of increasing number of spans. Similarly, Tables 89 to 92 summarize the deck superstructure details of all bridges, and Tables 93 to 96 summarize the bearing details of all bridges in the order of increasing number of spans. Tables 97 to 100 show the span-to-depth ratios of the different bridges.

Table 85. Cross-frame details of simple-span bridges.

	Bearing Cross Frame			Intermediate Cross Frame			
Bridge	**Type**	**Connection to Girder**	**Remarks**	**Type**	**Connection to Girder**	**Remarks**	**Fit Condition**
F1	Inverted V	Skewed Connection Plate	Staggered	V	Perpendicular Connection Plate	Contiguous	Not Available
F2	Inverted V	Alternate Bent Connection Plate	Contiguous	V	Perpendicular Connection Plate	Contiguous	Total Dead Load Fit
F3	V	One side Skewed Connection Plate and other side Alternate Bent Connection Plate	Staggered	V	Perpendicular Connection Plate	Staggered	Total Dead Load Fit
F4	V	One side Skewed Connection Plate and other side Alternate Bent Connection Plate	Staggered	V	Perpendicular Connection Plate	Staggered	Total Dead Load Fit
F5	Inverted V	Alternate Bent Connection Plate	Contiguous (half width)	V	Perpendicular Connection Plate	Contiguous	Not Available
F6	Inverted V	Not Available	Contiguous (half width)	V	Not Available	Contiguous	Not Available
F7	Inverted V	Not Available	Contiguous (half width)	V	Not Available	Contiguous	Not Available
F8	Inverted V	Skewed Connection Plate	Staggered	V	Perpendicular Connection Plate	Contiguous	Not Available
F9	Welded Plate Girder Diaphragm	Skewed Connection Plate	Staggered	V	Perpendicular Connection Plate	Contiguous	Not Available
F10	Inverted V	Bent Gusset Plate	Contiguous (parallel to skew)	X	Bent Gusset Plate	Contiguous (parallel to skew)	Not Available
F11	Welded Plate Girder Diaphragm	Bent Gusset Plate	Contiguous (spanning into bearing cross frame)	Alternate Inverted V (No gusset plate)	Perpendicular Connection Plate	Contiguous	Not Available
F12	Alternate V (No gusset plate)	Skewed Connection Plate	Contiguous	Alternate V (No gusset plate)	Perpendicular Connection Plate	Contiguous	Not Available
F13	Alternate Inverted V (No gusset plate)	Skewed Connection Plate	Contiguous (half-width)	Alternate V (No gusset plate)	Perpendicular Connection Plate	Contiguous	Not Available
F14	Alternate V (No gusset plate)	Not Available	Contiguous	V	Perpendicular Connection Plate	Contiguous	Erected Fit

Table 85 (contd.). Cross-frame details of simple-span bridges.

	Bearing Cross Frame			Intermediate Cross Frame			
Bridge	**Type**	**Connection to Girder**	**Remarks**	**Type**	**Connection to Girder**	**Remarks**	**Fit Condition**
F15	Welded Plate Girder Diaphragm	Skewed Connection Plate	Contiguous	V	Perpendicular Connection Plate	Contiguous	Not Available
F16	Welded Plate Girder Diaphragm	Skewed Connection Plate	Contiguous	V	Perpendicular Connection Plate	Contiguous	Not Available
F17	Inverted V	Alternate Bent Connection Plate	Staggered	V	Perpendicular Connection Plate	Contiguous	Not Available
F18	Inverted V	Alternate Bent Connection Plate	Staggered	V	Perpendicular Connection Plate	Contiguous	Not Available
F19	Welded Plate Girder Diaphragm	Skewed Connection Plate	Contiguous (half-width)	V	Perpendicular Connection Plate	Contiguous	Not Available
F20	Welded Plate Girder Diaphragm	Skewed Connection Plate	Contiguous (half-width)	V	Perpendicular Connection Plate	Contiguous	Not Available
F21	V	One side Perpendicular Connection Plate and other side Alternate	Staggered	V	Perpendicular Connection Plate	Contiguous	Erected Fit
F22	V	One side Perpendicular Connection Plate and other side Alternate	Staggered	V	Perpendicular Connection Plate	Contiguous	Erected Fit
F23	Diaphragm MC Section	Alternate Bent Connection Plate	Staggered	Diaphragm MC Section	Perpendicular Connection Plate	Contiguous	Not Available
F24	Inverted V	Alternate Bent Connection Plate	Staggered	V	Perpendicular Connection Plate	Contiguous	Erected Fit
F25	Inverted V	Alternate Bent Connection Plate	Staggered	V	Perpendicular Connection Plate	Contiguous	Not Available
F26	Alternate Inverted V (No Gusset Plates)	Skewed Connection Plate	Contiguous	Alternate Inverted V (No Gusset	Perpendicular Connection Plate	Contiguous	Not Available

Table 86. Cross-frame details of two-span continuous bridges.

	Bearing Cross Frame			Intermediate Cross Frame			
Bridge	**Type**	**Connection to Girder**	**Remarks**	**Type**	**Connection to Girder**	**Remarks**	**Fit Condition**
F27	Inverted V	Bent Gusset Plate @ pier, Alternate Bent Connection Plate @ End Bents	Staggered	V	Perpendicular Connection Plate	Contiguous	Erected Fit
F28	Inverted V	Alternate Bent Connection Plate	Staggered	X	Perpendicular Connection Plate	Contiguous	Total Dead Load Fit
F29	Welded Plate Girder Diaphragm	Skewed Connection Plate	Contiguous	V	Perpendicular Connection Plate	Contiguous	Not Available
F30	Inverted V (only @ end bents), No cf along intermediate pier	Alternate Bent Connection Plate @ end bents, Perpendicular connection plate for intermediate cf framing into intermediate pier bearing line	Staggered near End Bents, Contiguous @ intemediate pier (Intermediate Cf framing into Bearing line @ intermediate pier)	Inverted V	Perpendicular Connection Plate	Contiguous	Not Available
F31	Inverted V (only @ end bents), No cf along intermediate pier	Alternate Bent Connection Plate @ end bents, Perpendicular connection plate for intermediate cf framing into intermediate pier bearing line	Contiguous (Intermediate Cf framing into Bearing line @ intermediate pier)	Inverted V	Perpendicular Connection Plate	Contiguous	Not Available
F32	Inverted V (only @ end bents), No cf along intermediate pier	Alternate Bent Connection Plate @ end bents, Perpendicular connection plate for intermediate cf framing into intermediate pier bearing line	Contiguous (Intermediate Cf framing into Bearing line @ intermediate pier)	Inverted V	Perpendicular Connection Plate	Contiguous	Not Available
F33	Inverted V (only @ end bents), No cf along intermediate pier	Skewed Connection Plate	Staggered	Inverted V	Perpendicular Connection Plate	Staggered	Not Available
F34	Not Available	Not Available	Contiguous	Not Available	Perpendicular Connection Plate	Contiguous	Not Available
F35	Eccentric V	Skewed Connection Plate	Contiguous (for half-width)	Alternate Eccentric V (without gusset plates), Alternate V between girders S3 & S4 (without	Perpendicular Connection Plate	Contiguous	Not Available
F36	Alternate V (No Gusset Plates)	Skewed Connection Plate	Contiguous	Alternate V (No Gusset Plates)	Perpendicular Connection Plate	Contiguous	Not Available
F37	Alternate V (No Gusset Plates)	Skewed Connection Plate	Contiguous	Alternate V (No Gusset Plates)	Perpendicular Connection Plate	Contiguous	Not Available
F38	Alternate V (No Gusset Plates)	Skewed Connection Plate	Contiguous	Alternate V (No Gusset Plates)	Perpendicular Connection Plate	Contiguous	Not Available
F39	Inverted V (2 cf framing into end bearing line)	Alternate Bent Connection Plate	Staggered	V	Perpendicular Connection Plate	Contiguous	Total Dead Load Fit
F40	Inverted V (2 cf framing into end bearing line)	Alternate Bent Connection Plate	Staggered	V	Perpendicular Connection Plate	Contiguous	Total Dead Load Fit

Table 86 (contd.). Cross-frame details of two-span continuous bridges.

	Bearing Cross Frame			Intermediate Cross Frame			
Bridge	**Type**	**Connection to Girder**	**Remarks**	**Type**	**Connection to Girder**	**Remarks**	**Fit Condition**
F41	Alternate V (No Gusset Plates)	Skewed Connection Plate	Contiguous	Alternate V (No Gusset Plates)	Perpendicular Connection Plate	Contiguous	Erected Fit
F42	Inverted V	Alternate Bent Connection Plate	Staggered	Alternate V (No Gusset Plates)	Perpendicular Connection Plate	Contiguous	Not Available
F43	Inverted V (only @ end bents), No cf along intermediate pier	Alternate Bent Connection Plate	Contiguous (Intermediate Cf framing into Bearing line @ both end abutments and intermediate pier)	Inverted V	Perpendicular Connection Plate	Contiguous	Erected Fit
F44	Not Available	Not Available	Staggered near End Abutments, Contiguous (Intermediate Cf framing into Bearing line @ intermediate pier)	V	Perpendicular Connection Plate	Contiguous	Total Dead Load Fit
F45	Welded Plate Girder Diaphragm	Alternate Bent Connection Plate	Staggered near End Abutments, Contiguous (Intermediate Cf framing into Bearing line @ intermediate pier)	Alternate V (No Gusset Plates)	Perpendicular Connection Plate	Contiguous	Not Available
F46	Alternate V (No Gusset Plates for Top Channel)	Not Available	Staggered near End Bents &@ intermediate pier	V	Perpendicular Connection Plate	Contiguous	Erected Fit
F47	Alternate V (No Gusset Plates for Top Channel)	Not Available	Staggered near End Bents &@ intermediate pier	V	Perpendicular Connection Plate	Contiguous	Erected Fit
F48	Alternate V (No gusset plate)	Bent Gusset Plate, intermediate cross-frame also connected on the same connection plate	Contiguous (Intermediate Cf framing into Bearing line @ intermediate pier from both side)	Alternate V (No gusset plate for the bottom chord)	Perpendicular Connection Plate	Contiguous	Not Available
F49	Inverted V	Alternate Bent Connection Plate	Contiguous	Alternate V (No Gusset Plates)	Perpendicular Connection Plate	Contiguous	Not Available
F50	Inverted V	Alternate Bent Connection Plate	Contiguous (half-width)	Alternate V (No Gusset Plates)	Perpendicular Connection Plate	Contiguous	Not Available
F51	Inverted V	Alternate Bent Connection Plate	Contiguous (half-width)	Alternate V (No Gusset Plates)	Perpendicular Connection Plate	Contiguous	Not Available
F52	Inverted V	Bent Gusset Plate	Contiguous (half-width)	V (Alternate V for closure pour)	Perpendicular Connection Plate	Contiguous	Not Available
F53	W Section Diaphragm	Skewed Connection Plate	Contiguous (parallel to skew)	Inverted V	Skewed Connection Plate	Contiguous (parallel to skew)	Not Available

Table 87. Cross-frame details of three-span continuous bridges.

	Bearing Cross Frame			Intermediate Cross Frame			
Bridge	**Type**	**Connection to Girder**	**Remarks**	**Type**	**Connection to Girder**	**Remarks**	**Fit Condition**
F54	Inverted V @ left end, Double Inverted V @ right end	Alternate Bent Connection Plate	Contiguous (for half-width), Intermediate Cf framing into Bearing line @ intermediate pier from both side	V	Perpendicular Connection Plate	Contiguous	Total Dead Load Fit
F55	V	Bent Web Plate	Staggered	Alternate V (No gusset plate)	Perpendicular Connection Plate	Contiguous	Not Available

Table 88. Cross-frame details of three-span continuous bridges.

	Bearing Cross Frame			Intermediate Cross Frame			
Bridge	**Type**	**Connection to Girder**	**Remarks**	**Type**	**Connection to Girder**	**Remarks**	**Fit Condition**
F56	V	Alternate Bent Connection Plate	Staggered	V	Perpendicular Connection Plate	Contiguous	Not Available
F57	Inverted V	Alternate Bent Connection Plate	Staggered	Inverted V	Perpendicular Connection Plate	Contiguous	Total Dead Load Fit

Table 89. Deck superstructure details of simple-span bridges.

Bridge	Grade of Concrete	Width of Deck	Structural Thickness	Type of Deck Form	Casting Sequence		Remarks
					# of Phases	# of Stages	
F1	4.5 ksi	71 ft 1 in	8 in	SIP Metal Deck	3	1	Replacement of an existing bridge, Each phase shall be completed in a single pour.
F2	4.5 ksi	30 ft 1 in	9 in	SIP Metal Deck	1	1	Deck Casting to start from the right end of the bridge, 9 in thick deck includes 0.5 in sacrificial thickness
F3	31 MPa	17.75 m	215 mm	Not Available	Not Available	Not Available	
F4	31 MPa	17.75 m	215 mm	Not Available	Not Available	Not Available	
F5	Not Available	Not Available	Not Available	Not Available	Not Available	Not Available	
F6	4.5 ksi	59 ft 1 in	9 in	Not Available	3 (including closure pour)	Not Available	
F7	4.5 ksi	59 ft 1 in	9 in	Not Available	3 (including closure pour)	Not Available	
F8	31 MPa	12.641 m	200 mm	SIP Metal Deck	Not Available	Not Available	
F9	4.5 ksi	123 ft 1 in	8 in	SIP Metal Deck	5 (including closure pours)	Not Available	Existing 2 bridges to be replaced by 1 single wide bridge
F10	4.5 ksi	135 ft 1 in	8.5 in	SIP Metal Deck	5 (including closure pours)	1	Existing 2 bridges to be replaced by 1 single wide bridge
F11	Not Available	43 ft 1 in	8.75 in	SIP Metal Deck	1	1	
F12	4.5 ksi	43 ft 1 in	8.5 in	SIP Metal Deck	Not Available	Not Available	Scope for future expansion
F13	31 MPa	35.160 m	200 mm	SIP Metal Deck	5 (including closure pours)	Not Available	Existing 2 bridges to be replaced by 1 single wide bridge

Table 89 (contd.). Deck superstructure details of simple-span bridges.

Bridge	Grade of Concrete	Width of Deck	Structural Thickness	Type of Deck Form	Casting Sequence		Remarks
					# of Phases	# of Stages	
F14	4.5 ksi	64 ft 8 in	9.25 in	SIP Metal Deck	Not Available	Not Available	
F15	4.5 ksi	43 ft 1 in	8 in	SIP Metal Deck	Not Available	Not Available	
F16	4.5 ksi	30 ft 1 in	8 in	SIP Metal Deck	Not Available	Not Available	
F17	4.5 ksi	43 ft 1 in	9 in	SIP Metal Deck	Not Available	Not Available	9 in thick deck includes 0.5 in sacrificial thickness
F18	4.5 ksi	43 ft 1 in	9 in	SIP Metal Deck	Not Available	Not Available	9 in thick deck includes 0.5 in sacrificial thickness
F19	31 MPa	19.3 m	200 mm	SIP Metal Deck	1	1	
F20	31 MPa	22.885 m	200 mm	SIP Metal Deck	3 (including closure pour)	1	
F21	31 MPa	12.95 m	210 mm	SIP Metal Deck	Not Available	Not Available	
F22	31 MPa	16.55 m	210 mm	SIP Metal Deck	Not Available	Not Available	
F23	31 MPa	16.772 m	8.5 in	SIP Metal Deck	1	1	
F24	Not Available	73 ft	8.5 in	SIP Metal Deck	1	1	Deck Casting to start from the right end of the bridge, maximum width reported for the splayed girder bridge
F25	Not Available	87 ft 1 in	8.5 in	SIP Metal Deck	1	2	Deck Casting from both ends of the bridge
F26	4.5 ksi	55 ft 1 in	8 in	SIP Metal Deck	Not Available	Not Available	

Table 90. Deck superstructure details of two-span continuous bridges.

Bridge	Grade of Concrete	Width of Deck	Structural Thickness	Type of Deck Form	Casting Sequence		Remarks
					# of Phases	# of Stages	
F27	4.5 ksi	91 ft 11 in	8.5 in	SIP Metal Deck	1	5	
F28	4.5 ksi	43 ft 1 in	8.5 in	SIP Metal Deck	1	3	
F29	Not Available	50 ft 2 in	9 in	SIP Metal Deck	1	1	Continuous concrete placement from left end abutment to right end abutment (revised)
F30	4.5 ksi	65 ft	8.5 in	SIP Metal Deck	1	3	
F31	4.5 ksi	59 ft	9 in	SIP Metal Deck	1	3	
F32	4.5 ksi	84 ft 2 in	9 in	SIP Metal Deck	1	3	
F33	4.5 ksi	101 ft 1 in	9 in	SIP Metal Deck	1	1	Deck to be cast all at once with no construction joint
F34	5.5 ksi	47 ft 1 in	8.5 in	SIP Metal Deck	1	3	
F35	31 MPa	27.66 m	200 mm	SIP Metal Deck	3 (including closure pour)	3	
F36	Not Available	30 ft 1 in	9 in	SIP Metal Deck	1	3	
F37	Not Available	55 ft 1 in	9 in	SIP Metal Deck	1	3	
F38	Not Available	51 ft 1 in	9 in	SIP Metal Deck	1	3	
F39	Not Available	71 ft 1 in	9 in	SIP Metal Deck	1	3	
F40	Not Available	59 ft 1 in	9 in	SIP Metal Deck	1	3	Deck thickness includes 0.5 in sacrificial thickness

Table 90 (contd.). Deck superstructure details of two-span continuous bridges.

Bridge	Grade of Concrete	Width of Deck	Structural Thickness	Type of Deck Form	Casting Sequence		Remarks
					# of Phases	# of Stages	
F41	4.5 ksi	35 ft 1 in	8.5 in	SIP Metal Deck	3 (including closure pour)	3	
F42	4.5 ksi	55 ft 3 in	8.5 in	SIP Metal Deck	3 (including closure pour)	3	
F43	4.5 ksi	43 ft 1 in	9 in	SIP Metal Deck	1	3	Deck pour transverse direction perpendicular to girders
F44	4.5 ksi	54 ft	8.5 in	SIP Metal Deck	Not Available	Not Available	
F45	4.5 ksi	37 ft 1 in	8.5 in	SIP Metal Deck	1	3	
F46	Not Available	56 ft 1 in	9 in	SIP Metal Deck	1	3	
F47	Not Available	67 ft 1 in	9 in	SIP Metal Deck	1	3	
F48	4.5 ksi	102 ft 1 in	9.5 in	SIP Metal Deck	1	5	
F49	31 MPa	9.05 m	200 mm	SIP Metal Deck	1	3	
F50	31 MPa	29.75 m	200 mm	SIP Metal Deck	3 (including closure pour)	3	
F51	31 MPa	9.05 m	200 mm	SIP Metal Deck	1	3	
F52	4.5 ksi	112 ft 2 in	8 in	SIP Metal Deck	5 (including closure pour)	2	Staged construction begins from the two ends of the bridge
F53	4.5 ksi	73 ft 1 in	8 in	SIP Metal Deck	Not Available	Not Available	

Table 91. Deck superstructure details of three-span continuous bridges.

Bridge	Grade of Concrete	Width of Deck	Structural Thickness	Type of Deck Form	Casting Sequence		Remarks
					# of Phases	# of Stages	
F54	4.5 ksi	42 ft 5.5 in	8.5 in	SIP Metal Deck	Not Available	Not Available	
F55	4.5 ksi	67 ft 1 in	8 in	SIP Metal Deck	1	5	2 pairs of stages identical

Table 92. Deck superstructure details of four-span continuous bridges.

Bridge	Grade of Concrete	Width of Deck	Structural Thickness	Type of Deck Form	Casting Sequence	
					# of Phases	# of Stages
F56	4.5 ksi	43 ft 1 in	9.5 in	SIP Metal Deck	1	7
F57	Not Available	18.35 m	220 mm	SIP Metal Deck	1	7

Table 93. Bearing details of simple-span bridges.

	Bearing Articulation			
Bridge	**Left End**	**Right End**	**Type of Bearing**	**Remarks**
F1	Expansion	Fixed	Elastomeric: Composite Neoprene Pads	Slotted Holes in Longitudinal direction at expansion end with seismic bars
F2	Fixed	Expansion	Elastomeric: Composite Neoprene Pads	Slotted Holes in Longitudinal direction at expansion end with anchor bolts
F3	Expansion	Fixed	Elastomeric: Composite Neoprene Pads	Slotted Holes in Longitudinal direction at expansion end with anchor bolts
F4	Fixed	Fixed	Elastomeric: Composite Neoprene Pads	Slotted Holes in Longitudinal direction at expansion end with anchor bolts
F5	Expansion	Fixed	Not Available	
F6	Expansion	Expansion	Not Available	
F7	Expansion	Expansion	Not Available	
F8	Fixed	Expansion	Elastomeric: Composite Neoprene Pads	Slotted Holes in Longitudinal direction at expansion end with anchor bolts
F9	Expansion	Fixed	Elastomeric: Composite Neoprene Pads	Slotted Holes in Longitudinal direction at expansion end with anchor bolts
F10	Expansion	Expansion	Elastomeric: Composite Neoprene Pads	Slotted Holes in Longitudinal direction at expansion end with anchor bolts
F11	Expansion	Expansion	Elastomeric: Composite Neoprene Pads	Slotted Holes in Longitudinal direction at expansion end with anchor bolts
F12	Expansion	Fixed	Elastomeric: Composite Neoprene Pads	Slotted Holes in Longitudinal direction at expansion end with anchor bolts
F13	Expansion	Fixed	Elastomeric: Composite Neoprene Pads	Slotted Holes in Longitudinal direction at expansion end with anchor bolts
F14	Expansion	Expansion	Elastomeric: Composite Neoprene Pads	Slotted Holes in Longitudinal direction at expansion end with anchor bolts

Table 93 (contd.). Bearing details of simple-span bridges.

	Bearing Articulation			
Bridge	**Left End**	**Right End**	**Type of Bearing**	**Remarks**
F15	Expansion	Fixed	Elastomeric: Composite Neoprene Pads	Slotted Holes in Longitudinal direction at expansion end with anchor bolts
F16	Fixed	Expansion	Elastomeric: Composite Neoprene Pads	Slotted Holes in Longitudinal direction at expansion end with anchor bolts
F17	Expansion	Expansion	Elastomeric: Composite Neoprene Pads	Slotted Holes in Longitudinal direction at expansion end with anchor bolts
F18	Expansion	Expansion	Elastomeric: Composite Neoprene Pads	Slotted Holes in Longitudinal direction at expansion end with anchor bolts
F19	Fixed	Expansion	Elastomeric: Composite Neoprene Pads	Slotted Holes in Longitudinal direction at expansion end with anchor bolts
F20	Fixed	Expansion	Elastomeric: Composite Neoprene Pads	Slotted Holes in Longitudinal direction at expansion end with anchor bolts
F21	Expansion	Expansion	Elastomeric: Composite Neoprene Pads	Slotted Holes in Longitudinal direction at expansion end with anchor bolts
F22	Expansion	Expansion	Elastomeric: Composite Neoprene Pads	Slotted Holes in Longitudinal direction at expansion end with anchor bolts
F23	Expansion	Fixed	Elastomeric: Composite Neoprene Pads	
F24	Expansion	Fixed	Elastomeric: Composite Neoprene Pads	Slotted Holes in Longitudinal direction at expansion end with anchor bolts
F25	Fixed	Expansion	Elastomeric: Composite Neoprene Pads	Slotted Holes in Longitudinal direction at expansion end with anchor bolts
F26	Fixed	Expansion	Elastomeric: Composite Neoprene Pads	Slotted Holes in Longitudinal direction at expansion end with anchor bolts

Table 94. Bearing details of two-span continuous bridges.

	Bearing Articulation				
Bridge	**Left End**	**Intermediate Pier**	**Right End**	**Type of Bearing**	**Remarks**
F27	Expansion	Fixed	Expansion	Elastomeric: Composite Neoprene Pads	Slotted Holes in Longitudinal direction (actual) at expansion end with anchor bolts
F28	Uni-directional Pot Bearing	Fixed Pot Bearing	Uni-directional Pot Bearing	Pot Bearing	Masonry Plate with Swedged Anchor Bolt
F29	Expansion	Fixed	Expansion	Elastomeric: Composite Neoprene Pads	Slotted Holes in Longitudinal direction at expansion end with anchor bolts
F30	Uni-directional Pot Bearing	Fixed Pot Bearing	Uni-directional Pot Bearing	Pot Bearing	Swedged anchor bolt with longitudinal slotted holes at end bents 1 & 3
F31	Uni-directional Pot Bearing	Fixed Pot Bearing	Uni-directional Pot Bearing	Pot Bearing	Swedged anchor bolt with longitudinal slotted holes at end bents 1 & 3
F32	Uni-directional Pot Bearing	Fixed Pot Bearing	Uni-directional Pot Bearing	Pot Bearing	Swedged anchor bolt with longitudinal slotted holes at end bents 1 & 3
F33	Uni-directional Pot Bearing	Fixed Pot Bearing	Uni-directional Pot Bearing	Pot Bearing	Swedged anchor bolts at 4 corners with longitudinal slotted holes at end bents 1 & 3
F34	Expansion	Fixed	Expansion	Not Available	
F35	Expansion	Fixed	Expansion	Elastomeric: Composite Neoprene Pads	Slotted Holes in Longitudinal direction at expansion end with anchor bolts
F36	Expansion	Fixed	Expansion	Elastomeric: Composite Neoprene Pads	Slotted Holes in Longitudinal direction at expansion end with swedged anchor rods
F37	Expansion	Fixed	Expansion	Elastomeric: Composite Neoprene Pads	Slotted Holes in Longitudinal direction at expansion end with swedged anchor rods
F38	Expansion	Fixed	Expansion	Elastomeric: Composite Neoprene Pads	Slotted Holes in Longitudinal direction at expansion end with swedged anchor rods
F39	Expansion	Fixed	Expansion	Elastomeric: Composite Neoprene Pads	Slotted Holes in Longitudinal direction at expansion end with swedged anchor rods
F40	Expansion	Fixed	Expansion	Elastomeric: Composite Neoprene Pads	Slotted Holes in Longitudinal direction at expansion end with swedged anchor rods

Table 94 (contd.). Bearing details of two-span continuous bridges.

	Bearing Articulation				
Bridge	Left End	Right End	Type of Bearing	Remarks	
F41	Expansion	Fixed	Expansion	Elastomeric: Composite Neoprene Pads	Slotted Holes in (actual) Longitudinal direction at expansion end with swedged anchor rods
F42	Expansion	Fixed	Expansion	Elastomeric: Composite Neoprene Pads	Slotted Holes in Longitudinal direction at expansion end with anchor bolts
F43	Expansion	Fixed	Expansion	Elastomeric: Composite Neoprene Pads	Slotted Holes in Longitudinal direction at expansion end with swedged anchor rods
F44	Expansion	Fixed	Expansion	Not Available	Not Available
F45	Expansion	Fixed	Expansion	Elastomeric: Composite Neoprene Pads	Slotted Holes in Longitudinal direction at expansion end with swedged anchor rods
F46	Expansion	Fixed	Expansion	Elastomeric: Composite Neoprene Pads	Slotted Holes in (actual) Longitudinal direction at expansion end with swedged anchor rods
F47	Expansion	Fixed	Expansion	Elastomeric: Composite Neoprene Pads	Slotted Holes in (actual) Longitudinal direction at expansion end with swedged anchor rods
F48	Expansion	Fixed	Expansion	Multirotational Pot Bearing	Swedge anchor bolt
F49	Expansion	Fixed	Expansion	Elastomeric: Composite Neoprene Pads	Not Available
F50	Expansion	Fixed	Expansion	Elastomeric: Composite Neoprene Pads	
F51	Expansion	Fixed	Expansion	Elastomeric: Composite Neoprene Pads	
F52	Expansion	Fixed	Expansion	Elastomeric: Composite Neoprene Pads	Slotted Holes in Longitudinal direction at expansion end with swedged anchor rods
F53	Expansion	Fixed	Expansion	Elastomeric: Composite Neoprene Pads	Slotted Holes in Longitudinal direction at expansion end with anchor bolts

Table 95. Bearing details of three-span continuous bridges.

	Bearing Articulation					
Bridge	Left End	Left Intermediate	Right Intermediate	Right End	Type of Bearing	Remarks
F54	Expansion	Expansion	Fixed	Expansion	Not Available	
F55	Expansion	Expansion	Expansion	Expansion	Elastomeric: Composite Neoprene Pads	Slotted Holes in Longitudinal direction at expansion end with swedge anchor bolts

Table 96. Bearing details of four-span continuous bridges.

	Bearing Articulation						
Bridge	**Left End**	**Left Intermediate**	**Center**	**Right Intermediate**	**Right End**	**Type of Bearing**	**Remarks**
F56	Expansion	Expansion	Fixed	Expansion	Expansion	Elastomeric: Composite Neoprene Pads	Slotted Holes in Longitudinal direction at expansion end with swedge anchor bolts
F57	Expansion	Expansion	Fixed	Expansion	Expansion	Elastomeric: Composite Neoprene Pads	Slotted Holes in Longitudinal direction at expansion end

Table 97. Maximum span-depth ratios for girders of simple-span bridges.

Bridge	Max L/D
F1	26.90
F2	27.82
F3	28.72
F4	30.26
F5	28.79
F6	29.41
F7	29.41
F8	27.13
F9	27.55
F10	28.34
F11	25.84
F12	24.30
F13	29.51
F14	24.36
F15	27.92
F16	27.52
F17	28.39
F18	25.47
F19	28.34
F20	28.34
F21	28.04
F22	28.04
F23	29.39
F24	30.08
F25	40.33
F26	25.76

Table 98. Maximum span-depth ratios for girders of two-span continuous bridges.

Bridge	Max L/D
F27	29.04
F28	26.99
F29	27.07
F30	33.35
F31	32.50
F32	32.14
F33	28.79
F34	27.78
F35	30.29
F36	35.46
F37	35.46
F38	35.46
F39	33.68
F40	33.68
F41	36.16
F42	29.11
F43	26.19
F44	34.48
F45	24.68
F46	30.79
F47	30.55
F48	28.13
F49	31.11
F50	29.09
F51	28.54
F52	35.64
F53	32.32
F54	34.19
F55	30.43

Table 99. Maximum span-depth ratios for girders of four-span continuous bridges.

Bridge	Max L/D
F56	29.66
F57	28.31

APPENDIX 2. SIMPLE –SPAN AND TWO-SPAN CONTINUOUS BRIDGES NOT SELETED FOR FURTHER STUDY

This appendix shows the plan geometry of the bridges that have not been selected for further study at this time.

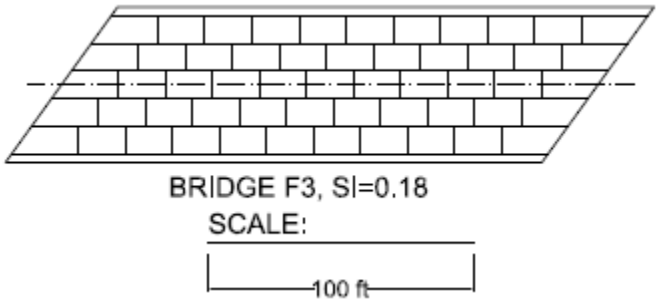

Figure 127. Other simple-span bridges with staggered cross-frame arrangement.

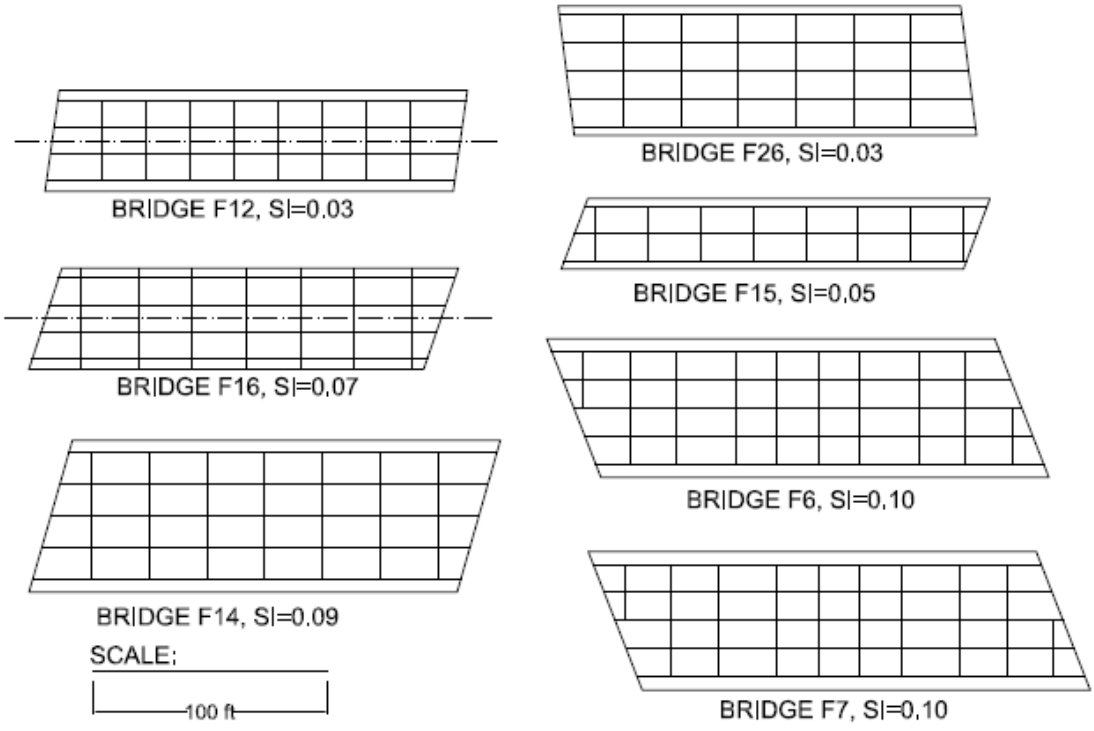

Figure 128. Other simple-span bridges with contiguous cross-frame arrangement.

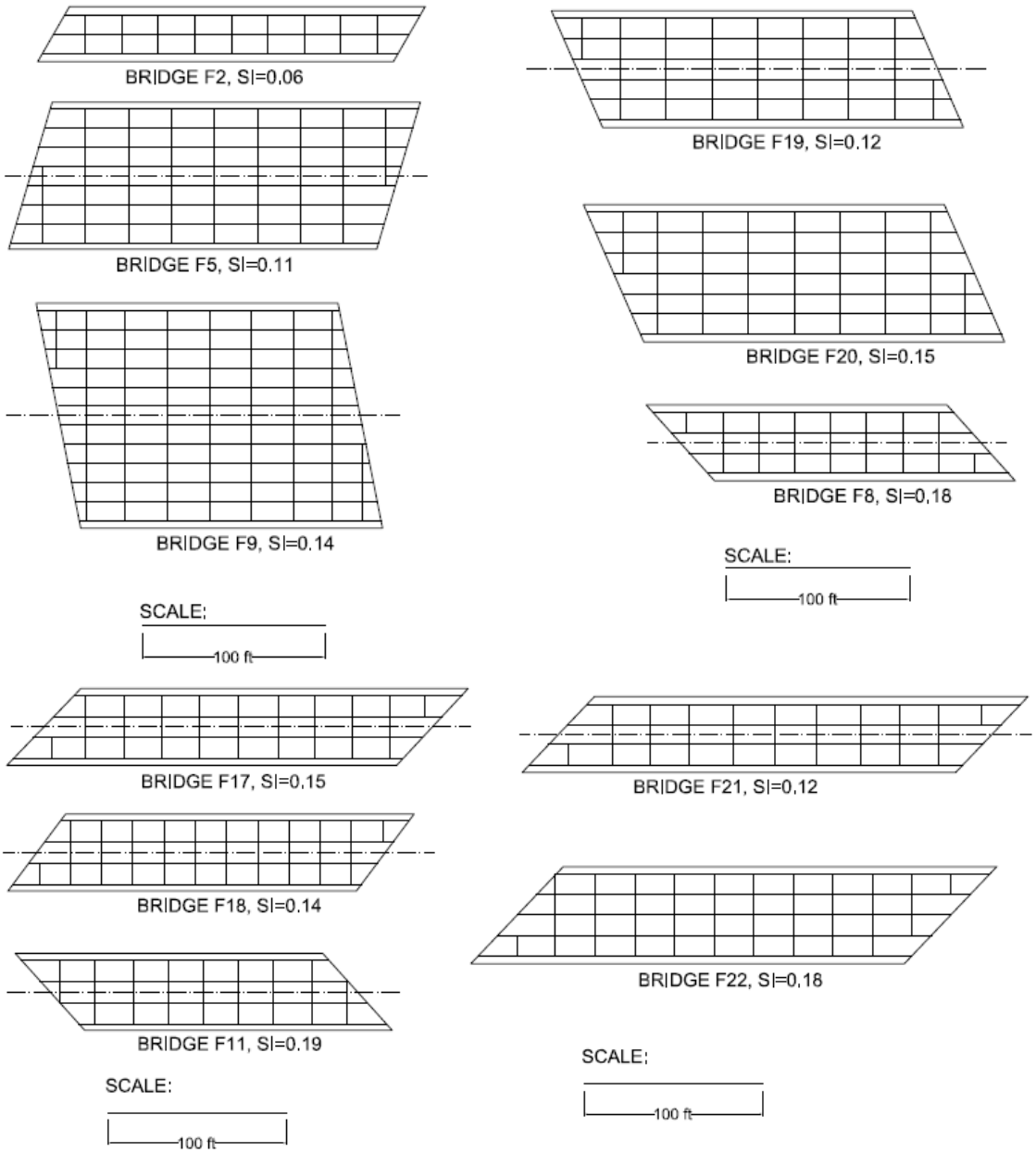

Figure 128 (contd.). Other simple-span bridges having contiguous cross-frame arrangement.

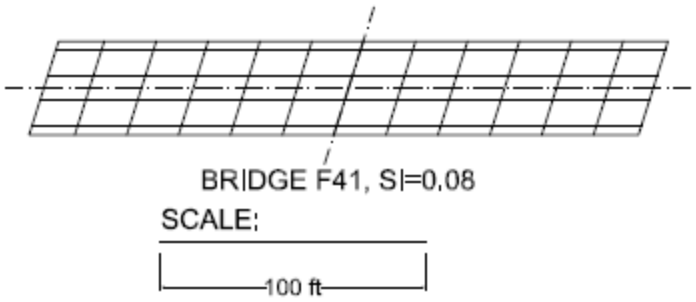

Figure 129. Other two-span continuous bridges having cross-frames parallel to skew.

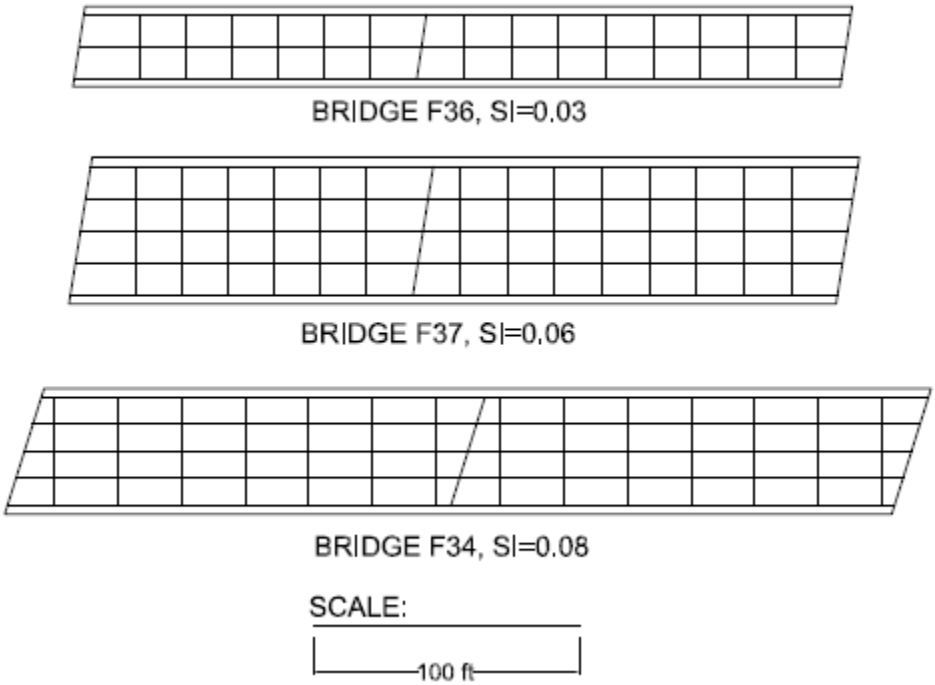

Figure 130. Other two-span continuous bridges having contiguous cross-frame arrangement.

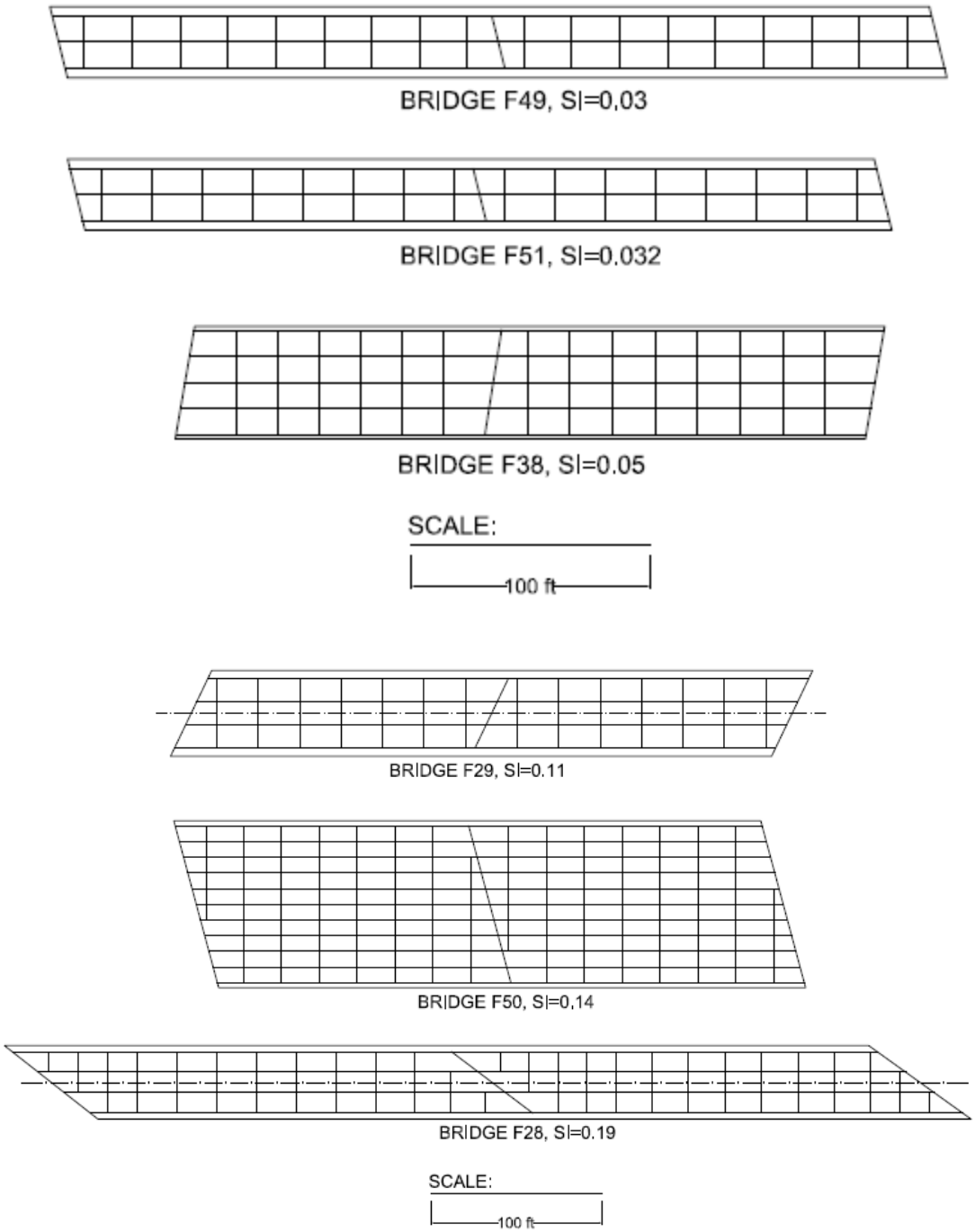

Figure 130 (contd.). Other two-span continuous bridges having contiguous cross-frame arrangement.

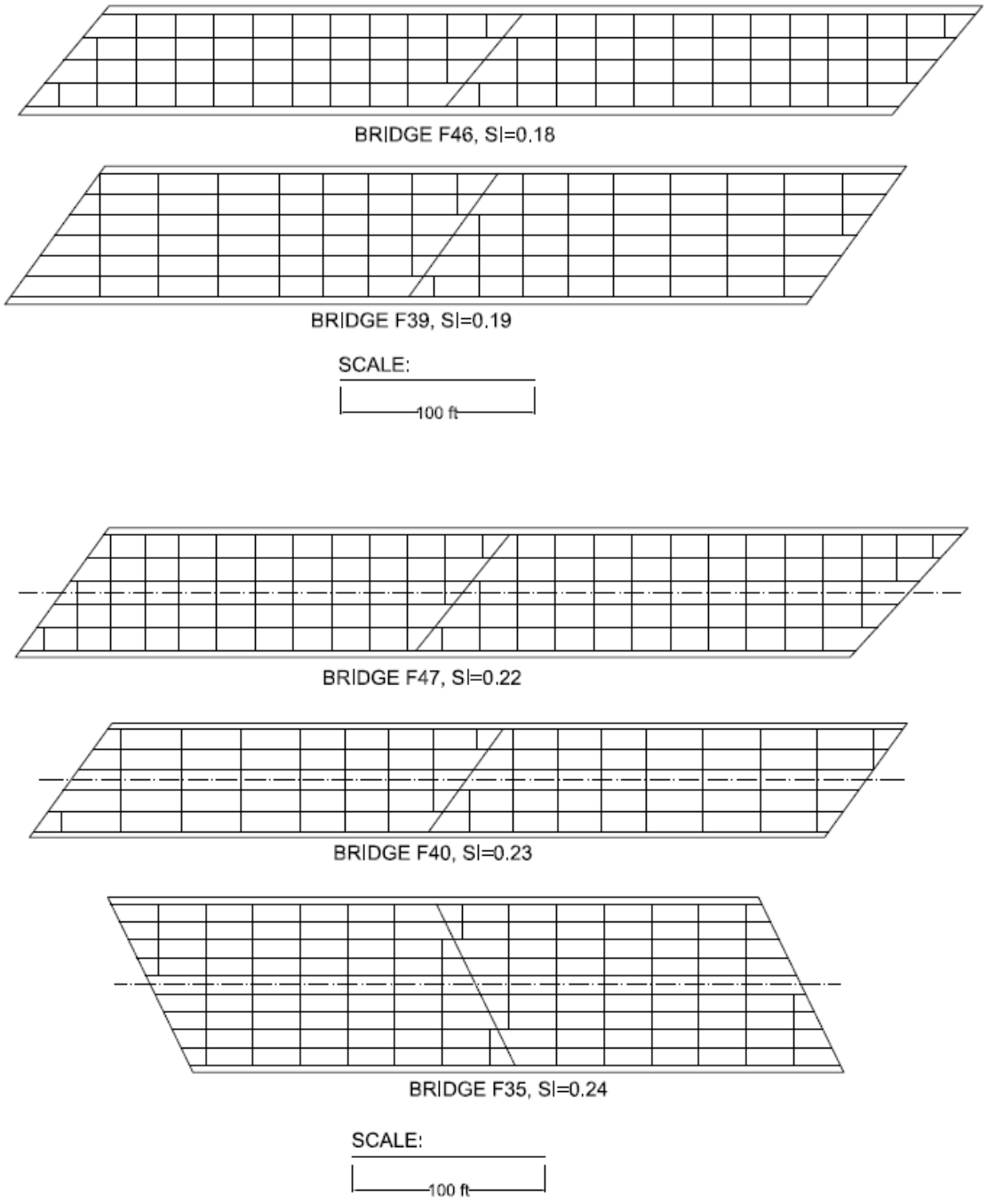

Figure 130 (contd.). Other two-span continuous bridges having contiguous cross-frame arrangement.

APPENDIX 3. SYNTHESIS OF DATA AND PLOTS FOR EACH BRIDGE

Appendix 3 Sections for individual bridge are furnished separately as electronic files

APPENDIX 4. SYNTHESIS OF DATA AND PLOTS FOR STAGED DECK PLACEMENT STUDIES

Appendix 4 Sections for individual bridge are furnished separately as electronic files

REFERENCES

AASHTO (2002). Standard Specifications for Highway Bridges, 17th Edition, American Association of State Highway and Transportation Officials, Washington, D.C.

AASHTO/NSBA (2004). Steel Bridge Bearing Design and Detailing Guidelines, G9.1, AASHTO/NSBA Steel Bridge Collaboration, American Association of State Highway and Transportation Officials, Washington, D.C. and National Steel Bridge Alliance, Chicago, IL.

AASHTO/NSBA (2006). Guidelines for Design Details, G1.4-2006, AASHTO/NSBA Steel Bridge Collaboration, American Association of State Highway and Transportation Officials, Washington, D.C. and National Steel Bridge Alliance, Chicago, IL.

AASHTO/NSBA (2011). Guidelines for the Analysis of Steel Girder Bridges, G13.1, AASHTO/NSBA Steel Bridge Collaboration, American Association of State Highway and Transportation Officials, Washington, D.C. and National Steel Bridge Alliance, Chicago, IL.

AASHTO (2015). AASHTO LRFD Bridge Design Specifications, 7th Edition with 2015 Interims, American Association of State Highway and Transportation Officials, Washington, DC.

AASHTO (2017). AASHTO LRFD Bridge Design Specifications, 8th Edition, American Association of State Highway and Transportation Officials, Washington, DC.

ANSYS (2019) .ANSYS Structures, ANSYS Inc., Canonsburg, PA.

Bishara, A.G., Liu, M.C., El-Ali, N.D., (1993). “Wheel Load Distribution on Simply Supported Skew I-Beam Composite Bridges”, J. Struct. Eng., 1993, 119(2): 399-419

Computers and Structures (2018). CSiBridge Version 21.0.2, Computers and Structures, Inc., Berkeley, CA.

Ebeido, T., and Kennedy, J. B. (1996a). “Girder moments in continuous skew composite bridges.” J. Bridge Eng., 1(1), 37–45.

FDOT (2018). “Simplified Method to Determine Girder Layover at Simply Supported Girder Ends,” private communication from the project steering group.

FDOT (2019a). “Structures Design Guidelines,” Structures Manual, Volume 1, Florida Department of Transportation, Tallahassee, FL, January.

FDOT (2019b). “Standard Specifications for Road and Bridge Construction July 2019”, Florida Department of Transportation, Tallahassee, FL, July.

Gull, J.H., Azizinamini, A., (2014a). “Steel Plate Girder Diaphragm and Cross Bracing Loads” FDOT Contract No. BDK80 977-20 Final Report, Florida Department of Transportation, Tallahassee, FL.

Gull, J.H., Azizinamini, A., (2014b). “Steel Framing Strategies for Highly Skewed Bridges to Reduce/Eliminate Distortion near Skewed Supports,” FDOT Contract No. BDK80 977-21 Final Report, Florida Department of Transportation, Tallahassee, FL.

Helwig, T.A. and Yura, J.A. (2015). “Bracing System Design,” Steel Bridge Design Handbook, Publication No. FHWA-HIF-16-002 - Vol. 13, December. 91 pp.

Huang, H., Shenton, H.W., Chajes, M.J., (2004). “Load Distribution for a Highly Skewed Bridge: Testing and Analysis”, J. Bridge Eng., 10.1061/(ASCE)1084-0702(2004)9:6(558).

Huo, S.X., Wasserman, E.P., Iqbal, R.A., (2005). “Simplified Method for Calculating Lateral Distribution Factors for Live Load Shear”, J. Bridge Eng., 10.1061/(ASCE)1084-0702(2005)10:5(544).

IOWA DOT (2018). “LRFD Bridge Design Manual”, Iowa Department of Transportation, Ames, IA.

Kupricka, G., and Poellot, B. (1993). “Nuisance Stiffness,” Bridgeline, HDR Engineering, Inc., 4(1), 3 pp.

Mabsout, M. E., Tarhini, K. M., Frederick, D. R., and Tayar, C., (1997). “Finite-element analysis of steel girder highway bridges.” J. Bridge Eng., 2(3), 83–87.

McConnell, J.R, Radovic, M., Ambrose, K., (2016). “Field Evaluation of Cross-Frame and Girder Live Load Response in Skewed Steel I-Girder Bridges”, J. Bridge Eng., 10.1061/(ASCE)BE.1943-5592.0000846.

Modjeski and Masters (2002). “Shear in Skewed Multi Beam Bridges,” NCHRP Project 20-7/Task 107, Transportation Research Board, National Research Council, Washington, D.C.

Morrill, J.L. (2016). “Live –Load Test and Finite-Element Model Analysis of a Steel Girder Bridge”, Masters. Dissertation, School of Civil and Environmental Engineering, Utah State University, Logan, Utah, 165 pp.

NHI (2011). “Analysis and Design of Skewed and Curved Steel Bridges with LRFD, Reference Manual”, NHI Course No. 130095, Publication No. FHWA-NHI-10-087, National Highway Institute, Federal Highway Administration, 1476 pp.

NHI (2015). “Load and Resistance Factor Design (LRFD) for Highway Bridge Superstructures, Reference Manual”, NHI Course No. 130081, 130081A, and 130081B, Publication No. FHWA-NHI-15-047, National Highway Institute, Federal Highway Administration, 1694 pp.

NSBA (2019). LRFD Simon, Version 10.3 (AASHTO 8th edition), National Steel Bridge Alliance, Chicago, IL.

NSBA. (2016). “Skewed and Curved Steel I-Girder Bridge Fit,” NSBA Technical Subcommittee Fit Task Force, Guide Document, National Steel Bridge Alliance, Chicago, IL, November 2015.

ODOT (2007). “Bridge Design Manual”, Ohio Department of Transportation, Columbus, OH.

PennDOT (2015). “Design Manual, Part 4”, Pennsylvania Department of Transportation, Harrisburg, PA

Quadrato, C.E. (2010). “Stability of Skewed I-Shaped Girder Bridges using ent Plate Connections,” Ph.D. dissertation, University of Texas at Austin, Austin, TX.

Romage, M.L. (2008). “Field Measurements on Lean-On-Bracing for Steel Girder Bridges with Skewed Supports,” M.S. thesis, University of Texas, Austin, TX.

Sanchez, T.A. (2011). “Influence of Bracing Systems on the Behavior of Steel Curved and/or Skewed I-Girder Bridges during Construction,” Ph.D. Dissertation, School of Civil and Environmental Engineering, Georgia Institute of Technology, Atlanta, GA, 335 pp.

Sotelino, E.D., Liu, J., Chung, W., Phhuvoravan, K. (2004). “Simplified Load Distribution Factor for Use in LRFD Design”, FHWA/IN/JTRP-2004/20 Final Report, Indiana Department of Transportation, Indianapolis, IN.

Sumner, E.A., Rizkall, S., Fisher, S.T., Whisenhunt, T.W., Paoinchantara, N. (2006). “Development of a Simplified Procedure to Predict Dead Load Deflections of Skewed and Non-skewed Steel Plate Girder Bridges”, NCSU-CFL Report No. RD-06-05, NCDOT Report No. FHWA/NC/2006-13, North Carolina DOT, Raleigh, NC.

TxDOT (2015). “Bridge Design Manual - LRFD” Section 14 Straight Plate Girders, Texas Department of Transportation, Austin, TX

White, D.W., Coletti, D., Chavel, B.W., Sanchez, A., Ozgur, C., Jimenez Chong, J.M., Leon, R.T., Medlock, R.D., Cisneros, R.A., Galambos, T.V., Yadlosky, J.M., Gatti, W.J., and Kowatch, G.T. (2012). “Guidelines for Analytical Methods and Construction Engineering of Curved and Skewed Steel Girder Bridges,” NCHRP Report 725, Transportation Research Board, National Research Council, Washington, D.C.

White, D.W., Nguyen, T.V., Coletti, D.A., Chavel, B.W., Grubb, M.A., and Boring, C.G. (2015). “Guidelines for Reliable Fit-Up of Steel I-Girder Bridges,” NCHRP 20-07/Task 355, Transportation Research Board, National Research Council, Washington, D.C.

WisDOT (2019). “Bridge Manual” Chapter 24- Steel Girder Structures, Wisconsin Department of Transportation, Madison, WI.

Zhou, C. (2006). “Utilizing Lean-On Cross-Frame Bracing for Steel Bridges,” Ph.D. dissertation, University of Houston, Houston, TX.

Zhou, J., Bennett, C., Matamoros, A., Li, J., (2017). “Skewed Steel Bridges, Part II: Cross-Frame and Connection Design to Ensure Brace Effectiveness,” Report No. K-TRAN: KU-13-7, Kansas Department of Transportation, Topeka, KS.

Zokaie, T., Osterkamp, T.A., Imbsen, R.A., (1991). “Distribution of wheel Loads on Highway Bridges,” NCHRP Report 12-26, Transportation Research Board, National Research Council, Washington, D.C.